THE EFFECT OF FOREST-TO-BOG RESTORATION ON NET ECOSYSTEM EXCHANGE IN FLOW COUNTRY PEATLANDS

Graham Hambley

A Thesis Submitted for the Degree of PhD
at the
University of St Andrews

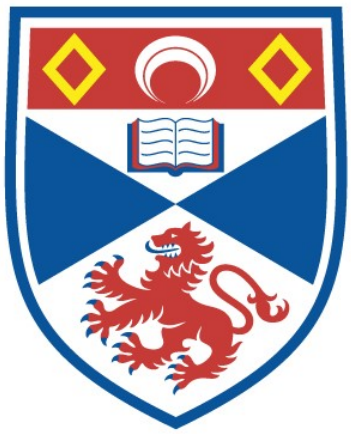

2016

The effect of forest-to-bog restoration on net ecosystem exchange in Flow Country peatlands

University of
St Andrews

School of Geography & Geosciences

Supervisors: Dr Robert Wilson and Dr Vincent Rinterknecht

Graham Hambley

This thesis is submitted in partial fulfilment for the degree of PhD at the University of St Andrews

October 2016

~ Declaration ~

1. Candidate's declarations:

I, Graham Hambley, hereby certify that this thesis, which is approximately 58,500 words in length, has been written by me, and that it is the record of work carried out by me, or principally by myself in collaboration with others as acknowledged, and that it has not been submitted in any previous application for a higher degree.

I was admitted as a research student in September 2012 and as a candidate for the degree of Doctor of Philosophy (Science Faculty), Geography and Geosciences in October 2016; the higher study for which this is a record was carried out in the University of St Andrews between 2012 and 2016.

Date ……..…….… Signature of candidate ……

2. Supervisor's declaration:

I hereby certify that the candidate has fulfilled the conditions of the Resolution and Regulations appropriate for the degree of Doctor of Philosophy (Science Faculty), Geography and Geosciences in the University of St Andrews and that the candidate is qualified to submit this thesis in application for that degree.

Date ……..……..… .Signature of supervisor ……

3. Permission for publication:

In submitting this thesis to the University of St Andrews I understand that I am giving permission for it to be made available for use in accordance with the regulations of the University Library for the time being in force, subject to any copyright vested in the work not being affected thereby. I also understand that the title and the abstract will be published, and that a copy of the work may be made and supplied to any bona fide library or research worker, that my thesis will be electronically accessible for personal or research use unless exempt by award of an embargo as requested below, and that the library has the right to migrate my thesis into new electronic forms as required to ensure continued access to the thesis. I have obtained any third-party copyright permissions that may be required in order to allow such access and migration, or have requested the appropriate embargo below.

The following is an agreed request by candidate and supervisor regarding the publication of this thesis:

Embargo on all of the print and all of the electronic copy for a period of one year on the following ground(s):

- Publication would preclude future publication

Date ……...… Signature of candidate. …… Signature of supervisor……

~ Statement of Collaboration ~

This research was carried out in collaboration with The James Hutton Institute and The Centre for Ecology and Hydrology (Edinburgh). A memorandum of understanding (MOU) was agreed between the three institutions for access to high frequency eddy covariance data and low frequency meteorological data. I carried out all of the data analysis and wrote everything in this thesis. Co-authors for each chapter are listed below.

Chapter 4: Graham Hambley (University of St Andrews), Dr Timothy Hill (University of Exeter), Dr Roxane Andersen (University of Highlands and Islands), Dr Peter Levy (Centre for Ecology and Hydrology), Dr Matthew Saunders (Trinity College Dublin), Dr Neil Cowie (RSPB), Dr Mark Hancock (RSPB), Dr Yit Arn Teh (University of Aberdeen).

Chapter 5: Graham Hambley (University of St Andrews), Dr Timothy Hill (University of Exeter), Dr Roxane Andersen (University of Highlands and Islands), Dr Peter Levy (Centre for Ecology and Hydrology), Dr Matthew Saunders (Trinity College Dublin), Dr Neil Cowie (RSPB), Dr Mark Hancock (RSPB), Dr Yit Arn Teh (University of Aberdeen).

Chapter 6: Graham Hambley (University of St Andrews), Dr Timothy Hill (University of Exeter), Dr Roxane Andersen (University of Highlands and Islands), Dr Jens-Arne Subke (University of Stirling) Dr Neil Cowie (RSPB), Dr Mark Hancock (RSPB), Dr Yit Arn Teh (University of Aberdeen).

Chapter 7: Graham Hambley (University of St Andrews), Dr Timothy Hill (University of Exeter), Dr Roxane Andersen (University of Highlands and Islands), Dr Peter Levy (Centre for Ecology and Hydrology), Dr Matthew Saunders (Trinity College Dublin), Dr Neil Cowie (RSPB), Dr Mark Hancock (RSPB), Dr Yit Arn Teh (University of Aberdeen).

~ Acknowledgments ~

I am grateful for the opportunity to carry out this postgraduate research with financial support from the University of St Andrews and the Royal Society of Protection of Birds (RSPB), whose funding made it possible. Additional thanks are extended to Scottish Natural Heritage (SNH) for providing funding for a fuel cell without which the project could not have continued and to the RSPB for allowing access to the sites on the Forsinard Flows Reserve and allowing the installation of eddy covariance towers on this fragile landscape. Unreserved thanks are extended to my, ever-growing list of, supervisors, Dr Robert Wilson, Dr Vincent Rinterknecht, Dr Timothy Hill, Dr Neil Cowie and Dr Yit Arn Teh for their invaluable expertise, guidance and support throughout this research project. Additionally, I would like to thank Professor John Moncrieff, Dr Robert Clement, and Dr Peter Levy for providing much of the eddy covariance equipment and technical support during the many equipment failures.

I would also like to thank the other collaborators involved in this and the wider Flow Country project, specifically, Dr Matthew Saunders, Dr Jens-Arne Subke, Dr Roxane Andersen, Dr Mark Hancock, Norrie Russell, Paul Gaffney, Rebecca McKenzie, Renée Hermans, Dr Ed Turner and all of the staff and volunteers at RSPB Forsinard Flows who have all provided valuable insights into eddy covariance, the Flow Country, provided on the ground support during issues with the flux towers, as well as providing great friendship. Further thanks are extended to Dr Melanie Chocholek and Dr Cheryl Wood for all of their support – as well as opening my eyes to the world of gin!

I would like to thank all of the staff in the Department of Earth and Environmental Sciences for providing feedback, criticism, praise and laughter during my near 4 years in the department as a postgraduate student and previous year and a half as a technician. Additionally, big thanks to the whole postgraduate community within the School of Geography and Geosciences for providing comic relief, friendship and moral support throughout my time in the department, in particular my fellow office workers Christopher Sargeant and Viktoria Oliver. Special thanks to Helen McMorris for spending many hours proofreading the thesis and listening to my stresses.

Finally, the biggest thank you is extended to friends and family for their support but in particular my mum and dad, who have provided unequivocal encouragement and support (as well as hot dinners and laundry services) throughout the process, without which I may not have made it to this point.

~ Abstract ~

Northern peatlands play a critical role in the regulation of atmospheric carbon (C) and are estimated to store approximately 550 Gt C, which is around a quarter of the world soil C pool. Saturated conditions means aboveground net primary productivity is low, but also results in low decomposition and subsequently low respiratory losses. The Flow Country of Caithness and Sutherland, Northern Scotland is the one of the largest areas of contiguous blanket bog in Europe encompassing an area in excess of 4000 km^2. However, these peatlands were badly degraded in the 1970s and 1980s by large-scale forestry plantations with around 17% of the Flow Country drained and planted with Sitka spruce and Lodgepole pine altering net ecosystem C functioning. Restoration efforts have been on going since the 1990s to restore these sites to blanket bog and return them to net C sinks. Using eddy covariance techniques this research sought to understand C dynamics over two sites restored at different times, assess their C sink/source status and the key environmental factors driving changes in C dynamics.

Results showed the youngest restoration site (Lonielist; restored in 2003/04) to be a net source of C to the atmosphere of 80 g C m^{-2} yr^{-1}, while the older restoration site (Talaheel; restored in 1997/98) was a net C sink of -71 g C m^{-2} yr^{-1}. Partitioning of the net exchange into its constituent parts of respiration (R_{eco}) and photosynthesis (GPP) found significant differences in R_{eco} between the two sites, whilst no significant differences were observed in GPP. Soil temperature and soil moisture were found to be the greatest controls on R_{eco}, with higher R_{eco} associated with drier, warmer conditions. Incident solar radiation controlled GPP, however dry periods coupled with high vapour pressure deficit resulted in a limitation of photosynthesis. These results highlight that peatland restoration is successful at returning sites to net C sinks over multi-decadal timescales.

~ Abbreviations and Notation ~

ABL	Atmospheric boundary layer
A_{max}	Light saturated photosynthetic rate
amsl	Above mean sea level
AGC	Automatic gain control
α	Quantum yield
C	Carbon
c	Scalar mixing ratio
CEH	Centre for Ecology and Hydrology
CO_2	Carbon Dioxide
CH_4	Methane
EBC	Energy balance closure
EC	Eddy covariance
E_o	Activation Energy
F	Turbulent Flux
F	Forested Control site (Chapter 6)
FG	Flux Gradient
G	Soil heat flux
GC	Gas chromatography
GHG	Greenhouse gas
GPP	Gross Primary Productivity
GPPmax	Difference between highest measured GPP flux and A_{max}
H	Sensible heat
H_2O	Water Vapour
IPCC	Intergovernmental Panel on Climate Change
IRGA	Infrared Gas Analyser
k	Von karman constant (0.4)
L	Leir – Felled in 2008/9 (Chapter 6)
LE	Latent energy
LO	Lonielist – Felled in 2003/4 (Chapter 6)
LSD	Least significant difference
MDS	Marginal distribution sampling

MDV	Mean diurnal variation
MODIS	Moderate resolution imaging spectroradiometer
N	Nitrogen
n	Number of samples
NASA	National Aeronautics and space administration
N_2O	Nitrous oxide
NO_x	Nitrogen oxides
NDVI	Normalised difference vegetation index
NEE	Net ecosystem exchange
NGO	Non Governmental Organisation
NPP	Net Primary productivity
NR	Newly Restored
O_3	Ozone
ρa	Air density
PAR	Photosynthetically Active Radiation
PFT	Plant functional traits
PPFD	Photosynthetic photon flux density
Q_{10}	Temperature coefficient for rate of change in respiration for a 10°C temperature increase
QC	Quality Control
Q_{pg}	Photon flux Density
R_1	Initial respiration rate
R_2	Final respiration rate
R_{10}	Basal ecosystem respiration at 10°C
r^2	Coefficient of determination
R_a	Autotrophic respiration
REA	Relaxed eddy accumulation
R_{eco}	Ecosystem respiration
R_h	Heterotrophic respiration
R_{net}	Net Radiation
RMSE	Root mean square error
SNH	Scottish Natural Heritage
SOC	Soil organic carbon
SMC	Soil moisture content

T_0	Temperature at which respiration reaches zero (-46.02°C)
T_1	Initial temperature
T_2	Final temperature
T14	Talaheel – Felled in 1997/98 Sampled in 2011/12 (Chapter 6)
T16	Talaheel – Felled in 1997/98 Sampled in 2014/15 (Chapter 6)
Ts	Sonic Temperature
T_{ref}	Reference Temperature (10°C)
*u**	Friction velocity
u/v/w	3-dimensional wind components
V	Volts
VMC	Volumetric moisture content
VOCs	Volatile organic compounds
VPD	Vapour pressure deficit
w	Vertical velocity
WPL	Webb-pearman-leuning density correction
z/L	Monin-Obukhov stability parameter
Zm	Height

~ Table of Contents ~

~ Chapter 1 ~

Introduction

1.1 The Earth's climate system

Climate change presents a serious threat to ecosystems all over the world and with it the human socio-economic system, which is dependent on the health of ecosystems for food and other services (Stern, 2007). Although variations in the climate have been recorded in the past (Peyron *et al.*, 1998, Steffensen *et al.*, 2008) there is now unequivocal evidence that the Earth's energy balance is changing due to increasing greenhouse gas (GHG) emissions caused by anthropogenic activities (Ciais *et al.*, 2013). As well as changes in atmospheric GHG concentrations, changes to land surface properties, and emissions of radiatively important atmospheric gases and aerosols can influence the Earth's energy balance (Cubasch *et al.*, 2013). These changes can alter the albedo of the Earth and the balance of incoming solar radiation that is absorbed or reflected resulting in a warming of the Earth (Wielicki *et al*., 2005). The rising concentration of atmospheric GHGs resulted in a 0.85°C increase in mean global surface temperature between 1880 and 2012 (Ciais *et al.*, 2013). This increase in temperature has the potential to affect natural, semi-natural and man-made ecosystems around the world with almost all areas of the Earth having experienced surface warming (Morice *et al.*, 2012).

Changes to the Earth's climate have been recognised as a major threat to the flora and fauna of the Earth's surface, as well as potentially affecting the integrity of ecosystems across the world (Erwin et al., 2009, Hulme 2005). Tree rings and peat cores can be used to identify changes to the Earth's climate and atmospheric GHG concentrations over the most recent few thousands of years (Charman *et al.*, 2013, Wilson *et al.*, 2016), whilst ice cores can go back as far as hundreds of thousands of years (Steffensen *et al.*, 2008, Yamamoto *et al.*, 2012). To understand deeper time changes in climate and atmospheric GHG concentrations the geological record, which can go back millions of years, can be used (Foster and Rohling, 2013). However, since March 1958 the Mauna Loa observatory has been used to reveal multi-decadal changes in the atmospheric concentration of carbon dioxide (Kane and dePaula, 1996, Lintner *et al.*, 2006).

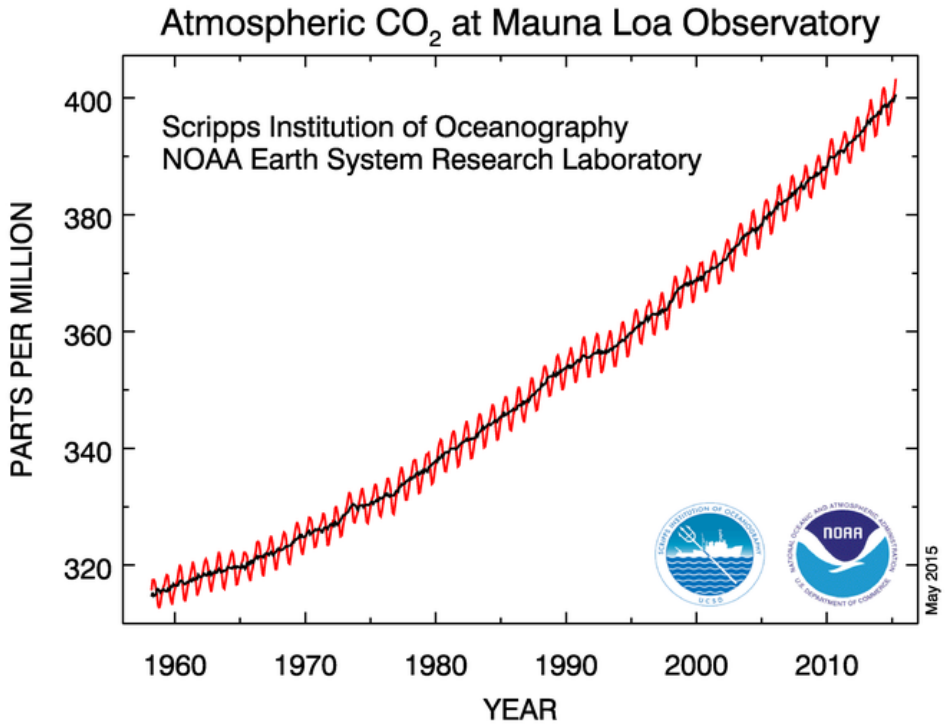

Figure 1.1 Mean monthly atmospheric CO_2 concentrations at the Mauna Loa Observatory, Hawaii. The red curve represents the mean monthly data measured as the mole fraction in dry air. The black curve represents the seasonally corrected data. (Image Source: http://www.esrl.noaa.gov/gmd/ccgg/trends/)

Despite seasonal scatter in the data, there is a strong signal for year on year increases (Figure 1.1) in atmospheric CO_2 concentrations (Solomon *et al.*, 2009). Between 1958 and 1996 there was a recorded increase in measured CO_2 concentrations of 12% (Kane and dePaula, 1996) and there is no evidence that this rate of increase is slowing down. It has been estimated that by the year 2100, if fossil fuel emissions and carbon (C) sequestration levels continue at their current rates. then humans will have released around 5000 Gt C to the atmosphere since the start of the industrial revolution (Zachos *et al.*, 2008) and atmospheric CO_2 concentrations will be in the range of 540 to 970 ppm (Stocker *et al.*, 2013). However, large uncertainties exist due to economic growth, technological advances and carbon sequestration by geological and biological processes (Nowak *et al.*, 2004, Stocker *et al.*, 2013). The world's oceans are also a sink of CO_2 and increasing CO_2 concentrations have been linked with the acidification of oceans, reducing their productivity (Cao and Caldeira, 2008, Doney *et al.*, 2009, Murphy and Measures, 2014, Guo *et al.*, 2015). To fully understand climate change and its relationship with C it is imperative that we improve our knowledge of the C cycle and understand all of the potential C sinks and sources between the land surface and atmosphere.

1.2 The C Cycle

In its simplest form the C cycle can be considered as a series of C reservoirs connected by the exchange of C in various gaseous and aqueous forms between the different reservoirs (Figure 1.2) (Ciais *et al.,* 2013). Anthropogenic activities do not physically create more C but cause a shift in the fluxes between the different reservoirs. It is thought that feedbacks from the terrestrial C cycle will have a significant impact on climate change in the future (Friedlingstein *et al.*, 2001, Davidson and Janssens, 2006). However, the CO_2 concentration dependence of the global terrestrial C storage is one of the largest and most uncertain feedbacks (Ciais *et al.*, 2013). There are two mechanisms, which result in terrestrial ecosystem feedbacks being affected by atmospheric CO_2 concentrations. Firstly, there is the effect of a direct increase in concentrations of CO_2 in the atmosphere on photosynthesis and secondly, the effects of climate change on photosynthesis and respiration (Ainsworth and Long, 2005, Taub, 2010).

As this thesis is centred on terrestrial ecosystems, further discussions of the global C cycle will be focussed on the terrestrial C reservoir and the interactions this has with the atmospheric reservoir. However, it should be noted that the oceanic and terrestrial reservoirs are not separate and that linkages between them exist through exchange with the atmosphere and the transport of sediments and dissolved C species in rivers.

CO_2 emissions from fossil fuel combustion and cement production were 8.3 [7.6 to 9.0] PgC yr^{-1} between 2002 and 2011 (Stocker *et al.,* 2013). These represent the greatest anthropogenic source of CO_2 followed by land use and land use change. Annual net CO_2 emissions from land use change between 2002 and 2011 were estimated to be 0.9 [0.1 to 1.7] PgC yr^{-1} (Stocker *et al.*, 2013). However, most global estimates do not include emissions from peat fires or decomposition of drained peat systems, estimated at 0.1 to 0.23 PgC yr^{-1} (Hooijer *et al.*, 2010). Although land use is the second largest source of GHG emissions, the terrestrial environment is estimated to remove approximately one-third of the CO_2 released by fossil fuel combustion (Canadell *et al.*, 2007), slowing the rate of CO_2 accumulation in the atmosphere (Raupach *et al.*, 2008). Atmospheric radiative forcing (RF) is a quantification of the change in energy fluxes caused by changes in natural and anthropogenic substances and processes that alter the energy budget relative to 1750. The RF through anthropogenic forcing for 2011 was 2.29 W m^{-2}, of which emissions of CO_2 alone caused an RF of 1.68 W m^{-2} (Ciais *et al.,* 2013).

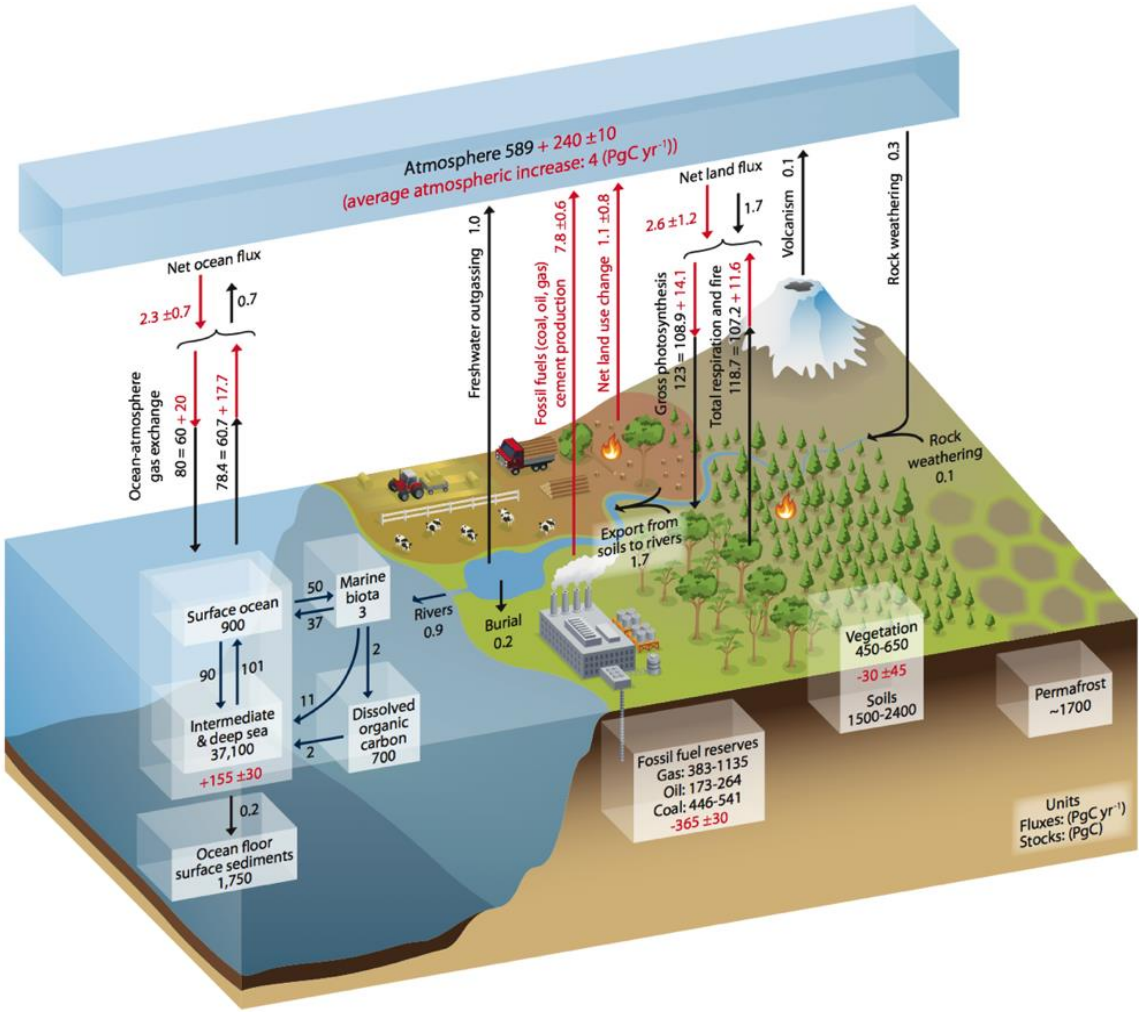

Figure 1.2 Simplified diagram of the C cycle, annotated with an estimation of the amount of C stored in each of the reservoirs. Numbers and arrows in black indicate reservoir mass and exchange fluxes estimated for the time prior to the industrial era (1750). The red numbers and arrows indicate anthropogenic fluxes averaged over a time period of 2002 – 2011 (Ciais *et al.*, 2013)

The net emission of C-related GHGs to the atmosphere is defined as the balance between the amount released to the atmosphere and the amount assimilated by C sinks in the biosphere[1] (Canadell *et al*., 2010). While increases in emissions have been seen globally, a decline in the efficiency of biospheric C sinks has been proposed as a potential explanation for the faster accumulation of GHGs in the atmosphere (Cox *et al.*, 2000, Canadell *et al.*, 2007, Raupach *et al.*, 2008, Le Quéré, 2010). If a decline in the biospheric sink is persistent, this could accelerate atmospheric CO_2 accumulation and climate warming (Canadell *et al.*, 2010). Additionally, vast C reservoirs in the terrestrial environment are vulnerable to destabilisation due to disturbances such as thawing of permafrost, releasing stored C (Schaefer *et al.*, 2014, Schuur *et al.*, 2015),

[1] A carbon sink is defined as an ecosystem in the biosphere (e.g. forest, ocean, peatland) with an ability to absorb carbon dioxide from the atmosphere

potentially resulting in increased C emissions from natural ecosystems (Nepstad *et al.*, 2008, Tarnocai *et al.*, 2009, Hooijer *et al.*, 2010). One possible mitigation strategy, at least in the short term, is through better management of known terrestrial C sinks. Managing ecosystems for GHG sequestration or biomass production could enhance C capture or prevent C loss from large reservoirs such as peatlands or forests (Obersteiner *et al.*, 2010). For example, Lal (2004) suggested that restorative land use and management practices on agricultural soils could reduce the enrichment of atmospheric CO_2, whilst improving food security, water quality and the environment. It is estimated that the increase in soil C sequestration through the adoption of these practices could globally result in an increase in soil C sequestration by 0.9 ± 0.3 Pg C/yr, offsetting approximately 1/4 to 1/3 of the annual increase in atmospheric CO_2 estimated at between 3 and 3.3 Pg C/yr (Lal, 2004, Stocker *et al.*, 2013).

Uncertainties associated with observations and models are large and there is an urgent need to reduce these uncertainties through better monitoring of CO_2 sources and sinks (Le Quéré, 2010). An improved knowledge of the dynamics of terrestrial C sinks and sources is essential for: i) not only predicting future climate, but understanding how ecosystems may react to different climate scenarios (Cao and Woodward, 1998); ii) identifying pathways in which GHG emissions from ecosystems can be stabilised (House *et al.*, 2010); and iii) helping to design future climate change mitigation policies (Canadell *et al.*, 2010).

1.3 Peatlands

Peat is defined as an accumulation of material, consisting of at least 30% dead organic material (Belyea and Clymo, 2001, Joosten and Clarke, 2002, Holden *et al.*, 2004), with a deposit depth of at least 30cm, depending on which country's definition is accepted (Gorham, 1991). In Scotland the minimum depth is 50 cm (Bruneau and Johnson, 2014). Peat begins to accumulate when the surface organic matter input (typically *Sphagnum spp*.) is greater than the decomposition rate with the saturated state helping to keep the decomposition rate low. Due to this need for saturated conditions, peatlands are most commonly formed in areas of positive water balance (i.e. precipitation greater than export - Gorham, 1991) such as upland areas of temperate and boreal zones (Billett *et al.*, 2010) or lowland areas where natural barriers such as shallow gradients or underlying impermeable substrates maintain saturation. Peatlands are also known to form in warmer climates with high precipitation inputs such as the tropics. Tropical peatlands account for around one fifth of the global peatland area (4 million km^2) (Holden, 2005). Peatlands are primarily found at northern latitudes with significant deposits in northern Europe, Canada, and USA (Limpens *et al.*, 2008).

There are two common types of peatland; minerotrophic and ombrotrophic. These peatlands differ in their source of water and nutrient inputs. An ombrotrophic peatland (From the greek ombros, rain, and trephein, to feed - Fritz *et al.*, 2014) only receives water and nutrients from precipitation, whilst minerotrophic peatlands can derive water and nutrients from both precipitation and groundwater (Shotyk, 1996, Holden, 2005). Ombrotrophic peatlands tend to be acidic (pH < 4) (Shotyk, 1996) with low concentrations of calcium and magnesium, while minerotrophic peatlands tend to be less acidic (Holden, 2005). Peat is characterised by its high carbon content; peaty soil typically has a C content on the order of 25 – 30%, while peat typically has a C content greater than 50% (Bruneau and Johnson, 2014). Blanket bogs are ombrotrophic and so called due to the peat appearing to create a blanket over the landscape with varying peat depth. Blanket bogs are found all over the world although they are more commonly found in the northern Hemisphere (Botch *et al.*, 1995, Joosten, 2010).

1.3.1 Peatlands as a C-store

Peatlands only cover ~3% of the global land surface (Gorham, 1991), but northern peatlands alone are estimated to hold around 500 ± 100 Pg C (Yu, 2012), which equates to around a third of the world's total soil C pool (approximately 1500 Pg C Scharlemann *et al.*, 2014). C is accumulated in peatlands due to an imbalance caused by a net excess of primary production over microbial decomposition. The net uptake of C can sometimes be offset by the release of methane (CH_4), which in terms of global warming potential is a more potent greenhouse gas with a 25 times greater warming potential than CO_2 over a 100-year timescale (Ciais *et al.*, 2013, Artz *et al.*, 2014). It is recognised that over longer timescales, such as centuries, peatlands globally have a cooling effect as the net uptake of long-lived atmospheric CO_2 outweighs the release of the relatively short-lived CH_4 (Frolking *et al.*, 2006). Therefore peatlands around the world play a key role in the modulation of regional and global climate (Frolking and Roulet, 2007). The net accumulation of peat and long-term stability of C storage is driven by saturated conditions which give rise to anaerobic conditions within the soil and thus slow decomposition rates (Bain *et al.*, 2011, Parry *et al.*, 2014).

1.3.2 Peatlands in the UK

In the UK, peatlands are estimated to cover ~25000 km^2, which equates to around 15% of the total land area, with peatlands in Scotland accounting for 17000 km^2 (Billett *et al.*, 2010). The Flow Country of Caithness and Sutherland is the largest area of contiguous blanket bog in the UK covering an area in excess of 4000 km^2 (Lindsay *et al.*, 1988). In the UK, extensive areas of peat are thought to have begun forming during the last 10,000 years (McMillan and Powell, 1999) with accumulation rates fluctuating on an annual basis as a result of changing

environmental conditions related to temperature and precipitation (JNCC, 2011) . UK peatlands are estimated to store 2302 Mt C (2.3Pg C) (Billett *et al.*, 2010) with Scottish peats contributing 1620 ± 70 Mt C (1.6 Pg C) to this total figure (Chapman *et al.*, 2009). Gorham (1991) estimated northern Hemisphere peatland carbon stocks to be 455 Pg C (1 Pg = 1 Gt), which equates to around one third of the total global soil carbon pool (1395 Pg C). A more recent study by Yu (2012) estimated northern peatland C stocks at around 500 ± 100 Gt C. Net exchange from northern peatlands is thought to be on the order of -23 g C m^{-2} yr^{-1}(Gorham, 1991), and although this is an old figure, it has been more recently re-affirmed by studies in Sweden and Canada where figures of -24 ± 4.9 g C m^{-2} yr^{-1} (Nilsson *et al.*, 2008) and -21.5 ± 39 g C m^{-2} yr^{-1} (Roulet *et al.*, 2007) were presented. Clymo *et al.* (1995) broadly agreed with the figure of -23 g C m^{-2} yr^{-1} with values of between -32.5 g C m^{-2} yr^{-1} and -13 g C m^{-2} yr^{-1} reported. It was believed that the variation in these values was due to changes in topography of the peat surface. Due to the maritime climate in the UK, there are some suggestions that net exchange rates for peatlands in the UK may be higher, with figures of -40 to -70 g C m^{-2} yr^{-1} (Cannell, 1993) presented.

1.3.3 Peatland Disturbance

Britain is one of the most extensively drained countries in Europe (Baldock, 1984), with more than half of UK agricultural activity occurring on drained land (Newson, 1992 in Holden et al., 2004). The post war "feed Britain" campaign resulted in government grants for the expansion of drainage works paid at 70% (Holden *et al.*, 2004). It is estimated that in total approximately 15,000 km^2 of UK blanket peatlands have been drained since the 1930s (Holden *et al.*, 2004) with the bulk of this occurring in the 1970s when the peak rate of peatland drainage was on the order of 1000 km^2 yr^{-1} (Green, 1973, Robinson and Armstrong, 1988),

Approximately 150,000 km^2 of northern peatlands and wetlands have been drained for plantation forestry predominantly in northern and eastern Europe since the 1800s (Paavilainen, 1995, Joosten and Clarke, 2002). A quarter of forestry plantations in Finland are situated on drained peatlands, equating to around 57,000 km^2 of peatlands having been drained. In Britain, around 1900 km^2 of deep peats and 3450 km^2 of shallow peats have been drained and planted with coniferous plantations, predominantly Sitka spruce (Cannell, 1993). Changes in land cover type can have a profound effect on the soil microclimate, especially where changes in the canopy or bulk density of the soil have occurred. Previous studies have shown that humid environments are more vulnerable to changes to land cover than drier regions, as the impact of precipitation is greater (Lugo and Brown, 1992, Don *et al.*, 2011). These changes can enhance C emissions to the atmosphere by increasing the area of peat under aerobic conditions and enhance microbial activity.

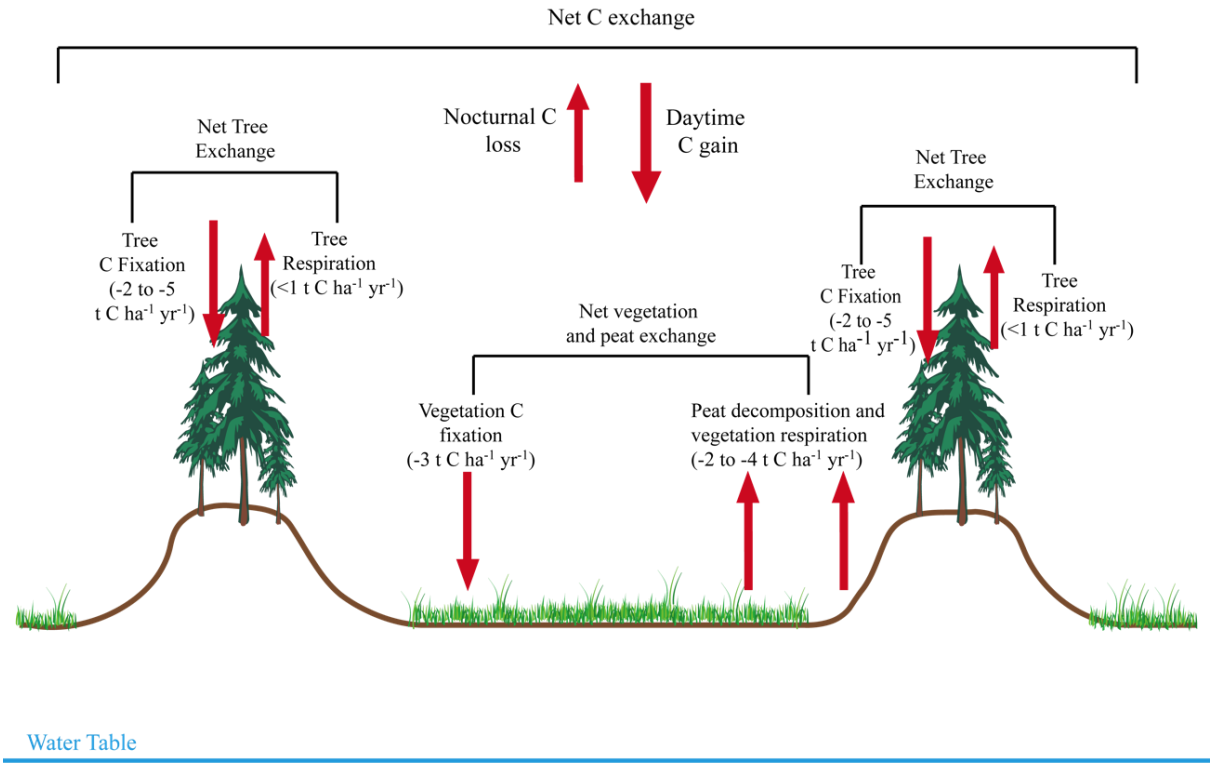

Figure 1.3 Schematic representation of the C cycling within an afforested peatland based on work by Hargreaves *et al.* (2003). Negative values indicate movement from the atmosphere to land surface and positive values indicate movement from the land surface to the atmosphere.

Peatland disturbance, either through drainage or cutting, reduces short- and long-term C sequestration potential by reducing C uptake through photosynthesis, enhancing soil C mineralisation and increasing the aqueous loss of dissolved and particulate C (Strack and Waddington, 2007, Limpens *et al.*, 2008). Peatland drainage increases the area of soil under aerobic conditions making conditions more suitable for the aerobic decomposition of the underlying peat, which had previously been protected from microbial decomposition by the unfavourable redox conditions. The result of this is the release of C through aqueous and gaseous pathways, which begins to exceed the gain of C from photo-assimilation (Armentano and Menges, 1986, Glenn *et al.*, 1993, Waddington *et al.*, 2002). Little is known about the effect of forestry conversion on biogeochemical processes (Fowler, 1995, Hargreaves *et al.*, 2003) and even less is known about the reversal of this conversion.

1.3.4 Peatland Afforestation

Figure 1.3 shows a characteristic afforested peatland and the C cycling expected to occur within it. In order to establish and successfully grow trees on peatlands it is essential for the water table to be lowered (Anderson *et al.*, 2000). On a peatland this is achieved through ploughing of the peat, creating closely spaced, narrow (*ca.* 50cm) plough furrows, within a few metres of each

other (Figure 1.4B). The peat that is lifted during the ploughing process, to create the furrow, forms two new structures either side of the furrow, which are referred to as ridges, typically around at least 50 cm in height immediately after ploughing, however, slumping and oxidation results in these reducing in height. These – the driest locations after ploughing – are where the trees are planted. Depending on how widely spaced the furrows are ploughed, the original bog surface may still be visible. In addition to this, deeper, wider drainage ditches are ploughed at intervals of hundreds of metres (Anderson *et al.*, 2000) to gather water from many smaller ditches and furrows. These lower the water table (Figure 1.4), increasing the area of peat under aerobic conditions, leading to decomposition and erosion of the peatland. This can also result in downstream flooding as the peatland is no longer able to hold as much water as it can drain away more freely than prior to drainage (Holden *et al.*, 2004).

Ombrotrophic peatlands are generally known to be nutrient poor, as they only receive atmospheric inputs such as precipitation or atmospheric deposition (Holden, 2005). Therefore, trees are typically treated with fertilisers after planting, to help them establish. Anderson *et al.* (2000) found that trees not fertilised with phosphorus and potassium at planting, expressed poor growth and required fertiliser inputs within a few years of planting to ensure the trees' survival.

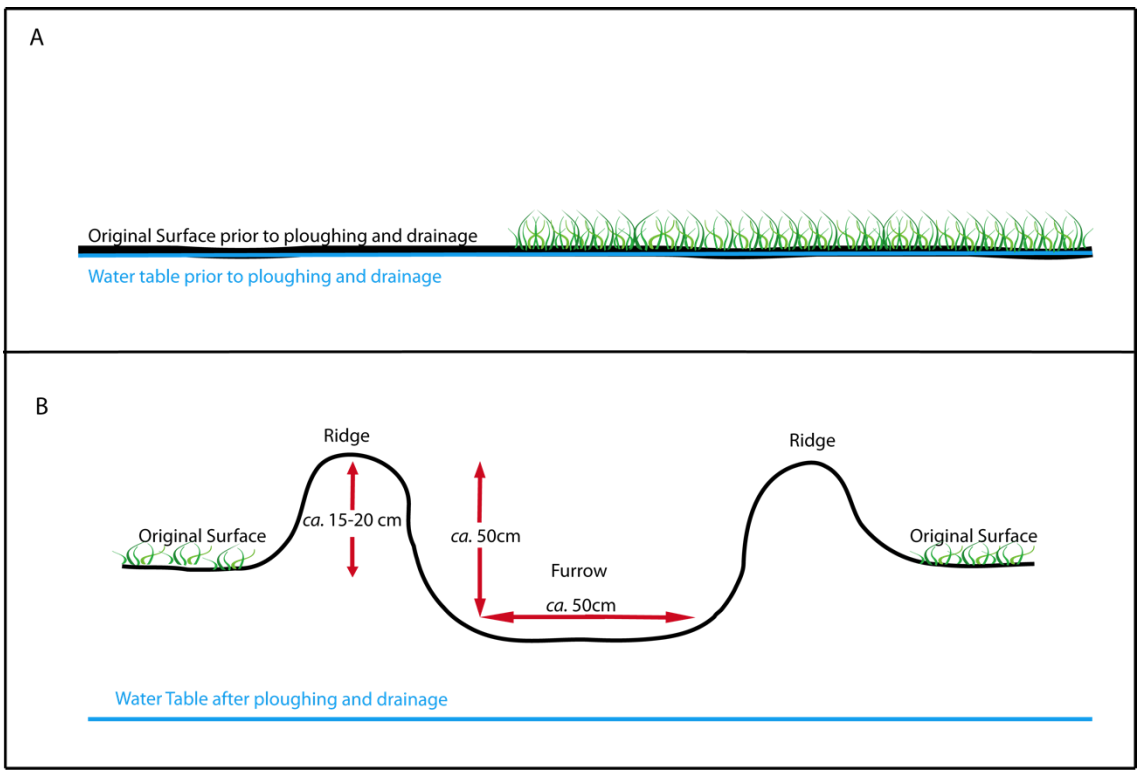

Figure 1.4 Diagrammatic representation of the typical micro topographic structures found on an afforested peatland. Panel A indicates a peatland prior to ploughing and panel B indicates a typical ploughed peatland structure, with approximated measurements of each structure. Heights and widths will vary depending on who carried out the ploughing, the type of plough used, and the soil thickness.

In addition to the physical changes to the peatland, the eventual establishment of a closed canopy forest leads to decreased light levels, increased transpiration, and interception rates (Parry *et al.*, 2014). This combined with the use of furrows and drainage ditches, can considerably alter peatland conditions both within the forested area and the intact blanket bog surrounding the forest. When the peat is drained and trees planted it is expected that the peatland becomes a net source of C to the atmosphere as the peat begins to oxidise leading to erosion and loss of C to the atmosphere and aqueous pathways.

The fixation of C in vegetation will also be greatly reduced due to the disturbance caused by the ploughing of the peat, and although this will also reduce heterotrophic respiration, it will be far outweighed by the peat decomposition C loss. As trees become established, C losses to the atmosphere will be reduced due to the increased atmospheric C fixation by the trees. Hargreaves *et al.* (2003) suggested that it takes approximately 4 – 8 years to return to net C uptake after planting on drained peat at which point the trees are expected to become a greater C sink than the peatland would have been if left undisturbed. However, although the trees may, over short time scales (i.e. decades), be greater C sinks than peatlands, they will not be able to exceed the peatland C stock. It is therefore hypothesised that over multi-decadal to century timescales it is beneficial to restore these afforested sites to peatlands in order to increase long-term C storage as a means of helping to mitigate climate change (Cannell, 1993).

1.3.5 Peatland restoration

Peatland restoration commonly occurs in two stages. Firstly, the water table must be returned to the surface of the peat to reduce the amount of peat under aerobic conditions. Increasing the water table stops the oxygenation of the peat. Secondly, the re-colonisation of peat-forming vegetation cover must be re-established. *Sphagnum* mosses are known to be key species for the growth of a peatland (Mitchell *et al.*, 2002). As *Sphagnum* are poikilohydric, meaning their survival is dependent on water content, re-established high water tables must be maintained and stabilised in order for the *Sphagnum* to re-grow and survive.

The first step in forest-to-bog restoration is to remove the trees from the site before blocking ditches to try to restore the water table to previously high levels. This is achieved through damming, which reduces water loss from the peatland, eventually resulting in a raising of the water table. Peat is the most commonly used damming technique in the UK as it can be carried out inexpensively and with no extra materials required to be brought onto the site (Armstrong *et al.*, 2009). However, this is not always possible either due to the width or depth of the drainage ditch or through peat not being readily available to block the ditch. In this case, other methods such as pile dams, and heather bales are used (Parry *et al.*, 2014). Dams are typically

constructed at regular intervals along the drainage channel or furrow. In order for the dam to be successful the drain blocking techniques must be adapted to the topographical features of the site. Once damming has occurred the *Sphagnum* mosses, will begin to regrow, provided the water table stays high. In North America restored peatlands are typically re-colonised with *Sphagnum*, whilst in the UK natural regeneration is typically favoured due to the high cost of trans-locating *Sphagnum* and the large areas of land involved (Quinty and Rochefort, 2003, Rochefort *et al.*, 2003). Although this is dependent on the land use prior to restoration with harvested peatlands typically showing little natural *Sphagnum* regeneration (Rochefort *et al.*, 2003).

Little or no empirical data exist on eddy covariance derived GHG fluxes from forest-to-bog restoration and thus it is not known whether it is possible to return an afforested peatland to an active C assimilating ecosystem as conditions, such as climate, peat depth and peatland geometry will have all changed since the original onset of peat formation (Price *et al.*, 2003). It is most likely that any form of peatland restoration will result in the formation of a new type of wetland with hydrologic and biogeochemical dynamics that are similar, but not identical, to undisturbed peatlands. Research undertaken on the restoration of drained peatlands has not been able to clarify how closely the hydrologic and biogeochemical behaviour of the newly restored ecosystem mimics that of the unmanaged environment (Hendriks *et al.*, 2007, Hatala *et al.*, 2012, Herbst *et al.*, 2013).

1.4 Uncertainties in scientific knowledge of managed peatlands

Peatland management and restoration needs to be undertaken in the context of anthropogenic climate change (Friedlingstein and Solomon, 2005). Peatlands are one of the largest terrestrial C sinks, with larger carbon storage densities per unit ecosystem area than other terrestrial system (Freeman *et al.*, 2012), but major uncertainty surrounds the resilience of the C sink under future climatic change (Sottocornola and Kiely, 2010). One of the largest uncertainties in climatic predictions remains the spatial and temporal changes in terrestrial C sinks including managed or restored peatlands (Cox *et al.*, 2000, Canadell *et al.*, 2010).

The response of peatlands to climatic change, in terms of net ecosystem exchange (NEE) of C, is likely to focus upon whether gross primary productivity (GPP) and ecosystem respiration (R_{eco}) are both affected equally or differently under different climatic conditions (Cai *et al.*, 2010). The peatland C balance is largely controlled by the interactions between hydrological and biogeochemical processes (Ise *et al.*, 2008). In simulations using a coupled-biogeochemical model, Ise *et al.* (2008) found that feedbacks between the water table and peat depth could increase the sensitivity of decomposition to temperature, intensifying the loss of carbon. Long-

term simulations suggest that a 4°C increase in temperature could result in the loss of 40% of organic carbon from shallow peat and 86% of organic carbon from deep peat (Ise *et al.*, 2008). Coupled with increased temperature, changing precipitation patterns are likely to result in a negative response to the peatland water balance, accelerating CO_2 losses (Cai *et al.*, 2010). Enriched atmospheric CO_2 concentrations, increasing CO_2 fertilisation could lead to an intensification of the below ground allocation of labile carbon by roots enhancing microbial activity and decomposition of "old" carbon previously believed to be stable (Heimann and Reichstein, 2008). Conversely, higher temperatures and extended growing seasons could aid ecosystem productivity (Heimann and Reichstein, 2008). Previous research undertaken during significant dry periods supports the modelled evidence with elevated CO_2 losses due to a reduction in the water table and increased temperatures (Alm, 1999, Bubier *et al.*, 2003a, Aurela *et al.*, 2009, Strack and Zuback, 2013).

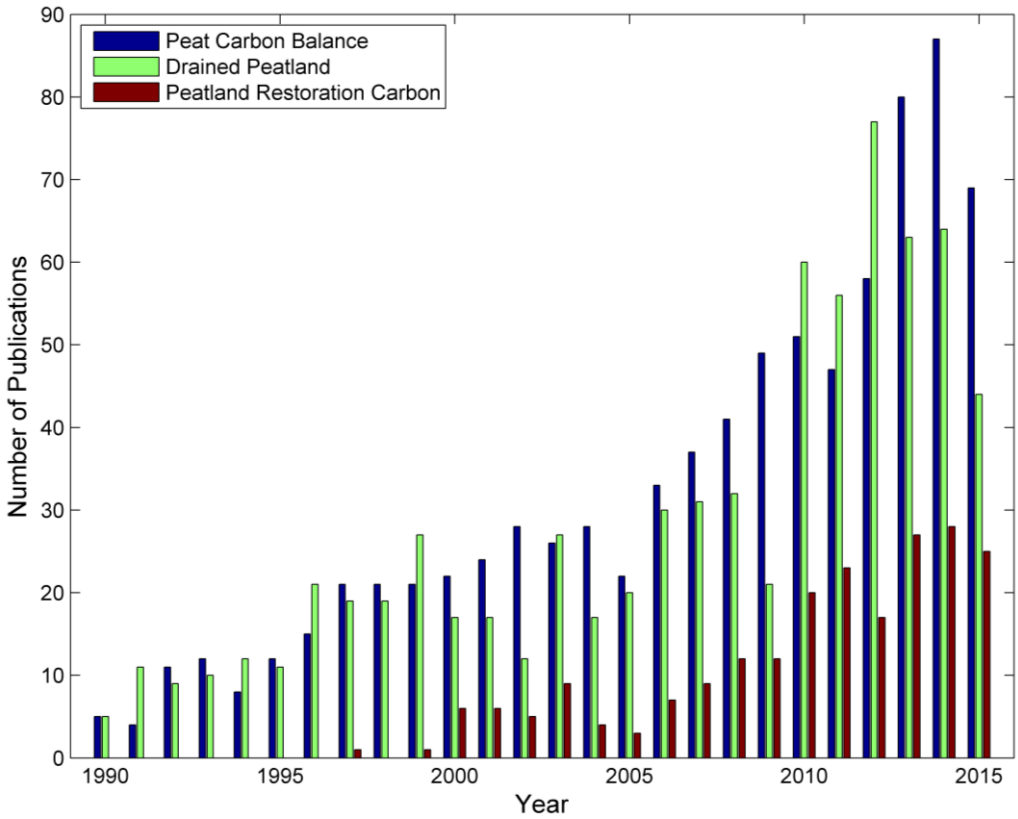

Figure 1.5 Number of publications per year between 1990 and October 2015 with the words Peat Carbon Balance, Drain Peatland and Peatland Restoration Carbon as key words from the Web of Science [Accessed 6th October 2015].

Despite a rapid increase in peatland carbon research over the last 15-20 years (Figure 1.5), there remains a lack of knowledge and understanding of the effects of restoration on C dynamics. It is currently unknown what impact management techniques such as drain blocking and tree removal have on C cycling in these ecosystems. The drainage of the peat is likely to have

physically altered the peat by changing the biogeochemical composition of the peat by reducing the C content of the peat through decomposition. It is unknown what effect this will likely have upon long-term C turnover due to the altered C:N ratio within the soil, and the impact on individual flux terms (GPP and R_{eco}) (Billett *et al.*, 2010). Long-term monitoring of these sites is required to better understand the impacts of management on the carbon balance and the individual flux terms. However, although there are several comprehensive studies of the status of peatland C sinks in North America and Fennoscandia, a lack of long-term direct measurements in the UK presents difficulties in assessing the sink status of UK peatlands. This casts doubt upon models of Northern Hemisphere peatlands (Billett *et al.*, 2010, Levy and Gray, 2015). Furthermore, the majority of research undertaken in restored peatlands has focussed on growing season fluxes over small areas using static chamber techniques (Komulainen *et al.*, 1998, Waddington and Warner, 2001, Kivimaki *et al.*, 2008). Eddy covariance, which measures at the larger ecosystem scale, is rarely used on peatland restoration sites due to the typically limited size of the sites (Waddington and Warner, 2001).

The impact of ploughing and the creation of distinct microtopographic features in blanket bogs on the C cycle is another major uncertainty. These microtopographic features provide another drainage pathway, and allow a greater surface area of peat to be opened up to aerobic conditions, speeding up the decomposition and erosion process of these sites. As the carbon balance of blanket bogs is tightly controlled by hydrological and biogeochemical processes (Ise *et al.*, 2008, Erwin, 2009) it is likely that these microtopographic features will have an effect upon the carbon balance and change the relative influence of the individual flux terms.

Understanding how C dynamics change with time since restoration and under different climatic conditions will provide an understanding of how these ecosystems are likely to react to future climatic change. Current predictions suggest that the UK will become warmer and wetter (Prudhomme and Davies, 2009). For northern Scotland, temperatures are predicted to increase by approximately 2 – 3 ºC with larger increases in summer than winter. Precipitation is expected to increase with a 10% rise, although summers are predicted to become drier (Stocker *et al.*, 2013).

1.5 Aims and research questions

This research forms part of a wider collaborative effort to understand the carbon dynamics of the restored, forested and intact blanket bogs of the Flow Country. This thesis focuses upon landscape scale measurements of NEE. Fluxes of CH_4 were not obtained as part of the data collection for this thesis, but are currently being researched by colleagues at the University of

Stirling, the James Hutton Institute, the University of Highlands and Islands, and the Centre for Ecology and Hydrology (CEH).

The aim of this thesis is to improve our current understanding of the land/atmosphere exchange of CO_2 at restored and unmanaged blanket bogs in the Flow Country of Northern Scotland. Investigating the individual flux terms, ecosystem respiration (R_{eco}) and gross primary productivity (GPP), providing an understanding of how restoration affects these fluxes.

Eddy covariance (EC) measurements are reported for two restored sites of differing ages at the Forsinard Flows National Nature Reserve in Northern Scotland during 2014 and 2015. In addition EC measurements were also undertaken over an area of unmanaged blanket bog on the same reserve during 2014.

This research represents the first measurements of land/atmosphere CO_2 exchange across two restored areas and one unmanaged area of blanket bog on one of the largest areas of contiguous blanket bog in Europe. The thesis aims to address the following questions:

1. How do fluxes of R_{eco} and GPP change with time since restoration and what are the key environmental drivers?

2. What effect do microtopographic features created by the ploughing of the peat for plantation forestry have on NEE and what are the key environmental drivers?

3. What impact does the restoration of blanket bogs from plantation forestry have on the net ecosystem exchange of CO_2?

This research aims to provide an understanding of how restoration affects the land/atmosphere exchange of NEE, whilst helping to provide an understanding of the factors influencing NEE and how this may be affected in the future under climatic change.

1.6 Thesis Structure

This thesis structure is detailed in table 1.1, with Chapter 2 providing a description of each of the sites. Chapter 3 provides a discussion of the EC theory, along with the processing and post-processing methods employed to turn the raw data into the final fluxes used throughout this thesis. Chapter 4 and 5 discuss respiration and assimilation and the environmental factors driving each of the fluxes. Chapter 6 discusses the role of microtopographic features on fluxes at restored sites before Chapter 7 brings all of these aspects together to discuss annual C budgets

and whether significant differences exist between restored sites. The results are discussed in the context of other northern peatlands.

Table 1.1 Structure of the thesis

Chapter Number	Title
2	Site Descriptions
3	Methods
4	Ecosystem respiration dynamics in restored Flow Country peatlands
5	Gross primary productivity dynamics in restored Flow Country peatlands
6	Microtopographic influences on CO_2 exchange in restored Flow Country peatlands
7	Net ecosystem exchange of restored peatlands in the Flow Country of Northern Scotland
8	Conclusions and Future Work
Appendix A	Gas analyser calibration co-efficients
Appendix B	EdiRe processing list
Appendix C	Eddy covariance – Description of important terms

~ Chapter 2 ~

Site Descriptions

2.1 The Flow Country

The Flow Country[2] is situated in Caithness and Sutherland, Northern Scotland (Figure 2.1) and is the largest expanse of contiguous blanket bog in the UK, encompassing an area in excess of 4000 km^2 (400,000 ha) of the UK's 15,000 km^2 (1,500,000 ha) of blanket bog (Lindsay *et al.*, 1988, Charman, 1995, Billett *et al.*, 2010). The Flow Country accounts for around 5% of the total global resource of blanket bog (Lindsay *et al.*, 1988).

Figure 2.1 Outline map of Scotland, with the approximate location of the Forsinard Flows National Nature Reserve highlighted by the red arrow.

[2] The Flow Country was so named due to the huge expanse of level bog land and flow being a colloquial term for an area of flat, deep, wet bog (Lindsay *et al.*, 1988).

Radiocarbon dating of peat deposits in the Flow Country indicates that it began forming soon after the last ice age, approximately 10,000 years ago (Lindsay *et al.*, 1988, Gilbert, 2007). The Flow Country is the single largest peat and soil C repository in the UK and thus plays a key role in mediating regional atmospheric exchanges of greenhouse gases such as carbon dioxide (CO_2), methane (CH_4) and water vapour (H_2O) (Gallagher *et al.*, 1994, Fowler, 1995). The combination of the underlying geology, topography and climate provides the Flow Country with ideal conditions for the formation and continued growth of blanket bog.

2.1.1. Underlying Geology

The Flow Country blanket bog spreads over the Old Red Sandstone of Caithness, the large granitic intrusion along the Caithness-Sutherland boundary, whilst Moine granulites and schists dominate the remaining areas of the Flow Country (Lindsay *et al.*, 1988) (Figure 2.2A). The Moine Supergroup covers the majority of the northern Scottish highlands and are a thick succession of metamorphosed sedimentary rocks, such as psammites and pelites (Trewin, 2003). Rocks of the Moine series are characteristically hard, highly weather resistant, generally non-calcareous and acidic, giving rise to largely infertile soils un-conducive to agriculture and timber production(Lindsay *et al.*, 1988). The bedrock is overlain by glacial till and alluvium, formed during deglaciation.

During the last age (2.4 million years ago), Scotland witnessed several cold, glacial periods interspersed by shorter, warmer, interglacial periods, approximately every 100,000 years; the last major glaciation peak occurred around 22,000 years ago (Auton *et al.*, 2011). Approximately 11,500 years ago, the cool, wet climate that we see today was established as the Gulf Stream dominated. As the ice retreated, sheets of till were deposited and over time thin stony soils developed on the sediments, which became colonised by herbaceous plants and shrubs such as heather, dwarf birch and juniper (Auton *et al.*, 2011). This glacial material can act as a considerable groundwater store, whilst glacial clay materials are likely to create impermeable layers that impede flow through to groundwater. The cool, wet climate led to the formation of peat mosses between 10,000 and 6,000 years ago (Belyea and Baird, 2006). The mixed superficial geology of clay, sands and gravels, coupled with a cool, wet climate, gentle topography and acidic substrates led to the development of ombrotrophic peat bogs (Figure 2.2B) (Lindsay *et al.*, 1988)

A

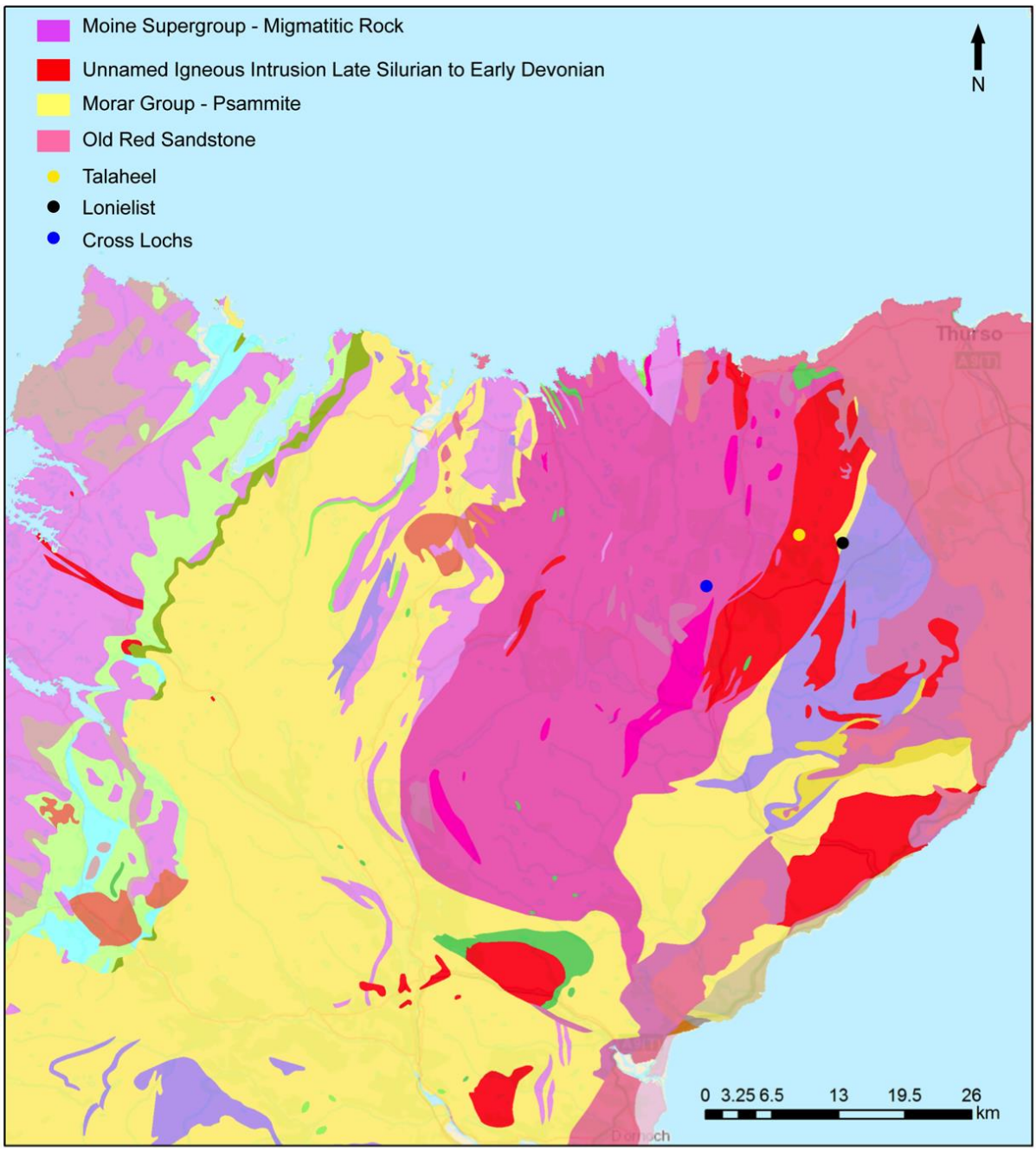

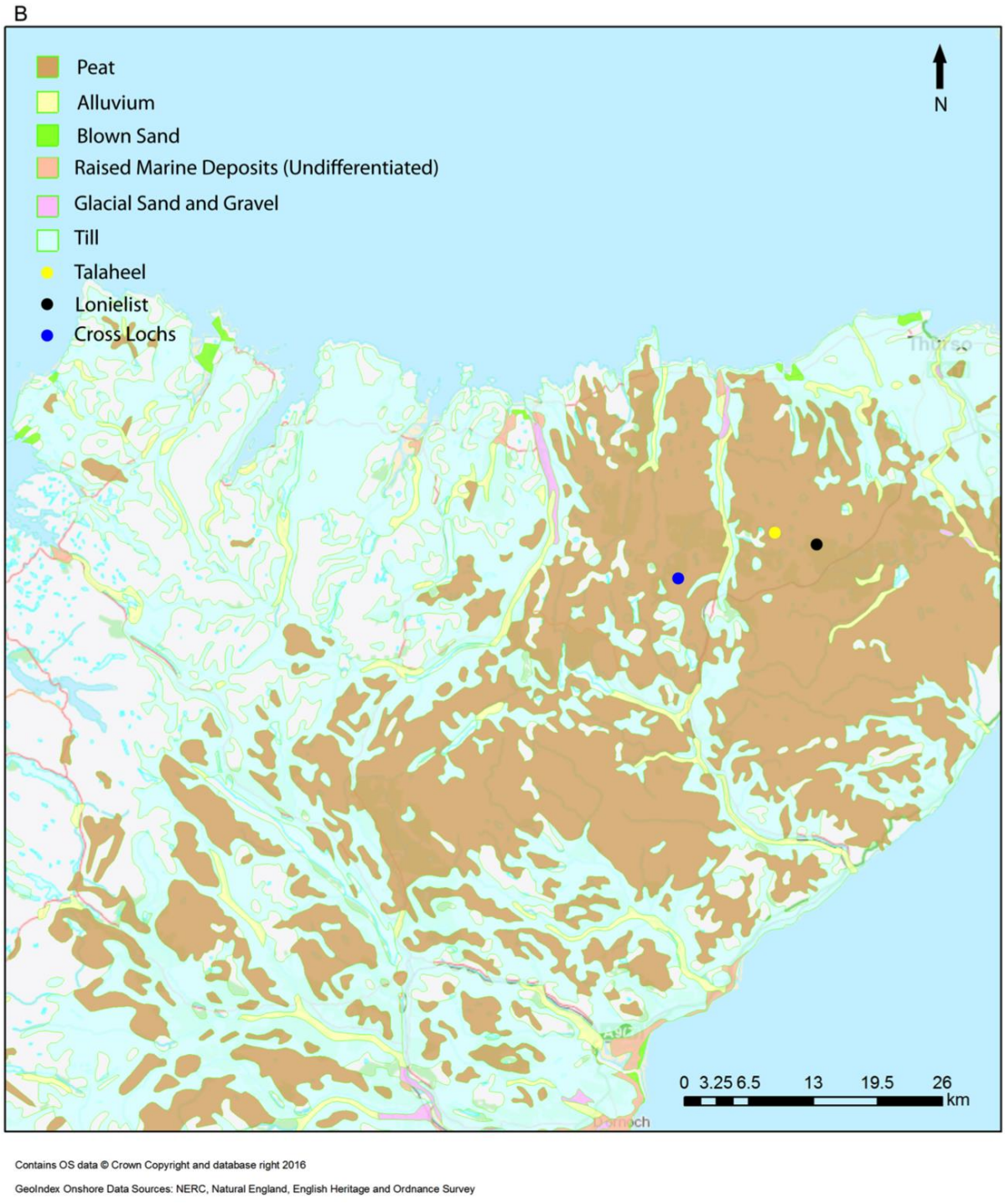

Figure 2.2 Geology of Caithness and Sutherland. A) Bedrock geology of the area, with the three sites used in this study highlighted. B) Superficial Geology, with the three sites used in this study highlighted.

2.1.2 Climate

The climate of the Flow Country is generally cool and wet, with mean annual precipitation between 1981 – 2010 of 970.5 mm and a mean annual temperature of 11.4°C recorded at the Kinbrace weather station (Location: NC 87530 28742; Altitude: 103 m amsl) (Met Office, 2015). Over the same time period, the mean UK annual maximum temperature was 12.4°C and precipitation was 1154 mm, but the Kinbrace weather station recorded a greater annual number of days with rainfall >= 1 mm at 179.4 compared with 156.2 for the whole of the UK (Met Office, 2015). The cool, wet climate provides ideal conditions for the formation of ombrotrophic peat due to the high precipitation input and low evaporation rates. A marked rain shadow effect is prevalent in the Flow Country, with the most westerly areas of Sutherland receiving high amounts of rainfall (up to 2500 mm per year) before rapidly declining to around 1200 mm per year in central areas and falling to around 700 mm per year in the north-east of Caithness (Lindsay *et al.*, 1988).

Between March 2014 and March 2015, an independent weather station at Talaheel (Location: NC 95161 48728, Altitude 196 m - Section 2.3.2) recorded slightly above mean precipitation for the site, with a total of 1132.1 mm (Figure 2.3) and an average temperature of 8.2°C (Figure 2.3). The maximum and minimum daily air temperatures recorded during the period of study were 26.8°C in July 2014 and -8.1°C January 2015, respectively. The highest daily precipitation recorded was 51.8 mm in October 2014. The thermal growing season is defined as a period beginning at the first of five days with a mean daily temperature above 5°C and ending on the day preceding the first of five days with a mean daily temperature below 5°C (Barnett *et al.*, 2006). Here, the thermal growing season began on 4^{h} April 2014 and ended on 4th December 2014, a total of 245 days equating to a mean daily temperature of 10.1°C during the thermal growing season. In northern Scotland the mean thermal growing season is 250 days (Barnett *et al.*, 2006).

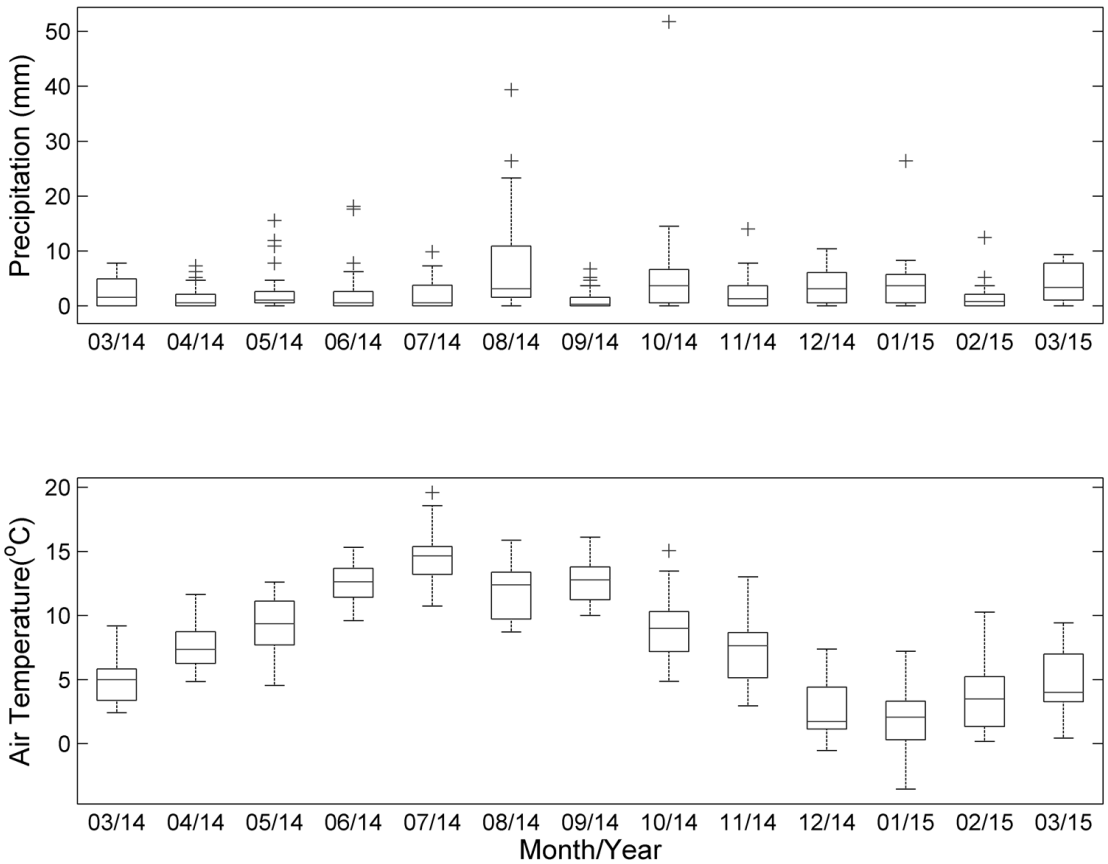

Figure 2.3 Top Panel: Daily precipitation levels in each month at Talaheel between March 2014 and August 2015. Bottom panel: Daily Air temperatures each month from the weather station deployed at Talaheel between March 2014 and March 2015. The central line represents the median, the box edges represent the 25th and 75th percentiles, the whiskers extend to the data points not considered to be outliers with outliers plotted individually.

The dominant wind direction in the UK is a southwesterly (Lapworth and McGregor, 2008) . However, annual dominant wind directions have been shown to vary over the British Isles, with a major cause of the variation being topography. High ground of Wales, northern England and Scotland has an effect on mean isobars, which turn clockwise over western coasts and anti-clockwise over the eastern half of the country (Lapworth and McGregor, 2008) .

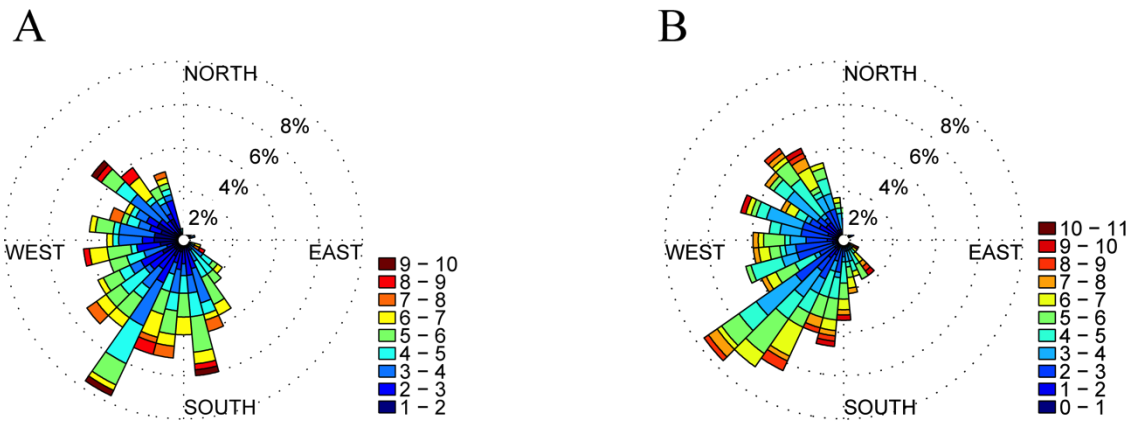

Figure 2.4 Daily average wind directions over the period of study. Wind directions are weighted by the average intensity of the wind (m/s) shown in the legend, A) Data obtained from the Lonielist (2.3.1) eddy covariance flux tower, measured using a Gill HS3-50 sonic anemometer (Gill Instruments, Lymington, UK). B) Data from CSAT3 Sonic Anemometer (Campbell Scientific, Shepshed, UK) on EC tower at Talaheel (2.3.2).

Over the course of the research, the dominant wind directions were from the northwest and southwest (Figure 2.4). The highest half-hourly mean wind speed was 31.3 m/s (~70mph) in January 2015, as a storm passed over the area from a northwesterly direction.

2.2 Land use & Ownership in the Flow Country

The Flow Country has historically thought to have been treeless (Lindsay *et al.*, 1988), however, this has been contested with palaeoenvironmental studies indicating the presence of birch species in the central part of the Flow Country in the early to mid-Holocene (Charman, 1995). However, although it is likely that birch-dominated woodlands would have existed in parts of the Flow Country in the past, particularly alongside water courses, large areas would have been open and as treeless as they are today (Lindsay *et al.*, 1988). Woodland has disappeared due to grazing by sheep and deer, as well as land management practices by man, such as burning. Land use maps from the 1930s (Figure 2.5) show there to be very little land use diversity in the Flow Country, with only a few small crofts and the majority of the land being classified as rough pasture. The largely infertile and inaccessible lands of the area, and of the Scottish highlands in general, make this area unattractive for large scale farming practices and industry, giving rise to a very low population density. The latest census shows the Highlands of Scotland to have a population density of just 9 people per km^2 (Scotland, 2013).

The large areas of blanket bog are used for sheep and cattle grazing by crofters and farmers, as well as grouse shooting and deer management, generating income for the big estates (Lindsay *et al.*, 1988, Warren, 2000). Fishing is a major tourist attraction in areas of the Flow Country with the Halladale and Helmsdale rivers both being major Atlantic salmon (*Salmo salar*) fishing

rivers, whilst the lochs are attractive for tourists looking to fish for brown trout (*Salmo trutta*). However, between the 1940s and 1980s forestry planting in the Flow Country has given rise to large-scale disturbance of the area and the loss of large areas of blanket bog (Figure 2.1).

2.2.1 Afforestation in the Flow Country

Due to the large expanse of saturated, inaccessible blanket bog with little, if any, natural tree cover the Flow Country was not an obvious choice for forestry plantations. However, since the 1940s, the UK government forest agency, Forestry Commission, and other private forestry companies had been planting on blanket bogs using a mixture of shallow and deep plough methods. Advances in ploughing technology combined with cheap land and favourable tax regimes in the 1970s and 1980s allowed, for the first time, the ploughing and planting of deeper and wetter blanket bog areas (Warren, 2000).

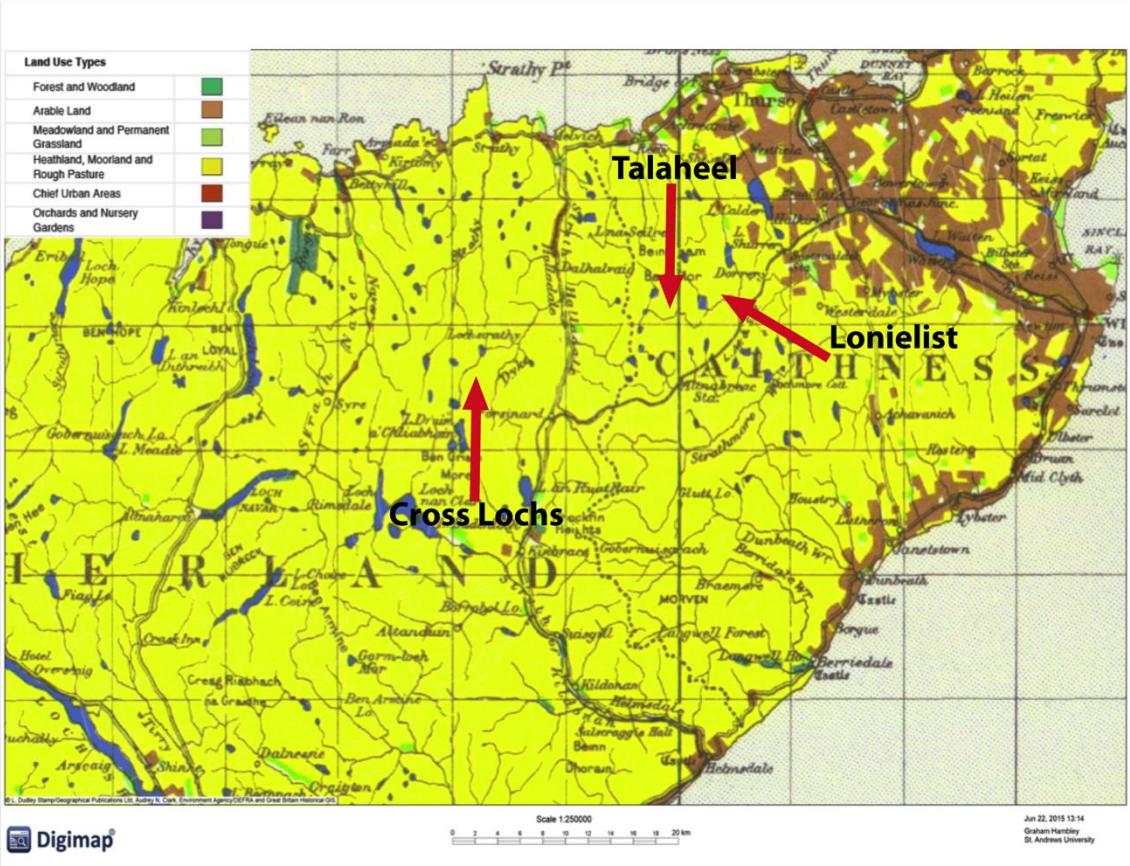

Figure 2.5 Land use in the Flow Country during 1930s. The majority of the land is mapped as heath, moorland and rough pasture. Arable land tends to be confined to the coastlines, except for an area to the far north east of Caithness. Locations of each of the study sites used in this study are marked. Image source: Digimap, 2015.

Tax regimes during the Thatcher government (1979 – 1990) to encourage increased timber production attracted rich investors to Scotland with 76% of private sector afforestation undertaken by non-local investors (Mather and Murray, 1988). In addition to the tax regimes

and corporate purchasing of the forestry, one of the private forestry companies - Fountain Forestry- envisaged a commercial opportunity for large-scale forestry plantations. They quickly became a major player in the afforestation of the Flow Country in the 1980s, purchasing approximately 40,000 ha of land in the Flow Country between 1980 and 1986 (Warren, 2000). The overall result of the tax regimes, advances in ploughing technology and silviculture, was that 67,000 ha of blanket bog (*ca.* 17% of the total blanket bog) were ploughed - creating two distinct microforms, ridge and furrow - and planted with non-native conifer species (Stroud *et al.*, 1987). Lodgepole pine (*Pinus contorta*) was typically used in these areas as a nurse crop for the more valuable Sitka spruce (*Picea sitchensis*) (Avery and Leslie, 1990). Recently, studies have shown that forestry plantations adjacent to intact blanket bogs are associated with a negative 'edge effect' on key bird species (Hancock *et al.*, 2009, Wilson *et al.*, 2014). Breeding numbers of golden plover (*Pluvialis apricaria*) and dunlin (*Calidris alpina*) are lower within a few hundred metres of forestry plantations than expected on the basis of bog habitat quality. This combined with the need for climate change mitigation strategies resulted in an even greater desire to remove large-scale forestry plantations on deep peat.

2.2.2 Deforestation and restoration to blanket bog

In the late 1980s, conservationists, including non-governmental organisations (NGOs) such as the RSPB, and the government nature conservation agency (Nature Conservancy Council) campaigned to stop the afforestation of deep peats. Much of the argument at this time centred around the wind throw risk of planting trees on waterlogged peat substrates where the trees had a very shallow root depth and were therefore susceptible to being blown over in gale force winds (Bainbridge *et al.*, 1987). Eventually, the government removed the tax incentives when the degree of ecological damage caused by tree planting on deep peat was realised. This was a highly controversial subject and eventually became known as the "birds, bogs and forestry" controversy (Warren, 2000) which was ended when the Secretary of State adjudged that the Flow Country should be divided in two halves for forestry and birds.

Although half of the Flow Country was designated for planting, the removal of tax incentives put an end to large scale silviculture (Warren, 2000). In 1980, the Forestry Commission took a decision to purchase no further land in this area due to the low returns - typically only around 1.25% (Bainbridge *et al.*, 1987). The cessation of large scale planting allowed nature conservation designations to be placed over much of the remaining undamaged blanket bog resulting in large parts of the Flow Country being named as part of the Caithness and Sutherland Special Areas of Conservation (SAC) and Special Protection Area (SPA) totalling 143,538 ha (1435.38 km^2) and 145,516 ha (1455.16 km^2), respectively (SNH, 2005) .

In the late 1990s, NGOs including the Royal society for the protection of birds (RSPB) and Scottish wildlife trust (SWT) began the process of restoring afforested areas. However, due to poor tree growth, high costs associated with the felling of trees on wet ground and the extreme remoteness of these locations from markets, it was not economically viable for the trees to be sold for timber. Therefore, felled trees were left to decompose on site, adding organic matter back into the peat. Initially, tree removal was done by chainsaw, but as technology developed, low ground pressure tracked vehicles came to the fore and allowed trees to be felled more easily and quickly. It was decided by peatland managers in the Flow Country not to block furrows rather only block the main collector drains using plastic pile dams. It was hoped that this would eventually allow the water table to rise sufficiently for the regrowth of *Sphagnum* mosses, which would naturally infill the furrows.

2.3 Site Selection

All the sites used in this research were situated within the RSPB Forsinard Flows National Nature Reserve (Figure 2.6 - 58°23'N, 3°49'W). Covering an area of 20000 ha (200 km^2), it is home to many endangered bird species, such as golden plover (*Pluvialis apricaria*), dunlin (*Calidris alpina*) and common greenshank (*Tringa nebularia*) (Hancock *et al.*, 2009, Wilson *et al.*, 2014). In order to collect data that was comparable between all sites (Table 2.1), it was essential that the restored sites were typical of the restoration age, had similar peat depths (>1m), were at similar altitudes (>150m & <250m) and had similar meteorological conditions. Additionally, sites needed to be large (hundreds of metres) and flat (< 3° slope) to satisfy the major assumptions of the eddy covariance (EC) method (Chapter 3). The main criteria for the undrained blanket bog site were that it was representative of blanket bogs in the area and was on a deep peat (i.e. >1m). The sites chosen were; Talaheel– restored in 1997/98 (red star in figure 2.5); Lonielist – restored in 2003/04 (yellow star in figure 2.5) and an area of undrained blanket bog (blue star in figure 2.5) referred to as Cross Lochs.

Table 2.1 Locations of each site, along with the altitude, year of restoration, mean carbon content, water table depth, soil moisture content, dominant vegetation type.

Site	**Lonielist**	**Talaheel**	**Cross Lochs**
Location	NC 96874 46076	NC 95161 48728	NC 85151 44251
Altitude (m)	180	196	210
Slope (°)	1 - 3	1 - 3	0 – 1
Restoration year	2003/04	1997/98	N/A
Mean carbon content (%/w ± SEM)	49.7 ± 0.28	50.0 ± 0.55	50.0 ± 0.43
Water table depth (m)	0.1 ± 0.02	0.11 ± 0.05	0.06 ± 0.06
Average volumetric soil moisture content at 10cm (m^3 m^{-3})	0.58 ± 0.04	0.71 ± 0.05	N/A
Peat depth range (mean) (m)	1.2 – 3.8 (2.2)	1.1 – 3.6 (2.03)	0.55 – 7 (2.19)
Dominant vegetation families	*Poaceae* *Mosses & Liverworts* *Sphagnaceae*	*Hypnaceae* *Sphagnaceae* *Cyperaceae*	*Sphagnaceae* *Ericaceae* *Cyperaceae*

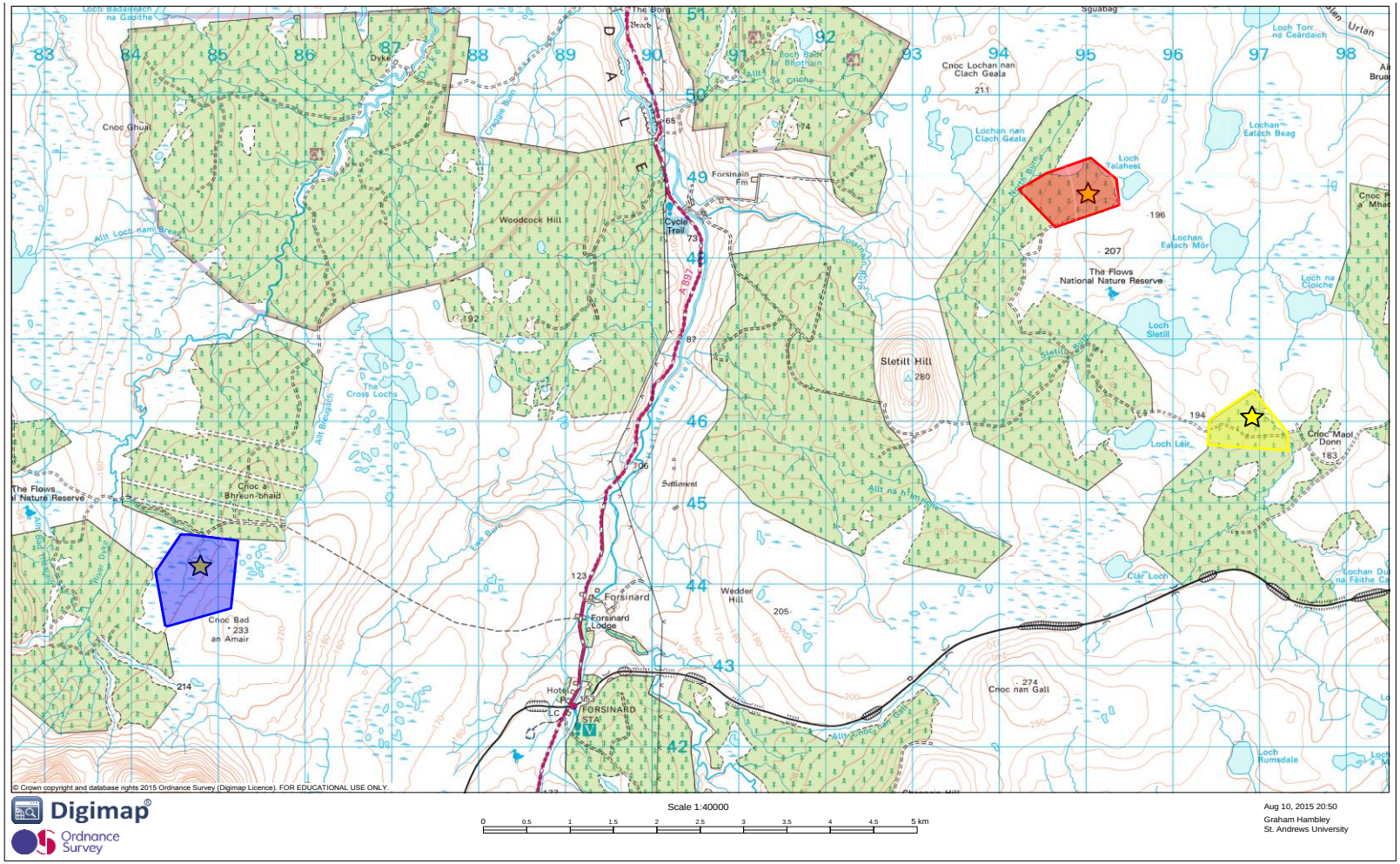

Figure 2.6 Map of the locations of the EC towers within the Forsinard Flows National Nature Reserve. The red polygon denotes Talaheel and the areal extent of the measurement site; the yellow polygon denotes Lonielist and the areal extent of the measurement site. The blue polygon represents Cross Lochs and the areal extent of the measurement site. Image Source: Digimap (2015).

2.3.1 Lonielist

Lonielist (Table 2.1) was restored in 2003/04 and was considered to be representative of a peatland at an intermediate stage of restoration. The site encompassed an area of approximately 200 ha (2 km^2). The site provided a large, flat area (Slope 1 - 3°) with a peat depth of around 2 m. Lonielist was planted in 1981 with a mix of Sitka spruce (*Picea sitchensis*) and lodgepole pine (*Pinus contorta*). Due to the poor growth of the trees, as previously mentioned (2.2.2), closed canopy status had only just been achieved prior to felling. Equipment at this site was provided and maintained by The James Hutton Institute, with agreements in place for access to CO_2 and environmental data for the purposes of this thesis.

2.3.1.1 Topography & Aspect

Three microforms were present at the site; furrow, ridge and original surface which had an east to west aspect. Furrow bases were around 0.3 m below the original peat surface and ridge peaks around 0.15 to 0.25 m above the original peat surface. Lonielist was a flat site with a slope of around 1-3°, which flattened to around 0-1° on the northern side of the site.

2.3.1.2 Vegetation Composition

Furrows were dominated by *Sphagnum spp* - mainly *Sphagnum cuspidatum* and *Sphagnum capillifolium*, which in some areas had begun to overgrow the woody debris. Lichens, liverworts and mosses, interspersed with *Trichophorum cespitosum*, *Hypnaceae* spp and small amounts of *Calluna vulgaris* dominated ridges. The original surface was dominated by *Trichophorum cespitosum*, *Molinia caereulea*, *Carex panicea*, *Eriophorum vaginatum*, *Eriophorum angustifolium*. The vegetation was generally quite short at Lonielist as a result of deer grazing. As can be seen in Figure 2.7, the levels of woody debris on site were greater than that of Talaheel (Figure 2.9), which reflects that the site was not as far through the restoration process as Talaheel, whilst trees were also slightly bigger and older at Lonielist prior to felling. It is also therefore likely that there was less pre-felling ground vegetation cover at this site compared to Talaheel. This site was affected by a heather beetle outbreak in 2010/11 (N. Russell, 2011 pers. comm. 27th April).

Figure 2.7 View to the southeast of Lonielist, showing the difference relative to Talaheel (Figure 2.9). Vegetation is short with small tussocks of *Eriophorum spp*., visible in the picture. Woody debris is clearly visible in each of the furrows and more abundant than Talaheel. Image Source: Author, September 2014.

2.3.2.3 Environmental Conditions

The water table depth (Figure 2.8A) at Lonielist was measured at much lower frequencies than that of Talaheel and Cross Lochs, due to the lack of an automated pressure transducer. However, five piezometers placed around the site were measured at least once a month, except in February 2015 where weather prevented access. The mean water table depth at Lonielist was 0.10 ± 0.02 m below the surface, which is similar to Talaheel. The lowest water table depth was recorded in October 2014 at depth of -0.28 m below the surface of the peat. In December 2014, a positive water table of 0.0037 m was recorded. Soil moisture content (Figure 2.8B) showed greater variation than Talaheel and a distinct seasonal signal, with the lowest value observed in the summer of 2014 (0.43 m^3 m^{-3}) and the highest value observed in November 2014 (0.68 m^3 m^{-3}).

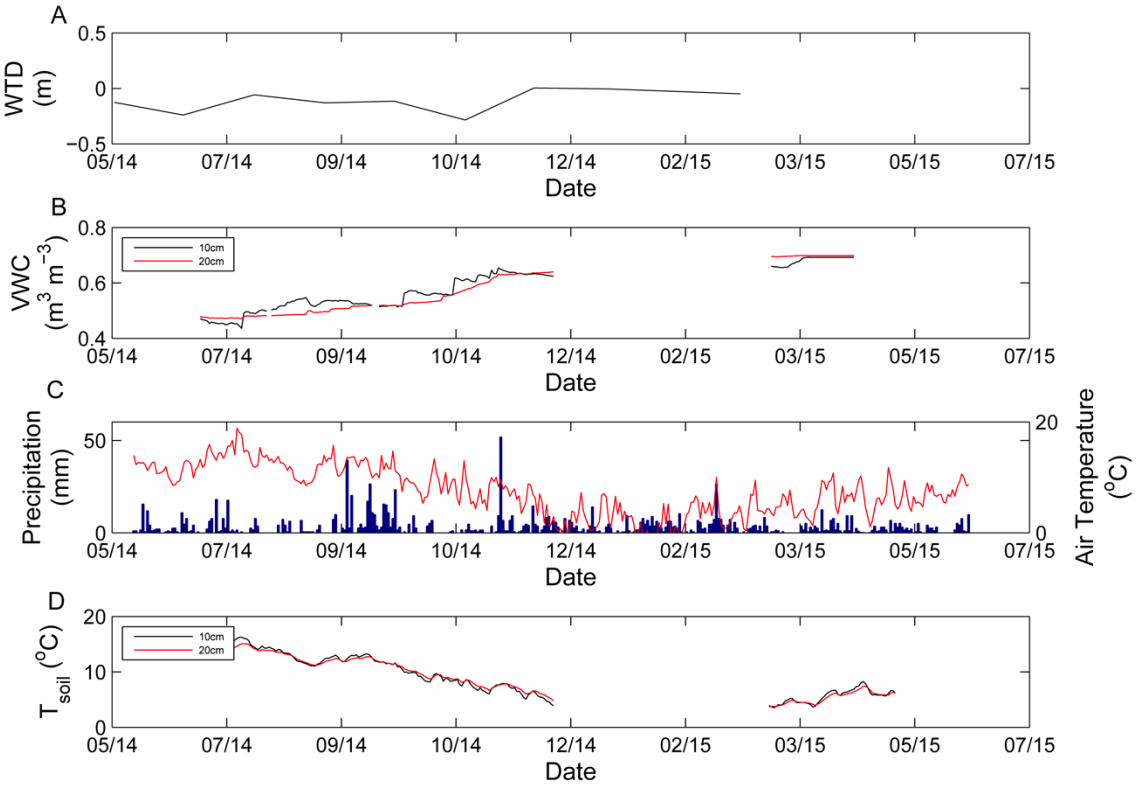

Figure 2.8 Selected environmental variables (Methods - Chapter 3) measured at Lonielist over the course of the study period. A) Water table depth measured manually on a monthly basis from 5 piezometers around the site, except February 2015 when weather blocked access to site. Negative values denote water table depth below the surface of the furrow. B) Daily mean Volumetric water content (VWC) at a depth of 10 cm (black) and 20 cm (red). C) Daily precipitation and mean air temperature from Lonielist. D) Daily mean soil temperature measured at a depth of 10cm (black) and 20 cm (red).

At almost all points, the soil moisture content was higher at 10 cm than 20 cm. However, problems with the sensor meant data collection from December 2014 onwards was patchy. Air temperature (Figure 2.8C) also showed a distinct seasonal signal, with highest temperatures observed in summer and lowest temperatures observed in winter. Soil temperatures (Figure 2.11D) were similar at both 10 cm and 20 cm with an observed seasonal signal. Similar to the soil moisture content, issues with the sensor meant data collection from December onwards was patchy.

2.3.2 Talaheel

Talaheel (Table 2.1) was the oldest restored site on the Forsinard Flows National Nature Reserve. This site encompassed an area of around 380ha (3.8 km^2) and was planted in 1981 with a mix of *Picea sitchensis* (Sitka spruce) and *Pinus contorta* (lodgepole pine) before undergoing restoration in 1997/98. As this was the oldest restored site, it gave vital information on how long these sites take to restore ecosystem functioning of blanket bog like systems. The trees at the site were felled using chainsaws and then left to decompose in situ. As at the

Lonielist site, poor growth of the trees prior to felling meant the canopy was felled before a fully closed canopy was achieved.

2.3.2.1 Topography & Aspect

Similar to Lonielist, Talaheel had a mean peat depth of around 2 m. Furrows were spaced around 1.5 to 2 m apart across the site. As seen in Figure 2.9, woody detritus was still visible in the furrows at Talaheel although, in many areas, this had been overgrown by *Sphagnum* moss. Microtopography was similar in magnitude to Lonielist. The site had a gentle slope of 1-3° from south to north before rising (4 - 6°) on the northern side.

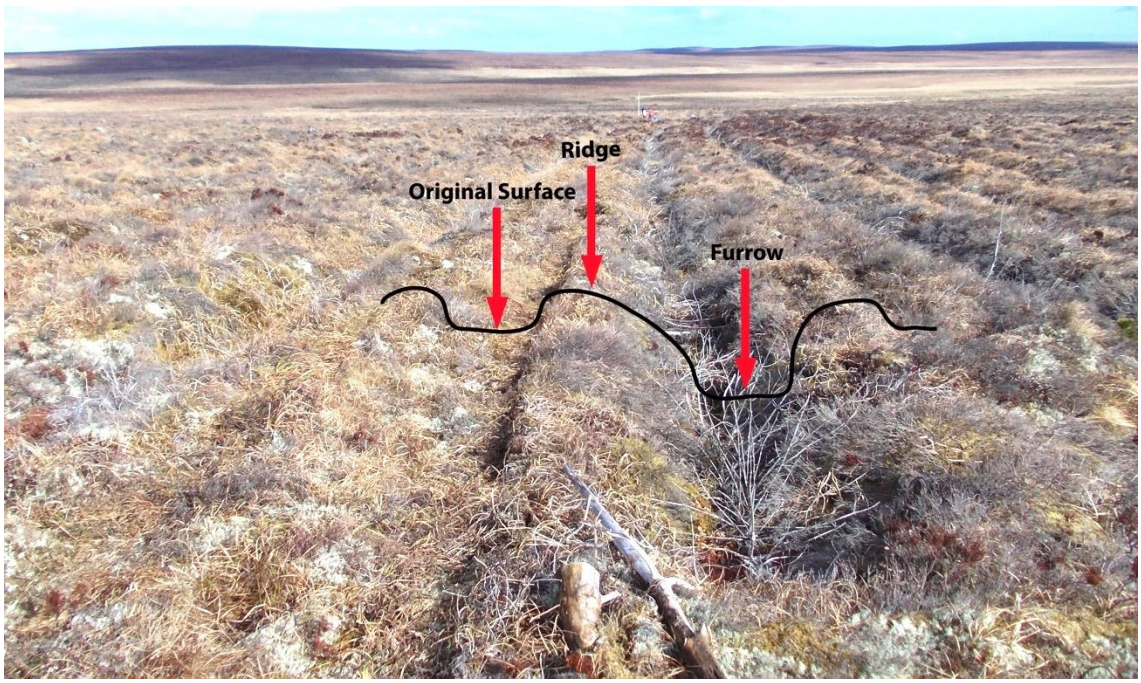

Figure 2.9 View of Talaheel facing north, showing the different microforms, the vegetation present on the site. Also visible are the remains of the trees felled in 1997/98. Image Source: Author, April 2013.

2.3.2.2 Vegetation Composition

The vegetation on the site was dominated by sedges (*Cyperaceae*), particularly cottongrasses (*Eriophorum vaginatum* and *Eriophorum angustifolium*), with a high percentage of *Hypnaceae*, *Molinia caerulea, Carex panicea* and *Trichophorum cespitosum* on the original surface. The wetter furrows were dominated by bog mosses, especially *Sphagnum cuspidatum, Sphagnum papillosum and Sphagnum capillifolium*. Ericaceous shrubs such as *Calluna vulgaris* and *Erica tetralix* dominated the ridges, however between 2010 and 2011, the heather beetle (*Lochmaea suturalis*) severely reduced the *Calluna vulgaris* community (N.Russell, 2011 pers. comm. 27th April). Other species found on the ridges included *Racomitrium lanuginosum* and *Carex panicea*.

2.3.2.3 Environmental Conditions

Talaheel had a mean water table of 0.11 ± 0.005 m below the peat, measured from the base of the furrow using an automatic logging pressure transducer (GE Sensing, Co. Clare, Ireland). The water table (Figure 2.10A) was relatively stable over the course of the study period, between 0.15 and 0.1 m below the furrow bottom, except in July 2014 when the water table dropped to nearly 0.3 m below the furrow bottom. The steady water table is also reflected in the soil moisture content, which varied between 0.71 and 0.73 m^3 m^{-3}. Spikes in soil moisture (VMC – Figure 2.10B) generally coincided with increases in the height of the water table or precipitation events (Figure 2.10C).

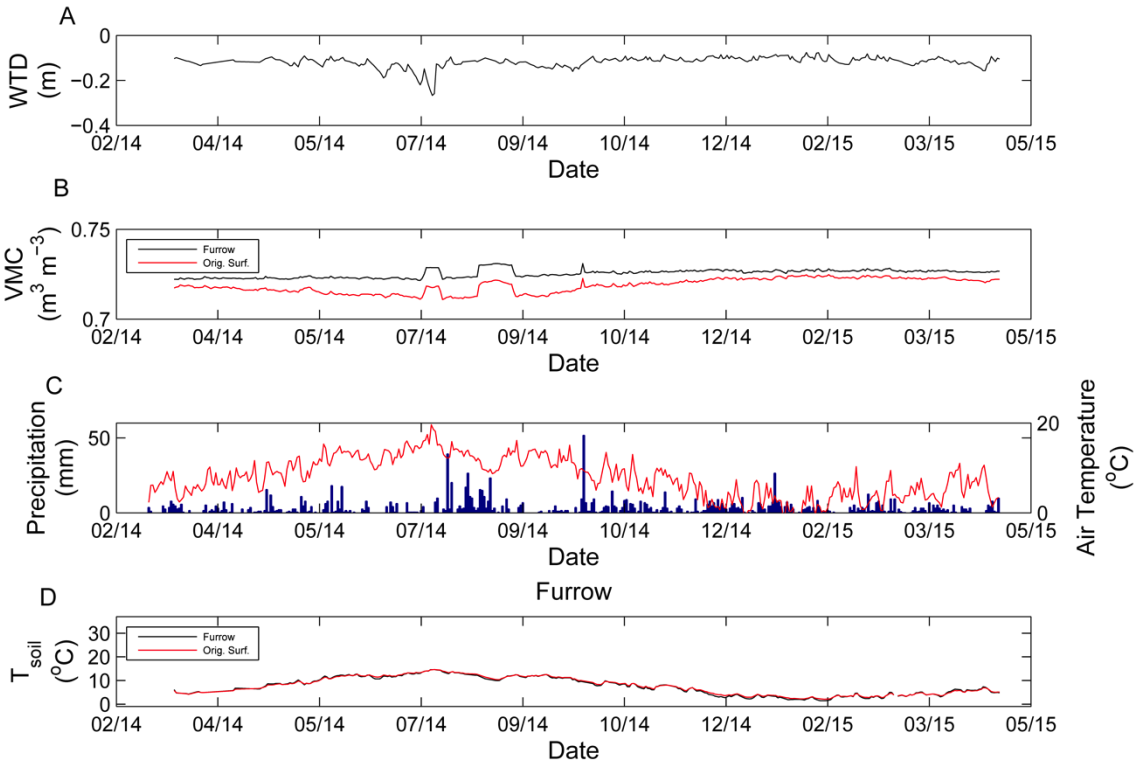

Figure 2.10 Selected environmental variables (Methods - Chapter 3) measured at Talaheel over the course of the study period. A) Daily mean water table depth from a pressure transducer in the furrow closest to the EC flux tower. Negative values denote water table depth below the surface of the furrow. B) Daily mean Volumetric water content (VMC) from a furrow and original surface measured at a depth of 10cm. C) Daily precipitation and mean air temperature from Talaheel. D) Daily mean soil temperature from the original surface and furrow measured at a depth of 10cm.

The mean soil temperatures (Figure 2.10D) showed little difference in temperature between microforms. The mean soil temperatures in the original surface and furrow were 7.65 ± 0.42°C and 7.50 ± 0.41°C respectively. It would be expected that the original surface would have a slightly higher temperature due to thermal properties of dry peat giving rise to greater temperature fluctuations.

2.3.3 Cross Lochs

Cross Lochs (Table 2.1) was chosen as the undrained blanket bog control as it already had an established EC system on site, as well as being representative of an intact blanket bog. The advantage of using the existing site was that it was already established and historical data were available, providing a baseline (2008 – 2012) from which to compare data collected during the course of this study (2013 – 2015). The Cross Lochs site had no known history of land management other than deer management, although there were managed areas approximately 600 metres to the north of the site.

2.3.3.1 Topography & Aspect

Cross Lochs is almost flat, with a slope of 0-1°. However, approximately 400 m to the south of the tower a more discernible slope of around 2° was present. The peatland featured the hummock/hollow pattern (Lindsay *et al.*, 1988) that is common in many peatlands. The hummocks tended to be drier and the hollows slightly below the level of the water table giving a positive water table at these points. The site had a mean peat depth of around 2.2 m with a maximum depth of 7 m. Approximately 500 m to the north of the site there was a large peatland pool complex, which was subject to research into gaseous and aqueous carbon fluxes from peatland pools, conducted across a number of peatlands in Scotland and Ireland by researchers from The University of Leeds, Centre for Ecology and Hydrology and The University of Stirling.

2.3.3.2 Vegetation Composition

Cross Lochs (Figure 2.11) was similar in vegetation composition to other undrained blanket bogs in the area. The site was dominated by cottongrasses especially *Eriophorum vaginatum and Eriophorum angustifolium,* and bog mosses such as *Sphagnum cuspidatum* and *Sphagnum capillifolium* in the wetter areas, such as small pools, which in some cases also contained bog bean (*Menyanthes trifoliata).* Also present were ericaceous plants such as *Erica tetralix* and *Calluna vulgaris,* as well as mosses and lichens such as *Racomitrium lanuginosum,* which were usually found on the drier hummocks. Other vegetation found included *Trichophorum cespitosum, and Drosera rotundifolia*.

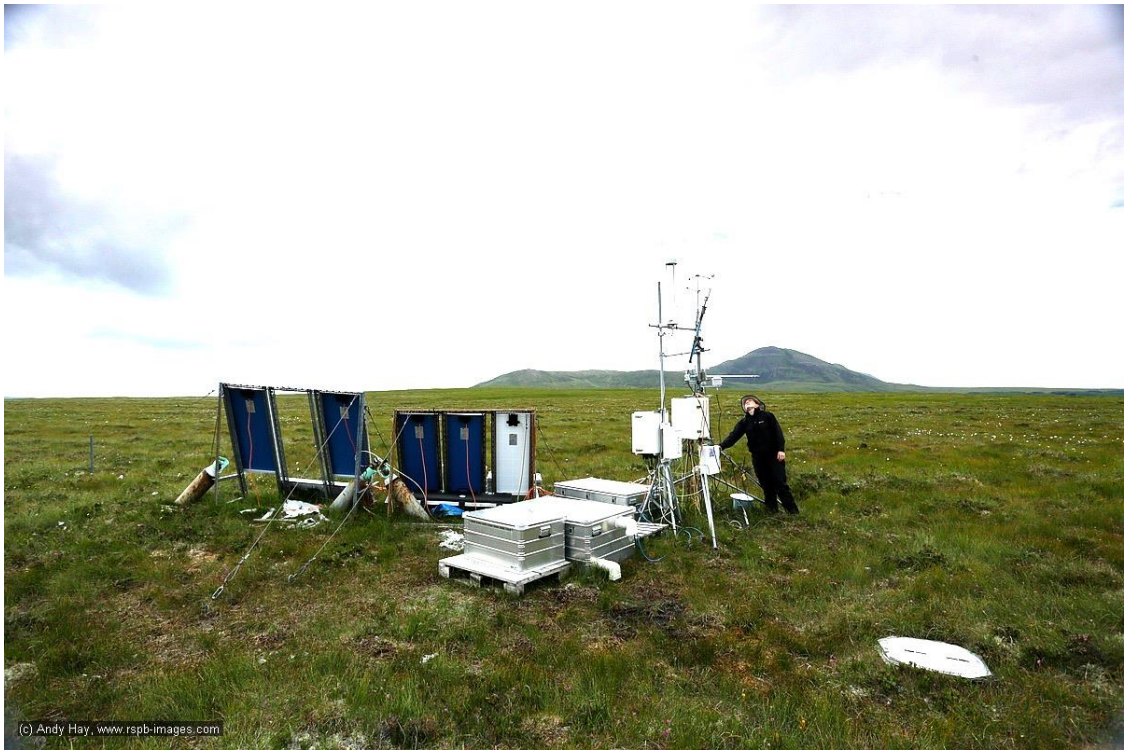

Figure 2.11 Southwesterly view of Cross Lochs and of a volunteer at the Cross Lochs EC flux tower, displaying the flat surface required for the EC method and the absence of the ploughed microforms present at the restored sites. Image Source: © Andrew Hay, rspb-images.com

2.3.3.3 Environmental Conditions

The water table at Cross Lochs was always within 0.13 m of the soil surface during the period of study (Figure 2.12A) and at times was above the surface at the measurement point. The lowest water table measured was 0.13 m in July and August 2014, when similar drops in the water table were also seen in the restored sites. The mean water table depth was 0.06 ± 0.06 m, which is higher than the mean water tables measured at the restored sites. This is to be expected, given that the site has no modern history of drainage. The soil temperature (Figure 2.12D) showed distinct seasonal patterns, with the highest soil temperature of 15.8°C in July and a minimum temperature of 2.3°C in February. Soil moisture was not measured at this site, but with the height of the water table it would be expected that the soil moisture would be saturated for most, if not all of the year. Air temperature (Figure 2.12C) showed a seasonal signal with the lowest temperatures observed in the autumn and early winter. Logger issues resulted in no environmental conditions being measured in spring and early summer 2014.

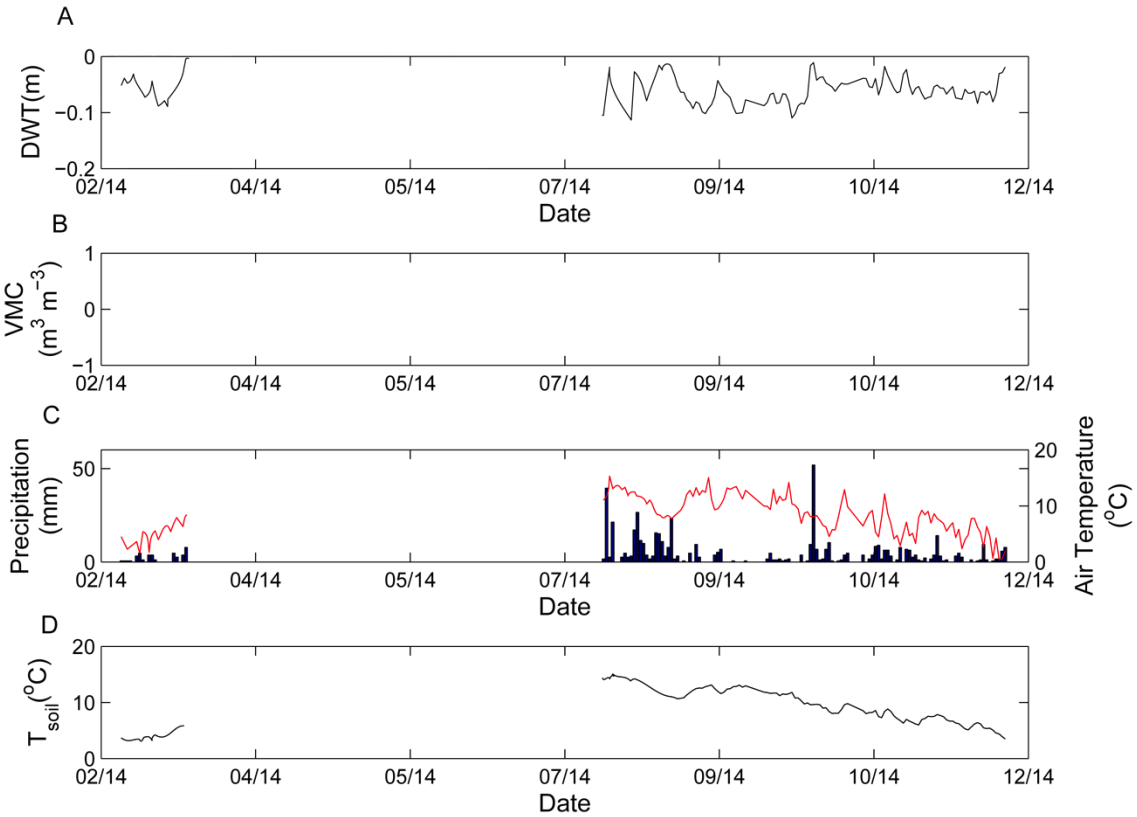

Figure 2.12 Selected environmental variables measured at Cross Lochs over the course of the study period. A) Daily mean water table depth from pressure transducer. Negative denotes water table depth below the surface. C) Daily precipitation and mean air temperature from Cross Lochs. D) Daily mean soil temperature measured at a depth of 10cm within the footprint of the net radiometer.

2.3.3.4 Human Interaction

There is some recorded history of low level human occupation around the Cross Lochs site with an old settlement around 500 – 600 metres to the east of the site and also an old Victorian pony track running around 500 m to the north east of the flux tower down to Forsinard Lodge (M. Hancock 2015 pers. comm. 29th June). This previous small scale human occupation would have been concentrated on the better soils, near rivers, as the blanket bogs would only have provided poor grazing and been of little use for livestock (M. Hancock 2015 pers. comm. 29th June). Around 600 to 800 metres to the north of the site there is an area of felled Sitka spruce and lodgepole pine plantation forestry.

2.4 Summary

This chapter has provided a background on the Flow Country, giving details of the typical land uses and history. The circumstances surrounding the planting of non-native conifer trees on around 17% of the total blanket bog have been explained along with details of the subsequent restoration in the late 1990s. Furthermore, descriptions and site characteristics of each of the main sites used in this research have been provided.

~ Chapter 3 ~

Methods

3.1 Methods for quantifying ecosystem carbon balance

Multiple methods are currently used to quantify the carbon balance of terrestrial ecosystems at the soil-atmosphere interface. Eddy covariance (EC) quantifies gas exchange rates by measuring the movement of gases within the atmospheric boundary layer. Whilst EC is becoming the method of choice for ecosystem-scale trace gas measurements due to its ability to carry out measurements at a high temporal resolution, it is not able to pick up the small-scale (<1m) processes occurring within the soil atmosphere (Baldocchi, 2003). In order to quantify the small-scale processes occurring in ecosystems, closed static and dynamic chambers are often used to compliment larger scale (>100 m) EC measurements or where EC is not suitable (Wang *et al.,* 2013). Chambers enclose an area of soil and vegetation to allow the accumulation of gases within the chamber; the flux is quantified by changes in the headspace gas concentration over the enclosure time. Due to their low cost and mobility, chambers are easy to replicate giving a greater understanding of the spatial variability and key environmental variables driving the flux. However, due to the intensive labour requirement, static or dynamic chambers cannot provide the temporal resolution of EC. Identified errors in chamber measurements include changes in the enclosed microclimate, and pressure artefacts, which can cause a sudden gas efflux (Livingston and Hutchinson, 1995).

Other direct methods of quantifying the exchange of CO_2 and other greenhouse gases include flux gradient (FG) and relaxed eddy accumulation (REA). The FG method is based on the measurement of gas concentration gradients and transport properties (Maier and Schack-Kirchner, 2014). Assuming molecular diffusion dominates gas transport in soils, the flux can be calculated using the concentration gradient of the soil gas and the effective gas diffusivity of the porous medium (Goffin *et al.*, 2014, Maier and Schack-Kirchner, 2014). This has an advantage over the EC and chamber methods by providing information on the profile of net gas production and consumption. However, it can be difficult to replicate, whilst also being labour intensive and expensive. REA is an ideal method for continuous measurement of gas species for which fast response analysers are not available, such as ammonia and sulphur (Businger and Oncley, 1990, Meyers *et al.*, 2006). REA samples air depending on the magnitude and direction of the vertical wind velocity (Ren *et al.*, 2011) with the sample air separated into two reservoirs, an upward and downward draft, at a constant flow rate based upon the sign (positive or negative) of the vertical wind. The flux is calculated proportional to the difference in concentration between the up and down drafts (Meyers *et al.*, 2006). However, measurements of vertical wind velocity must be accurate and free from bias, as data cannot be corrected later (Pattey *et al.*, 1993). Additionally, because concentration differences in the updrafts and downdrafts are generally small, a high level of detection is required for gas analysis. For most gases, high

detection can only be achieved under laboratory conditions (Pattey *et al.*, 1993), therefore samples must be stored and regular visits made to collect samples for analysis, making REA a more labour intensive method than EC.

Whilst EC methods can provide ecosystem-scale measurements, larger landscape scale measurements can be obtained using aircraft (Hill, 2011, Saeki *et al.*, 2013, Sasakawa *et al.*, 2013). Aircraft measurements quantify land – atmosphere exchange at larger scales (>1km) than that measured by EC (Sasakawa *et al.*, 2013). Aircraft measurements are often carried out in conjunction with EC to provide a point on the landscape where flux is known and can be cross-calibrated (e.g. Saeki *et al.*, 2013, Sasakawa *et al.*, 2013). These data can be used independently or combined with satellite-derived measurements of environmental variables such as soil moisture, vegetation indices and temperature (Mahadevan *et al.*, 2008) to provide top-down Earth observation models or inversion models to constrain ecosystem C fluxes (Houborg *et al.*, 2009). Top-down models are often limited by their spatial resolution and inability to determine processes occurring within ecosystems (Hill, 2011). EC combined with eco-physiological measurements, such as vegetation indices, chamber measurements or soil qualities can be used as a bottom-up approach to constrain C fluxes from ecosystems. However, the number and areal extent of sampling locations often limits the bottom-up approach (Houborg *et al.*, 2009).

For this research it was decided that the most appropriate methods, given the scale of the restoration work, was eddy covariance (EC) to quantify the ecosystem carbon (C) balance and closed-dynamic chambers to quantify small-scale variations in C dynamics.

3.2 Eddy Covariance

3.2.1 Method development

Although EC development has accelerated over the last 30-40 years, the theoretical framework behind the method can be dated back to Sir Osborne Reynolds in 1895 (Reynolds, 1895). This research suggested a process that allowed the energy of mean motion to be continually transferred into energy of heat motion without the need for an intermediate stage. However, Reynolds' research was hindered by a lack of equipment able to test his theory and thus it remained in this untested state until around 1930, when Scrase (1930) conducted research into momentum transfer with simple analogue instruments and strip chart loggers (Baldocchi, 2003). A theoretical breakthrough occurred in 1946, when Obukhov (1946) found a universal length scale for exchange processes in the surface layer, leading to the inception of the Monin-Obukhov similarity theory (Appendix C) later in 1954. Whilst theoretical work gathered pace, technological advancement always lagged until after World War II. Swinbank (1951) was able to measure vapour pressure fluctuations using two wet bulb thermocouples built into an

electrical network over open, level grassland near Melbourne, Australia. The network behaved in a similar manner to Regnaults psychrometric equation for small changes in vapour pressure, saturation vapour pressure at the wet bulb temperature and depression. This set down the theoretical and experimental framework upon which EC is based (Baldocchi, 1996, Jarvis *et al.*, 1997, Hargreaves *et al.*, 2003, Teh *et al.*, 2011, Smallman *et al.*, 2014).

3.2.2 Early EC Measurements and Developments

The first EC measurements were made in the early 1970s using a propeller wind vane and closed-path CO_2 analyser modified with a capacitance detector (Desjardins, 1974). However, this research was heavily criticised for being unable to perform the required high frequency measurements. The 0.5s measurement intervals, gave a 5% underestimate in the eddy flux under neutral or unstable atmospheric conditions and 20% under stable atmospheric conditions. In the late 1970s, a fast response open-path CO_2 analyser, capable of the required high frequency measurements, was developed using a solid state selenium (PbSe) detector (Bingham *et al.*, 1978, Jones *et al.*, 1978). While this development permitted the high frequency measurements, other limitations such as data logging systems, power supplies and the long-term performance of the analysers limited studies to time scales of just a few days or weeks (Anderson *et al.*, 1986, Verma *et al.*, 1989, Kim and Verma, 1990).

A new system using infrared absorbance spectroscopy was proposed by Auble and Meyers (1992), allowing fluxes of CO_2 and H_2O to be reliably measured at timescales on the order of months to years. This system, combined with the earlier development of reliable data acquisition products and sonic anemometers (Zhang *et al.*, 1986), was the springboard for the long-term EC measurements being undertaken today.

3.2.3 Current Methodological State

The development of the continuous measurement system led to the formation of international flux networks, such as FLUXNET (Baldocchi *et al.*, 2001). The concept of a global flux network was first proposed in 1993 in the science plan of the International Geosphere-Biosphere Program/Biospheric Aspects of the Hydological cycle (Baldocchi *et al.*, 2001). The first flux networks were established in 1996 when the Euroflux and AmeriFlux projects began, with the broad aim of monitoring long-term fluxes of CO_2 and H_2O from a range of ecosystems across Europe and the Americas (Aubinet *et al.*, 2000, Valentini *et al.*, 2000). In 1998, following the success of the flux networks and the impending launch of the Earth Observation *Terra* satellite (MODIS), the National Aeronautics and Space Administration (NASA) decided to fund the global FLUXNET programme to validate the products of MODIS (Baldocchi *et al.*, 2001). Today, comprising over 650 flux sites across 5 continents and a variety of ecosystems, the

network measures land-atmosphere fluxes of CO_2, H_2O and energy to validate the computations of net primary productivity (NPP), evaporation and energy absorption being made by MODIS. Aside from providing MODIS validation, FLUXNET seeks to (Baldocchi *et al.*, 2001):

1) Quantify spatial differences in CO_2 and H_2O exchange rates across natural ecosystems and climatic gradients

2) Quantify temporal dynamics and variability of carbon, water and energy flux densities

3) Quantify variations of CO_2 and H_2O fluxes due to changes in environmental conditions such as temperature, soil moisture content, canopy structure and photosynthetic capacity

Eddy covariance has become a widely used method for quantifying the exchange of greenhouse gases and energy between the land surface and atmosphere. In 1995, the year before the start of the EuroFlux project, only 19 published articles listed Eddy Covariance as a keyword. In 2005 over 200 articles were published and in 2015 over 500 published papers cited eddy covariance as a keyword (Figure 3.0).

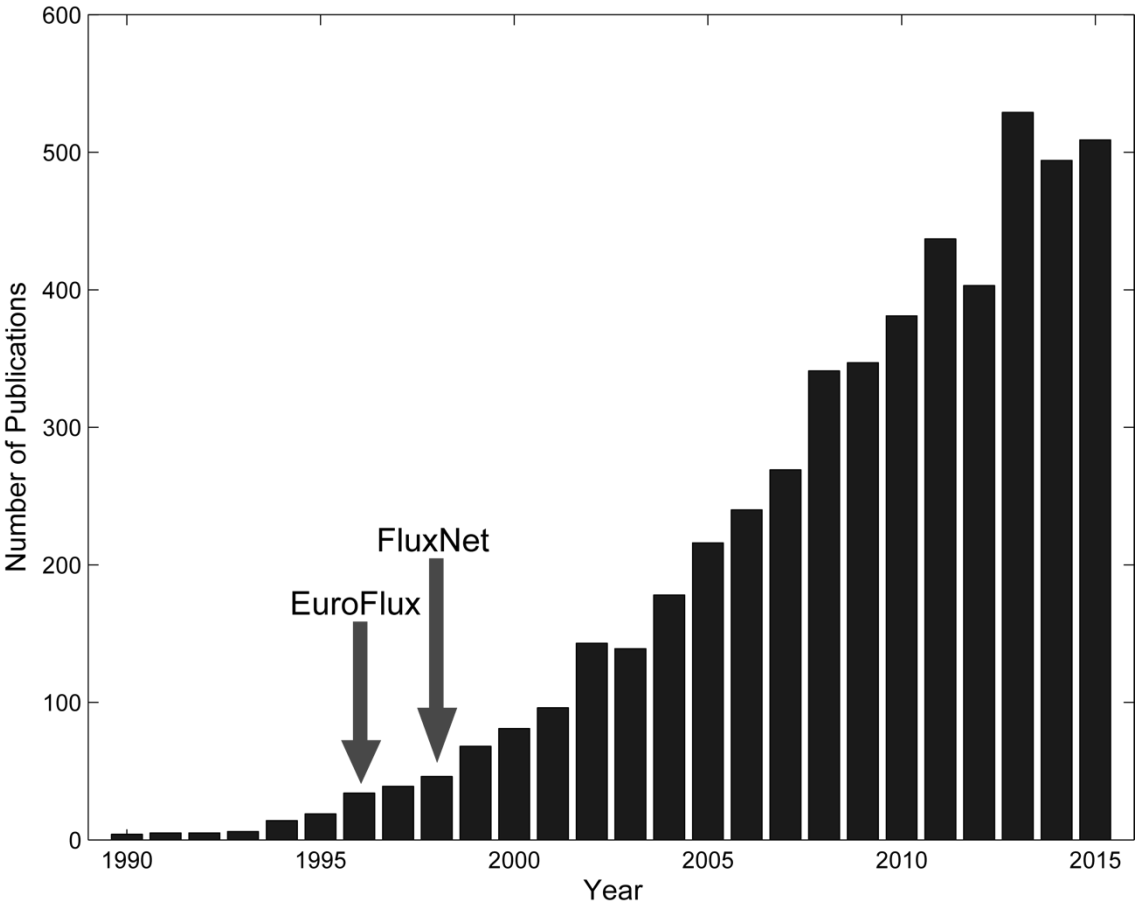

Figure 3.0 Number of articles published each year listing Eddy Covariance as a keyword between 1990 and 2015. Key milestones such as the inception of the flux networks have been added to the plot. Data Source: Web of Knowledge, May 2016.

The increased use of EC has allowed the development of both the science and technology in studying soil-atmosphere interactions across a range of ecosystems. A prime example of this is the design, testing and implementation of enclosed CO_2/H_2O analysers, which maximise the strengths and minimise the weaknesses of the open-path and closed-path systems (Burba *et al.*, 2010). Open-path technology has been used to develop methane (CH_4) analysers, which can be easily integrated into existing EC systems and run without the need for mainline power connections (McDermitt *et al.*, 2011). The development of cavity ring down spectrometry (CRDS) has also led to easier closed-path measurements of CH_4 and nitrous oxide (N_2O) through the production of smaller, more energy efficient analysers that can be used in the field without the need for cryogenic cooling (Hendriks *et al.*, 2008, Miles *et al.*, 2012, Andrews *et al.*, 2014, Stowasser *et al.*, 2014, Winderlich *et al.*, 2014).

In addition to the measurement of CO_2, H_2O, CH_4, and N_2O, recent work has also looked at the measurement of ozone (O_3) using the EC method (Wohlfahrt *et al.*, 2009, Muller *et al.*, 2010, Stella *et al.*, 2013). As well as being a greenhouse gas, O_3 is also an air pollutant dangerous to

human and ecosystem health. Ozone is produced through photochemical reactions with nitrogen oxides (NOx) and volatile organic compounds (VOCs). As atmospheric concentrations of NOx and VOCs have increased over the last decade, primarily due to fossil fuel combustion, background levels of O_3 have also increased (Derwent *et al.*, 2007). The development of an EC methodology for O_3 measurement provides a continuous measurement of O_3, which may help to inform models predicting when O_3 levels may be dangerous to human health.

3.3 Theory of Eddy Covariance

3.3.1 Atmospheric Structure

In order to understand how an ecosystem functions, we must first understand the boundaries across which heat, mass and momentum can be exchanged. Ecosystems can typically be divided into three parts; soil, vegetation and atmosphere. The boundaries between these components are able to exchange matter, but the timescales upon which this happens are variable. The lowest boundary comprises the soil and underlying geology, the processes here occur on timescales of years to decades (Revelle and Suess, 1957) and are not able to be fully captured in the short time scales of most studies. Vegetation provides a transportation mechanism for the exchange of gases between the soil and atmosphere (Greenup *et al.*, 2000, Kim *et al.*, 2000, Hamilton *et al.*, 2014). These processes occur on time scales of a few hours to days, making them key for studying land-atmosphere CO_2 exchange.

The atmosphere is a highly mobile area, where many of the resources required for ecosystem functioning, such as CO_2, N_2 and H_2O, are exchanged. The character of the atmosphere makes monitoring simple, although it is necessary to choose an appropriate position and method to robustly measure the exchange of atmospheric constituents between the atmosphere and ecosystem. The area of interest for EC research is the atmospheric boundary layer (ABL). Stull (1988) defined the ABL as:

"The part of the troposphere that is directly influenced by the presence of the Earth's surface and responds to surface forcing on a timescale of one hour or less"

The ABL responds quickly to changes occurring at the surface, with the depth ranging from tens of metres under more stable nocturnal conditions, to as much as 2 km under extreme convective conditions (Stull, 1988). Generally, the ABL can be split into 4 layers; the interfacial layer, the roughness sublayer, the surface layer and the outer layer (Figure 3.1). Above the ABL, the free atmosphere is characteristically well mixed, with temperature and humidity decreasing with height (Stull, 1988). The outer layer, or mixed layer, as the name suggests is well mixed, but does not have the structure of the free atmosphere. The outer layer is characterised by

convection and a near constant horizontal velocity profile (Stull, 1988). The depth of the layer varies diurnally from approximately 100 m to over 1000 m due to surface forcing from energy inputs. On top of the outer layer is a layer called the entrainment zone, where drier, warmer air from the free atmosphere mixes with air from the outer layer.

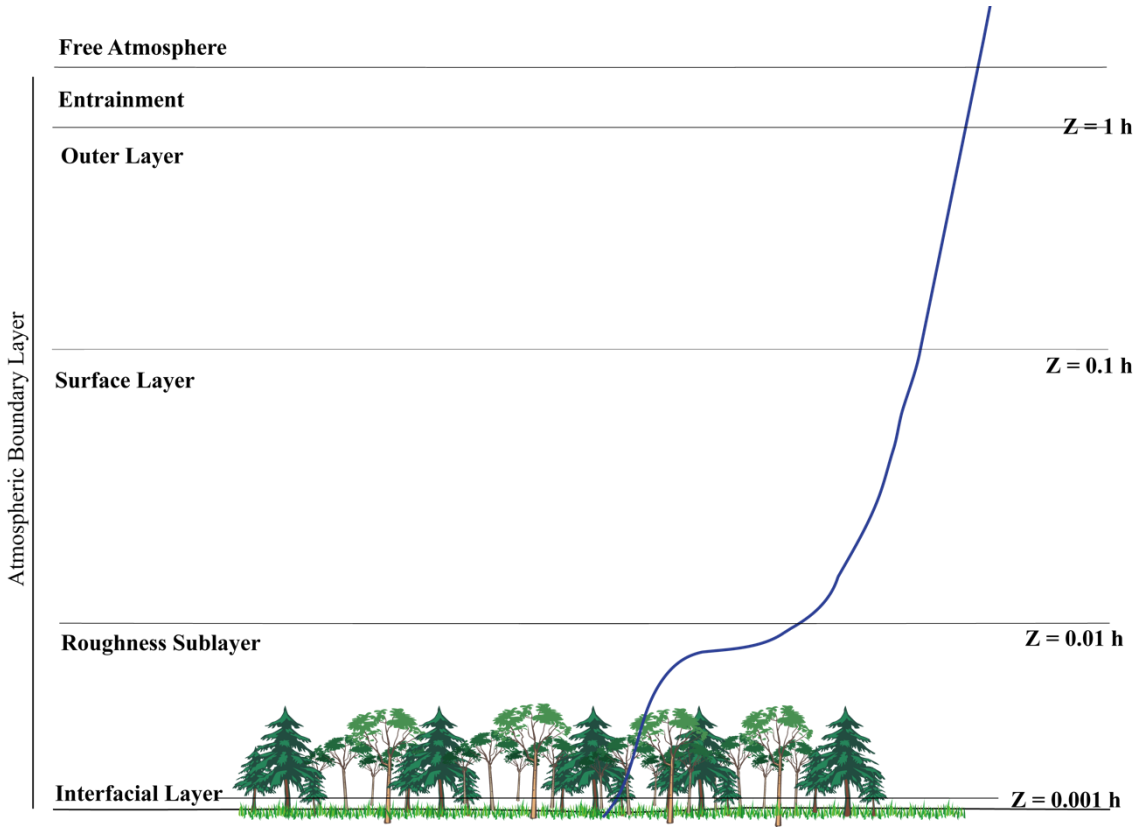

Figure 3.1 The layers within the atmospheric boundary layer (ABL). Heights (z) are given relative to the height of the ABL (h) and are order of magnitude approximations. The blue line represents the behaviour of horizontal wind speed.

The lowest 10% of the ABL is referred to as the surface layer and is defined by a logarithmic velocity profile and turbulent mixing. Fluxes in the surface layer are thought to be nearly constant with height, making fluxes measured within the surface layer representative of the underlying surface. The base of the surface layer is referred to as the roughness sublayer and is characterised by turbulent mixing. However, roughness of the underlying surface results in spatial variability and an unpredictable flux distribution. A small layer underneath this with a depth of a few millimetres to a few centimetres is referred to as the interfacial layer and is defined by molecular diffusive transport. This behaviour of the ABL, specifically the constant flux nature and turbulence of the surface layer, has led to the development of EC and other methods.

3.3.2 EC Measurement Principle

EC measures the turbulent motions and concentrations of atmospheric constituents (scalars) within the surface layer of the ABL. Turbulence in the ABL is generated by mechanical and thermal processes such as shearing and convection, which generate eddies of varying frequencies and sizes (Stull, 1988). As eddies are the primary method of scalar transport in the surface layer, and the vertical variation of turbulent transport is independent of height, the measurement of the turbulent structures at a fixed height (*Zm*) is representative of fluxes across the land surface (Stull, 1988, Foken *et al.*, 2012a). As these processes occur rapidly within the ABL, high frequency (10 – 20 Hz) measurements are required to resolve the full range of flux transporting turbulent motions (Foken *et al.*, 2012a). The turbulent flux is equal to the mean product of the air density (ρ_a), vertical velocity (w) and mixing ratio of the scalar (c):

$$F = \overline{\rho_a w c}$$

(Eqn 3.1)

Using Reynolds rule of averaging (Reynolds, 1895 and Appendix C), Eqn 3.1 can be broken down into means (overbars) and deviations (primes) (Baldocchi, 2003):

$$F = \overline{(\overline{\rho_a} + \rho_a')(\overline{w} + w')(\overline{c} + c')}$$

(Eqn 3.2)

The terms in Eqn 3.2 now describe air density, vertical velocity and mixing ratio as a mean over some time (half an hour for example) and an instantaneous deviation from this mean for every unit of time, such as 0.05 or 0.1 seconds. The parenthesis can be opened on Eqn 3.2 to remove unnecessary terms. These unnecessary terms are denoted by the strikes in Eqn 3.3.

$$F = (\overline{\overline{\rho_a}\overline{w}\overline{c} + \cancel{\overline{\overline{\rho_a}\overline{w}c'}} + \cancel{\overline{\overline{\rho_a}w'\overline{c}}} + \overline{\overline{\rho_a}w'c'} + \cancel{\overline{\rho_a'\overline{w}\overline{c}}} + \overline{\rho_a'\overline{w}c'} + \overline{\rho_a'w'\overline{c}} + \overline{\rho_a'w'c'}})$$

(Eqn 3.3)

These terms are removed as averaged deviations from the average are equal to zero (denoted by the strikes in Eqn 3.3), therefore these can be removed, and the equation simplified to equation 3.4.

$$F = (\overline{\rho_a}\overline{w}\overline{c} + \overline{\rho_a}\overline{w'}\overline{c'} + \overline{w}\overline{\rho_a' c'} + \overline{c}\overline{\rho_a' w'} + \overline{\rho_a' w' c'})$$

(Eqn 3.4)

A number of assumptions are made in EC such as density fluctuations are negligible and there is no divergence or convergence in the flow such that the mean vertical flow is negligible for horizontally homogeneous terrain. Therefore Eqn 3.4 can be simplified further to:

$$F = \overline{\rho_a} \cdot \overline{w'c'}$$

(Eqn 3.5)

If all the assumptions of EC - discussed in 3.5 - are met, the eddy flux (Eqn 3.5) is equal to the product of the mean air density (ρ_a) and mean covariance between instantaneous deviations in the vertical wind speed (w) and scalar-mixing ratio (c). Although Eqn 3.5 is based upon CO_2 land-atmosphere exchange, similar equations exist for fluxes of latent heat, sensible heat and other atmospheric constituents.

3.4 Eddy covariance implementation

Before discussing errors and assumptions associated with EC, it is prudent to discuss EC instrumentation in order for the errors and assumptions to be fully understood. From here on in, discussions on the EC method and data processing are focussed on the procedures implemented in this research.

3.4.1 Anemometer

Three-dimensional sonic anemometers are used in micrometeorological research to quantify fluxes of momentum and virtual temperature (Lee, 1998, Mahrt *et al.*, 2000). A sonic anemometer (Figure 3.2) measures wind speed using the flight time of sonic pulses between transducer pairs arranged a fixed distance apart. There are two types of sonic anemometer; orthogonal and non-orthogonal (Horst 2015). A non-orthogonal sonic such as the CSAT3 (Campbell Scientific, Shepshed, UK) has 3 transducers at angles of 60°, but does not physically have a transducer in the vertical plane, while an orthogonal sonic, such as the ATI-K (Applied Technologies Inc. Longmont, Colorado, USA) has three transducer paths (x, y and z), which are set perpendicular to each other (Horst *et al.*, 2015).

3.4.2 Open-Path CO_2/H_2O analysers

Open-path analysers (Figure 3.2) quantify concentrations of CO_2/H_2O *in situ*, using a non-dispersive infrared light source. Open-path analysers do not rely on intake tubes, allowing them to respond to small changes in concentration very quickly. However, they are sensitive to precipitation and dirt, which can result in the optical path becoming blocked, and measurements being affected. As these analysers do not use pumps to draw air into a cell they are very

efficient and are typically used on EC systems where power is limited. This type of analyser was used at Talaheel (Chapter 2 - 2.3.2) and Cross Lochs (Chapter 2 - 2.3.3).

3.4.3 Closed-path CO_2/H_2O Analysers

Closed-path CO_2/H_2O analysers use intake tubes (Figure 3.2) to draw air into a sample cell where the density of gas is quantified over an enclosed sample path using a non-dispersive infrared source. These analysers are free from the problems of meteorological conditions faced by open-path sensors. However, as closed-path analysers require tubing to draw sample air down into the analyser, this can result in the physical or chemical modification of the sample as well as a delay between the measurement of vertical wind velocity and scalar concentration. Tube attenuation results in high-frequency losses through a lack of turbulent flow and adsorption of the analyte to the tubing wall. During periods of laminar flow, parabolic velocity profiles are established in the tube with a maximum velocity which is twice that of the mean velocity at the centre of the tube (Philip, 1963a, Philip, 1963b, Philip, 1963c). This results in the physical mixing of different air streams and the smoothing of high frequency fluctuations. Additionally, the analyte can become "stuck" to the tubing wall (Foken *et al.*, 2012b), particularly in humid conditions and results in a further lag between vertical wind velocity and scalar concentration. A closed path analyser was used at Talaheel (Chapter 2 – Section 2.3.2) but no data is presented in this thesis due to the large gaps in the data caused by high amounts of analyser and pump downtime.

3.4.4 Enclosed-Path CO_2/H_2O analysers

More recently, enclosed path analysers have become available and these devices bridge the gap between open- and closed-path analysers. Enclosed path analysers use open path technology encased within a weatherproof housing eliminating the precipitation sensitivity. As these analysers can be placed closer to the sonic anemometer, only a small, straight intake tube (~ 1 m) is required, reducing tube attenuation (Clement *et al.*, 2009, Burba *et al.*, 2010). This type of analyser was used at Lonielist (Chapter 2 - Section 2.3.1).

3.4.4 Data Management

As EC systems work at high frequencies, fast response data loggers are required to store all of the data. Typically, stand-alone data loggers or a computer are used. For sites without main line power, data loggers are a great advantage as they are robust, compact and efficient. Data loggers typically store raw data on USB drives or compact flash cards.

Computers generally require main line power, but are able to carry out other tasks alongside raw data acquisition, such as flux processing which allows the user to obtain processed fluxes on site

and fix instrumentation problems immediately. Due to the limited power supply and remote nature of the sites in this study, a data logger was used rather than a computer.

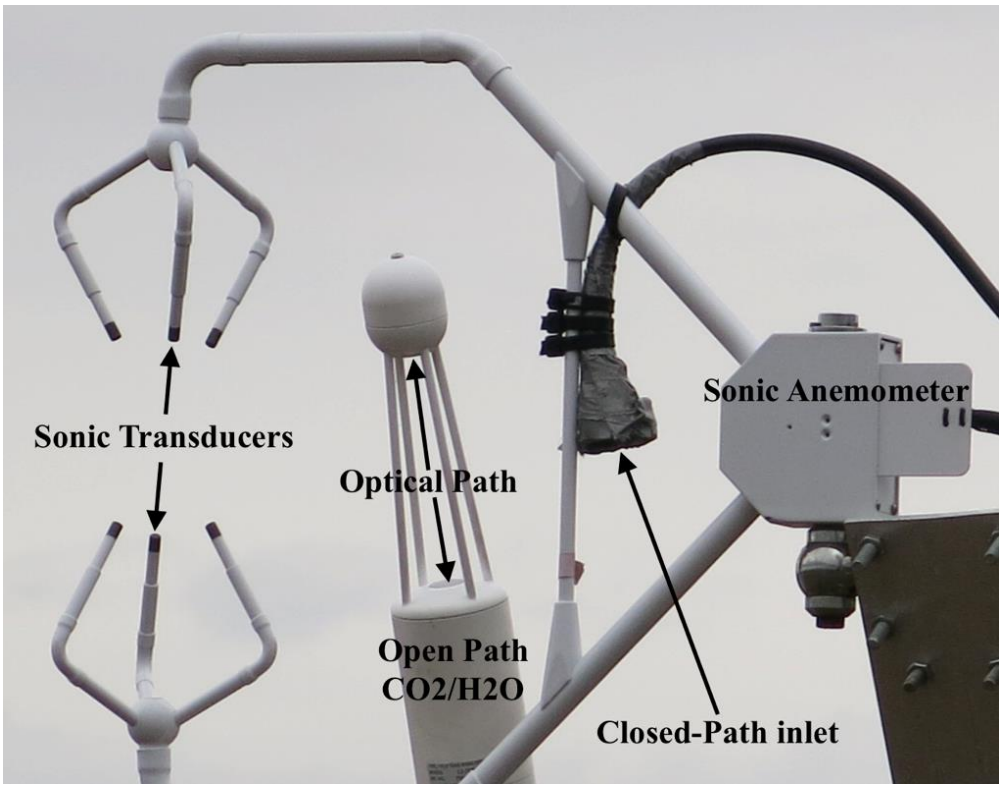

Figure 3.2 Sonic Anemometer and IRGAs deployed at Talaheel (Chapter 2, Section 2.3.2). Arrows are pointing to paired sonic transducers. Each transducer is set at an angle of 60° and faces its paired transducer. The open-path analyser sits at an angle allowing water to run off the optical windows. The closed path inlet is labelled for reference, but no data were used from this analyser.

In this study, non-orthogonal sonic anemometers were used at every site with open-path CO_2 analysers used at Talaheel and Cross Lochs and an enclosed-path analyser used at Lonielist. At every site, data were recorded on data loggers.

3.5 Assumptions of EC Measurements

In order to implement the EC technique a number of theoretical assumptions need to be made:

I. Measurements at one point are representative of an upwind area (Aubinet *et al.*, 2012).
II. Measurements are undertaken inside the surface or constant flux layer (Malhi *et al.*, 2004).
III. Fetch/footprint is of adequate size such that fluxes originate from the surface of interest (Aubinet *et al.*, 2012).

IV. The flux is fully turbulent, such that eddies are the dominant method of vertical transport (Foken, 2008).

V. The terrain is horizontal and uniform thus the average of the fluctuations is zero, and the density fluctuations, flow convergence and divergence are all negligible (Webb *et al.*, 1980, Baldocchi, 2003, Leuning, 2004, Foken, 2008).

VI. Instruments are able to detect very small changes in the scalar and vector quantities at very high frequencies (Moore, 1986).

VII. As scalar sensors do not measure mixing ratios it is assumed that the product of mean air density and mean covariance between instantaneous deviations in the vertical velocity and mixing ratio is equal to the mean covariance between instantaneous deviations in the vertical velocity and gas density (Baldocchi, 2003, Burba and Anderson, 2005).

In practice, the theoretical assumptions are rarely fully met (Moncrieff *et al.*, 2004). However, the errors associated with these assumptions can be reduced by the setup of the EC system. An appropriate site and tower location along with a number of post-processing and quality control methods can result in reliable flux estimates being obtained from EC (Rebmann *et al.*, 2012).

3.6 Errors

Errors associated with the EC technique (Table 3.0) can broadly be broken down into three categories:

I. Representation errors

II. Instrumentation errors

III. Methodological errors

These errors rarely occur independently of each other and can potentially add up to over 100% of the measured flux (Foken *et al.*, 2012b).

One of the main representational errors is the footprint/fetch associated with the tower. The footprint is constantly changing on a semi-predictable basis. During the day, while there is a turbulent structure within the surface layer, the footprint is smaller than at night when laminar flow dominates. Temporal variability of wind speed and direction can also cause variations in the footprint area (Post *et al.*, 2015). Additionally, representational errors can be caused by the flux averaging time. If the averaging period is too small, larger eddies will not be sampled resulting in an underestimation of the flux and if the period is too large, smaller eddies will not be captured (Moncrieff *et al.*, 2004). In practice, fluxes are calculated over timescales of

between 30 minutes and up to one hour as this is thought to be a sufficient time for the largest scale eddies to be sampled by the system, whilst not missing the smaller eddies (Moncrieff et al., 2004).

Instrumental errors are caused by fundamental failings of the sensors such as sensor separation and sensor drift. Sensor separation occurs due to the physical separation of the scalar sensor from the anemometer, resulting in the covariance being calculated from two different points in space and time (Moore, 1986, Twine *et al.*, 2000). This error can be minimised by placing the scalar sensor as close to the anemometer as possible without causing flow distortion (Laubach and McNaughton, 1998). Errors in gas concentration measurements occur due to instrumental drift, thermal expansion, contamination or operational errors. Occurring on timescales of hours to days, it has generally been assumed that these errors are not important as the mean gas concentration does not affect the estimation of turbulent fluctuations (Fratini *et al.*, 2014). However, for instruments with a curvilinear calibration it can lead to flux errors on the order of 30-40% (Fratini *et al.*, 2014). A large instrumental error occurs with open path analysers and sonic anemometers, which are affected by precipitation events, water droplets and dew formation. This scatters the infrared or sonic signal and can result in a weakened or no signal leading to abnormal CO_2 concentration or wind velocity measurements (Haslwanter *et al.*, 2009).

Methodological errors are caused by deviations from the assumptions of the EC technique. As mentioned in section 3.3, one of the assumptions is that density fluctuations are negligible. However, due to water vapour density and temperature variations not associated with the net transport of the scalar, density fluctuations can cause an error. This can be corrected through the WPL correction (Appendix C), and although this correction can affect all trace gases, it tends to be large for CO_2. Additionally, the EC technique assumes that the surface of interest is horizontally homogeneous such that flow convergence and divergence is negligible. Errors caused by these assumptions not being met can be eliminated through sensible site selection. The EC technique assumes that the flux is fully turbulent, however this is generally not the case at night when the boundary layer collapses into a quasi-laminar boundary, resulting in the loss of the turbulent structure (van de Wiel *et al.*, 2011). As laminar flow becomes the dominant transport mechanism the assumption that the flux is fully turbulent is invalidated.

Table 3.0 Typical errors associated with eddy covariance measurements, which fluxes they affect, the error range and the correction applied in order to correct the error. Table modified from (Burba and Anderson, 2005)

Error	Flux Affected	Range (%)	Correction
Frequency Response	All	5 – 30	Frequency response correction
Sensor response	All	5 - 15	Adjust for delay
Spikes	All	0 - 15	Spike removal
Unlevelled instrumentation	All	0 – 25	Co-ordinate rotation
Density fluctuation	CO_2, H_2O, CH_4	0 – 50	WPL
Sonic temperature error	Sensible Heat	0 - 10	Sonic temperature correction
Gap filling	All	0 - 20	Methodology/tests

3.7 Frequency Response Corrections

Frequency corrections compensate for the loss of flux at different frequencies due to a diminished response caused by instrumental time response, sensor separation, scalar-path averaging and tube attenuation (Massman, 2000). All sensors display some form of high frequency attenuation due to instruments not being fast enough to capture rapid changes in gas densities or wind velocities (Massman and Clement, 2004). Moreover, the physical separation of scalar and wind sensors introduces further frequency attenuation as the covariance is based on measurements at two different points in space and time (Kristensen and Jensen, 1979). Tube attenuation (Massman, 1991) is an error, unique to closed path analysers, where long intake tubes (>1m) cause high frequency fluctuations in gas densities to be smoothed due to velocity profiles within the tube.

The correction of frequency dependent flux losses requires knowledge of the proportion of the flux attenuated across all measured frequencies, the true flux spectral behaviour and/or the attenuated flux at a certain frequency. However, attenuation can reduce the flux at high frequencies to magnitudes that are so low that the true flux cannot be accurately recovered. The

frequency response of a system is described by co-spectra, which are a set of equations describing the response for different atmospheric conditions (stable, unstable and neutral) and use measured and calculated parameters such as stability (z/L), non-dimensionalised frequency (f=n(z-d)/U), measurement height (z), zero plane displacement (d) and mean wind speed (U) to obtain the co-spectral energy at each frequency (nC(n)).

The frequency response correction of fluxes required knowledge of the true and attenuated cospectra. However, true cospectra are not measureable and therefore assumptions are required to be made about their form. In EC experiments, the true cospectra is assumed from model cospectra based on measurements undertaken under ideal conditions such as Kaimal *et al.* (1972). Attenuated cospectra are readily calculable from measurements by multiplying the model true cospectra with the frequency response transfer functions. The flux correction factor can then be calculated as the ratio of the integrated true model cospectra to the integrated attenuated model cospectra.

A number of approaches can be used to estimate the frequency loss experienced by an EC system. These approaches can be broadly split into three categories; integration, analytical and pass band ratio. All of these methods are conceptually similar but differ in their implementation. The integration method, such as Moore (1986), uses co-spectral shape for an assumed unattenuated flux and a transfer function, which describes the loss of true flux at different frequencies. The transfer function and true cospectra are multiplied to obtain the attenuated cospectral shape. The analytical method (Massman, 2000) can be described as an updated version of the integrated method, but uses a general analytical solution to the integration method to obtain the flux correction factor. This method reduces the number of calculations required to calculate the flux correction. Whilst both the intergration and analytical methods employ transfer functions, the pass band ratio method employs the true and attenuated cospectra directly, by assuming that a spectral region exists where no attenuation occurs in the attenuated cospectra. The corrected attenuated flux is obtained by multiplying the ratio of attenuated to true flux within the unattenated spectral region by the true flux. Frequency correction methods are discussed in more detail in Appendix C or see Moore (1986), Massman (2000) or Kaimal *et al.* (1972).

The integration and analytical approaches are most commonly used with the EC method and for the purposes of this study, the analytical method proposed by Massman (2000), hereafter referred to as Horst/Massman, was used to correct for frequency response flux loss. The Horst/Massman method uses a transfer function to correct for the loss of flux at different frequencies. The total transfer function is generated as the product of transfer functions for each

of the sensors describing flux losses at different frequencies due to errors such as tube attenuation or sensor separation. The transfer functions for each variable (Sonic temperature (Ts), CO_2 and H_2O) are applied to a co-spectral model, in this case the Horst/Massman model. The co-spectral model is adjusted for the transfer function at each frequency and a correction value determined. More details on frequency response corrections can be found in Appendix C.

3.8 Flux Processing

EC data are processed using software packages, such as EdiRe (University of Edinburgh, Edinburgh, UK) or EddyPro (LI-COR Biosciences Inc., Lincoln, NE, USA). A study by Mauder et al. (2008) found that the difference in processed fluxes between EC processing software packages was around 5-10% for 30-minute CO_2 flux values. However, the authors concluded that conceptually different ideas about the selection and implementation of processing steps had the biggest influence on CO_2 flux estimates rather than the use of different programmes. The workflow for the processing of EC data in this research can be seen in Figure 3.3.

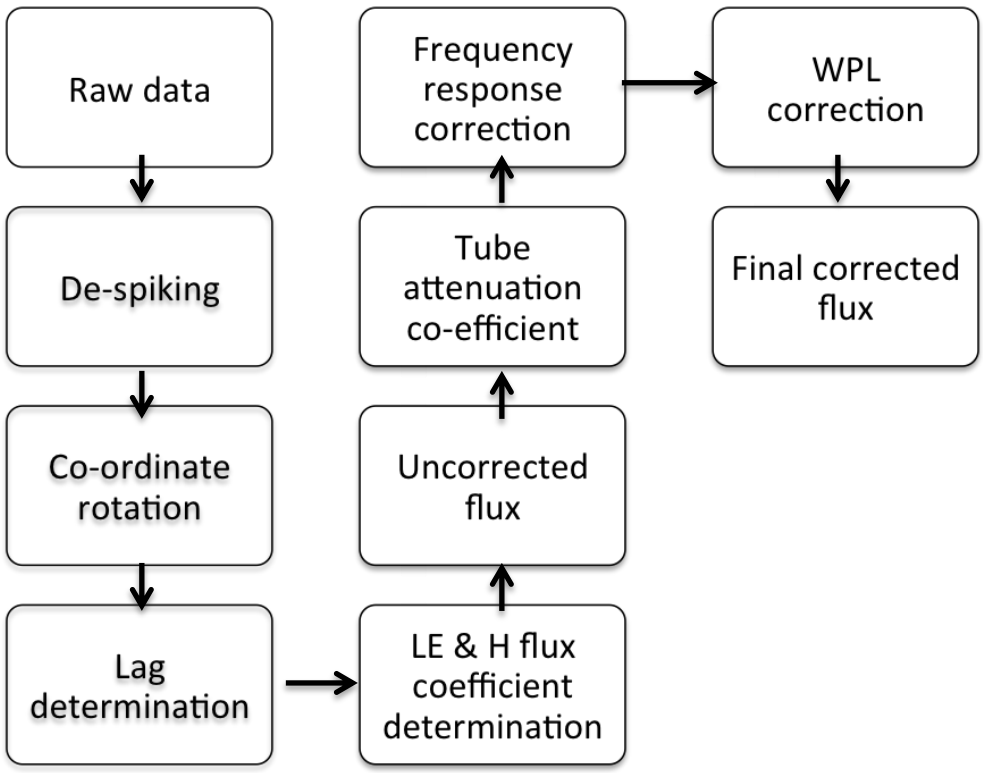

Figure 3.3 Flow chart describing the main steps required for processing raw high frequency EC data into final corrected fluxes. This is not exhaustive and is based upon the general flux processing procedures used in this research. LE is latent energy, H is sensible heat, WPL is the Webb Pearman Leuning correction (Appendix C)

The first part of flux processing is to remove spikes and non-physical values in the raw EC data due to instrument or electrical noise. This is performed through de-spiking, where data more than a set number of standard deviations from the population mean are removed; in this study 5

standard deviations were used. Co-ordinate rotations account for imperfect sonic mounting and are used to bring Cartesian rotation coefficients into a stream-wise coordinate system. This also removes any contamination of the vertical wind vector by the horizontal components of atmospheric turbulence (Burba and Anderson, 2005). Lag determination calculates the lag between sensors and is performed using a cross-correlation technique to maximise the covariance between the measurements of vertical wind velocity and the scalar (Foken, 2008, Aubinet *et al.*, 2012). Uncorrected fluxes of latent energy (LE), sensible heat (H) and net ecosystem exchange (NEE) are calculated after coefficients of H and LE have been determined. The co-efficients are required to account for associations with temperature and humidity. These are applied to the covariance of vertical wind velocity and water vapour and temperature for each thirty-minute period to calculate the latent heat of evaporation (LE) and sensible heat flux (H) in W m^{-2}. The uncorrected flux for LE, H and NEE is calculated by the covariance of vertical wind speed with the scalar.

If a closed path analyser is used, tube attenuation needs to be calculated before frequency response corrections are applied to account for the imperfect sensors. The corrected flux can then be calculated by adding the frequency correction to the uncorrected flux. The WPL correction (Appendix C) is a procedure applied to LE and NEE fluxes in order to account of changes in concentration measurements that are related to fluctuations in density and temperature and not changes in the trace gas concentration. An additional correction to account for surface heating of the LI-COR LI7500 (LI-COR Biosciences Inc., Lincoln, NE, USA) analyser window (Burba *et al.*, 2008) by the body of the analyser should be applied at this point. However, this only applies to vertically mounted analysers, as the heat from the analyser rises straight up onto the window; mounting the analyser at an angle results in heat being dissipated away from the window (Burba *et al.*, 2008, Ueyama *et al.*, 2012, Levy and Gray, 2015). A fuller description of the individual terms in Figure 3.3 can be found in Appendix C and an example of the processing list used in this research found in Appendix B.

3.9 Post Processing

Flux post processing ensures that the data used in analyses are of the highest quality. This begins with friction velocity (u^*) filtering to remove or correct periods of low turbulence, which invalidate the EC theory. Data validation is assessed through energy balance closure, co-spectral and footprint models (Rannik *et al.*, 2012). Furthermore, gaps in the time series caused by instrumental problems, power breaks or periods of data acquisition under non-ideal conditions can be filled (Foken *et al.*, 2011, Papale, 2012). The gap filling in this study is discussed in section 3.9.4.

3.9.1 Quality Control

Quality control procedures ensure that only data within a range of tolerances are used. Although there are no set QC procedures for EC (Foken *et al.*, 2004), there are commonly used QC procedures such as tolerance ranges for each variable, flagging of precipitation events and the removal of non-stationarity periods (Foken *et al.*, 2012b). Night time quality control can be handled differently to daytime quality control due to stability issues. Due to the dominance of non-turbulent flows following the collapse of the boundary layer, stationarity tests are commonly applied to "clean" night time data. This test sets a criterion for the behaviour of airflow so that non-stationary periods can be flagged and not used in analyses.

3.9.2 *u** Filtering

Nocturnal fluxes are thought to be controlled by plant and soil respiration and should therefore be independent of *u**. However, EC is sensitive to *u** and nocturnal fluxes are typically observed to decrease with *u** (Goulden *et al.*, 1996, Aubinet *et al.*, 2012). Usually, a threshold is used to remove data during stable nocturnal conditions which invalidate the EC measurement principle, and can systematically underestimate the nocturnal C efflux (Goulden *et al.*, 1996). However, Miller *et al.* (2004) showed that small variations in the *u** threshold calculation, below which data are rejected, can change the sign of NEE, which is particularly important if the data are to be used for C budgeting. Although *u** filtering is commonly used by EC studies for correcting nocturnal NEE (Papale *et al.*, 2006, Lohila *et al.*, 2011), it is recognised that the estimation of nocturnal NEE needs to be re-investigated both theoretically and experimentally (Falge *et al.*, 2001, Van Gorsel *et al.*, 2007).

Typically, *u** values below the calculated threshold are removed, however, these data could also be corrected depending upon the final use of the data. If the data are to be used to assess functional traits of an ecosystem then values below the threshold can be removed, as it is not required for budgeting. If however, the data are required for annual C budgeting then data should be corrected. To do this, periods where the flux is observed to decrease with *u** are identified (See Goulden *et al.*, 1996, Papale *et al.*, 2006). Once thresholds have been identified, nocturnal NEE data are binned by *u** value in 0.05 increments. An absolute correction is applied to the data using modelled respiration data so a relationship with decreasing *u** is no longer observed. This is undertaken on each *u** bin individually to avoid over-correction.

3.9.3 Flux Partitioning

NEE partitioning allows the dynamics of respiration and photosynthesis to be understood. The method by Reichstein *et al.* (2005) uses an algorithm defining the short term temperature sensitivity of R_{eco}, avoiding biases introduced by confounding factors in seasonal data. To do

this, a short-term exponential approach is used to model nocturnal NEE as a function of air or soil temperature. Nocturnal NEE data are used to parameterise the Lloyd and Taylor (1994) respiration model:

$$R_{eco} - R_{ref} e^{Eo(1/Tref - To)-1/(T-To))}$$

(Eqn 3.6)

Where T_{ref} is the reference temperature, set to 10°C, Eo is the activation energy, a free parameter that determines the temperature sensitivity. T_o is the temperature at which ecosystem respiration reaches zero and is kept constant at -46.02°C to prevent over parameterisation of the model; T is the measured temperature.

Once R_{eco} has been calculated from nocturnal NEE measurements, daytime R_{eco} is calculated from daytime measurements of temperature. Gross primary productivity (GPP) is then calculated as the difference between NEE and R_{eco}:

$$GPP = R_{eco} - NEE$$

(Eqn 3.7)

3.9.4 Gap Filling

QC procedures and analyser down time results in time series gaps that need to be filled. Methods such as marginal distribution sampling (MDS), mean diurnal variation (MDV), look up tables and non-linear regressions, are all commonly used to fill these gaps (Falge *et al.*, 2001, Reichstein *et al.*, 2005). The MDS method was used in this study and is detailed below. In the MDS technique, three different scenarios are identified:

I. EC (H, LE, NEE) time series data are missing, but solar radiation, air temperature and vapour pressure deficit (VPD) are present.
II. Air temperature and VPD data are missing alongside the missing EC data, but solar radiation data are available.
III. As II, but solar radiation data are also missing.

In scenario I, missing data are replaced by a mean value under similar meteorological conditions, during a time window of ±7 days. Similar meteorological conditions are defined as; solar radiation, air temperature and VPD with a deviation equal to 50 W m^{-2}, 2.5°C and 5.0 hPa, respectively. If similar meteorological conditions are not identified during the ±7 day window it is increased to ±14 days.

In the 2nd scenario the same approach is taken, however similar meteorological conditions are defined by deviation of less than 50 W m^{-2} in solar radiation. In the case of scenario 3, missing values are replaced by mean values at the same time of day, ±1hr. In this case window size starts at ±0.5 days and becomes a linear interpolation from available data at adjacent hours. If after these steps all the values cannot be filled, the procedure repeats with increased window sizes until the value is filled. The quality of the data are classified depending on the averaging time window as shown in Table 3.1, where A is the highest quality gap filling, B is considered to be of acceptable quality, while C is considered to be of dubious quality. Gap filling is performed using the R programme REddyProc (Reichstein and Moffat, 2014), which also provides partitioned fluxes of GPP and R_{eco}.

Table 3.1 Classification of the quality for gap-filled values, depending on the method used and the averaging time window. Where it is not possible for a method to be used over a certain time averaging window, N/A is used. (Table adapted from: http://www.bgc-jena.mpg.de/%7EMDIwork/eddyproc/method.php)

Averaging-time window (days)	**Method**		
	1	2	3
0.5	N/A	N/A	A
1.5 – 2.5	N/A	N/A	B
> 2.5	N/A	N/A	C
7	A	A	N/A
14	A	B	N/A
>28	B	C	N/A
>56	C	C	N/A

3.9.5 Energy Balance

The energy balance is used as a means of data validation (Foken *et al.*, 2004, Leuning *et al.*, 2012), with key components being net radiation (R_{net}), latent energy, sensible heat flux, soil heat flux and soil heat storage. The energy balance validation theory is that if all key components sum to zero as required by the conservation of energy, then all possible transfers have been incorporated. Energy balance closure is determined by the linear regression of the sum of the turbulent energy fluxes (LE + H) against the measured available energy (R_{net} – ground heat – ground storage). However, it has been suggested that the energy balance of the Earth's surface cannot be fully represented with experimental data (Foken and Oncley, 1995). The research by Foken and Oncley (1995) found that at many sites the sum of available energy was larger than

the sum of turbulent energy. A synthesis from 50 site years of data across 22 FLUXNET sites shows that at half-hourly timescales, the average turbulent energy was underestimating the available energy by around 20% and proposed a half-hourly EBC range of 70 – 90 % (Wilson *et al.*, 2002). There are a number of reasons (Table 3.2) for the lack of energy balance closure (EBC).

Table 3.2 Reasons for the lack of energy balance closure using the eddy covariance method and references containing information on each of the possible reasons.

Possible reason for lack of EBC	Reference
Assumptions of EC not met	Leuning (2004)
Radiation measurement error	Halldin and Lindroth (1992)
Energy storage incorrectly measured	Meyers and Hollinger (2004); Haverd *et al.* (2007)
Advective flux divergence	Katul *et al.* (2006)
Low frequency meso-scale transport	Foken (2008)
Averaging period inadequacies	Finnigan *et al.* (2003)
High frequency losses	Moore (1986); Massman (1991); Massman (2000)
Coordinate system	Finnigan (2004)

Variations in soil heat capacity in peatlands due to changes with depth and soil moisture content over temporal and spatial scales make it difficult to measure ground storage (Leuning *et al.*, 2012). It has been suggested that commercially available heat flux plates do not work well in peat substrates due to these variations (Harding and Lloyd, 2008). This is therefore likely to have an effect on the energy balance closure and could in part explain the lack of complete energy balance closure at many peatland sites (Leuning *et al.*, 2012). Over a day this variation averages out, which is why a better EBC is achieved when assessed on a daily scale. EBC from other peatland sites in the Northern Hemisphere at similar latitudes has been found to be 75% (Runkle *et al.*, 2014) and 91% (Lohila *et al.*, 2011). It is currently not recommended to scale measurements to the surface energy budget due to the EBC problems (Baldocchi, 2003, Foken *et al.*, 2011).

3.9.6 Flux Footprint Calculations

The flux footprint defines the area influencing the turbulent flux. The flux footprint can sometimes be confused for fetch, which is used to refer to the upwind distance from the tower when describing the footprint. The source area is a fraction of the upwind surface containing

sources and sinks, contributing to the flux measured at a point (Rannik *et al.*, 2012). The source area is dependent upon the measurement height and wind direction, however the footprint is also sensitive to atmospheric stability and surface roughness (Leclerc and Thurtell, 1990). There are a number of models that can be used to determine the flux footprint such as Lagrangian models (Leclerc and Thurtell, 1990), one-dimensional models (Horst and Weil, 1992) and analytical models (Kormann and Meixner, 2001). In this research the method of Kormann and Meixner (2001) was used. This is an analytical method which uses power law profiles for wind speed and eddy diffusivity. The Monin-Obukhov similarity relationship is also added to this method after calculation of the power law profiles. However, this method assumes steady-state conditions during the course of the flux period and that there is no downwind contribution of point sources to the flux.

3.9.7 Uncertainty Analysis

All measured flux data are subject to some degree of uncertainty due to several sources of error such as instrumental error, poor sample design, calibration error and imperfect measurement conditions (Richardson *et al.*, 2012). Whilst uncertainties are unavoidable, they can be reduced through activities such as good sample design and careful equipment set up and maintenance. In order to statistically analyse modelled or measured data it is essential to understand the uncertainties associated with the data to help with its interpretation (Hollinger and Richardson, 2005).

Where possible, uncertainty is ascertained by repeated paired independent measurements from two flux towers within close proximity under identical conditions. Measurement uncertainty is therefore estimated as the standard deviation of the difference between the concurrent measurements. However, there are few flux sites that are able to undertake repeated paired independent measurements. Therefore another method proposed by Hollinger and Richardson (2005) uses paired measurements from one tower on successive days. In order for this to work, only measurements made under similar conditions are used. Similar conditions are defined as the same time of day to eliminate diurnal effects, half-hourly incident solar radiation within 75 $\mu mol\ m^{-2}\ s^{-1}$, air temperatures within 3°C and wind speeds within 1 ms^{-1}. The uncertainty is then calculated using the repeated paired independent measurement approach.

3.10 Implementation in the Flow Country

So far this chapter has discussed the theory of eddy covariance and procedures that were applied in this research to process raw data into final fluxes. In this section, the equipment used at each of the sites (Chapter 2) will be discussed before the performance of each system is discussed

with a focus on the energy balance closure, flux footprint and an analysis of the gap-filling procedures used.

3.10.1 Flux Towers

The research was carried out using three EC systems at the three sites outlined in Chapter 2. The set up at each site was kept as similar as possible to allow for easier inter-site comparison. However, some set up differences do exist between Lonielist (Chapter 2 - Section 2.3.1), Talaheel (Chapter 2 - Section 2.3.2) and Cross Lochs (Chapter 2 - Section 2.3.3)

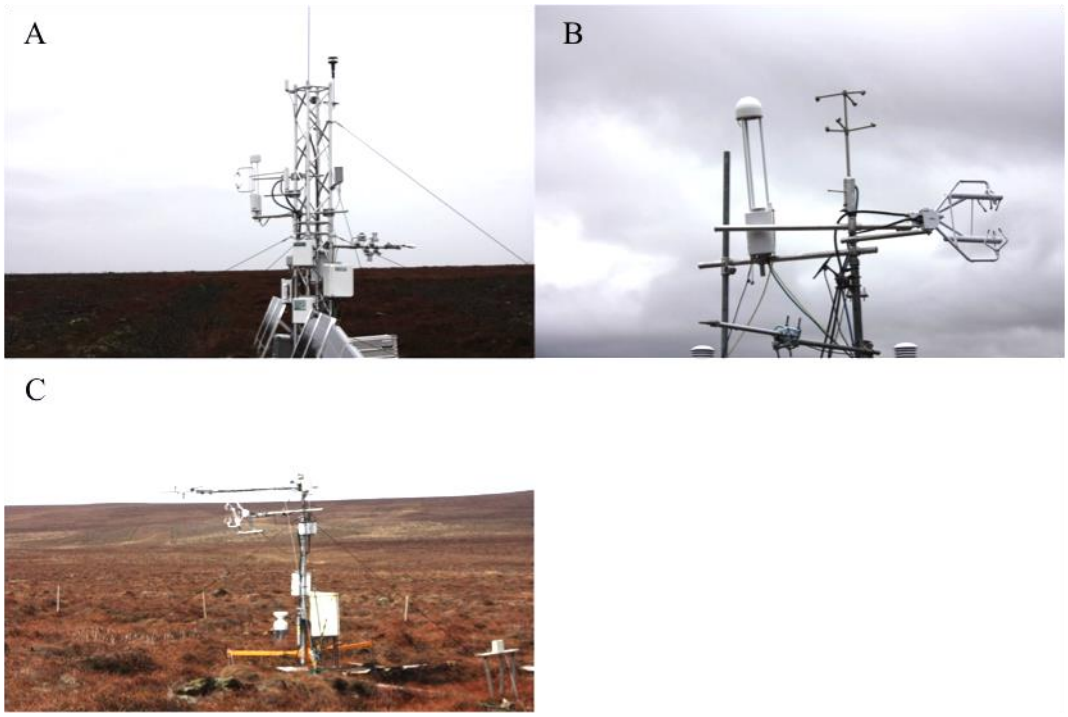

Figure 3.4 Photographs of the three flux towers at the three different sites. A) Lonielist; B) Cross Lochs; C) Talaheel.

The equipment deployed at each site is described in Table 3.3 and can be seen in Figure 3.4. All of the towers were set-up as similar as possible in terms of the equipment used and measurement height. Talaheel and Cross Lochs used open-path systems, while Lonielist was equipped with the latest LI-7200 enclosed path system. All of the sonic anemometers were mounted to face into the prevailing southwesterly wind direction. Data were recorded at a frequency of 10 Hz and environmental data collected once a minute. Details of the calibration co-efficients for each of the gas analysers can be found in Appendix A.

Table 3.3 EC and environmental sensors deployed on the flux towers at each site. * An additional LI-COR LI-7000 was also used at this site with a 5.8 m intake tube. ** This logger only stored the high frequency EC data; lower frequency environmental data were stored on a Sutron 9210B Xlite datalogger.

Variable	**Site**		
	Lonielist	**Talaheel**	**Cross Lochs**
Measurement Height (m)	3	3.37	3
Wind Speed	Gill HS3-50	Campbell Scientific CSAT3	Campbell Scientific CSAT3
CO_2/H_2O	LI-COR LI7200 Enclosed-Path	LI-COR LI-7500 Open-Path*	Campbell Scientific EC150 Open-Path
High Frequency Data Logger	LI-COR Li7550 Analyser interface**	Campbell Scientific CR5000	Campbell Scientific CR3000
Air Temperature/Humidity	Vaisala HMP155 probe	Campbell Scientific CS215 probe	Campbell Scientific CS215 probe
Net Radiation	Kipp and Zonen CRN4	Kipp and Zonen NRLite	Kipp and Zonen NRLite
Incident PAR	LI-COR LI-190SL Quantum	Skye Instruments SKP215 Quantum	Skye Instruments SKP215 Quantum
Shortwave Radiation	Delta-T SPN1	Apogee instruments SP110	-
Soil Temperature	UMS-TH3-s profile probe	Thermocouple	Campbell Scientific 109T
Soil Moisture	Sentek EasyAg 50 profile probe	Delta-T ML2x	-
Soil Heatflux	Huskeflux HFP01	Huskeflux HFP01	Huskeflux HFP01
Precipitation	Young 52202 tipping bucket	ARG100 tipping bucket	Davis 7852 tipping bucket
Water-table depth	-	Druck PDCR1830 pressure sensor	Druck PDCR1830 pressure sensor
NDVI	Skye Instruments SKR1860D	Skye Instruments SKR1860D	-

3.10.2 Talaheel environmental sensors

Environmental sensors used at Talaheel are listed in Table 3.3. The air temperature/humidity probe was encased in a naturally aspirated radiation shield and mounted at a height of 3.5 m. All of the solar radiation measurements were undertaken on a separate arm of the tower 45° to the south of the sonic arm. Soil temperature and moisture measurements were undertaken within in the footprint of the net radiometer. Soil temperature was measured at two depths in the furrow and original surface (0.05 m and 0.1 m) with a soil heat flux plate in between the temperature probes at 0.08 m depth. Soil moisture was also measured in the original surface and furrow microforms at a depth of 0.1 m. Precipitation was measured 1.5 m away from the tower and 0.5 m above the ground, to avoid rain splashing and snow burial, using a tipping bucket rain gauge with a calibration of 0.19 mm per tip. Water table depth was measured in the furrow closest to the EC tower with the probe housed within a 1 m piezometer. Environmental data were logged every minute and averaged over 30 minutes.

In addition to the main EC tower, a small, independent basic automatic weather station (BAWS) was placed 10 m from the EC tower. The Campbell Scientific BWS200 weather station (Campbell Scientific, Shepshed, UK) was equipped with a Young 03002 wind sentry (RM Young, Traverse City, Michigan, USA) for wind speed and direction. A CS215 probe encased in a naturally aspirated radiation shield was used to measure relative humidity and air temperature (Campbell Scientific, Shepshed, UK) and was mounted at a height of 1.5 m above the ground surface. Solar radiation was measured using a SKS1110 pyranometer (Skye Instruments, Llandrindod Wells, UK). The weather station was also equipped with a rain gauge for back up precipitation measurements. This rain gauge had a calibration of 0.3 mm of precipitation per tip. The whole system was powered using a single solar panel mounted on the enclosure for the CR200x datalogger (Campbell Scientific, Shepshed, UK) and battery. Data were logged at 30-minute intervals. The logger was equipped with internal flash storage allowing approximately 125,000 data points to be stored. The logger saved two separate tables, a high frequency half-hourly table and a daily average table.

3.10.3 Lonielist environmental sensor set up

The air temperature/humidity probe was encased within a naturally aspirated radiation shield and mounted at a height of 3 m. All of the solar radiation measurements were undertaken on a separate arm of the tower at 180° to the EC measurements, whilst measurements of soil temperature and moisture were undertaken within half a metre of this area. Soil temperature and moisture were measured using profile probes, which gave measurements at 0.1 m increments in top 0.5 m of soil. Environmental data were logged at a frequency of once a minute

and averaged over 30 minutes using a Sutron 9210B Xlite data logger (Sutron Corporation, Sterling, Virgina, USA).

3.10.4 Cross Lochs environmental sensor set up

Air temperature and humidity were measured at a height of 1.8 m using a single probe encased within a naturally aspirated radiation shield to stop sun shining directly on the probe biasing the measurements. The net radiometer was mounted at a height of 2 m in a northerly direction so that measurements of soil temperature and soil heat flux were carried out within the net radiometer footprint. Soil temperature was measured at a depth of 0.1 m and the soil heat flux was measured below the temperature probe at a depth of 0.12m. Water table depth was monitored using a pressure transducer housed within a piezometer half a metre from the tower in a north westerly direction. Precipitation was measured 5 m west of the tower to eliminate the likelihood of contamination through water droplets falling from the arms holding EC equipment into the rain gauge, which had a calibration of 0.20 mm per tip.

3.10.5 Power

Power for all three sites was obtained mainly by solar panel arrays, ranging from 395 W at Cross Lochs to over 1 kW at Lonielist and Talaheel. Small wind turbines provided back up power at Lonielist and Talaheel whilst all three sites were equipped with Efoy Pro 800 methanol fuel cells (SFC Energy, Munich, Germany) as an additional backup power option. Battery banks provided power storage, allowing for the system to continue running during periods of low incident radiation or low wind. The loss of the wind turbine at Talaheel during a storm in January 2015 increased the need for the fuel cell.

3.11 Data processing

The raw data from Talaheel and Cross Lochs were processed using the processing software EdiRe (University of Edinburgh, Edinburgh, UK), whilst Lonielist data were processed using EddyPro (LICOR Biosciences Inc, Lincoln, NE, USA). EddyPro was used with Lonielist data as this was to be used with these data in the future so to keep it consistent with future datasets it was decided to process this with EddyPro, whilst Talaheel and Cross Lochs datasets had already been processed using EdiRe. The processing steps used were kept the same between all three datasets. Previous research has shown there to be little difference in the use of different packages for processing EC fluxes, and that the different use of processing steps is a bigger source of uncertainty (Mauder *et al.*, 2008). Post-processing of data were undertaken in MATLAB (R2013a). The processing of raw data followed the same process outlined in section 3.8 and post-processing followed the same as outlined in section 3.9. Flux footprints were calculated using the Kormann and Meixner (2001) model. For Talaheel and Cross Lochs this

was undertaken in EdiRe with the same procedures applied to the Lonielist data in EddyPro. The LI-7500 heat flux adjustment proposed by Burba *et al.* (2008) was not applied to the data at Talaheel due to the generally low insolation and mild temperature environment. Additionally, this correction was primarily meant for vertically mounted analysers and not those mounted at an angle (Reba *et al.*, 2009, Ueyama *et al.*, 2012, Levy and Gray, 2015). Sensor separation was not considered a source of error at Cross Lochs as the EC150 CO_2/H_2O analyser is designed to work within the transducer head of the CSAT3, allowing for vertical wind and scalar data to be collected at the site point with no separation.

3.11.1 Frequency response corrections

Frequency response corrections were undertaken on all the data using the Horst/Massman model described in section 3.7, which uses a transfer function to correct for the loss of flux at different frequencies. The area under each plot in Figure 3.5 is equal to the flux. In plots 3.5E and 3.5F the Horst/Massman model is shown in green. The darker grey line in Figure 3.5E shows the measured co-spectra from the CSAT3 and its departure from the Horst/Massman model. The lighter grey line displays the Kaimal (1972) model and the more extreme departure from the measured flux, highlighting that the Horst/Massman model was the more appropriate model to use for these data.

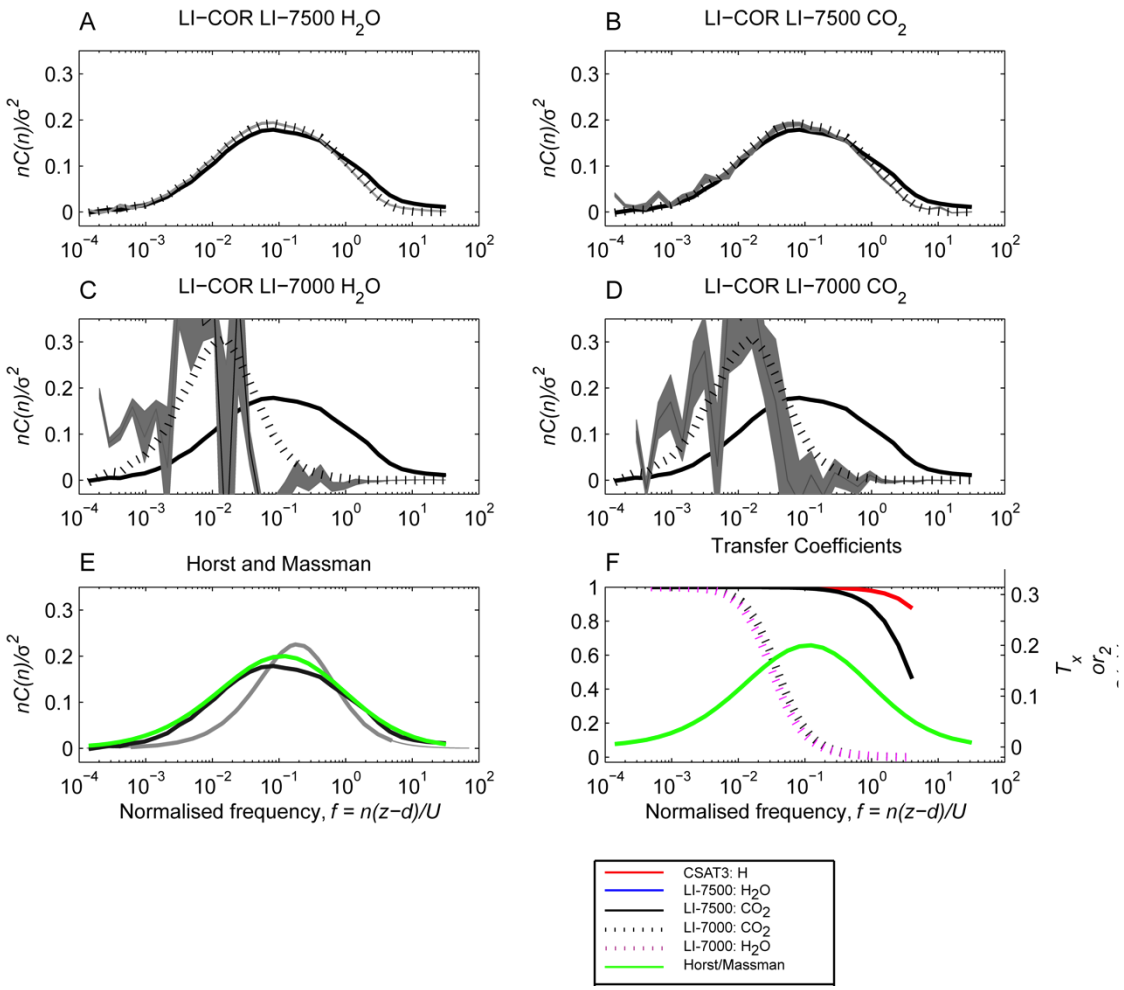

Figure 3.5 Example of co-spectra for A) LI-7500 H_2O with the attenuated signal as the solid line with trapezoidal error and the dotted line displaying the Horst/Massman corrected signal along with the CSAT3 Ts co-spectra B) LI-7500 CO_2 with the attenuated signal as the solid line with trapezoidal error and the dotted line displaying the Horst/Massman corrected signal along with the CSAT3 Ts co-spectra C) LI-7000 H_2O with the attenuated signal as the solid line with trapezoidal error and the dotted line displaying the Horst/Massman corrected signal along with the CSAT3 Ts co-spectra D) LI-7000 CO_2 with as the attenuated signal the solid line with trapezoidal error and with the dotted line displaying the Horst/Massman corrected signal along with the CSAT3 Ts co-spectra E) Sonic temperature (dark grey) and the departure of the measured co-spectra from the Kaimal (1972) model (light grey line) and the Horst/Massman model (green line). F) Transfer functions for sonic temperature, CO_2 and H_2O. Subplots of modelled and measured co-spectra. All of these data are from the instrumentation at Talaheel.

The loss of frequency for each of the measured components, CO_2, H_2O and sonic temperature, at Talaheel can be clearly seen in Figure 3.5. For CO_2, the frequency loss was relatively small with the co-spectra for CO_2, sonic temperature (Ts) and the modelled cospectra generally showing good correlation, while the H_2O was not quite as well correlated. At high frequencies, above 10^0 Hz, the co-spectra for CO_2 and H_2O began to drop off more quickly than Ts, caused by detection limits of the system. These losses at high frequencies resulted in an underestimation of CO_2 and H_2O fluxes.

Quality control (QC) procedures were kept as similar as possible across all sites. Firstly, threshold limits above which data would automatically be removed were set to extreme values, based on fluxes from published data (Levy and Gray, 2015), and allowed for seasonal cycling and spatial variation. In this study CO_2 fluxes above 50 μmol CO_2 m^{-2} s^{-1} were considered extreme and automatically removed. Data were then filtered to exclude any further outliers by binning the data by photosynthetic photon flux density (PPFD) into 20 bins so as to allow for variation in the fluxes due to the diurnal cycle and seasonality. Outlying values were excluded when they exceeded 5 standard deviations from the mean of the binned data. Data were then checked for diagnostic flags from the sonic or the infrared gas analyser (IRGA). The primary diagnostic flag for each of the IRGA's was the automatic gain control (AGC) value. This is a measure of the cleanliness of the optical path. As the optical path accumulates dirt, through particles in the air, or becomes blocked due to water accumulating on the window, the AGC value increases until the optical path is completely blocked at which point the AGC value reads 100. Data with AGC values 20% over the baseline value of 50 were excluded (Ruppert *et al.*, 2006). Sonic data were excluded when the diagnostic flag was greater than 0 suggesting a transducer path blockage. Data from wind directions where the power generation equipment were stored were excluded as this represented a significant source of disruption to the turbulent structures. Total EC data loss at Talaheel over the period of study was on the order of 52%, whilst EC data loss at Lonielist was slightly lower at 44%. However, data loss at Cross Lochs was significantly higher at 66% due to data logger issues, which resulted in the complete loss of high frequency data. It is estimated that most EC sites typically achieve around 40 – 60% data coverage over annual timescales, although 40% is considered adequate coverage in order to obtain defensible annual sums (Falge *et al.*, 2001). Due to the extreme data loss at Cross Lochs calculations of annual budgets were not attempted.

3.12 System Performance

The system performance was evaluated through some of the measured or calculated components, such as the energy balance (section 3.9.5) and flux footprint coverage (section 3.9.6). The gap-filling procedure can also be evaluated using some of the outputs from this procedure.

3.12.1 Energy balance closure

As mentioned in section 3.9.5 the EBC is determined by linear regression of the sum of the turbulent energy fluxes and measured available energy.

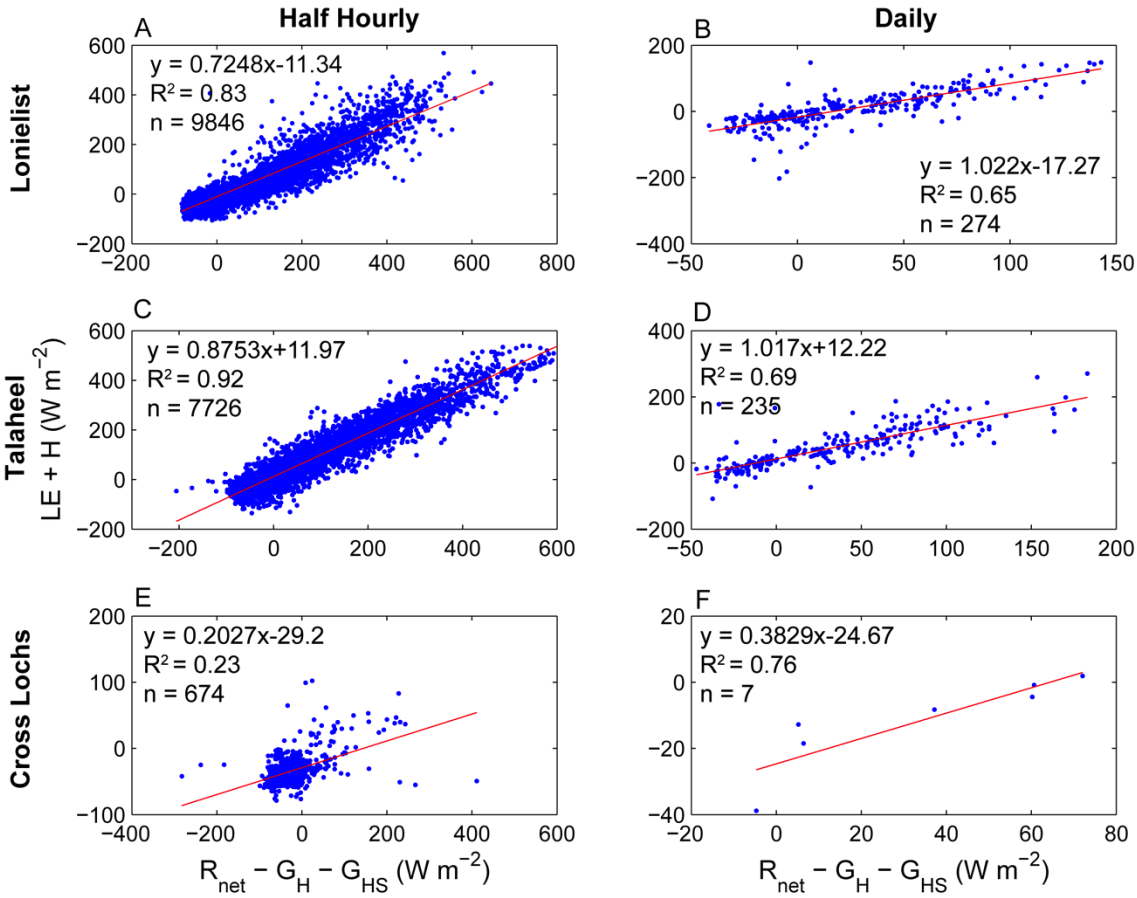

Figure 3.6 Energy balance closures from all sites using QC'd half-hourly LE and H fluxes. Available energy measured using corresponding QC'd data from net radiometer, soil temperature probes and soil heat flux plates. The equation and co-efficient of determination are displayed on each plot along with the number of data points used.

The half-hourly EBC at Talaheel was 87.5% (Figure 3.6C), in the range of energy balance closures from other northern peatland sites of 75% (Runkle *et al.*, 2014) and 91% (Lohila *et al.*, 2011). Lonielist had a slightly lower half-hourly EBC of 72.5% (Figure 3.6A), while EBC at Cross Lochs was significantly lower at only 20.3% (Figure 3.6E). This indicates that at all sites there is some energy, which remains unaccounted for either due to it not being physically measured or poor measurement by the sensors. The daily EBC at Lonielist (Figure 3.6B) and Talaheel (Figure 3.6D) was 101% and 102% respectively, which is within the range of 75% - 118% proposed after a FLUXNET multi-site EBC analysis (Leuning *et al.*, 2012). The improvement in closure over daily timescales compared to half-hourly timescales is likely indicative of lags relating to the storage of heat in the air, vegetation canopy and peat, and the minimised noise compared to half-hourly data (Leuning *et al.*, 2012). Lack of closure at the

half-hourly timescale is likely related to noisier data and the measurement of G_H as soil heat flux plates are known to perform poorly in peat substrates due to the large variations in soil heat capacity (Harding and Lloyd, 2008). It has also been demonstrated that it is difficult to accurately measure storage in peat substrates due to the large variation in soil heat capacity due to changes with depth and soil moisture content over temporal and spatial scales (Leuning *et al.*, 2012).

The data from Talaheel and Lonielist are within the typical ranges of other peatland sites and EBC from other ecosystems indicating that these data represent good quality. However, the data from Cross Lochs suggests that significant amount of energy remain unaccounted. Following current recommendations, no attempt was made at scaling NEE measurements to the surface energy budget (Baldocchi, 2003, Foken *et al.*, 2011).

3.12.2 Flux Footprint

Another tool that can be useful for understanding how good the recorded fluxes are is to assess the footprint of the EC tower. The footprint is the area of ecosystem that is seen by the sensors on the tower within the fetch and how much of this influences the flux.

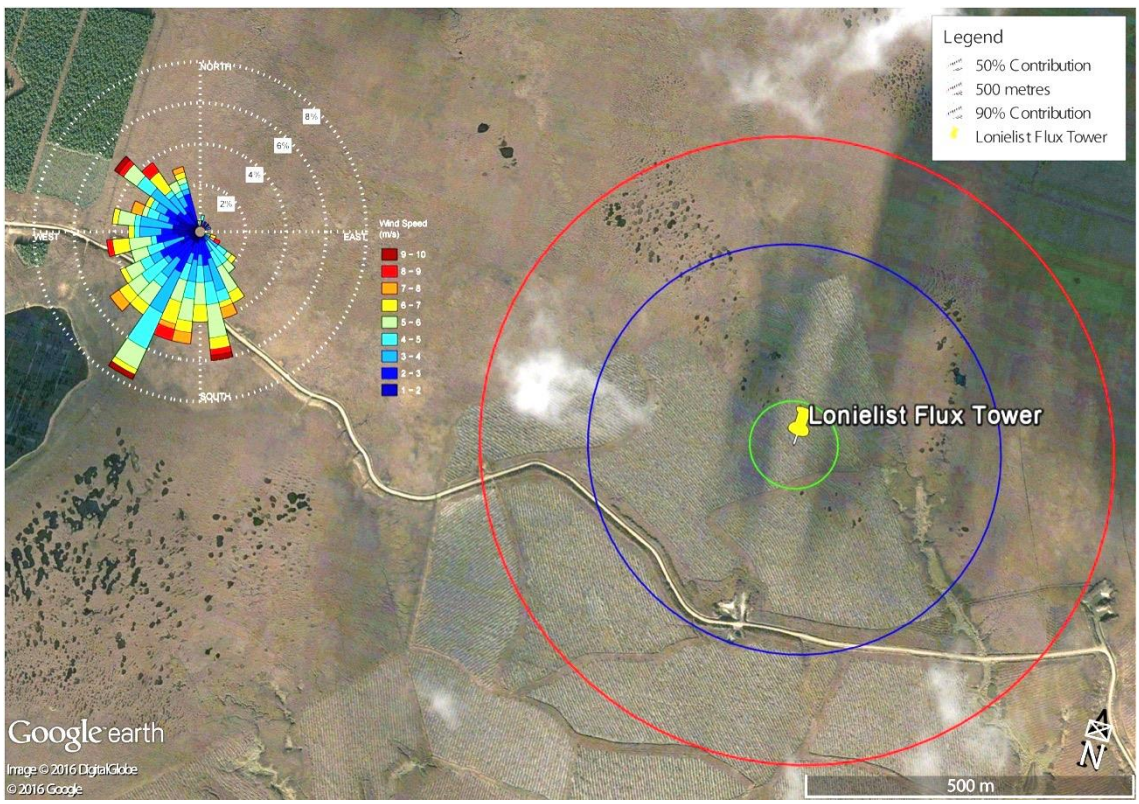

Figure 3.7 Map of the Lonielist flux tower (Yellow pin) footprint with a 500-metre radius around the tower marked in red. The distance contributing 90% of the flux is marked in blue and the distance contributing 50% of the flux is marked in green. Inset displays a wind rose of

daily mean wind speed (m/s) and direction (º) at Lonielist during the period of study (Map Data: Google, getmapping plc., 2016).

At Lonielist, a distance of 70 m contributed 50% of the measured flux, which as can be seen in Figure 3.7 is completely covered by blanket bog restored from plantation forestry. A distance of around 350 m contributed 90% of the measured flux, with the majority of this covered in the land use of interest (Figure 3.7). However in some cases, depending on the direction of the wind, there was potentially some influence from an area of unmanaged blanket bog to the north of the site within which was a small system of peatland pools. To the south of the site and right on the edge of the 90% contribution, was an access track. This track was rarely used and thus was likely to have had little influence on the data, especially given that the dominant wind direction was southwesterly (Figure 3.7 - Inset).

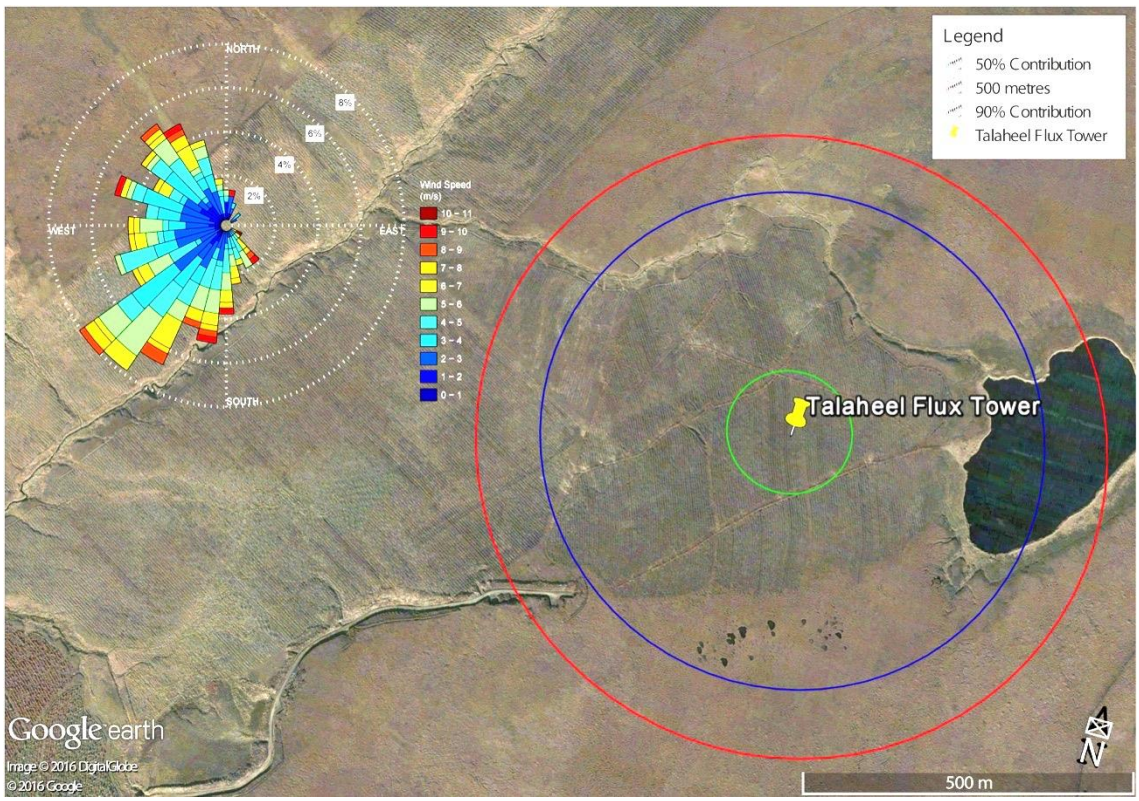

Figure 3.8 Map of the Talaheel flux tower (Yellow Pin) footprint with a 500-metre radius around the tower marked in red. The distance contributing 90% of the flux is marked in blue and the distance contributing 50% of the flux is marked in green. Inset displays a wind rose of daily mean wind speed (m/s) and direction (º) at Talaheel during the period of study (Map Data: Google, getmapping plc., 2016)

At Talaheel, a distance of around 85 m provided 50% of the measured flux (Figure 3.8). In all directions this was covered by the land-cover of interest, blanket bog restored from forestry plantation. A distance of approximately 380 m contributed 90% of the measured flux (Figure 3.8). To the north east of the site there was potential for influence from Loch Talaheel, however

due to the positioning of the solar array and wind turbine winds from this direction were excluded due to potential distortion of the eddies. An area of unmanaged blanket bog to the south of the site, which also had a small peatland pool system, had an influence on the 90% contribution. However, as the dominant wind direction was southwesterly (Figure 3.8 - Inset) this influence was rare.

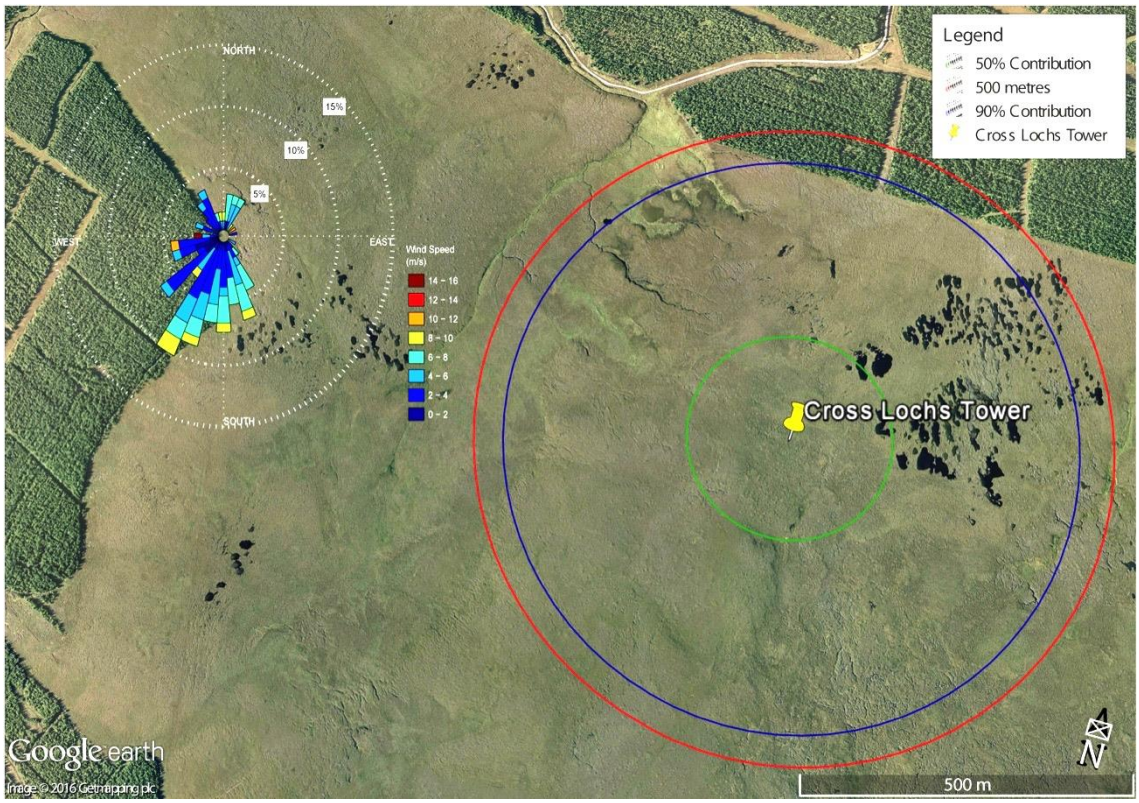

Figure 3.9 Map of the Cross Lochs flux tower (Yellow Pin) footprint with a 500-metre radius around the tower marked in red. The distance contributing 90% of the flux is marked in blue and the distance contributing 50% of the flux is marked in green. Inset displays a wind rose of daily mean wind speed (m/s) and direction (º) at Cross Lochs during the period of study. Areas of foresty to the north of this map have been felled since this image was obtained (Map Data: Google, getmapping plc., 2016)

A distance of around 150 m contributed 50% of the measured flux at Cross Lochs (Figure 3.9). On the northern edge of this 50% perimeter was a large peatland pool complex, which was subject to research on gaseous and aqueous greenhouse gas fluxes by other researchers. A greater contribution of this pool system was observed in the 90% contribution, when the wind was from a northerly direction. Data were rejected from a northeasterly direction due to the presence of the solar array and wind turbine, which had the potential to distort turbulent structures. As the dominant wind was southwesterly (Figure 3.9 - Inset) the majority of the flux was observed from blanket bog. To the north of the site, on the edge of the 90% contribution

there was an area of felled forestry, the influence of which upon the flux was likely to be small and dependent on the wind direction (Figure 3.9).

3.12.3 Gap filling procedure

In this study the Marginal Distribution Sampling (MDS) method (Reichstein *et al.*, 2005) was used, as discussed in section 3.9.4. Where necessary, meteorological data were filled from the independent automatic weather station at Talaheel. During the period of study, it was rare that meteorological data were missing, and data from the weather station only had to be used on two occasions. Other gaps in the data were confined only to the high frequency EC data and meteorological data tables were unaffected. However, a large gap in data at Cross Lochs between April and July 2014 due to data logger issues affected both the high frequency EC and lower frequency meteorological data. It was not possible to fill this gap due to the length of the gap, which spanned both the spring and summer. Gap filling of these data would have resulted in a bias in the final filled data. The quality of the gap filling across all the sites can be seen in Figure 3.10. At all sites over 85% of the gaps were filled using method one, where all meteorological variables were available. At each site, over 87% of the gaps were filled within a time window of 14 days or less.

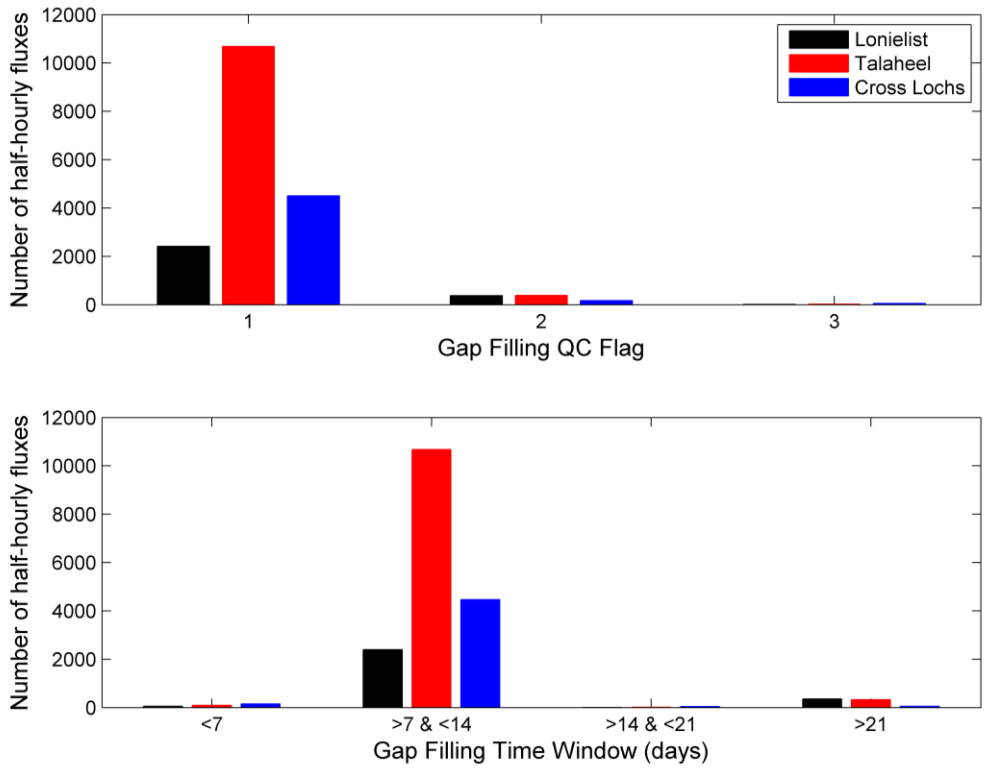

Figure 3.10 The top plot shows the gap filling methods used in the MDS gap filling procedure for NEE at Talaheel. The QC flags 1,2 and 3 refer to the 3 filling scenarios listed in Table 3.2. The bottom plot displays the time- averaged window length used, also displayed in Table 3.2.

In order to provide a means of evaluating the gap filling procedure, artificial gaps were created and filled to provide a comparison between gap-filled and measured fluxes. The gap filled and measured NEE at Talaheel (Figure 3.11C) show good correlation (R^2 = 0.88). The model residuals (Figure 3.11D) show a greater number of negative residuals when the gap filled NEE are high (i.e respiration); therefore the model is overestimating respiration in relation to the measured values. The RMSE shows a difference between the modelled and measured values of 0.61 μmol m^{-2} s^{-1}, which is in the range observed in a synthesis of 15 gap filling techniques (Moffat *et al.*, 2007). Similar relationships were also observed at Lonielist (Figure 3.11A) where a good correlation was observed between the gap filled and measured NEE (R^2 = 0.75), but there was an overestimation in the gap filled values at high NEE (Figure 3.11B), whilst RMSE showed a slightly bigger difference between gap filled and measured NEE 0.81 μmol m^{-2} s^{-1}. Gap filling performance at Cross Lochs was poorer (Figure 3.11E), with a weak correlation (R^2 = 0.62) and a larger RMSE (2.5 μmol m^{-2} s^{-1}). Several large gaps within the data set are likely to account for some of this, as this reduces the number of data points for the averaging procedure as well as changes in ecosystem properties, such as leaf senescence, influencing the gap filling (Moffat *et al.*, 2007). At all sites, the off-structure residuals were caused by the poor performance of the gap filling procedure during nocturnal periods. This poor performance is typical of the MDS and other gap-filling methods (Moffat *et al.*, 2007) due to inherent problems with eddy covariance data during nocturnal periods caused by the collapse of the turbulent structure within the atmosphere.

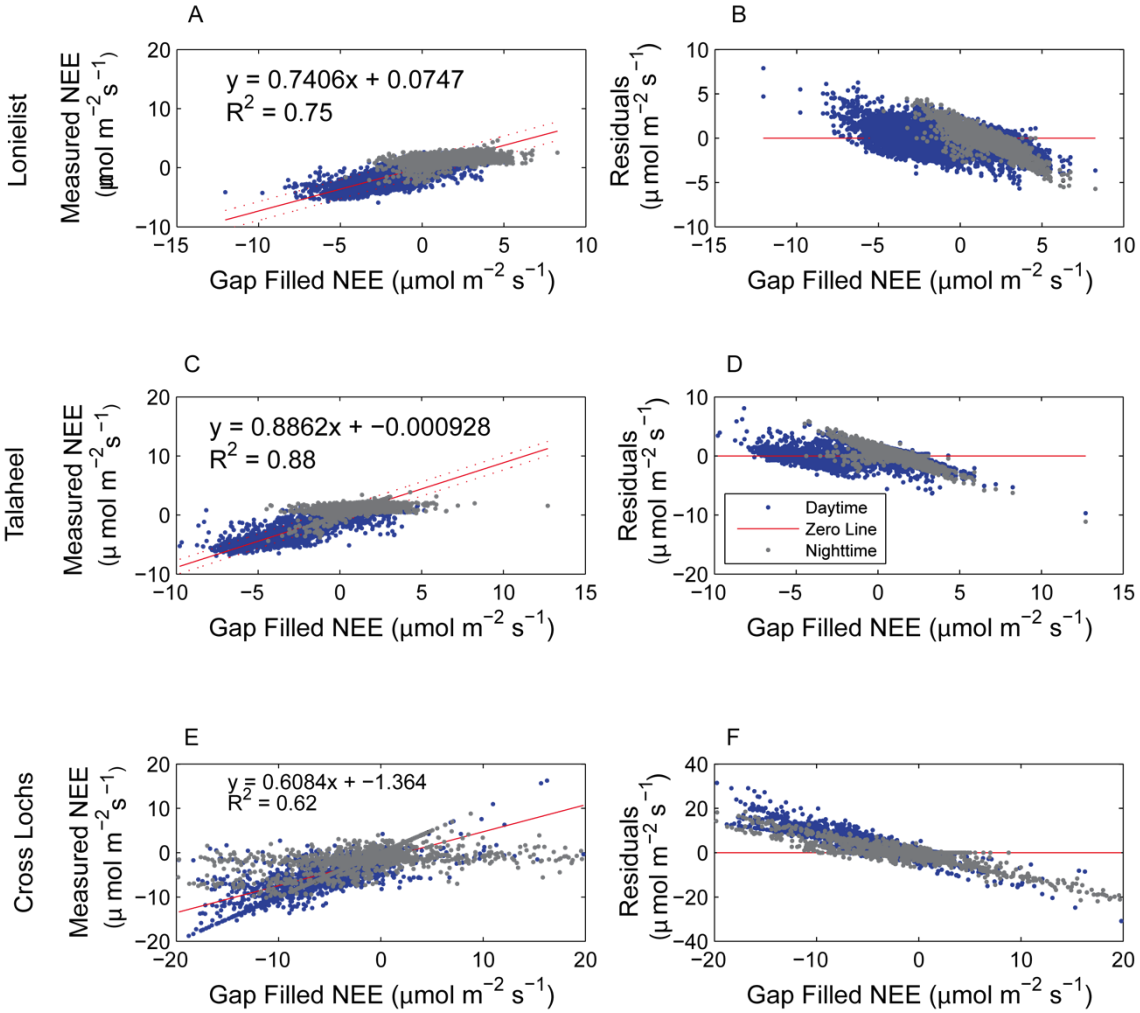

Figure 3.11 Gap-filling evaluation for data obtained from the three EC towers. Gap-filled NEE data are artificial gaps introduced by the gap-filling tool in order to assess the method. Data shown are half-hourly fluxes in units of µmol m^{-2} s^{-1}. Daytime (incident solar radiation >20 µmol m^{-2} s^{-1}) values are represented by blue markers, whilst nocturnal measurements (incident solar radiation <20 µmol m^{-2} s^{-1}) are denoted by black markers Residuals show any under- or over-estimation of the gap filling procedure.

3.12.4 Uncertainty analysis

Hollinger uncertainty analysis showed the least uncertainty in NEE measurements at Lonielist (0.93 µmol m^{-2} s^{-1}). This is to be expected as the analyser is enclosed, eliminating noise associated with precipitation events as occurs with open-path analysers, such as those at Talaheel and Cross Lochs. Uncertainty at Talaheel (1.8 µmol m^{-2} s^{-1}) was almost double that of Lonielist, primarily due to precipitation related errors, which reduced the number of paired measurements available with which uncertainty could be estimated. Uncertainty was higher again at Cross Lochs (2.8 µmol m^{-2} s^{-1}) due to a lower number of paired measurements, due to tower downtime and the same precipitation related errors observed at Talaheel due to the open-path analyser. Similar patterns were observed in latent energy with the least uncertainty observed at Lonielist (5 W m^{-2}) and the greatest observed at Cross Lochs (36 W m^{-2}).

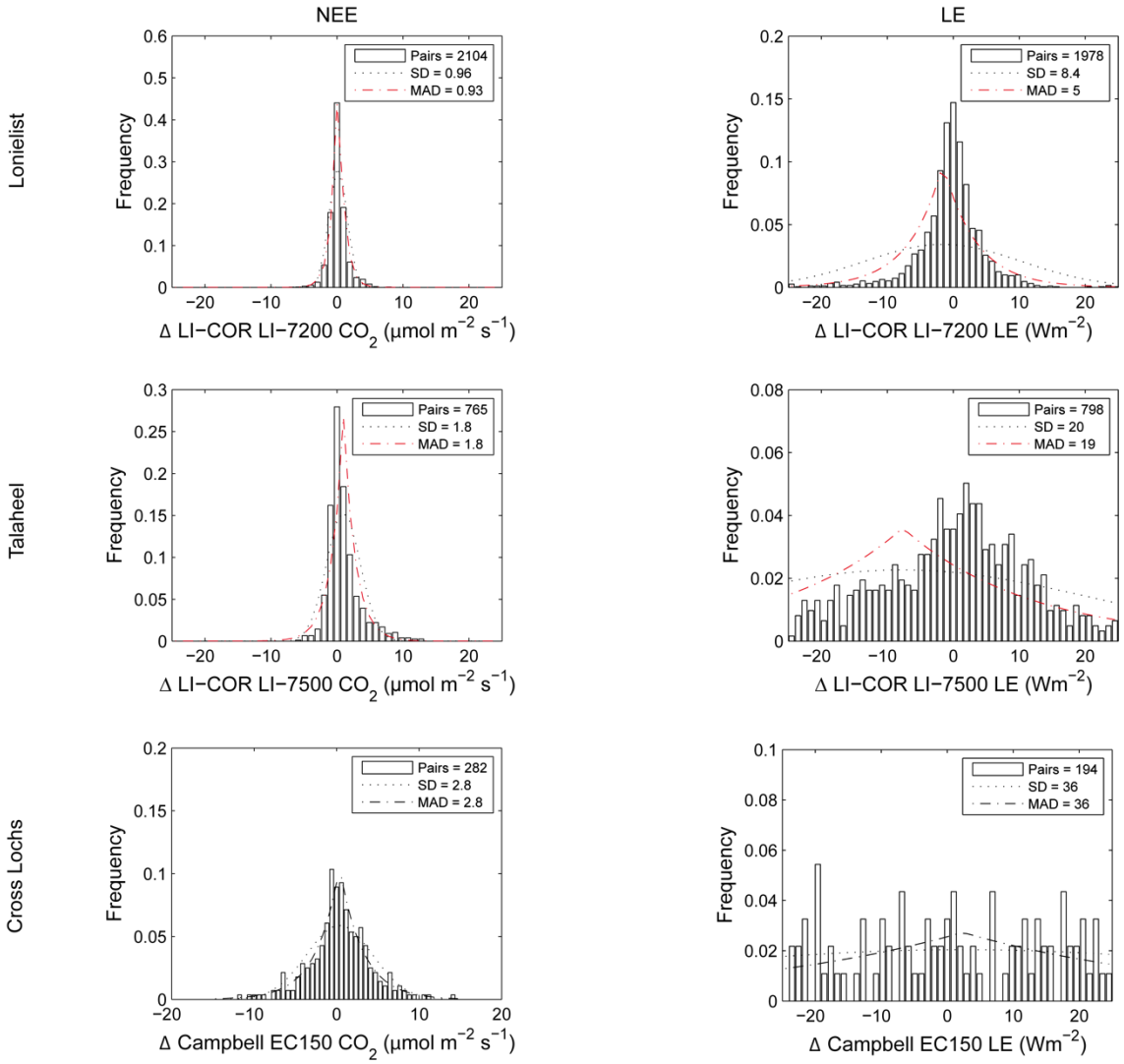

Figure 3.12 Hollinger uncertainty analyses carried out on net ecosystem exchange (NEE) and latent energy (LE) data. SD denotes the standard deviation and MAD the Hollinger uncertainty estimate derived as the standard deviation of the difference between two measurements on successive days during the same time period and under similar environmental conditions.

3.13 Other Methods

As mentioned in section 3.1, eddy covariance is good for resolving mesotope scale changes in CO_2 fluxes, but is unable to determine smaller microform scale changes in fluxes. To improve our knowledge of C dynamics in restored ecosystems it is important to understand the key drivers of C cycling at the microform scale and the influence of microtopography on this. Changes at the smaller microform scale have a big influence on mesotope scale fluxes and are likely to play an important role in C dynamics under future climatic change. Therefore, closed dynamic chamber measurements were carried out within the footprint of the flux towers at Talaheel (Chapter 2 - section 2.3.2) and Cross Lochs (Chapter 2 - Section 2.3.1). Additionally, data from a previous chamber study over a chronosequence of newly restored and older

restoration sites are presented. Alongside chambers, measurements of peat depth and peat C:N status were undertaken.

3.14 Chamber methods

Chamber methods were used to understand the influence of microtopography on C dynamics and key environmental drivers to aid understanding of C cycling at the microform scale in restored peatland ecosystems. Two different chamber studies were used, firstly I undertook dark chamber measurements for respiration with the samples analysed by gas chromatography in 2011/12 across a chronosequence of sites undergoing restoration, with data processing taking place in the first year of this PhD. Secondly, in response to the results gained from the first study, a second study was started using transparent chambers in order to be able to capture both photosynthesis and respiration. This study was focussed on Talaheel and Cross Lochs, and was more focussed on the influence of microtopography on C dynamics rather than understanding the influence of restoration on C fluxes.

3.14.1 Sample Design

As the main interest in this part of the research was concerned with understanding the influence of the different microtopographic features, the sampling was designed to cover these areas. In Talaheel, 3 chambers were placed on each microform and replicated 3 times (Figure 3.13C), to give a total of 9 chambers across the site. At Cross Lochs, the chambers were split by the hummock and hollow microform, with 3 chambers placed on each giving a total of 6 chambers (Table 3.4).

Table 3.4 Total number of measurements made at Talaheel and Cross Lochs using the static chamber method.

	Talaheel	Cross Lochs
Number of Chambers	9	6
Microform	Furrow	Hummock
	Ridge	Hollow
	Original Surface	
Sampling Campaigns	8	4
Total number of fluxes	648	288

In order to understand the light response of these different microforms, measurements were undertaken on each chamber with different degrees of shading. A coarse mesh of ~0.05 m, a finer mesh of ~0.002 m and finally a thick black bag to completely darken the chamber were

used to give shading of approximately 25%, 75% and 100%. Sampling was initially undertaken on a bi-monthly basis at Talaheel, before increasing to monthly sampling during spring and summer. This unintentionally decreased during autumn and winter due to weather conditions preventing safe access to sites. Efforts were made to ensure sampling was undertaken around the same time each month and around the same time of day.

Data from a previous study undertaken in 2011/12 which did not specifically look at microtopography but are nevertheless relevant to this study and included in the analyses. Due to the different focus the experimental design was different (Figure 2.14). Here, two chambers were placed on each microform and replicated three times across the sites, giving a total of 6 chambers on each microform and 18 in total across each site.

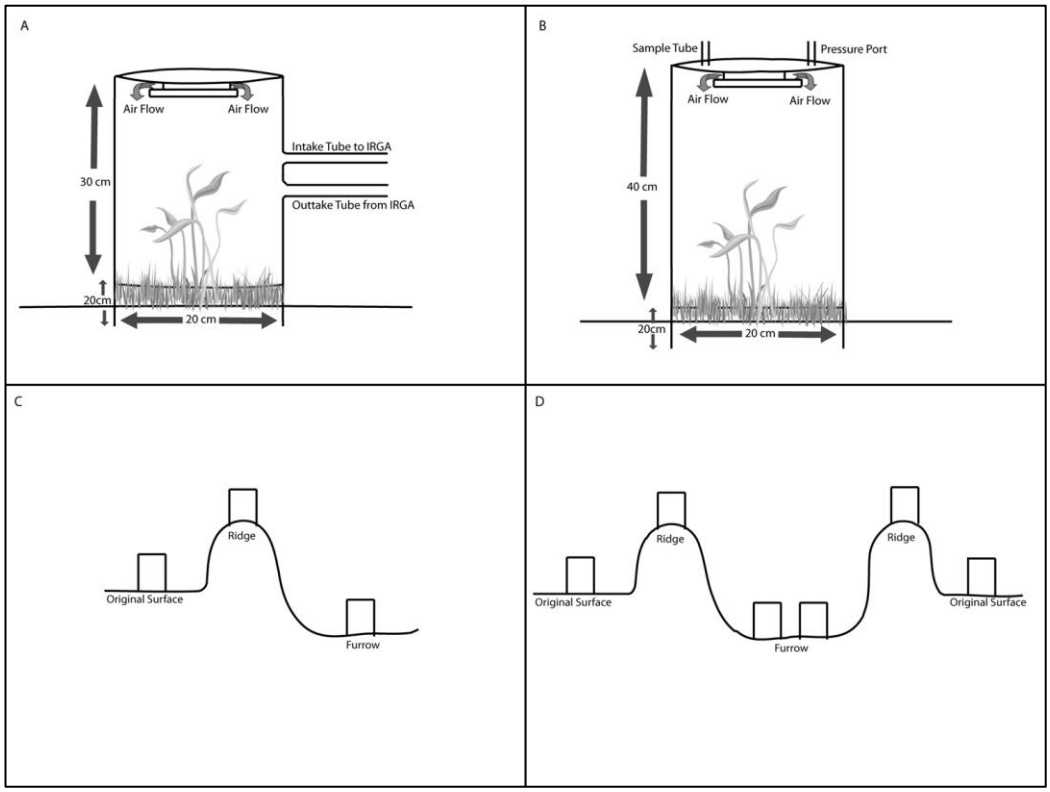

Figure 3.13 Diagrammatic representation of the chambers and the experimental setup used in this study. A) Chamber used in the 2014/15 research at Talaheel and Cross Lochs. B) Chamber used in the 2011/12 research across the chronosequence. C) Experimental set up used in 2014/15, which was replicated 3 times across the site. D) Experimental set up used in 2011/12, which was replicated 3 times across the site.

3.14.2 Chamber Design

A transparent cylinder (Figure 3.13A) with a diameter of 0.2 m, height of 0.3 m, and wall thickness of 0.003 m was used; the cylinder was sealed at one end with a transparent disc. A transparent computer fan with a diameter of 0.1 m was mounted to the disc, powered using an external 12 V battery to ensure good mixing of air within the chamber (Pumpanen *et al.*, 2004,

Christiansen *et al.*, 2011). The fan was mounted upside down and approximately 0.005 m from the top of the chamber to allow air to first move up and then back down. This was performed so as to reduce potential effects of turbulence and pressure gradients within the chamber (Denmead, 2008, Rochette, 2011). As this chamber was used for photosynthesis measurements, everything used within the chamber was kept as transparent as possible to reduce potential shading effects within the chamber footprint. Two holes were drilled in the side of the chamber, 0.08 m from the top of the chamber, and 0.08 m apart. These were equipped with pneumatic bulkhead tube connectors to give an input and output from the chamber to the IRGA. Percentage shading caused by equipment within the chamber was estimated at 20%. The percentage shading was calculated by measuring the light (PAR) outside the chamber on a clear day and then placing the chamber on the collar and measuring the light (PAR) levels within the chamber and calculating the difference between the light levels outside and inside the chamber.

The chambers used in 2011/12 (Figure 3.13B), were similar to these chambers, but were slightly taller at 0.4 m and were only used for respiration measurements so were constructed from opaque, heat reflecting materials and were fitted with sampling tubes in order to draw the sample out using a syringe for injection into pre-evacuated 12mL Exetainers® (Labco Ltd, Lampeter, UK).

3.14.3 Collar Installation

In both 2014/15 and 2011/12, permanent collars were installed to a depth of approximately 0.12 m to limit horizontal movement of gas within the top 0.1 m where most of the productivity was expected to take place. The collars were inserted approximately 6 weeks prior to the start of the sampling to allow settling of the system after disturbance (Holland *et al.*, 1999). However, due to a lack of equipment and issues with flux towers, which required significant amounts of labour time, Cross Lochs sampling did not begin until September 2014.

3.15 Sampling and analysis protocol

3.15.1 2011/12

Gas fluxes were measured by enclosing an area of 0.031 m^2 for a period of 18 minutes with chambers connected to the collars using a cross section of Land Rover inner tube (Teh *et al.*, 2014). Chamber placement was performed with as much care as possible so as not to lean on the chamber or stand next to the collar, potentially causing ebullition of soil gases (Christiansen *et al.*, 2011). Each chamber was equipped with a 1.5 m length of 0.06 m inner diameter bev-a-line tubing so as to prevent trampling near the chamber during sampling. This tube was flushed 3 times with a 20 mL syringe before each headspace gas sample was taken. Samples (20 mL) were collected at four regular time intervals (0, 6, 12, 18 minutes) using a gas tight syringe and

stored in pre-labelled, pre-evacuated 12 mL Exetainers® (Labco Ltd., Lampeter, UK). Prior to gas sampling, the soil temperature, air temperature and barometric pressure measurements were taken. At the end of sampling a reading of the chamber temperature was taken and a soil sample taken for soil moisture content.

Collected gas samples were analysed with a Thermo TRACE GC ULTRA (Thermo Fisher Scientific Inc., Waltham, Massachusetts, USA) at the University of St Andrews. The instrument was equipped with a HayeSep-Q column to give chromatographic separation and the analyte concentration quantified using a flame ionisation detector (FID) with methaniser. The precision of the instrument was determined by calculating the coefficient of variation of the standards analysed in each run, which were always below 5%. Certified standards of 372 ppm, 998 ppm and 5000 ppm were used to create a calibration curve to ascertain headspace concentration of each sample.

3.15.2 2014/15

Gas fluxes were measured by enclosing an area of 0.031 m^2 for a period of 120s with chambers connected to the collars using a cross section of Land Rover inner tube (Teh *et al.*, 2014). The chamber was connected to a PP-Systems EGM-4 CO_2 infrared gas analyser (PP-Systems, Amesbury, Massachusetts, USA) by two lengths of bev-a-line tubing, each approximately 1 m long. The analyser was always placed behind the chamber, so as not to cast a shadow on the chamber, potentially affecting the measurements. The EGM-4 was used in the closed system respiration mode (probe type 8), which stores data every 4.8 seconds over the length of run. The run duration was limited to a change of 50 ppm or 120 s if the concentration change was lower than this limit. Care was taken not to disturb the collar prior to positioning the chamber, potentially creating an efflux. If collar disturbance occurred, a visual check of the initial concentration of the chamber was performed, the measurement was stopped and the chamber was left for 5 minutes to allow CO_2 to disperse before repeating the measurement.

As this chamber was used to quantify the light response, two measurements were made with different levels of shading in the order: 0% shading (clear), ~25% shading (coarse), ~75% shading (fine) and 100% shading (Dark). At the end of each measurement, the chamber was removed to allow the conditions within the chamber to return to ambient conditions. Prior to taking measurements with the next level of shading, the shade cloth was placed over the collar to allow vegetation to adapt to the new light conditions. In each run, two measurements were made with each level of shading in the order: no shading, coarse, fine and black cover. Light levels were recorded on the outside of the chamber and underneath the shade cloth using an SKP-215 quantum PAR sensor (Skye Instruments, Llandrindod Wells, UK). As well as

recording light levels, measurements of air and soil temperature (10cm) were made using type-K thermocouples (Hanna Instruments Ltd., Woonsocket, RI, USA) and soil moisture probes (ML2x, Delta-T Devices, Cambridge, UK), concomitant with flux sampling. Chamber temperature was also recorded at the start and end of each measurement.

3.16 Processing and QC

The headspace concentration (ppm) was plotted against time (seconds) using R 3.1.2 (R, 2012) with the *HMR* flux estimation package (Pedersen *et al.*, 2010) used to determine flux rates. Lines of best fit were plotted to headspace concentration against time for each individual chamber (Pedersen *et al.*, 2010, Teh *et al.*, 2014). The ideal gas law (Eqn 3.8) was used to convert gas-mixing ratios to areal fluxes in order to solve for the quantity of CO_2 in the chamber headspace in moles (Livingston and Hutchinson, 1995):

$$n = \frac{PV}{RT}$$

(Eqn 3.8)

where P is the absolute pressure in pascals (pa), V is the volume of gas in cubic metres (m^3), n is the amount of gas in moles, R is the ideal gas constant (m^3 pa K^{-1} mol^{-1}) and T is the temperarure in kelvins (K). As per standard practices, this was normalised to the surface area of each chamber (Livingston and Hutchinson, 1995, Teh *et al.*, 2014).

QC procedures were performed on the data to define and exclude outlying values to limit erroneous results. The QC procedure occurred in two stages; firstly, fluxes with a recorded zero flux were removed by the *HMR* flux estimation programme as no change was detected in the headspace concentration, indicating a leak in the chamber or a problem with the analysis. Secondly, the *HMR* package provided a *P*-value for the null hypothesis of a zero flux, therefore fluxes with a *P*-value greater than 0.05 were removed.

3.17 Soil Analysis

Soil carbon (C) and nitrogen (N) analyses were undertaken for site characterisation and to see whether differences in C:N content existed between the restored and undrained sites. It was decided to only sample the original surface and ridge to keep the data consistent with a dataset previously recorded at Lonielist. A 1 m box corer was used to obtain a peat core from the original surface. This was split into 6 different measurement depths: 0 - 0.1 m, 0.1 - 0.2 m, 0.2 - 0.3 m, 0.3 - 0.4 m, 0.4 - 0.5 m and 0.9 - 1.0 m. At Talaheel and Cross Lochs, peat samples were obtained from a single transect running from the EC tower in a south-westerly direction and

taken at 3 points; 10 m, 75 m and 150 m with GPS co-ordinates recorded for each peat sample. At Talaheel, a smaller 0.3 m box corer was used to take a sample of peat from the nearest ridge surface to the point where it became level with the original surface. Peat depths were also recorded for each core, by taking a measurement of peat depth at the sampling point and at 4 points around the core. Collected samples were stored in zip-lock bags and kept cool prior to sample preparation and analysis.

Once in the lab, samples were split vertically to keep the 0.1 m profile intact. One half of each sample was placed in a sample tray and left to air-dry in the lab to avoid potential issues of the oven becoming too hot and beginning to burn off the organic fraction. Samples were milled before being sieved to remove vegetation and aggregates. The sieved sample was milled again until the sample was in a powder form, suitable for elemental analysis. Analyses of carbon and nitrogen content were performed at the James Hutton Institute using a Flash 1112 elemental analyser coupled via a conflo III to a Finnigan delta^{plus} XP gas source mass spectrometer (EA-IRMS - Thermo Finnigan, Bremen, Germany). After every ten samples a duplicate sample was run to test instrumental precision with a replicate error <5%.

The other half of the sample was placed in a pre-weighed, pre-labelled sample tray before being weighed to determine the initial wet weight. The samples were placed in a drying oven at 105°C for 24 hours (O'Kelly, 2007) before being weighed again to determine final dry weight. Volumetric water content, bulk density and water-filled porosity were then calculated using established methods (Breuer *et al.*, 2000).

3.18 Peat Depth

Peat depth was determined by walking 10 transects in a 100 x 100 m grid within the expected footprint of the EC tower (Figure 3.8). On each transect 10 peat depths were measured at 10 m intervals. A modified drain cleaning rod was used to measure the depth of the peat. To take a peat depth measurement, the rod was pushed into the ground until it could be pushed no further. If it was thought that this was due to some debris, and thus was not representative, the measurement was moved a metre to the right of the original measurement area. The measurement was recorded by observing the nearest pre-marked depth on the rod and measuring to the peat surface. In addition to recording the peat depth, a GPS recording was made and noted down along with the microform type. These measurements were in addition to those which were taken at the time of the C: N analysis.

3.19 Chapter Summary

This chapter has provided an overview of the EC and chamber methods employed in this thesis. The EC theory has been explained along with an overview of the required instrumentation to make the measurements. Details of the techniques used in taking raw vertical wind and scalar data and processing these into final fluxes were provided. A description of the QC procedures used in order to minimise erroneous data outwith set thresholds have been provided. Post-processing techniques such as gap filling, used to fill unavoidable gaps in the EC flux records, have been described along with the procedures used to partition NEE measurements into its constituent fluxes of GPP and R_{eco}. The role of the EBC as a means for validating the fluxes measured by the EC technique has been discussed. The use of dynamic chambers and the sampling, measurement and QC protocols used have been discussed along with other methods, such as soil analysis and peat depth measurements.

~ Chapter 4 ~

Ecosystem respiration dynamics in restored Flow Country peatlands

4.0 Abstract

Northern peatlands play a crucial role in the regulation of atmospheric CO_2 concentrations with uptake of carbon (C) from the atmosphere greater than respiratory losses to the atmosphere from decomposition. However, these systems have been severely degraded by drainage, switching the net C sinks to sources due to increasing aerobic decomposition and subsequently respiration. Peatland restoration aims to reverse this change and restore the net C sink status of peatlands by raising water tables, thereby reducing the area of peat under aerobic conditions and diminishing respiratory losses. Using eddy covariance techniques over a chronosequence of two restored peatlands during one year, this study sought to examine time dependent changes in ecosystem respiration (R_{eco}) as a result of peatland restoration in the Flow Country of Northern Scotland. Moreover, key environmental drivers were assessed to better understand R_{eco} dynamics and how these change with time since the onset of restoration.

Results showed that peatland restoration was successful at reducing C losses to the atmosphere, with the oldest site, restored in 1997/98 (Talaheel), emitting 480g C m^{-2} yr^{-1} whilst the younger site, restored in 2003/04 (Lonielist), emitted 581 g C m^{-2} yr^{-1}. Seasonal differences were observed, with the highest R_{eco} fluxes observed in summer and the lowest R_{eco} fluxes observed in winter. Significantly higher median daily R_{eco} was observed during the winter period at the younger site (Lonielist; 1.07 ± 0.43 CO_2 μmol m^{-2} s^{-1}) relative to the older site (Talaheel; 0.62 ± 0.24 μmol CO_2 m^{-2} s^{-1}). Soil moisture and temperature were key environmental drivers with higher R_{eco} fluxes observed during warm, dry conditions, particularly at the younger site, where higher measured soil temperatures, due to the lower peat moisture content, increased measured R_{eco}. Seasonal R_{eco} followed similar patterns to air and soil temperature, indicating they were the greatest drivers of R_{eco} across the restored sites. Observed R_{eco} fluxes were within the range of other northern peatland ecosystems, although the younger site's R_{eco} was at the top end of that range.

4.1 Introduction

Soil respiration is an important part of the C cycle and plays a critical role in regulating atmospheric CO_2 concentration with soils, globally, estimated to emit around 68 – 75 Pg CO_2-C yr^{-1}, which equates to approximately 10% of the atmospheric CO_2 pool (Raich and Schlesinger, 1992, Raich and Potter, 1995). It is estimated that around two-thirds of terrestrial carbon (C) is stored belowground with a substantial amount of this respired by roots and microbes in the soil (Hibbard *et al.*, 2005, Scharlemann *et al.*, 2014). Northern peatlands hold approximately one-third of the world's soil organic carbon (SOC), which is equivalent to more than half of the carbon (C) held in the atmosphere (Dorrepaal *et al.*, 2009). However, anthropogenic impacts on peatlands have led to the degradation of northern peatlands with approximately 15 million ha having been drained for forestry, predominantly in northern and eastern Europe (Paavilainen, 1995, Minkkinen and Laine, 1998). In the UK, over 1.5 million ha of blanket peat have been drained for various uses, such as agriculture, forestry and peat cutting since the early 1900s (Holden *et al.*, 2004). Over 500,000 ha of the drained UK peatlands have been afforested with non-native plantation forestry since World War II (Cannell, 1993). Significant efforts are now underway in the Northern Hemisphere to return degraded peatlands back to active peat forming ecosystems. In the Flow Country, over 2500 ha of forested peatlands have been restored to date, with significantly more planned for the future.

In undisturbed blanket bogs, R_{eco} is the second largest transfer of C between the land surface and atmosphere after gross primary productivity (GPP - Limpens *et al.*, 2008)**,** due to larger photosynthetic inputs than respiration losses (Ward *et al.*, 2007)**,** making these ecosystems net C sinks. Above-ground net primary productivity (ANPP) of northern peatlands is lower than the ANPP of other northern ecosystems because of saturated, anaerobic conditions and lower concentrations of essential nutrients (Frolking *et al.*, 1998). However, accompanied with this low productivity are small respiratory losses, giving rise to soil carbon accumulation rates that are approximately 10 times larger than other ecosystem soils (Schlesinger, 1990, Frolking *et al.*, 1998). Ecosystem respiration (R_{eco}) is the sum of the autotrophic and heterotrophic components of soil respiration (Yvon-Durocher *et al.*, 2012) and is directly measured by the eddy covariance (EC) method in the absence of light. Autotrophic respiration (Ra) is the metabolism of organic matter by plants with approximately 50% of the C fixed during photosynthesis re-emitted to the atmosphere through autotrophic respiration (Dawson and Smith, 2007, Smith *et al.*, 2010). Heterotrophic respiration (Rh) occurs during the decomposition of plant litter, root exudates and organic matter by soil microorganisms with the gaseous by-products transported to the atmosphere via diffusion, advection or ebullition (Hibbard *et al.*, 2005, Redeker *et al.*, 2015).

Heterotrophic respiration is dependent upon multiple factors such as substrate availability, aerobic status of the ecosystem and microbial activity.

In undrained peatlands, R_{eco} is thought to be controlled by a range of biotic and abiotic factors, such as vegetation composition, soil temperature and soil moisture (Armstrong *et al.*, 2015). The height of the water table has two potential impacts on R_{eco}, firstly by affecting gas diffusion rates through the peat profile (Levy *et al.*, 2012, Armstrong *et al.*, 2015) and secondly affecting the depth of the aerobic zone, which leads to greater decomposition and greater CO_2 release through Rh (Dorrepaal *et al.*, 2009). Furthermore, microbial communities affect the amount of Rh in the ecosystem, with substrate availability and chemical composition of the peat known to affect the composition of microbial communities (Bragazza *et al.*, 2012). Climatic conditions, such as temperature are thought to be one of the main controllers of R_{eco} (Freeman *et al.*, 2001, Dorrepaal *et al.*, 2009). Many northern peatlands show distinct seasonal changes in R_{eco} with warmer temperatures enhancing R_{eco} and C cycling in summer (Lafleur *et al.*, 2005b, Ward *et al.*, 2007, Clark *et al.*, 2008). These drivers of R_{eco} are not independent, with well-known interactions between R_{eco} and the thermal and hydrological conditions of the peat (Waddington *et al.*, 2002, Kettridge and Baird, 2008).

Peatland drainage reduces the height of the water table resulting in greater areas of peat under aerobic conditions and larger losses of CO_2 to the atmosphere with emissions to the atmosphere observed to increase by 100 – 400% after peatland disturbance or drainage (Nykanen *et al.*, 1995, Nykanen *et al.*, 1997, Waddington *et al.*, 2002). Furthermore, a loss of *Sphagnum* mosses and other peat-forming vegetation results in a reduction in productivity and Ra (Waddington *et al.*, 2002, Holden *et al.*, 2004). Waddington *et al.* (2002) found R_{eco} rates from drained sites were around three times higher than those measured from undrained sites, due to the lowering of the water table and a reduction in photosynthesis through vegetation loss. Peatland restoration seeks to return drivers of R_{eco} to pre-disturbance levels, such as restoring the water table height and stability (Holden *et al.*, 2008), reducing the thickness of the aerobic zone and thus reducing the Rh component of R_{eco} (Parry *et al.*, 2014). Research in Canada has shown that re-wetting drained peatlands can significantly decrease R_{eco} by approximately 80% (Waddington and Warner, 2001). Research undertaken at other sites in Canada also found similar reductions in R_{eco} thought to be due to the re-wetting and re-vegetation of the peat, (Strack and Zuback, 2013, Strack *et al.*, 2014).

Little empirical evidence exists across a wide range of northern peatlands of how R_{eco} and known drivers of R_{eco} respond to restoration over annual to decadal timescales. Moreover, peatland restoration projects are typically undertaken on scales of tens of metres making it

unsuitable for the eddy covariance (EC) technique (Waddington and Price, 2000). Chamber measurements are often undertaken at lower frequencies during winter compared to summer, which creates a bias in the data (Komulainen *et al.*, 1999, Juszczak *et al.*, 2013, Strack and Zuback, 2013). The aim of this research is to understand R_{eco} dynamics and the key environmental drivers across a chronosequence of two restored peatlands. To achieve this aim the following research questions are proposed:

1. How does peatland restoration affect R_{eco}?

2. How does restoration impact key drivers, such as temperature and moisture?

4.2 Site Descriptions

All work was undertaken on sites situated within the Forsinard Flow National Nature Reserve (58°23'59"N, 3°49'28"W) in Caithness and Sutherland, northern Scotland. Talaheel (58°24'49"N, 3°47'52"W) was the oldest site and encompassed an area of around 380ha. Before restoration began in 1997/98, the site was planted in the 1980s with a mixture of lodgepole pine (*Pinus contorta*) and Sitka spruce (*Picea sitchensis*. The site was relatively flat with a gentle slope of 1-3° at an altitude 196 m above mean sea level. The site had a mean peat depth of around 2 m. The furrows on the site were spaced approximately 1.5 to 2 m apart with a depth of 0.3 m below the original surface. Ridge peaks were approximately 0.1 to 0.15 m above the original surface. Some woody material was still present in the furrows, although in many places this had been overgrown by *Sphagnum* spp.

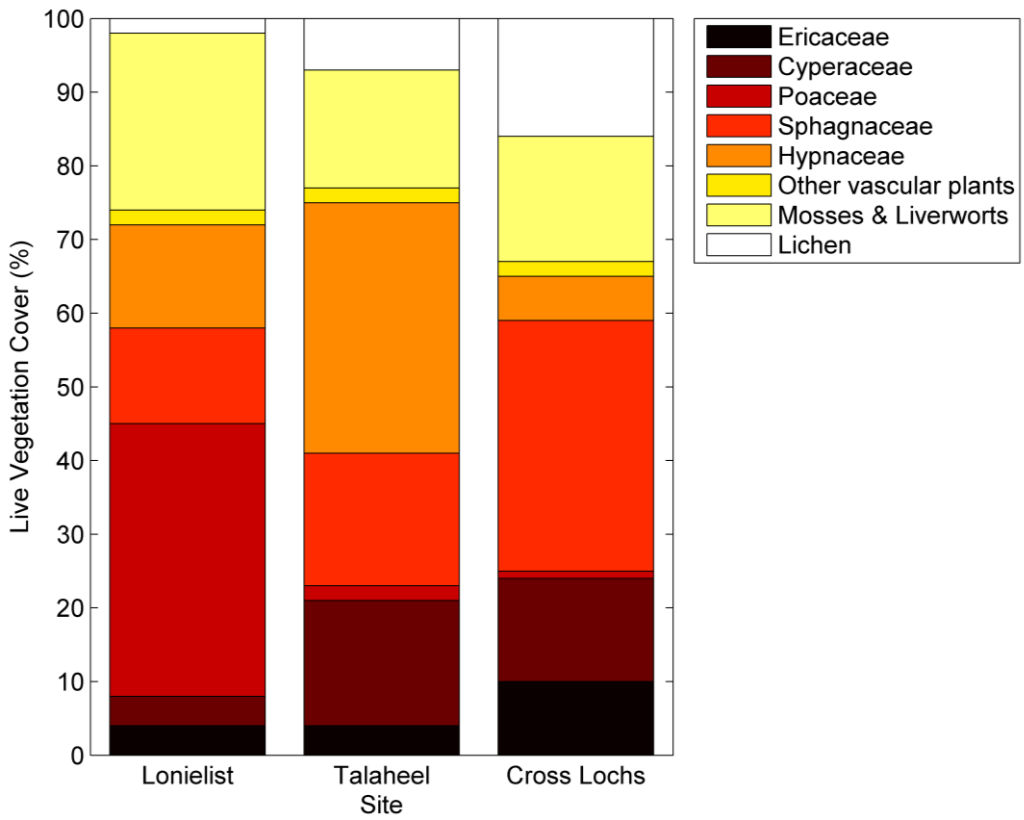

Figure 4.0 Percentage live vegetation coverage from the three sites. Vegetation data for Talaheel provided from Hancock & Cowie (manuscript in preparation).

Lonielist (58°23'29"N, 3°45'59"W) was planted in the 1980s with a mixture of lodgepole pine (*Pinus contorta*) and Sitka spruce (*Picea sitchensis*), with restoration commencing in 2003/04. Lonielist, situated at an altitude of 180 m above mean sea level, was relatively flat with a gentle slope of 1-3° and a mean peat depth of around 2 m. The furrow structure at Lonielist was

similar to Talaheel, however, significantly more woody material was present in the furrows at Lonielist than Talaheel.

Cross Lochs (58°22'13"N, 3°57'52"W) was considered to be representative of undrained blanket bog in the area and thus used as a control site. This site had never been drained and the only recorded human intervention was deer management. This site was the highest of all measurement sites at an altitude of 210 m above mean sea level. The site had a mean peat depth of 2 m, however, a peat depth of over 7 m was recorded at the site. Approximately 600 m north of the site is an area of felled forestry but due to the height of the instrumentation and location of the tower this area had minimal influence upon the fluxes (Chapter 3).

Further information on each of the sites is available in Chapter 2.

4.3 Methods

All R_{eco} data presented in this chapter were collected using the EC method described in Chapter 3. Eddy covariance measurements were undertaken on towers situated at the three sites, each equipped with a sonic anemometer and either an open-path or enclosed-path CO_2/H_2O analyser at a measurement height of 3m. Additionally, each site was equipped with environmental sensors such as soil moisture, soil temperature and air temperature. EC measurements were logged at a frequency of 10Hz and environmental measurements were recorded once a minute.

4.3.1 Analysis

All EC data were processed using the same protocols as described in Chapter 3. NEE data were gap-filled and partitioned into the constituent parts of ecosystem respiration (R_{eco}) and GPP using REddyProc (Reichstein *et al.*, 2005, Reichstein and Moffat, 2014) as described in Chapter 3 and described briefly below. Data were gap-filled using the MDS method where missing data are replaced using a mean value of periods with similar meteorological conditions over a moving window of ± 7 days.

Nocturnal NEE data, which represent R_{eco} in the absence of light necessary for photosynthesis, were used to parameterise the Lloyd and Taylor (1994) model (Eqn 4.0). Firstly, this was used to calculate daytime R_{eco} from daytime temperature measurements in order to partition NEE data into the constituent parts of R_{eco} and GPP. Secondly, the model was used to assess the impact of temperature on respiration,

$$R_{eco}(T) = R_{10} exp\left[E_o\left(\frac{1}{T_{ref} - T_o} - \frac{1}{T - T_o}\right)\right]$$

(Eqn 4.0)

where, R_{10} is the basal ecosystem respiration at 10°C (T_{ref}), E_o the activation energy or temperature sensitivity parameter, and T_o is the temperature at which R_{eco} reached zero; in this model it is set to a constant of -46.02°C to prevent over parameterisation.

The Q_{10} temperature coefficient was calculated (Eqn 4.1) as a measure of the rate of change in respiration as a result of a 10°C change in temperature,

$$Q_{10} = \left(\frac{R_2}{R_1}\right)^{10/(T2-T1)}$$

(Eqn 4.1)

where R_2 and R_1 are the final and initial respiration rates (μmol m^{-2} s^{-1}), and T_2 and T_1 are the final and initial temperatures (°C), respectively.

Where data were assessed seasonally, they were split into standard meteorological seasons (Table 4.0). All of the sites were subject to the same statistical analyses performed in MATLAB, Version 8.1.0.604 (R2013a) with Statistics Toolbox Version 8.2 (R2013a) (Mathworks Inc., Natick, MA, USA). Normality within the data were tested using a Kolmogorov-Smirnov test. As none of the data were normally distributed, and thus did not meet the assumptions of analysis of variance (ANOVA), non-parametric methods were employed. Values are therefore presented as median ± interquartile range unless otherwise stated.

Table 4.0 Classifications of seasons used in this research.

Season	Months
Spring	March, April and May
Summer	June, July and August
Autumn	September, October and November
Winter	December, January and February

Kruskal-Wallis tests were used along with Fishers LSD post hoc analysis to assess intra-annual variability and whether there were significant changes within the sample period. Wilcoxon rank sum analysis was used to assess inter-site variability. The impacts of environmental variables on R_{eco} were assessed using Spearman's rank correlation coefficient, with further analysis based

upon the strongest correlations, with the strength of correlation based on Table 4.1. Spearman's analyses were undertaken between environmental variables and nocturnal NEE, which is equal to R_{eco} due to the absence of light. The partitioning procedure uses temperature response to model daytime R_{eco} and therefore a strong relationship between temperature and R_{eco} would be expected, therefore it was decided to use nocturnal R_{eco} which would not display this coupled relationship with temperature. Further relationships were observed through multiple regression analysis. The normality of the residuals for each regression was checked to ensure they were normally distributed.

Table 4.1 Classification of the strength measure and Spearman's correlation coefficient used in this study.

Strength	Correlation Range
Very Weak	0 to 0.19
Weak	0.2 to 0.39
Moderate	0.4 to 0.59
Strong	0.6 to 0.79
Very Strong	0.8 to 1.0

4.4 Results

4.4.1 Restoration effect on R_{eco}

A significant difference (Kruskal-Wallis ANOVA $P < 0.0001$) in R_{eco} was observed with a decreasing R_{eco} flux associated with increasing time since restoration (Figure 4.1). The highest R_{eco} flux was observed from the most recently restored site (Lonielist; restored in 2003/04) with an annual flux of 581 g C m^{-2} yr^{-1}. The annual R_{eco} flux of the oldest restored site (Talaheel; restored in 1997/98) was over 100 g C m^{-2} yr^{-1} lower than Lonielist, with a flux of 480 g C m^{-2} yr^{-1}. However, annual fluxes from both Lonielist and Talaheel were higher than the published 6-year annual mean R_{eco} flux (461 g C m^{-2} yr^{-1}) from the undrained site at Cross Lochs (Levy and Gray, 2015).

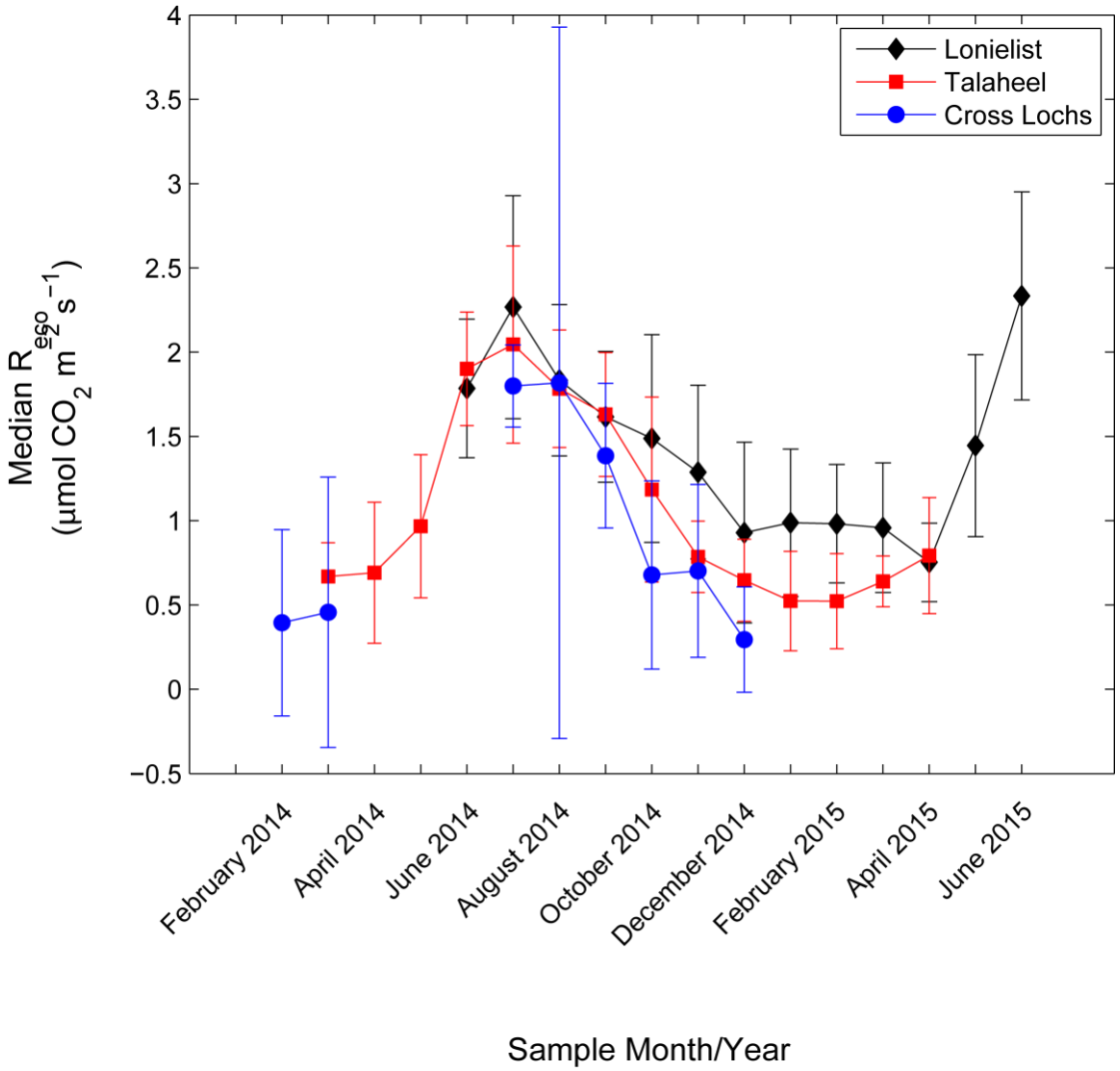

Figure 4.1 Median monthly R_{eco} fluxes from Lonielist (black), Talaheel (red) and Cross Lochs (blue). Error bars represent the interquartile range.

The data presented in Figure 4.1 shows distinct intra-site seasonality across all of the sites. The highest R_{eco} flux across all sites was observed at the undrained Cross Lochs sites (5.43 µmol CO_2 m^{-2} s^{-1}) in July 2014, and the highest R_{eco} fluxes from Lonielist (4.86 µmol CO_2 m^{-2} s^{-1}) and Talaheel (5.39 µmol CO_2 m^{-2} s^{-1}) were observed on the same day. Minimum fluxes were observed during winter at Lonielist (0.35 µmol CO_2 m^{-2} s^{-1}) and Talaheel (0.11 µmol CO_2 m^{-2} s^{-1}) on consecutive days in January 2015. The minimum flux at Cross Lochs was also observed during the winter but was observed earlier than Lonielist and Talaheel in December 2014 (0.06 µmol CO_2 m^{-2} s^{-1}). At Talaheel (restored in 1997/98), median daily intra-site seasonal R_{eco} fluxes (Table 4.2) were significantly different from one another (Kruskal-Wallis, $P < 0.0001$). A similar pattern was also observed at Lonielist (restored in 2003/04), with median intra-site seasonal R_{eco} observed to be significantly different (Kruskal-Wallis, $P < 0.0001$). Moreover, at

all points, except summer (Wilcoxon rank sum, $P = 0.2474$), inter-site seasonal R_{eco} fluxes were significantly lower at Talaheel than Lonielist (Wilcoxon rank sum, $P < 0.0001$). The same intra-site seasonality relationship was observed at Cross Lochs (Kruskal-Wallis, $P < 0.0001$). No significant difference was observed in seasonal R_{eco} between Talaheel and Cross Lochs, except in winter where Talaheel fluxes were significantly higher (Wilcoxon rank sum, $P = 0.0245$)

Table 4.2 Median daily seasonal R_{eco} fluxes (μmol m^{-2} s^{-1}) from Lonielist, Talaheel and Cross Loch. All values are ± interquartile range. Unique letters indicate significant differences, while common letters indicate no significant difference between sites. Note the difference in units for the annual flux. *Figure is a published 6-year mean between 2008 and 2013 (Levy and Gray, 2015).

	Lonielist (Restored 2003/04)	**Talaheel (Restored 1997/98)**	**Cross Lochs (Undrained)**
Spring (μmol CO_2 m^{-2} s^{-1})	1.07 ± 0.61 a	0.89 ± 0.41 b	0.89 ± 0.81 b
Summer (μmol CO_2 m^{-2} s^{-1})	2.19 ± 0.66 c	2.17 ± 0.48 c	2.16 ± 1.06 c
Autumn (μmol CO_2 m^{-2} s^{-1})	1.57 ± 0.43 d	1.18 ± 0.75 e	1.17 ± 0.41 e
Winter (μmol CO_2 m^{-2} s^{-1})	1.07 ± 0.43 f	0.62 ± 0.24g	0.25 ± 0.89 h
Annual flux (g C m^{-2} yr^{-1})	**581**	**480**	**461***

When assessed over the diurnal cycle (Figure 4.2), significant differences in R_{eco} were observed at all sites (Kruskal-Wallis, $P < 0.0001$) with the highest R_{eco} fluxes observed between the hours of 11:00 and 14:00, and R_{eco} fluxes were significantly higher at Lonielist than Talaheel (Wilcoxon rank sum, $P = 0.0046$). The strong diurnal cycle is indicative of a coupled relationship between R_{eco} (Figure 4.2 A – D) and temperature (Figure 4.2 E – H).

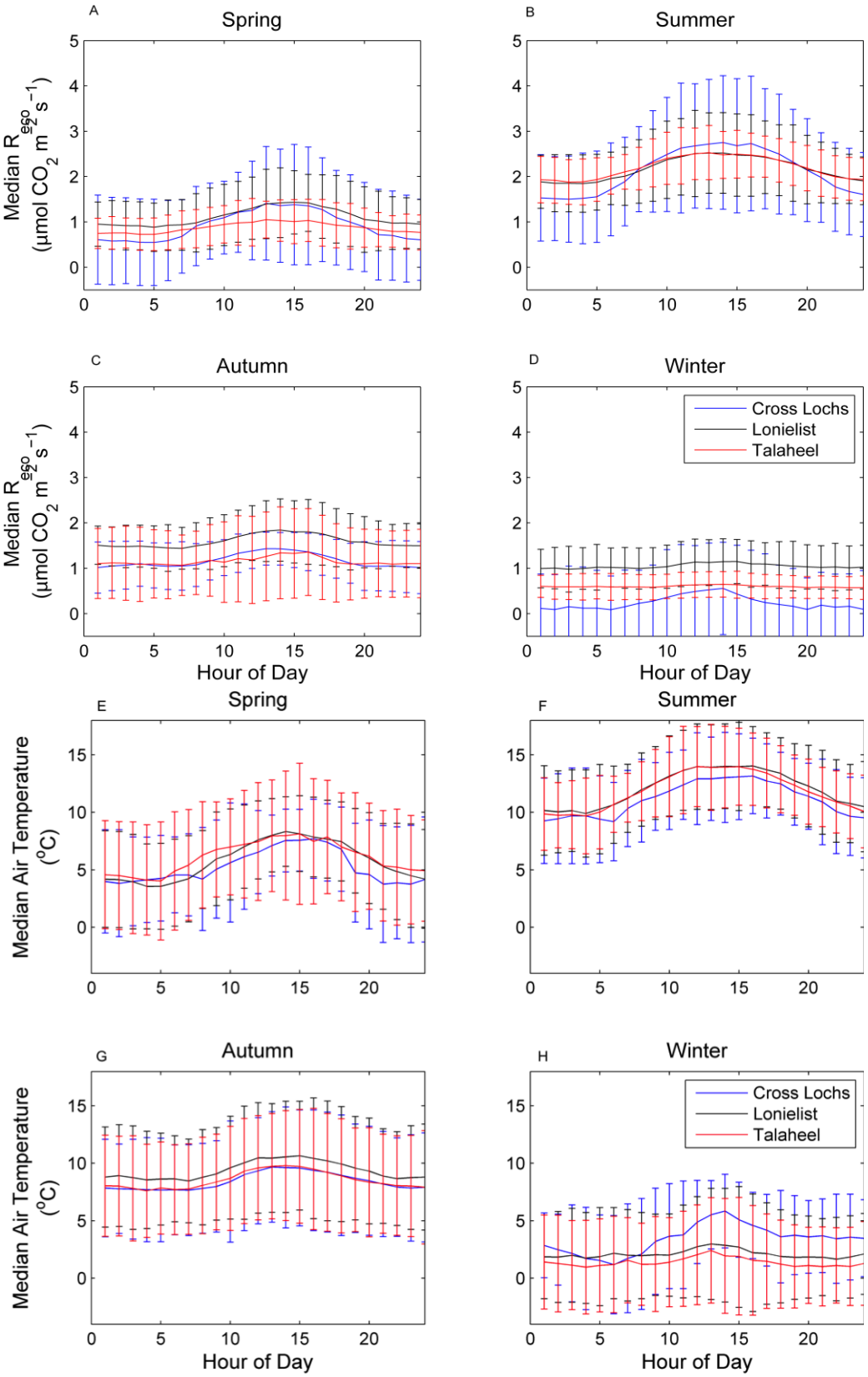

Figure 4.2 Seasonal diurnal R_{eco} and air temperature from the EC towers at Lonielist (black), Talaheel (red) and Cross Lochs (blue). All figures are median ± interquartile range

4.4.2 Environmental influences on respiration fluxes

Mean annual soil temperatures at Lonielist were significantly higher than both Talaheel (Wilcoxon rank sum, $P < 0.0001$) and Cross Lochs (Wilcoxon rank sum, $P = 0.0014$). Intra-site seasonal air and soil temperatures (Table 4.4) were significantly different at all sites (Kruskal-Wallis with Fishers LSD, $P < 0.0001$), with a strong seasonal pattern of higher temperatures in the summer and lower temperatures in the winter (Table 4.4). Whilst air temperatures were more variable, soil temperatures were always higher at Lonielist, except in spring where the highest temperatures were found at Talaheel, although this was not significantly different (Wilcoxon rank sum, $P = 0.2346$). Median seasonal soil moisture content (Table 4.4) was significantly different at Lonielist (Kruskal-Wallis with Fisher's LSD, $P < 0.0001$), but no significant differences were observed at Talaheel, where the soil moisture content was more stable (Kruskal-Wallis with Fisher's LSD, $P = 0.0674$). At Lonielist, soil moisture content was significantly lower than Talaheel across all seasons (Wilcoxon rank sum $P = 0.001$). Median annual water table depth (Table 4.4) was significantly lower at Talaheel than Cross Lochs (Wilcoxon rank sum $P < 0.0001$). This is reflected in the median seasonal water table depth measurements where the lowest water table measurement was recorded at Talaheel in the summer (-29.2 cm), whilst the highest median seasonal water table measurement was recorded at Cross Lochs at 1.2 cm above the surface of the peat.

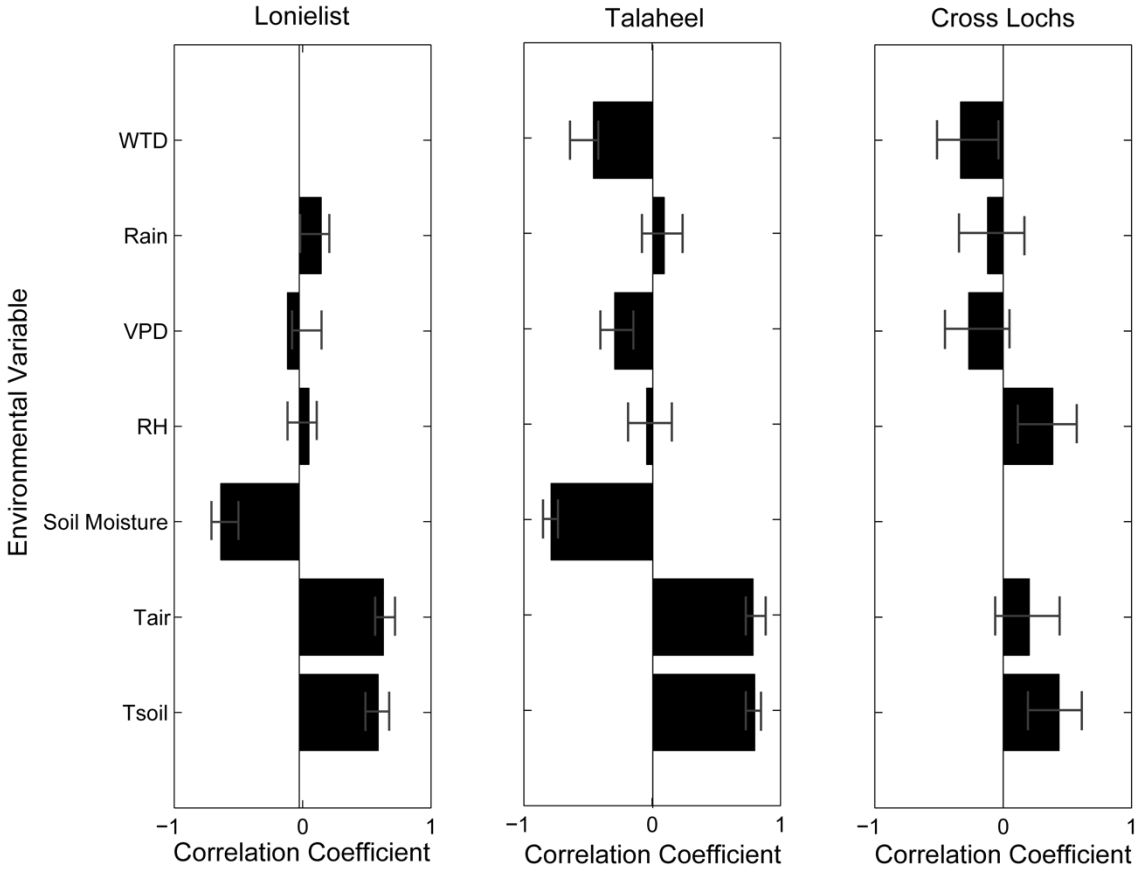

Figure 4.3 Correlation coefficients between QC'd Daily nocturnal R_{eco} and measured environmental variables. Error bars indicate the 95% confidence intervals.

Soil and air temperature were strongly correlated with daily nocturnal R_{eco} at Lonielist (Spearmans ρ = 0.6158, P = <0.0001; Spearmans ρ = 0.6559, P = <0.0001 respectively) and Talaheel (Spearmans ρ = 0.7820, P = <0.0001; Spearmans ρ = 0.7934, P = <0.0001 respectively). There was an increasing correlation between R_{eco} and soil temperature as time since restoration increased, whilst the correlation with air temperature decreased. At the undrained Cross Lochs site, soil temperature was moderately correlated with daily nocturnal R_{eco} (Spearman's ρ = 0.4359, P < 0.0001). Soil moisture was negatively correlated with daily nocturnal R_{eco} at both Lonielist and Talaheel, whilst a lack of usable suitable soil moisture data meant this could not be assessed at Cross Lochs. However, at Talaheel (Spearman's ρ = -0.4169; P < 0.0001) and Cross Lochs (Spearman's ρ = -0.3301, P = 0.01), where high frequency water table measurements were available, moderate to weak negative relationships were observed.

At all sites, higher soil and air temperatures (Figure 4.4) resulted in higher R_{eco} fluxes. Daily nocturnal Q10 values, describing the change in R_{eco} with a 10°C increase in temperature, showed that across all sites, increasing air temperature had a bigger influence on R_{eco} rate than

soil temperature. For both soil and air temperature the greatest increase in R_{eco} rates were observed at Lonielist with Q10 values of 3.3 and 3.4, respectively (Table 4.3).

Table 4.3 Daily nocturnal EC Q10 temperature response values for each site for both soil temperature and air temperature.

	Lonielist (Restored 2003/04)	**Talaheel (Restored 1997/98)**	**Cross Lochs (Undrained)**
Soil temperature	3.3	3.2	3.0
Air temperature	3.4	3.1	2.6

Cross Lochs had the lowest increase in respiration rate for both soil and air temperature increases of 10°C with Q10 values of 2.6 and 3.0, respectively. Talaheel Q10 values were approximately midway between Lonielist and Cross Lochs for both daily soil and air temperature (Table 4.3).

Table 4.4 Median, maximum and minimum seasonal air temperature, soil temperature, soil moisture content and water table depth from Lonielist, Talaheel and Cross Lochs. Negative water table depth denotes water table below the peat surface.

Air Temperature (°C)

	Lonielist			Talaheel			Cross Lochs		
	Median	Max	Min	Median	Max	Min	Median	Max	Min
Spring	5.8	16.7	-2.0	6.3	17.8	-3.1	6.6	13.2	-1.9
Summer	12.1	26.6	1.5	11.7	26.9	3.4	11.8	19.5	2.4
Autumn	9.4	20.2	1.0	8.5	19.6	0.3	8.6	19.5	0.0
Winter	2.1	12.1	-8.1	1.4	11.7	-8.1	3.4	8.6	-1.6
Annual	7.5	26.6	-8.1	6.9	26.9	-8.1	8.7	19.5	-1.9

Soil Temperature (°C)

	Lonielist			Talaheel			Cross Lochs		
	Median	Max	Min	Median	Max	Min	Median	Max	Min
Spring	5.7	8.7	3.2	5.6	11.0	2.3	4.0	6.6	2.3
Summer	14.0	17.3	3.3	12.3	15.6	8.9	13.0	15.9	9.4
Autumn	9.1	13.5	4.9	8.6	12.8	3.7	8.9	14.0	4.8
Winter	5.2	6.3	3.7	2.6	6.7	1.2	4.7	6.3	2.7
Annual	8.7	17.3	3.2	6.6	15.6	1.2	9.0	15.9	2.3

Soil Moisture Content (m^3 m^{-3})

	Lonielist			Talaheel			Cross Lochs		
	Median	Max	Min	Median	Max	Min	Median	Max	Min
Spring	0.70	0.69	0.65	0.72	0.72	0.71	N/A	N/A	N/A
Summer	0.50	0.54	0.43	0.71	0.72	0.71	N/A	N/A	N/A
Autumn	0.56	0.68	0.51	0.72	0.72	0.71	N/A	N/A	N/A
Winter	0.63	0.69	0.43	0.72	0.73	0.71	N/A	N/A	N/A
Annual	0.56	0.69	0.43	0.72	0.73	0.71	N/A	N/A	N/A

Water Table Depth (cm)

	Lonielist			Talaheel			Cross Lochs		
	Median	Max	Min	Median	Max	Min	Median	Max	Min
Spring	N/A	N/A	N/A	-11.4	-7.1	-17.5	-3.4	-1.6	-5.3
Summer	N/A	N/A	N/A	-12.2	-4.4	-29.2	-6.8	-4.2	-14.3
Autumn	N/A	N/A	N/A	-11.4	-6.1	-17.2	-3.0	-1.5	-7.1
Winter	N/A	N/A	N/A	-10.3	-5.6	-13.0	-0.1	1.2	-2.4
Annual	N/A	N/A	N/A	-11.4	-4.4	-29.2	-3.5	1.2	-14.3

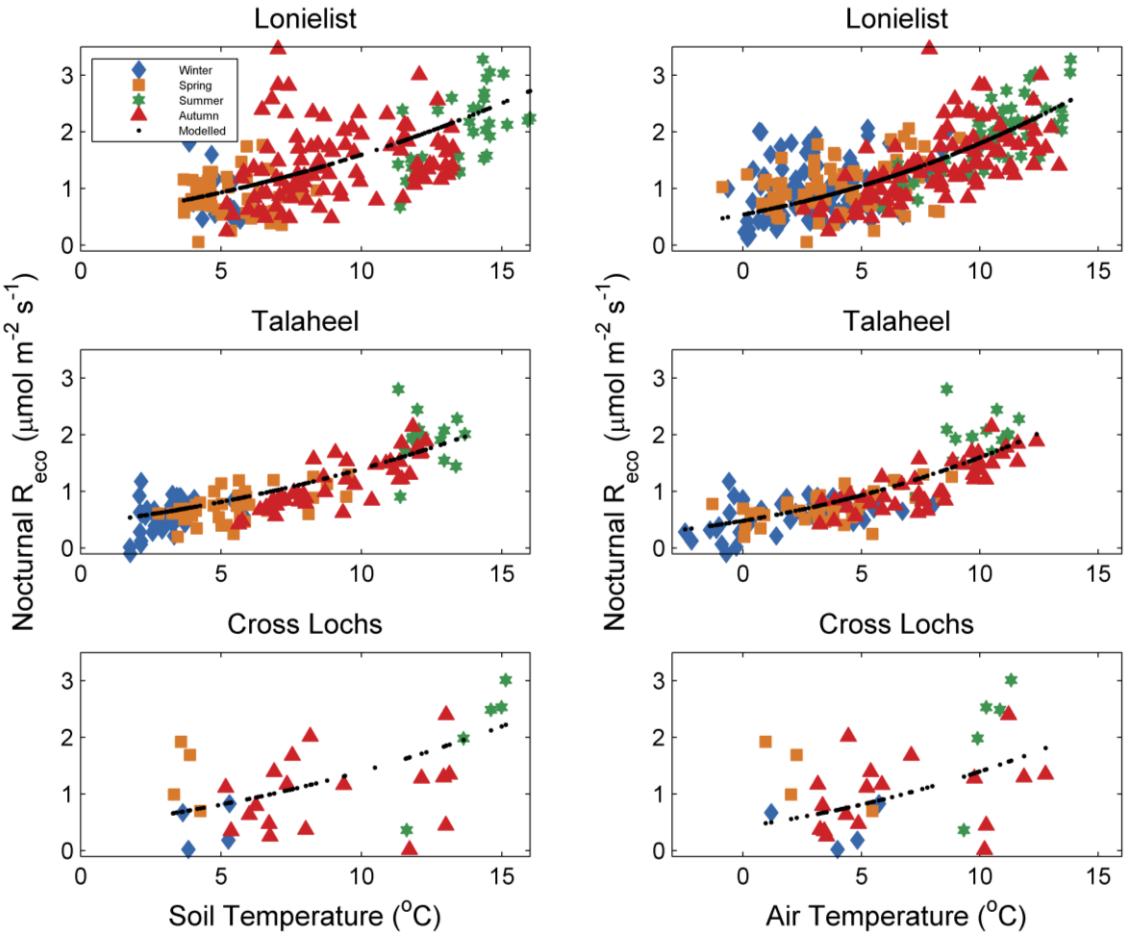

Figure 4.4 Daily nocturnal respiration responses to changes in soil and air temperature from Lonielist, Talaheel and Cross Lochs. Purple markers indicate modelled response using (Eqn 4.2).

The trend observed in Q10 analysis was also present when plotting the daily nocturnal R_{eco} flux against both air and soil temperature with the Lloyd and Taylor (1994) model (Eqn 4.2). The greatest response to a change in temperature was seen at Lonielist and the lowest response to changes in temperature seen at Cross Lochs (Figure 4.4).

Table 4.5 Seasonal daily nocturnal EC Q10 temperature response values for each site for both soil and air temperature

	Season	Soil Temperature	Air Temperature
Lonielist	Spring	3.0	3.5
	Summer	4.5	3.6
	Autumn	4.4	2.6
	Winter	3.5	3.5
Talaheel	Spring	1.8	1.7
	Summer	2.2	1.8
	Autumn	4.9	1.8
	Winter	1.3	2.0
Cross Lochs	Spring	3.8	1.9
	Summer	5.8	0.5
	Autumn	1.4	1.6
	Winter	1.8	2.8

Strong positive correlations between both soil and air temperature and R_{eco} suggested a possible seasonal influence causing both soil and air temperature to influence R_{eco} at different periods of the year. At both Lonielist and Talaheel, Q10 relationships suggested that soil temperature had a greater influence on R_{eco} during the summer and autumn (Table 4.5) and air temperature had a greater influence during spring and winter (Table 4.5). Whilst this is also supported at Cross Lochs during the summer (Table 4.5), Q10 relationships show that air temperature had a greater influence on R_{eco} during autumn rather than soil temperature, as observed at Lonielist and Talaheel. A significant weak correlation was found at Lonielist between R_{eco} and soil temperature during the summer (Spearmans $\rho = 0.2948$, $P = <0.0001$) and autumn (Spearmans $\rho = 0.2245$, $P = <0.0001$). Similar correlations were also observed at Talaheel during the summer (Spearmans $\rho = 0.2765$, $P = <0.0001$). However, in autumn at Talaheel, although both soil and air temperature correlated significantly, air temperature showed a stronger significant positive correlation (Spearmans $\rho = 0.4694$, $P = <0.0001$). The only significant correlation found at Cross Lochs was between R_{eco} and soil temperature in autumn (Spearmans $\rho = 0.1023$ $P = 0.003$), however this was a very weak correlation.

Soil moisture was assessed at Lonielist and Talaheel in order to understand two things: 1) is restoration resulting in wetter conditions and 2) what effect does this have on R_{eco} fluxes. The volumetric soil moisture content (Table 4.4) was significantly higher at Talaheel than at Lonielist (Wilcoxon Rank sum, $P < 0.0001$). Lower soil moisture content was observed at Lonielist throughout the sampling period with median moisture content of 0.56 ± 0.12 m^3 m^{-3},

maximum moisture content of 0.698 m^3 m^{-3}. Higher soil moisture conditions were observed at Talaheel with a median value of 0.72 ± 0.01 m^3 m^{-3} and maximum soil moisture of 0.73 m^3 m^{-3}.

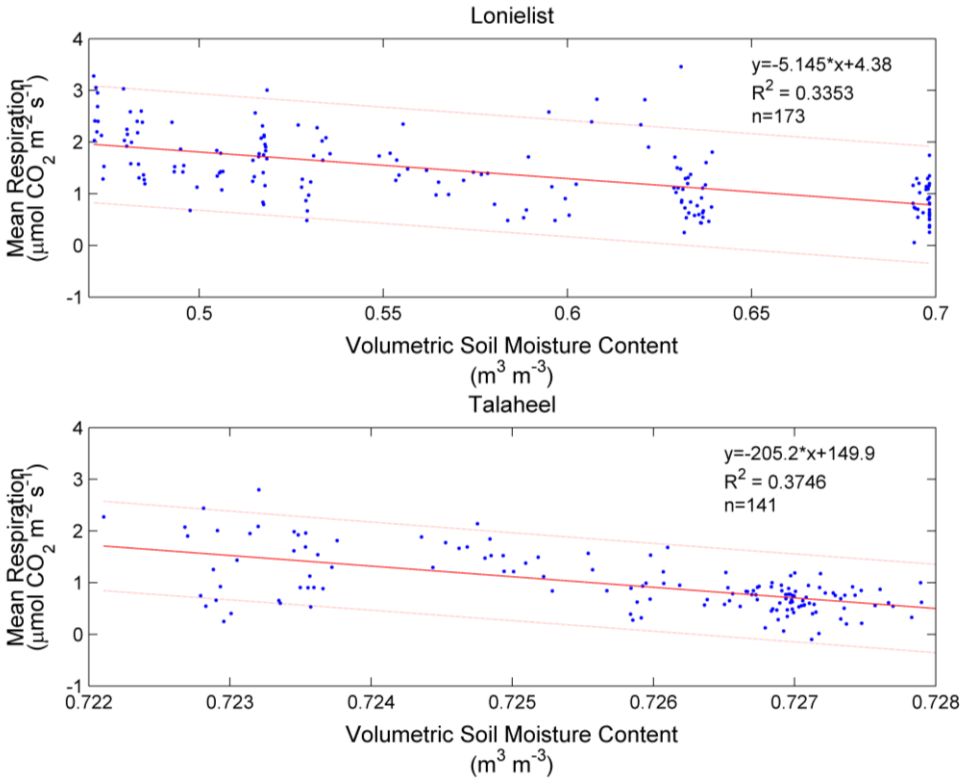

Figure 4.5 Daily nocturnal R_{eco} response to changes in volumetric soil moisture content. Fitted lines are linear fits with the equations given within each of the plots. Dotted lines represent the 95% prediction bounds.

At both sites, higher volumetric moisture content was associated with lower nocturnal R_{eco} fluxes (Figure 4.5). A significant negative correlation was observed at Lonielist (Spearmans ρ = -0.6100, $P < 0.0001$), and a similar relationship was also observed at Talaheel (Spearmans ρ =-0.7291, $P = < 0.0001$). When data were disaggregated seasonally, similar negative relationships were observed at both sites. However in winter, a weak positive correlation was observed at Lonielist (Spearmans ρ = 0.2305, P = <0.0001). A positive correlation was also observed at Talaheel, although this relationship was very weak and non-significant (Spearmans ρ = 0.0564, P = 0.0625).

To better understand the relationships between R_{eco} and the driving variables, a multiple linear regression was undertaken, the inputs for which were informed by the Spearman's rank correlation analyses. Similar to the Spearman's analyses, soil moisture and temperature explained the greatest amount of variation in the data at both Lonielist (R^2 = 0.79, $P < 0.0001$) and Talaheel (R^2 = 0.87, $P < 0.0001$) (Figure 4.6). The addition of air temperature to the model

accounted for slightly more of the variation (R^2 = 0.84, P < 0.0001 and R^2 = 0.91, P < 0.0001 respectively). In both models R_{eco} was observed to increase under drier, warmer conditions.

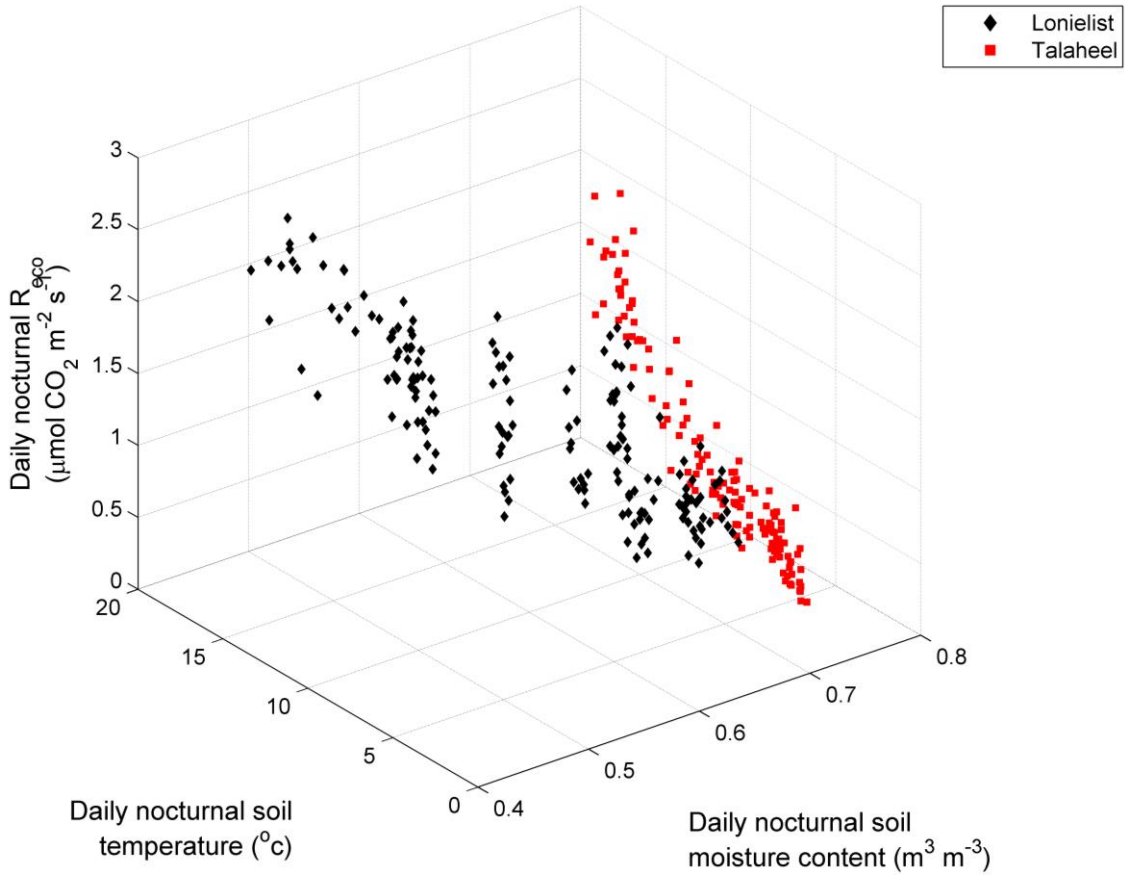

Figure 4.6 Three-dimensional scatter plot of the relationship between daily nocturnal R_{eco}, soil temperature and soil moisture content at Lonielist (Black diamonds) and Talaheel (Red squares).

At Cross Lochs, soil temperature and air temperature accounted for around 43% of the variance in R_{eco} (R^2 = 0.43, P < 0.0001). As soil moisture was not available at Cross Lochs, water table depth was substituted for this, however this did not have an impact upon the model and did not account for any more variance in the data (R^2 = 0.43, P < 0.0001).

4.5 Discussion

4.5.1 Effect of peatland restoration on R_{eco}

Current research on GHG exchange from peatland restoration suggests that these activities reduce respiration losses to the atmosphere (Samaritani *et al.*, 2011, Strack and Zuback, 2013, Strack *et al.*, 2014). However, these studies have been undertaken on peat extraction sites rather than sites restored from forestry, with data suggesting a reduction in respiration losses and a return of peatland ecosystem functioning within a few years (Tuittila *et al.*, 1999, Strack and Zuback, 2013). In contrast, other research has shown that in low productivity environments, such as those in boreal regions, it can take over 20 years to recover the net C sink functioning following restoration and re-vegetation of a site (Schulze *et al.*, 1999, Rannik *et al.*, 2002, Kowalski *et al.*, 2004). Few studies of peatland restoration work report annual R_{eco} rates as most studies focus on growing season fluxes and are thus unable to report annual flux rates (Strack and Zuback, 2013). Furthermore, few micrometeorological measurements have been performed over peatland restoration sites due to the typically limited size of these plots (Waddington and Price, 2000).

Table 4.6 Literature searches of annual R_{eco} flux rates from other peatland sites in the Northern Hemisphere. * Denotes this is a mean value from 12 sites in the Northern Hemisphere.

R_{eco} (g C m^{-2} yr^{-1})	Reference
278	Peichl *et al.* (2014)
461	Levy and Gray (2015)
411*	Lund *et al.* (2010)
569	Syed *et al.* (2006)

Annual R_{eco} fluxes from Lonielist (restored in 2003/04) and Talaheel (restored in 1997/98) were higher than reported R_{eco} from sites in the Northern Hemisphere (Table 4.6), however, research by Syed *et al.* (2006) reported higher annual R_{eco} than that observed at Talaheel from a stunted tree fen in the southern boreal forest of Canada. A strong correlation between R_{eco} and ecosystem photosynthesis during the growing season was observed, suggesting links between plant and microbial activity in the shallow layers of the peat. Moreover, the authors suggested that the presence of trees, as well as dwarf shrubs, was likely to have resulted in higher respiration rates. Throughout the study period, median R_{eco} fluxes were higher from Lonielist than Talaheel. Research by Strack and Zuback (2013) into the annual carbon balance of a cutover restored peatland site in Canada of similar age to Lonielist at the time of research presented a much lower annual R_{eco} flux. However, the authors noted that this research was undertaken during an exceptionally dry year and that chamber measurements were extrapolated

out over the site. Despite the higher R_{eco} compared to Cross Lochs and other northern peatlands, losses are reducing as demonstrated by the lower annual R_{eco} at the older Talaheel site. This relationship has also been observed at other peatland restoration sites in the Northern Hemisphere (Samaritani *et al.*, 2011, Strack and Zuback, 2013, Strack *et al.*, 2014).

The presence of decomposing woody material could, in part, explain the high respiration rate observed at Lonielist during the study period. Lonielist had a greater coverage of decomposing tree material than Talaheel, as observed in Figure 2.7 and 2.9 (Chapter 2). Temperature is known to directly affect decomposition through its influence on microbial activity, with higher soil temperatures strongly related to higher CO_2 respiration (Waddington *et al.*, 1998). Higher soil temperatures were observed at Lonielist compared to both Talaheel and Cross Lochs, and with greater substrate availability, decomposition is likely to result in a higher R_{eco} flux. Re-colonisation of the site by C-fixing vegetation increases the labile C pool, increasing the potential for higher respiration rates (Lagomarsino *et al.*, 2009). Accompanied with the re-vegetation is the input of woody material from deforestation, which is a much slower decomposition process (Laiho *et al.*, 2003)**,** but provides a persistent source of CO_2 to the atmosphere from the land surface. Typically these biotic factors are coupled with seasonal changes in temperature, making it difficult to assess the temperature-independent influence of these variables on R_{eco}.

4.5.2 Environmental controls on R_{eco}

Clear seasonal variation indicated differing influences of soil and air temperature throughout the year. However, both showed similar intra-annual trends to R_{eco}, which is suggestive of these having a strong influence on respiration. R_{eco} correlated better with soil temperature than air temperature over the summer and autumn at both Lonielist and Talaheel (Table 4.5), whilst in the winter and spring air temperature was better correlated with R_{eco} than soil temperature. Peat temperature is closely linked to hydrological conditions, with wet peats typically being lower in temperature than dry peats (Waddington *et al.*, 2002). It is therefore likely that the intra-annual variation in correlations between R_{eco} and air and soil temperature are related to changes in the water table and soil moisture content. Similarly, differences in moisture content between microforms (Chapter 6) are likely to be masked in this research as peat temperature was only measured from the furrow and original surface, whilst the ridges which account for around 2/3 of the land surface (M. Hancock, pers. comm. 2nd December 2015) were not measured and are associated with drier soil moisture conditions.

When assessed across a year, R_{eco} at both Talaheel and Lonielist increased following a non-linear relationship with increasing air temperature (Figure 4.4). The Q10 values (Table 4.3)

obtained from this research were in the range of other peatland sites in the Northern Hemisphere (Chapman and Thurlow, 1998, Lafleur *et al.*, 2005b). They suggest that R_{eco} at Lonielist (Q10 = 3.4) increases more with a 10°C increase in temperature than Talaheel (Q10 = 3.2). The strong dependence of temperature on R_{eco} is consistent with other studies across a range of ecosystems (Lloyd and Taylor, 1994, Kirschbaum, 1995, Lafleur *et al.*, 2005b, Bond-Lamberty and Thomson, 2010, Luo *et al.*, 2012, Borchard *et al.*, 2015). However, the stronger correlation of R_{eco} with air temperature opposed to soil temperature is inconsistent with research from other peatland sites in the Northern Hemisphere. Work undertaken by Lafleur *et al.* (2005b) at the Mer Bleue peatland in Canada found a stronger correlation between R_{eco} and peat temperature (r^2 = 0.62), although a strong correlation was also observed with air temperature (r^2 = 0.61). Additionally, the authors noted that near surface peat temperatures had a greater influence on R_{eco} than deeper layers and that a lack of a standardised method for the measurement of peat temperature is a likely cause for the amount of variation reported in literature. The differences in correlation between soil temperature and air temperature at both Lonielist and Talaheel are low and it is likely that the lack of a stronger correlation with soil temperature is due to measurements not being undertaken nearer the surface of the peat and only covering a small spatial extent.

The significant differences in soil and air temperature are likely to explain some of the differences in R_{eco} flux between Lonielist and Talaheel. However, it is unlikely given the low correlation values that this explains all of the variation in these fluxes and it is likely that some other factors are influencing the difference in R_{eco} between the sites.

Soil moisture content was negatively correlated with R_{eco} at both Lonielist (Spearmans ρ = -0.3593 $P < 0.0001$) and Talaheel (Spearmans ρ =-0.3024 $P < 0.0001$). Lonielist was associated with a significantly lower soil moisture content than Talaheel. Blanket bogs are associated with saturated soil moisture conditions, with little variation during the year (Holden *et al.*, 2011, Parry *et al.*, 2014), which is a key factor in their formation and continued growth. Soil moisture is inversely related to the rate of gas diffusion through the peat, due to diffusion of gases in water being approximately 10,000 times slower than in air (Waddington *et al.*, 2002). Additionally, this is likely to be most prevalent at sites with a variable soil moisture content, such as restored peatlands, where the frequency and magnitude of precipitation events can cause large shifts in the soil moisture content. The lower moisture content observed at Lonielist is likely to have resulted in a greater efflux of CO_2, which in turn is likely to explain the more variable fluxes at Lonielist during the period of December 2014 through February 2015.

Soil moisture content plays another important role in peatland environments by the controlling thermal conditions of the peat (Waddington *et al.*, 2002). Together, the hydrological and thermal dynamics can affect the flux rates of CO_2 from the peat. As soil moisture content decreases, the total thermal capacity of the peat also decreases, resulting in an increase in diurnal peat temperatures fluctuations. Changes to diurnal fluctuation of peat temperature and its effect on R_{eco} are seen by the changing influence of air and soil temperature (Figure 4.2), where soil temperature becomes more influential during the latter part of the day as the temperature builds throughout the day. As peat temperature increases, so does the potential for oxidation of the peat due to an increase in the rate of microbial activity thereby increasing respiration. Moreover, restoration of the hydrological conditions results in vegetation composition differences (Figure 4.0) with greater coverage of bog species such as *Sphagnum* and *Hypnum* at Talaheel than Lonielist. Although vegetation influences on R_{eco} were not specifically observed, they are likely to have had an influence on R_{eco} due to different plant functional traits influencing C dynamics (Diaz *et al.*, 2007, Ward *et al.*, 2009, Armstrong *et al.*, 2015).

The results of the multiple regression analyses suggested that interactive effects of soil moisture and temperature had the greatest influence on R_{eco} than any single environmental variable. Previous research in other peatlands has also observed similar relationships both in lab incubation and field studies (Waddington *et al.*, 2001, Wang *et al.*, 2010). This relationship between soil moisture, temperature and R_{eco} is likely to be important under future climate change. The Flow Country is predicted to become hotter and wetter, however summers are predicted to become drier and hotter, which is likely to stimulate large R_{eco} losses. However at Cross Lochs, in the absence of soil moisture measurements, the depth to the water table was added to the multiple regression model, but did not explain any more of the variation. This suggests that peat temperature had a greater influence on R_{eco} than the water table. Bubier *et al.* (2003b) suggested that water table depth has a bigger influence than temperature on R_{eco} fluxes during dry periods. The low hydraulic conductivity of peat means that decreases in the water table height can result in significant changes in the soil moisture content of the peat above the water table (Clymo, 2004, Lafleur *et al.*, 2005a). Due to the issues with data collection at Cross Lochs, dry periods were missed and therefore only small variations were observed in water table depth, which likely explains the lack of relationship between R_{eco} and water table depth. Furthermore, as daily water table changes are small (Lafleur *et al.*, 2005b), assessment over seasonal timescales may yield greater correlations between R_{eco} and water table depth. Further research is required to understand whether the interactions between soil moisture and temperature observed at Lonielist and Talaheel are also observed at Cross Lochs.

4.6 Conclusions

This chapter has presented the first year-round EC measured R_{eco} fluxes of a chronosequence from previously forested peatland sites in the Northern Hemisphere. Little or no published annual EC studies exist on peatland restoration sites often due to the scale of restoration activities not being suitable for the EC technique, as well as previous research typically focussing just on growing season fluxes.

The re-wetting and re-vegetation of the peat has facilitated the reduction of CO_2 emissions from restored sites. However, emissions at Lonielist remain high due to the presence of woody material from the felled trees, which are a persistent source of CO_2 to the atmosphere due to their slow decomposition rate. Significantly lower flux rates at Talaheel are indicative of the lower coverage of woody material and greater coverage of peat-forming vegetation. Whilst R_{eco} fluxes are still higher than those observed from undrained peatlands in the Northern Hemisphere, there is a significant decrease in CO_2 losses to the atmosphere through the process of restoration. Measured R_{eco} fluxes at Talaheel were observed to be significantly lower than the younger restoration site at Lonielist and indeed within the range of some other northern peatlands.

Interactions between temperature and soil moisture content were found to have the biggest influence on R_{eco} fluxes. Seasonal influences on R_{eco} followed similar patterns to those of air and soil temperature, indicating that these are the greatest drivers of R_{eco} across both restored and undrained sites. Although air temperature was found to have the greatest correlation with R_{eco} it is likely that soil temperature needs to be measured at more points over the expected footprint and closer to the surface in order to account for spatial differences. Temperature was found to influence soil respiration, whilst the soil moisture content of the peat enhanced the response of R_{eco} to temperature. Soil temperature is likely to be driven by changes in soil moisture content, resulting in changes to the thermal conditions of the peat. A drier peat has greater thermal conductivity leading to an increase in microbial activity and thus an increase in decomposition of organic matter releasing CO_2. Further research into partitioning respiration into the heterotrophic and autotrophic components, combined with greater monitoring of soil temperatures and soil moisture content and water table depth, will provide a better understanding of the interactions between soil temperature, moisture and R_{eco}.

~ Chapter 5 ~

Gross primary productivity dynamics in restored Flow Country peatlands

5.0 Abstract

Northern peatlands are estimated to hold up to one third of the world soil carbon (C) stocks (~550 Gt C) making them important ecosystems for regulating C exchange between the land surface and atmosphere. Above-ground net primary productivity (ANPP) is low due to saturated conditions, but this also results in low decomposition and low respiratory losses. Drainage of northern peatlands has resulted in the loss of C-fixing and peat forming vegetation, whilst increasing respiration (R_{eco}) losses. Peatland restoration seeks to re-balance R_{eco} and gross primary productivity (GPP) to return the ecosystems to net C sinks. Between March 2014 and June 2015, eddy covariance techniques were utilised along a chronosequence of restored peatland sites to examine time-dependent changes in GPP as a result of peatland restoration in the Flow Country of northern Scotland. Key environmental drivers were assessed to better understand GPP dynamics and how these change with time since the onset of restoration.

No significant difference was observed in GPP with the oldest restoration site (Talaheel; restored in 1997/98) taking up 551 g C m^{-2} yr^{-1}, while the younger restoration site (Lonielist; restored in 2003/04) took up 501 g C m^{-2} yr^{-1}. GPP from both restored sites was lower than the 6-year mean from an undrained bog in the Flow Country of 575 g C m^{-2} yr^{-1}. Seasonal variations were observed in the data. Significant differences were only observed in the summer between the youngest (Lonielist; restored in 2003/04 – 2.60 ± 0.84 μmol CO_2 m^{-2} s^{-1}) and the oldest site (Talaheel restored in 1997/98 – 3.34 ± 0.76 μmol CO_2 m^{-2} s^{-1}). Significant differences were also observed between the two sites in winter (0.28 ± 0.40 and 0.21 ± 0.22 μmol CO_2 m^{-2} s^{-1} respectively). Incident solar radiation was observed to be a primary driver of GPP, although strong relationships were also found with vapour pressure deficit (VPD) and soil moisture, resulting in a GPP limitation during periods of high VPD and low soil moisture.

5.1 Introduction

Despite only covering approximately 3% of the Earth's surface (Gorham, 1991), peatlands are estimated to contain at least one third of the world's soil carbon (C) pool (Jobbagy and Jackson, 2000, Yu, 2012, Scharlemann *et al.*, 2014, Armstrong *et al.*, 2015). Above-ground net primary productivity (NPP) is lower in peatlands compared to other ecosystems due to saturated conditions and a limited nutrient supply. However, low ecosystem respiration (R_{eco}) often results in high levels of net C uptake and net ecosystem exchange (NEE - Frolking *et al.*, 1998, Yu, 2006). Long-term northern peatland C accumulation is, on average, approximately 23 g C m^{-2} yr^{-1} (Gorham, 1991, Roulet *et al.*, 2007), a value that is approximately 10 times larger than the mean long-term soil C accumulation rates for other upland soils (Schlesinger, 1990, Post and Kwon, 2000). In the UK, peatlands cover around 12% of the land area and are estimated to store around 3.2Gt C, which is approximately 20 times more C than UK's forests, which cover around 13% of the land area (Worrall *et al.*, 2010).

Plant and soil characteristics are known to influence C dynamics in peatlands (Armstrong *et al.*, 2015). Peatland vegetation composition regulates gross primary productivity (GPP) with different plant functional traits (PFTs), such as nitrogen (N) use or the timing of phenological changes, influencing C dynamics (Diaz *et al.*, 2007, Ward *et al.*, 2009, Armstrong *et al.*, 2015). PFTs are well correlated with the growth rate of a plant (De Deyn *et al.*, 2008) with fast-growing plants typically associated with greater photosynthetic potential and higher quality litter inputs than their slower growing counterparts (Aerts and Chapin, 2000, Zhang *et al.*, 2012, Zinnert *et al.*, 2013). This can result in differences in rates of net C exchange between the plants, soils and atmosphere, depending on the dominant PFTs of the vegetation community (Diaz *et al.*, 2007, Armstrong *et al.*, 2015). Blanket peatlands are typically ombrotrophic, receiving all their water and mineral inputs from the atmosphere, resulting in an acidic, low base cation, less humified peat dominated by *Sphagnum* moss, sedges and ericaceous shrubs (Weltzin *et al.*, 2000). *Sphagnum* mosses only grow a few centimetres per year (Rydin *et al.*, 2006) and are poikilohydric; this means that their productivity is highly dependent on water availability, making them ideally suited to undisturbed peatlands where saturated conditions often prevail (Grosvernier *et al.*, 1997, Weltzin *et al.*, 2000, Haraguchi and Yamada, 2011). Northern peatlands are characterised by a low apparent quantum yield (α) and low light saturated photosynthetic capacity (A_{max} - Frolking *et al.*, 1998) in comparison to forests and grasslands, making them a unique ecological class. In undisturbed peatlands, it has been suggested that light response characteristics are a function of nutrient limitations (Clymo, 1984). Peatlands in the Northern Hemisphere have a long history of disturbance with large areas of Northern Europe, Canada and USA having been drained for forestry (Badorek *et al.*, 2011).

Drainage alters the chemical composition of the peat by modifying hydrological and biogeochemical dynamics leading to drier, warmer conditions, which increases aerobic decomposition, and transforms the structure and composition of vegetation. Soil microbial communities stimulate aerobic decomposition of the peat affecting the biogeochemical balance, potentially altering the vegetation composition. Changes to the vegetation composition may subsequently affect PFTs, which has knock-on effects for C dynamics; for instance, nutrient limitations affect chlorophyll production reducing GPP. Moreover, drainage lowers the water table increasing the thickness of the aerobic zone, intensifying carbon loss through aerobic decomposition, and a loss of productive, peat-forming vegetation such as *Sphagnum,* which requires water to maintain productivity (Grosvernier *et al.*, 1997, Weltzin *et al.*, 2000). Previous research has shown that the loss of *Sphagnum* can result in peatlands switching from a net C sink to a net C source by reducing GPP and increasing ecosystem respiration (R_{eco} - Maljanen *et al.*, 2010). Lohila *et al.* (2004) found that peatlands drained for agriculture were hotspots for C loss through high R_{eco}. Contrastingly, Hargreaves *et al.* (2003) suggested that drained and afforested peatlands in Scotland continue to be net C sources 2 – 4 years post drainage before returning to net sinks 4 – 8 years after planting, with the ecosystem a net sink on the order of 4 t C ha^{-1} yr^{-1}, of which GPP accounted for 5 t C ha^{-1} yr^{-1}. However, measurements were only undertaken during the growing season and fluxes extrapolated over the course of a year. Further research by Lohila *et al.* (2011) agreed with the work of Hargreaves *et al.* (2003) and found a drained peatland forest to be a large net sink for CO_2 with net ecosystem exchange on the order of -800 to -900 g CO_2 m^{-2} yr^{-1}. However, the authors noted that tree biomass only explained around 70% of this sink with the other 30% attributed to soil C accumulation.

A lack of knowledge concerning ecosystem scale GPP dynamics in restored peatlands at all temporal scales exists, particularly for peatlands restored from plantation forestry (Tuittila *et al.*, 1999, Waddington *et al.*, 2010, Strack and Zuback, 2013, Strack *et al.*, 2014). Previous research concerning the C balance of restored peatland sites has typically focussed on growing season fluxes so annual C balances could not be assessed. However, Strack and Zuback (2013) observed the annual carbon balance of a peatland 10 years after restoration in Canada, with carbon losses found to have greatly reduced compared to unrestored sites, in part due to re-vegetation and re-wetting increasing the plant productivity. However, this research was undertaken in 2010, which was a drier and warmer year (annual mean temperature 5.2° and precipitation 886 mm) than the 30-year mean (mean temperature 3.2°C and precipitation 963 mm) making all sites strong C sources. The authors noted higher R_{eco} through increased decomposition and lower GPP due to reduced stomatal conductance. Furthermore, research at the Sainte-Marguerite-Marie and Cacouna Station peatlands in Québec, Canada found that

restoration enhanced GPP and reduced R_{eco} (Waddington and Price, 2000). Similar to other research into the carbon balance of restored peatlands, the work of Waddington and Price (2000) focussed on growing season fluxes and did not take non-growing season fluxes into account.

The aim of this study in Flow Country was to examine year-round ecosystem scale dynamics of GPP and its key drivers across a chronosequence of restored peatlands and one undrained peatland using eddy covariance techniques. To achieve this aim the following questions are proposed:

1) How does the restoration of blanket bogs from forestry affect GPP?

2) What are the key drivers influencing change in GPP in restored blanket bogs?

5.2 Site Descriptions

All work was undertaken on sites situated within the Forsinard Flow National Nature Reserve (58°23'59"N, 3°49'28"W) in Caithness and Sutherland, Northern Scotland. Talaheel (Chapter 2 - 58°24'49"N, 3°47'52"W), the oldest restoration site on the reserve, underwent restoration in 1997/98 with trees felled and left to decompose. Vegetation coverage at Talaheel (Figure 5.0) was dominated by *Hypnaceae* (34% coverage*)* and *Sphagnum* mosses (18% coverage), with the majority of the *Sphagnum* found in the furrows (M. Hancock pers. comm. 2nd December 2015). Sedges (*Cyperaceae*) (17% coverage) showed similar coverage to *Sphagnum* spp.

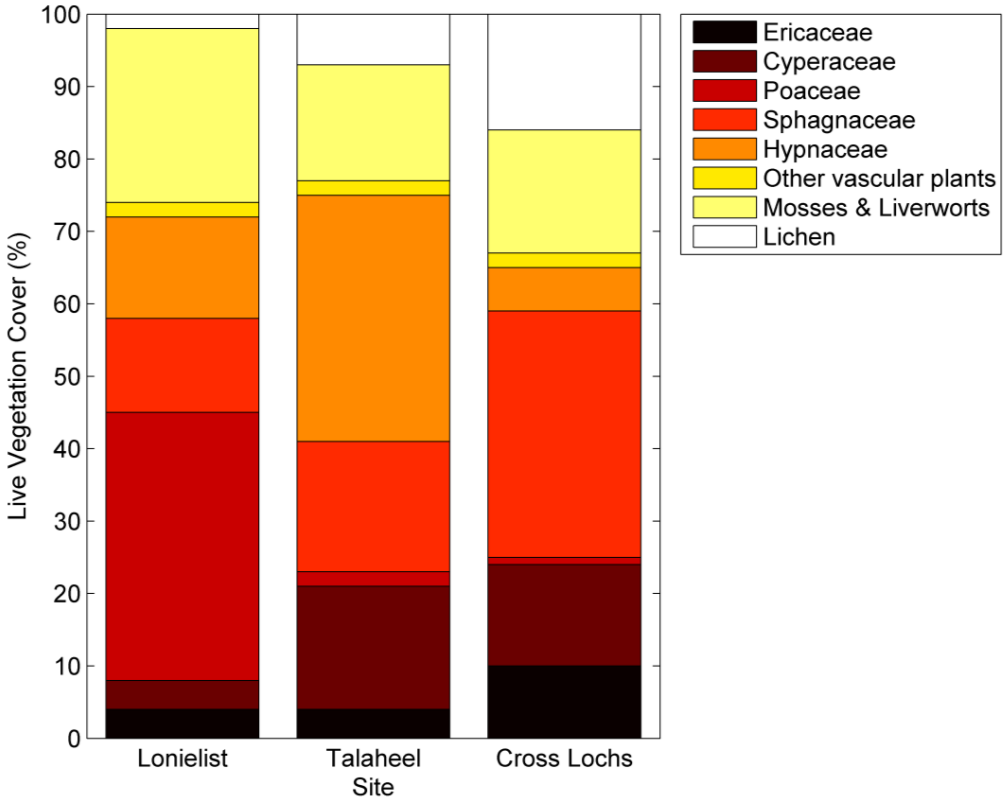

Figure 5.0 Percentage live vegetation coverage from the three sites. Vegetation data for Talaheel provided from Hancock & Cowie (manuscript in preparation). Data were collected from each site using 1 m x 1 m quadrats on each microform and replicated three times. Ellenberg values were used to infer the physical condition of vegetation. The data were corrected such that the quadrate total for all live vegetation summed to 100%.

Lonielist **(**Chapter 2 - 58°23'29"N 3°45'W) was considered representative of a peatland at an intermediate stage of restoration. Tree felling and main drain blocking occurred at the site in 2003/04, with felled trees left to decompose on site. Lonielist was characterised by a high coverage of grasses (*Poaceae*) (37%) and non-Hypnum or *Sphagnum* mosses (24%). Coverage of live *Sphagnaceae* (13%) and *Hypnaceae* (14%) was lower at Lonielist than Talaheel, most likely due to the more variable water table. The lowest coverage was of lichen (2%), whilst coverage of other vascular plants (2%) was similar to Talaheel and Cross Lochs.

Cross Lochs (Chapter 2 - 58°22'13"N, 3°57'52"W) was an undrained blanket bog, with the only human intervention being deer management. Approximately 600 m to the north of the site was an area of felled plantation forestry, however due to the height and location of instrumentation, this area likely had minimal influence on the footprint of the flux tower (Chapter 3). The vegetation (Table 5.0) was considered representative of undrained blanket bog stock in the area. Cross Lochs was dominated by *Sphagnaceae* (34%), whilst the coverage of *Hypnaceae* (6%) was significantly lower than in Talaheel. There was also a higher coverage of *Ericaceae* (10%) and lichen (16%), both of which were predominantly found on the drier hummock microforms. More detailed site descriptions are available in Chapter 2.

5.3 Methods

Eddy covariance (EC) techniques were used at the three sites described above (see also Chapter 2), each equipped with a sonic anemometer and either open-path or enclosed-path CO_2 analysers at a measurement height of 3m. Additionally, each site was equipped with environmental sensors such as soil moisture, soil temperature and air temperature. EC measurements (see Chapter 3 for more detail) were recorded at a frequency of 10Hz and environmental measurements recorded once a minute.

5.3.1 Analysis

All eddy covariance data were processed using the same protocols, (see Chapter 3). NEE data were gap filled and partitioned into the constituent parts of R_{eco} and GPP using REddyProc (Reichstein *et al.*, 2005, Reichstein and Moffat, 2014). Data were gap-filled using the marginal distribution sampling (MDS) method where missing data were replaced using a mean value of periods with similar meteorological conditions (incident radiation, air temperature and VPD with a deviation equal to 50 W m^{-2}, 2.5°C and 5.0 hPa, respectively) over a moving window of ± 7 days. Nocturnal NEE data were then used to parameterise the Lloyd and Taylor (1994) temperature-respiration model and calculate daytime R_{eco} from daytime temperatures. GPP fluxes were then calculated by subtracting the partitioned R_{eco} from NEE. Where data were assessed seasonally, they were split into standard meteorological seasons (Table 5.0).

Table 5.0 Classification of seasons used in this research.

Season	Months
Spring	March, April and May
Summer	June, July and August
Autumn	September, October and November
Winter	December, January and February

5.3.2 Assimilation Curve Fitting

Assimilation of carbon is the conversion of inorganic carbon (such as carbon dioxide) to organic compounds by living organisms, such as through photosynthesis. Assimilation is therefore a function of incident solar radiation and in this research is presented as a rectangular hyperbola. This type of relationship shows a near-linear increase in productivity with increasing incident light and an asymptotic approach to maximum productivity at high incident solar radiation. The curve was fitted using the method of Clement *et al.* (2012):

$$A = \frac{Amax \cdot \ \alpha \ \cdot Q_{pg}}{Amax + \ \alpha \ \cdot Q_{pg}}$$

(Eqn 5.0)

Where A is the assimilation, A_{max} the asymptotic CO_2 assimilation rate (μmol CO_2 m^{-2} s^{-1}), α the apparent quantum yield and Q_{pg} the photon flux density (μmol m^{-2} s^{-1}). Additionally, GPPmax was calculated as the difference between the highest measured flux and A_{max} as a means of accounting for the variability of light on the highest and lowest GPP fluxes.

5.3.3 Solar Angle

The solar angle was calculated using the MATLAB function SolarAzEl (Koblick, 2009), which calculated the solar azimuth and elevation based on the latitude, longitude and altitude of each site at half-hourly intervals over the research period.

5.3.4 Statistical Methods

All of the sites were subjected to the same statistical analyses, performed in MATLAB Version 8.1.0.604 (R2013a) with Statistics Toolbox Version 8.2 (R2013a) (Mathworks Inc., Natick, MA, USA). Data normality was tested using a Kolmogorov-Smirnov test, and if data were shown to be not normally distributed, and thus did not meet the assumptions of analysis of variance (ANOVA), non-parametric methods were used. All data are presented as median ± interquartile range unless otherwise stated.

Kruskal-Wallis tests were used along with Fishers LSD post hoc analysis to assess intra-annual variability and whether there were significant changes within the sample period. Wilcoxon rank sum analysis was used to assess inter-site variability. The impacts of environmental variables on GPP were assessed using Spearman's rank correlation coefficient, with the strength of correlation based on Table 5.1. Multiple regression analyses were used with the strongest correlations from the Spearman's rank correlation coefficient analyses used as the independent variables. Normality of residuals was checked to ensure normality and ensure validity of the analyses. Significance was accepted at $P < 0.05$ unless otherwise stated.

Table 5.1 Classification of the strength measure and Spearman's correlation coefficient used in this study.

Strength	Correlation Range
Very Weak	0 to 0.19
Weak	0.2 to 0.39
Moderate	0.4 to 0.59
Strong	0.6 to 0.79
Very Strong	0.8 to 1.0

5.4 Results

5.4.1 Restoration effects on GPP

No significant difference in GPP flux (Table 5.2) was observed between Lonielist and Talaheel over annual timescales (Kruskal-Wallis, $P = 0.2103$). The lowest flux was observed at Lonielist (restored in 2003/04) with an annual GPP flux of 501 g C m^{-2} yr^{-1}, whilst the annual GPP at Talaheel (restored in 1997/98) was 50 g C m^{-2} yr^{-1} higher (551 g C m^{-2} yr^{-1}). Both of these were lower than the published 6-year mean annual R_{eco} flux from the undrained site at Cross Lochs of 575 g C m^{-2} yr^{-1} (Levy and Gray, 2015).

Table 5.2 Median seasonal daily GPP fluxes from Lonielist, Talaheel and Cross Lochs. Values are ± interquartile range. Small letters indicate no significant intra-site intra-annual variability. Capital letters indicate no significant inter-site difference. Please note the difference in units for the annual flux. *Figure is a published 6-year mean between 2008 and 2014 (Levy and Gray, 2015)

	Lonielist (Restored 2003/04)	**Talaheel (Restored 1997/98)**	**Cross Lochs (Undrained)**
Spring (μmol CO_2 m^{-2} s^{-1})	1.21 ± 0.76 aA	1.07 ± 0.57 bA	3.79 ± 3.11 cB
Summer (μmol CO_2 m^{-2} s^{-1})	2.60 ± 0.84 dC	3.34 ± 0.76 eD	3.80 ± 1.87 fE
Autumn (μmol CO_2 m^{-2} s^{-1})	1.03 ± 1.51 gF	0.83 ± 1.51 hF	1.80 ± 2.18 iG
Winter (μmol CO_2 m^{-2} s^{-1})	0.28 ± 0.40 jH	0.21 ± 0.22 kI	1.19 ± 1.61 lJ
Annual flux (g C m^{-2} yr^{-1})	**501**	**551**	**575***

In contrast to annual fluxes, significantly higher daily GPP fluxes were observed at Cross Lochs compared to Lonielist (Wilcoxon rank sum, $P < 0.0001$) and Talaheel (Wilcoxon rank sum, $P < 0.0001$). However, in July 2014 no significant difference was found between Cross Lochs and the other two sites, Lonielist and Talaheel due to the large error associated with the small amount of noisy data collected at Cross Lochs in this month (July $n = 72$, August $n = 306$).

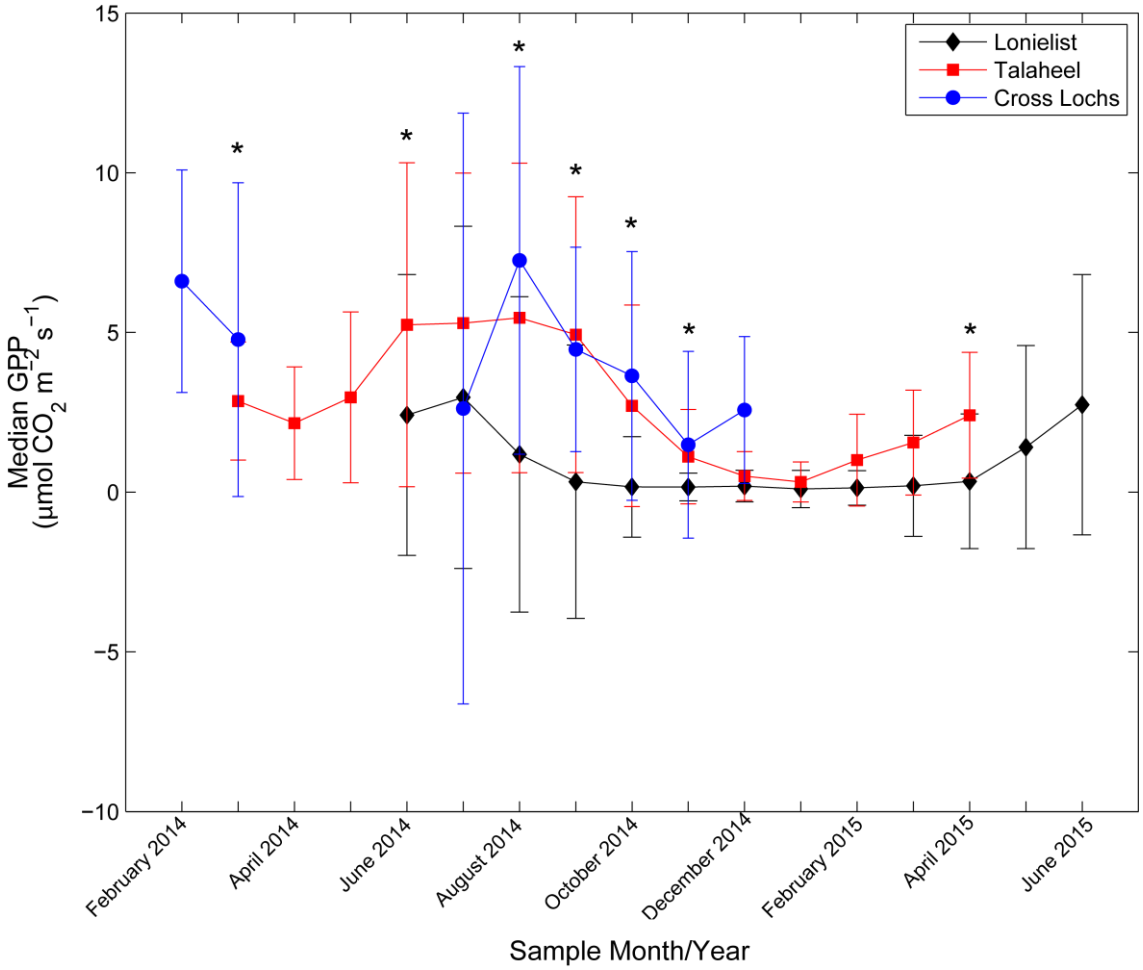

Figure 5.1 Median daily GPP fluxes (µmol m^{-2} s^{-1}) for each month of sampling from Lonielist (black), Talaheel (red) and Cross Lochs (blue). Error bars represent the interquartile range. * Denotes significant differences between sites in that sample month.

The data presented in Figure 5.1 shows distinct intra-annual variability across all sites. The greatest GPPmax (6.47 µmol CO_2 m^{-2} s^{-1}) was observed at Cross Lochs in July 2014, whilst the greatest GPPmax from Lonielist (0.78 µmol CO_2 m^{-2} s^{-1}) and Talaheel (2.99 µmol CO_2 m^{-2} s^{-1}) were observed in July and August 2014 respectively. Lowest GPPmax was observed in December 2014 at Cross Lochs (3.5693 µmol CO_2 m^{-2} s^{-1}), while the lowest GPPmax at Lonielist (0.3214 µmol CO_2 m^{-2} s^{-1}) and Talaheel (0.3464 µmol CO_2 m^{-2} s^{-1}) occurred in January 2015.

When assessed seasonally, both Lonielist (Kruskal-Wallis with Fisher's LSD, $P < 0.0001$) and Talaheel (Kruskal-Wallis with Fisher's LSD, $P < 0.0001$) showed significant intra-site differences in GPP with the highest fluxes observed in summer and the lowest fluxes observed in winter (Table 5.2). Inter-site seasonal median daily GPP fluxes were almost always significantly different between Lonielist and Talaheel (Wilcoxon rank sum, $P < 0.0001$).

However, in spring (Wilcoxon rank sum, P = 0.235) and autumn (Wilcoxon rank sum, P = 0.345) GPP fluxes between Lonielist and Talaheel were not significantly different.

At Cross Lochs, no significant difference in GPP fluxes during spring and summer were observed (Table 5.2) (Kruskal-Wallis with Fisher's LSD, P = 0.89), but autumn and winter fluxes were significantly different from spring and summer (Kruskal-Wallis with Fisher's LSD, $P < 0.0001$). At all points, inter-site seasonal daily GPP fluxes were significantly different (Wilcoxon rank sum, $P < 0.0001$)

5.4.2 Light Response Characteristics

The quantum yield describes the amount of CO_2 taken up during photosynthesis for each photon of light received by the leaf of a plant; this is described by the E_o parameter in Table 5.3. At all sites the apparent quantum yield (α) illustrated similar seasonal responses: peaking in summer, declining through autumn, reaching a minimum in winter, and rising again in spring.

All light response curves (Figures 5.2, 5.3 and 5.4) reached an asymptote indicating that other factors limited photosynthesis. Across all sites and seasons this occurred between 400 and 700 $\mu mol\ m^{-2}\ s^{-1}$ (Figures 5.2, 5.3, and 5.4). At this asymptote, GPP fluxes were in the range of 2 – 10 $\mu mol\ m^{-2}\ s^{-1}$, depending on the season. GPP fluxes were always slightly higher, although not significantly (Wilcoxon rank sum, P = 0.057), at Talaheel (Figure 5.3) relative to Lonielist (5.2) when the asymptote was reached, whilst the highest GPP fluxes were observed at Cross Lochs (Figure 5.4), despite the lack of data at high Photosynthetic Photon Flux Density (PPFD) due to tower downtime.

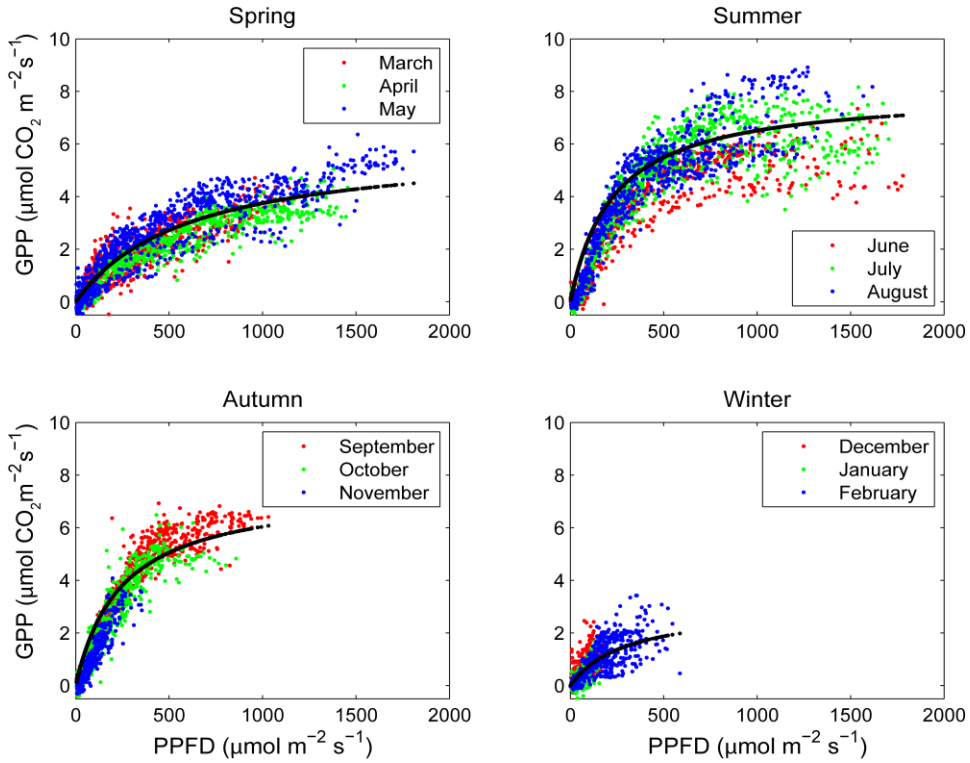

Figure 5.2 Half-hourly EC-derived GPP light response curves disaggregated seasonally at Lonielist. Different coloured markers are assigned to each month of the season to understand monthly variation within each season. Black markers indicate the fitted rectangular hyperbola.

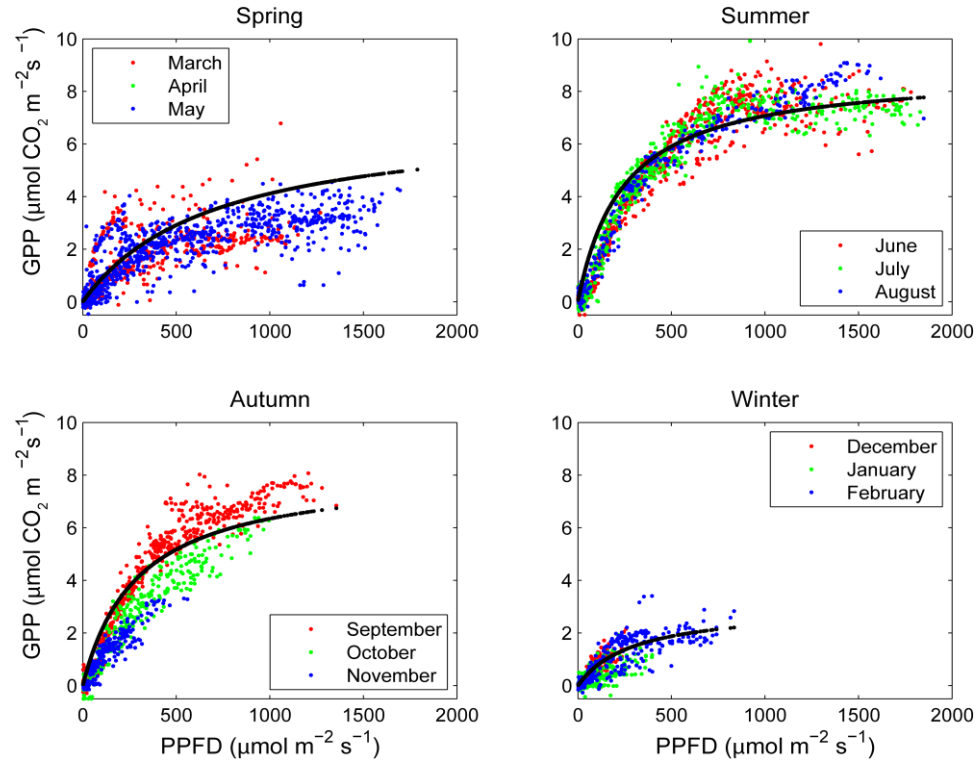

Figure 5.3 Half-hourly EC-derived GPP light response curves disaggregated seasonally at Talaheel. Different coloured markers are assigned to each month of the season to understand monthly variation within each season. Black markers indicate the fitted rectangular hyperbola.

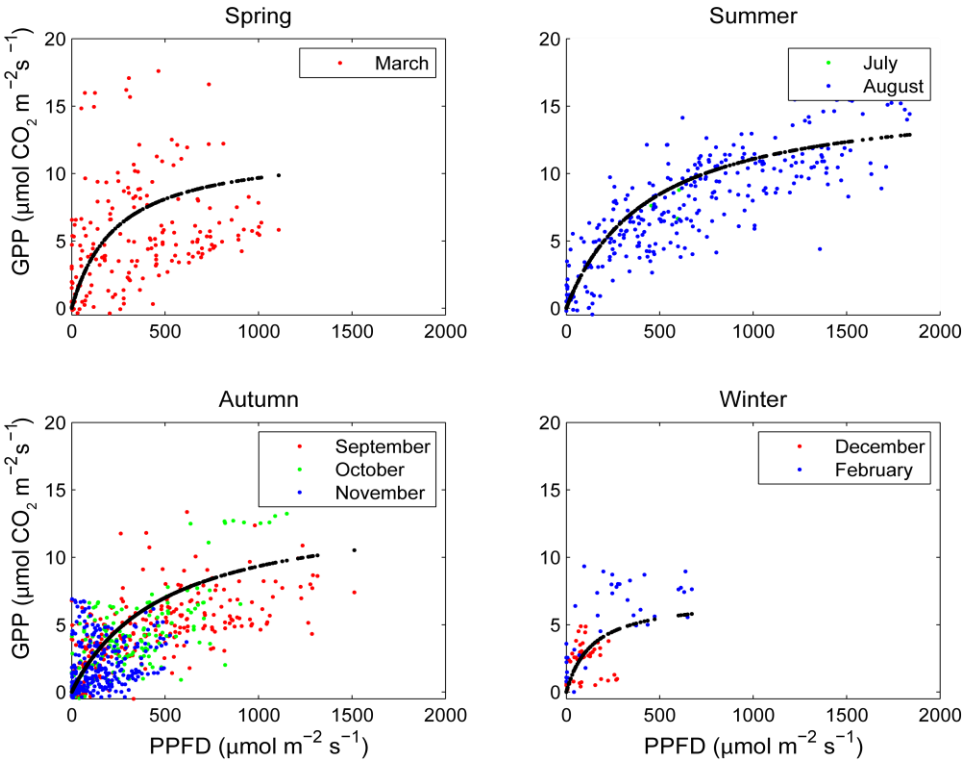

Figure 5.4 Half-hourly EC-derived GPP light response curves disaggregated seasonally at Cross Lochs. Different coloured markers are assigned to each month of the season to understand monthly variation within each season. Black markers indicate the fitted rectangular hyperbola.

Generally, higher fluxes were associated with higher photosynthetic photon flux density (PPFD). However, at Lonielist (Figure 5.2) during the summer, higher incident PPFD was not associated with the highest GPP fluxes (4.26 µmol CO_2 m^{-2} s^{-1} at PPFD of 1703 µmol m^{-2} s^{-1}), indicating that other factors suppressed CO_2 uptake. The apparent appearance of at least two light response curves in summer and autumn at Lonielist (Figure 5.2) and in autumn at Talaheel (Figure 5.3) is likely caused by the angle of the sun (Figure 5.5). In the summer, the response increases with each month of the summer with the lowest response observed in June at Lonielist and the greatest response observed in August. However, the highest sun angle appears in June (55.3°, GPP flux: 4.79 µmol CO_2 m^{-2} s^{-1}) (Figure 5.5), but does not correspond to the highest GPP flux (8.91 µmol CO_2 m^{-2} s^{-1}), which is observed at a lower sun angle (47.3°) in August. However, similar sun angles in spring do not result in similarly high fluxes, indicating that there is some other factor limiting GPP.

Table 5.3 Table of fitting parameters from the rectangular hyperbola fitted to the light response for each site. A_{max} denotes the maximum gross productivity and E_o the initial slope, which is also the apparent quantum yield (95% Confidence intervals).

	Spring		**Summer**		**Autumn**		**Winter**	
	A_{max}	**E_o**	**A_{max}**	**E_o**	**A_{max}**	**E_o**	**A_{max}**	**E_o**
Lonielist	**6.147** (5.837, 6.457)	**0.012** (0.008, 0.016)	**8.125** (7.967, 8.283)	**0.035** (0.029, 0.041)	**7.532** (7.197, 7.867)	**0.031** (0.025, 0.037)	**3.102** (2.894, 3.310)	**0.011** (0.007, 0.015)
Talaheel	**4.259** (3.876, 4.642)	**0.022** (0.018, 0.026)	**8.834** (8.464, 9.204)	**0.036** (0.030, 0.042	**8.213** (7.898, 8.528)	**0.028** (0.024, 0.032)	**3.157** (2.876, 3.438)	**0.013** (0.009, 0.017)
Cross Lochs	**9.674** (8.612, 10.736)	**0.035** (0.028, 0.042)	**12.498** (11.027, 13.969)	**0.043** (0.035, 0.051)	**10.127** (9.098, 11.156)	**0.036** (0.029, 0.043)	**5.762** (4.754, 6.770)	**0.029** (0.024, 0.034)

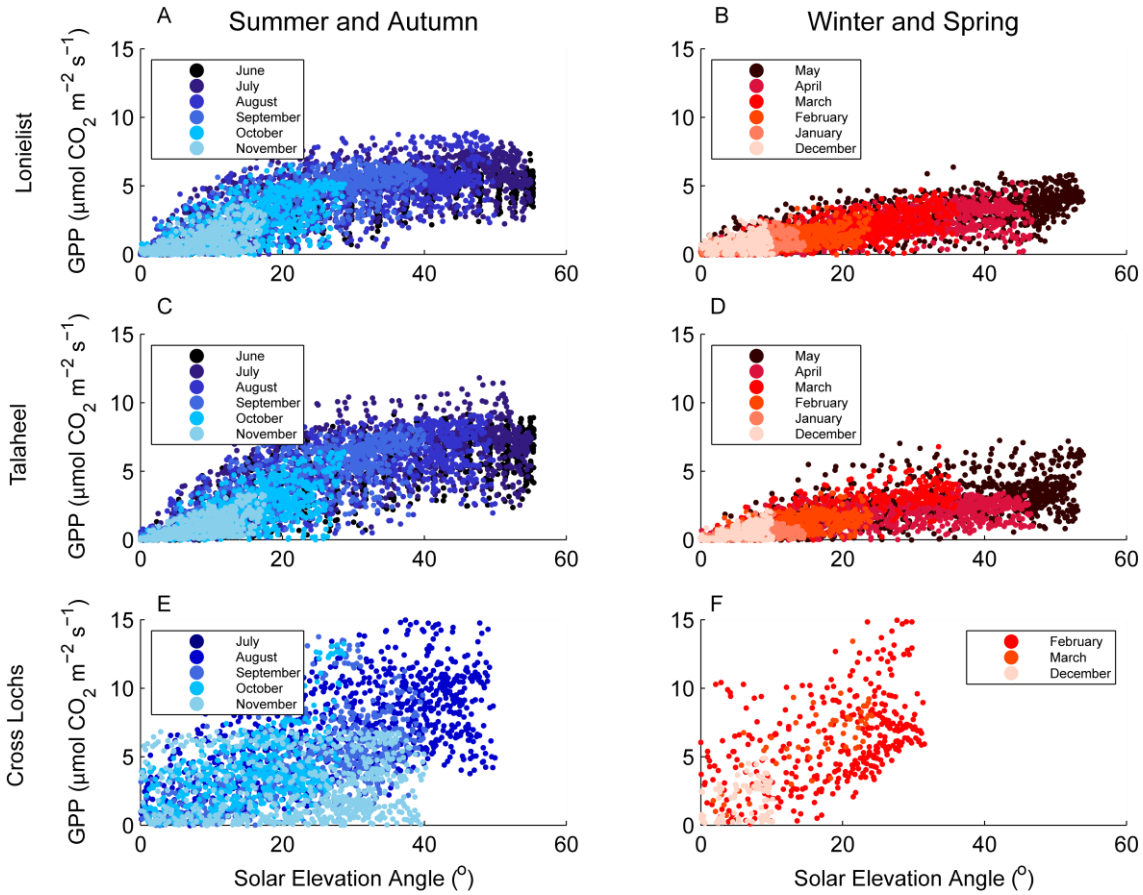

Figure 5.5 GPP fluxes relative the angle of the sun for each month at Lonielist (A and B), Talaheel (C and D) and Cross Lochs (E and F). Each month is represented by a different colour and the two columns split into summer, autumn and winter, spring.

A similar trend is observed at Talaheel, where the highest sun angles are not correlated with the highest GPP fluxes (Figure 5.5 C & D). All monthly summer fluxes between Lonielist and Talaheel were significantly different (Wilcoxon rank sum, $P < 0.0001$). The reverse trend of decreasing response with each month of autumn is very clear at both Lonielist and Talaheel and is further evident in Figure 5.5 where lower sun angles result in lower fluxes as less solar radiation penetrates down into the canopy. No significant differences were found between Lonielist and Talaheel in the months of October 2014 (Wilcoxon Rank Sum, $P = 0.0474$), November 2014 (Wilcoxon Rank Sum, $P = 0.0189$).

Further analysis showed a strong positive correlation between the solar angle and PPFD at Lonielist (Figure 5.6B), Talaheel (Figure 5.6D) and Cross Lochs (Figure 5.6F), (Spearman's ρ = 0.8475, 0.8978, 0.8053, $P < 0.0001$ respectively). Analysis of residuals from the GPP light response model (Figures 5.2 – 5.4) indicate an overestimation in GPP fluxes of up to 4 μmol CO_2 m^{-2} s^{-1} under high solar angles (>50°), particularly at Lonielist (Figure 5.6A). This suggests a potential limitation in the GPP flux not accounted for by PPFD. This is most prevalent in the summer (dark blue markers) when PPFD is highest (Figure 5.6B). The GPP overestimation at high solar angles was not observed as strongly at Talaheel (Figure 5.6C). However, in the autumn (blue markers), there was a move towards under-estimation at higher solar angles (~30 to 40°) and over-estimation at lower sun angles. At both Lonielist and Talaheel, there appeared to be no bias towards an under-estimation or over-estimation of GPP in winter and spring.

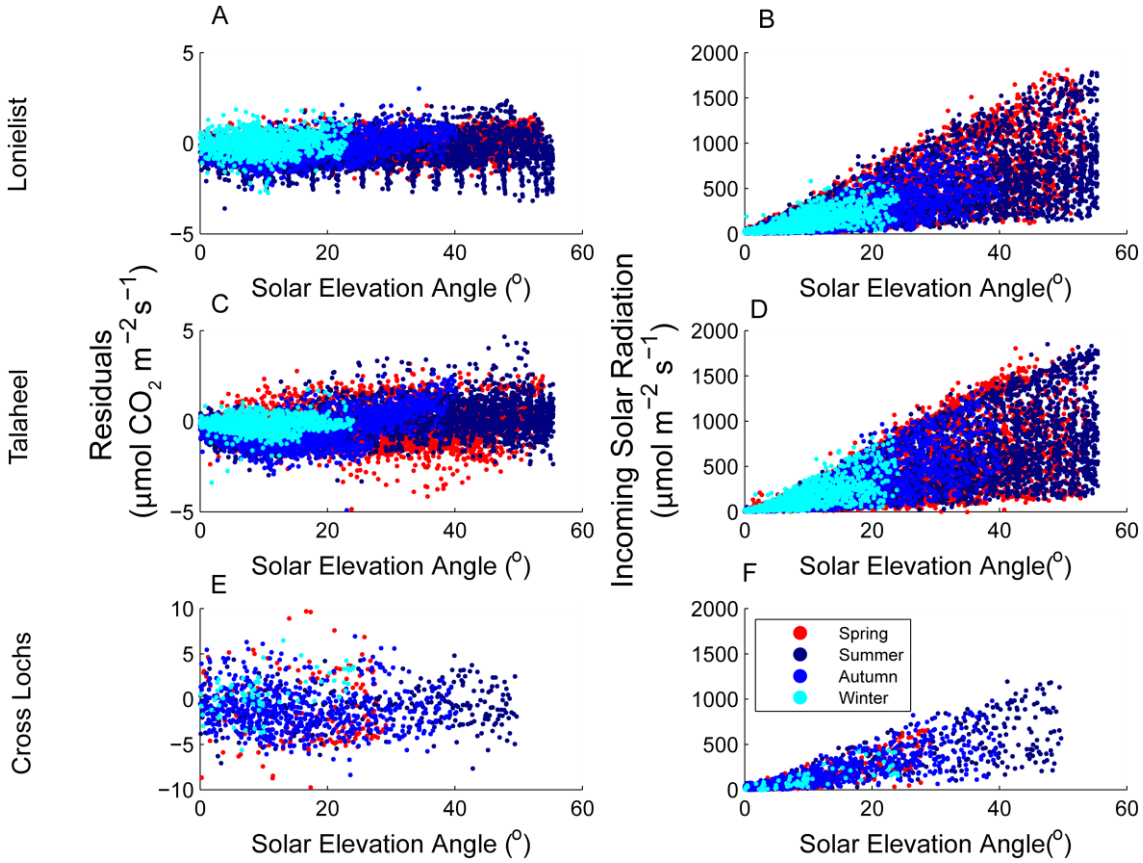

Figure 5.6 Plots A, C and E show residuals from the GPP model plotted against the solar elevation angle, and the influence of solar angle on GPP. Plots B, D and E show the relationship between incoming solar radiation (PPFD) and solar elevation angle.

At Cross Lochs, the highest sun angles did correlate with the highest GPP (Figure 5.5E and F), however due to a lack of data at the start of summer, it is not clear whether this is a robust result, as the highest sun angles are typically observed in June. Unlike Lonielist and Talaheel, GPP does not appear to reach an asymptote with increasing solar elevation at Cross Lochs, suggesting that this is not a limiting factor as it is at Lonielist and Talaheel. Residual analysis (Figure 5.6E) does not appear to show any bias towards an under-estimation or over-estimation in GPP by the model. However, further data are required particularly at higher PPFD levels to better understand GPP at Cross Lochs.

5.4.2 Environmental Drivers

At both Lonielist (Spearman's ρ = 0.8396, $P < 0.0001$) and Talaheel (Spearman's ρ = 0.8630, $P < 0.0001$), GPP was very strongly correlated with PPFD (Figure 5.7), however; only a moderate correlation was observed at Cross Lochs (Spearman's ρ = 0.3812, $P < 0.0001$).

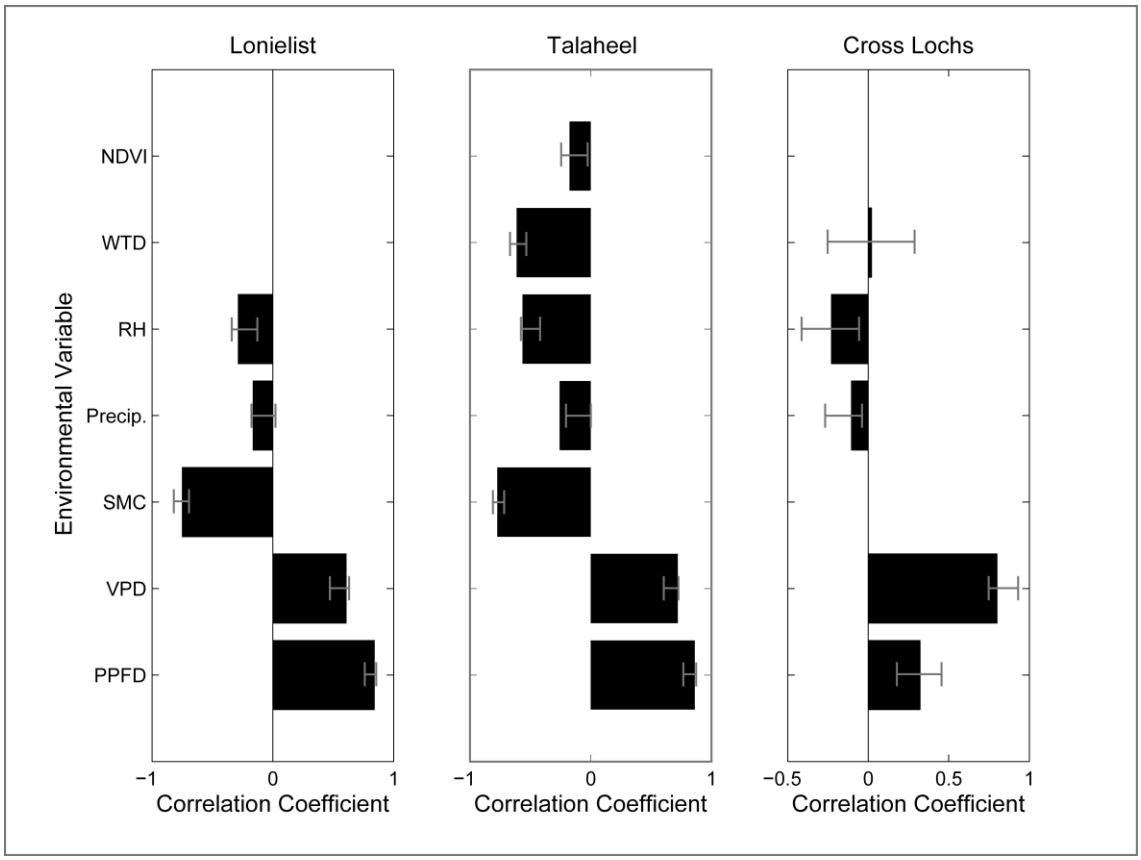

Figure 5.7 Spearman correlation coefficients for environmental drivers of Daily EC-derived GPP at Lonielist, Talaheel and Cross Lochs. Temperature was not included in these analyses, as the effect of temperature will still be present from the partitioning procedure and therefore may not be a true reflection of the correlation between temperature and GPP. Error bars represent the 95% confidence intervals.

At Lonielist, strong positive correlations (Figure 5.7) were found between GPP and Vapour Pressure Deficit (VPD - Spearman's ρ = 0.6006, $P < 0.0001$). A strong negative correlation was observed between GPP and soil moisture content at Lonielist (SMC - Spearman's ρ = - 0.7492, $P < 0.0001$) and Talaheel (Spearman's ρ = -0.7734, $P < 0.0001$), whilst negative correlations were observed with relative humidity at Lonielist (Spearman's ρ = - 0.2860, $P <0.0001$) and Talaheel (Spearman's ρ = -0.5638, $P < 0.0001$). Similar to Lonielist significant positive correlations were observed between VPD and GPP at Talaheel (Spearman's ρ = 0.7217, $P <0.0001$). Further analysis of the correlation between GPP and VPD at pressure greater than

1kPa found the correlation became strongly negative at Lonielist (Spearman's ρ = -0.6446, $P < 0.0001$) and weakly negative at Talaheel (Spearman's ρ = -0.3921, $P < 0.0001$).

The depth of the water table was strongly negatively correlated with GPP at Talaheel (Spearman's ρ = -0.6137, $P < 0.0001$), whilst a non-significant negative correlation was observed at Cross Lochs (Spearman's ρ = 0.0207, $P = 0.8029$). Additionally, normalised difference vegetation index (NDVI) was measured at Talaheel, showing a very weak but significant correlation with GPP (Spearman's ρ = 0.1761, $P = 0.001$).

When data were pooled, soil moisture content showed a negative correlation with soil moisture content. However, when assessed seasonally (Figure 5.9), both positive and negative relationships were observed, for example in summer a weak positive correlation was observed at both Lonielist (Spearman's ρ = 0.1242, $P = 0.2714$) and Talaheel (Spearman's ρ = 0.1307, $P = 0.2139$), although neither of these were significant. However, a strong negative correlation was observed in the autumn at both Lonielist (Spearman's ρ = -0.8211, $P < 0.0001$) and Talaheel (Spearman's ρ = -0.8248, $P = < 0.0001$).

VPD and SMC were found to have a limiting effect on GPP at Lonielist (Figure 5.8A). During periods of high VPD (>1kPa), low SMC (<0.5 m^3m^{-3}), and high incident PPFD (>1000 μmol m^{-2} s^{-1}), suppression was found in GPP. This effect is less pronounced at Talaheel (Figure 5.8B) due to the more stable SMC.

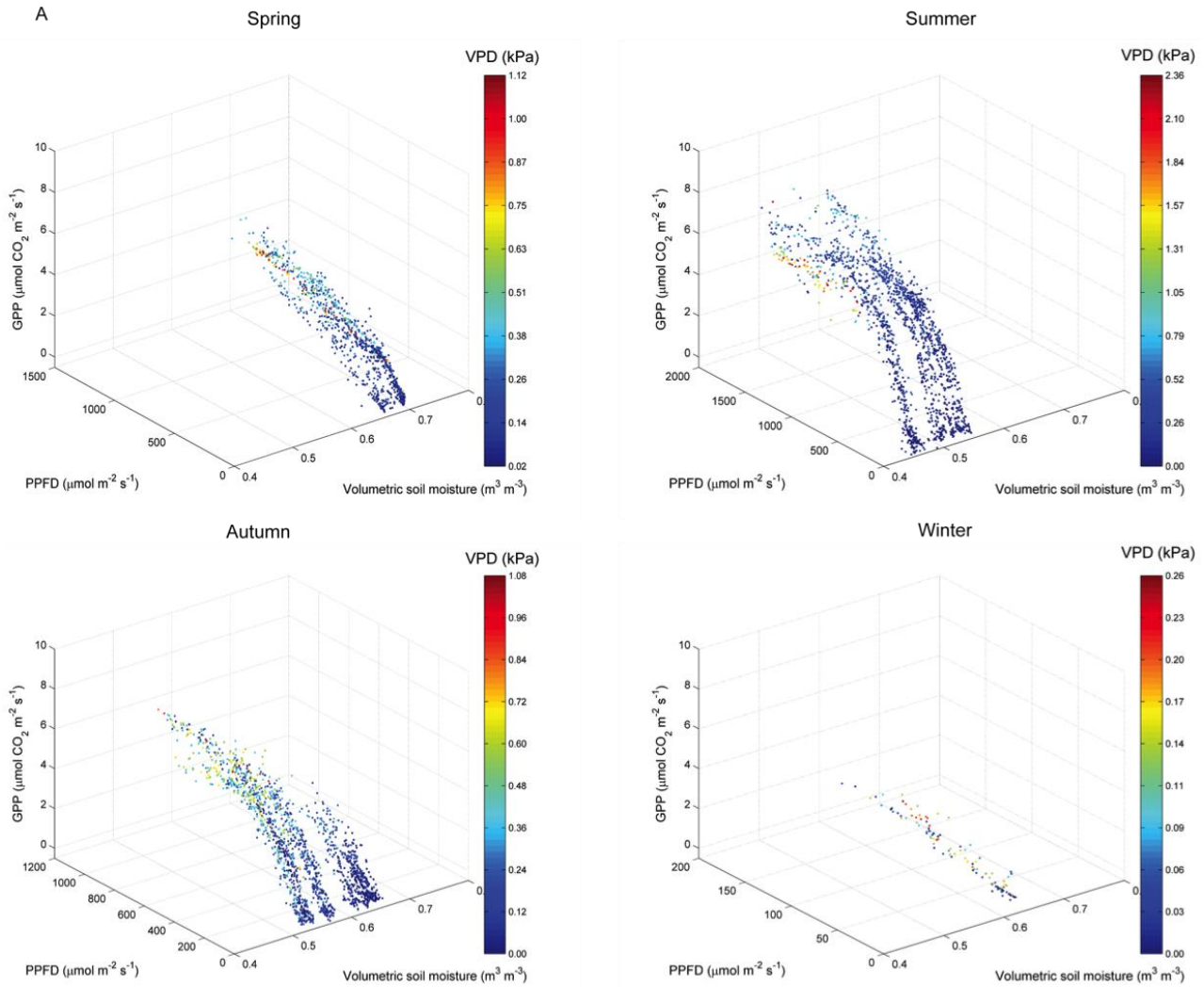
A
Spring
Summer
Autumn
Winter
VPD (kPa)
GPP (μmol CO2 m-2 s-1)
PPFD (μmol m-2 s-1)
Volumetric soil moisture (m3 m-3)

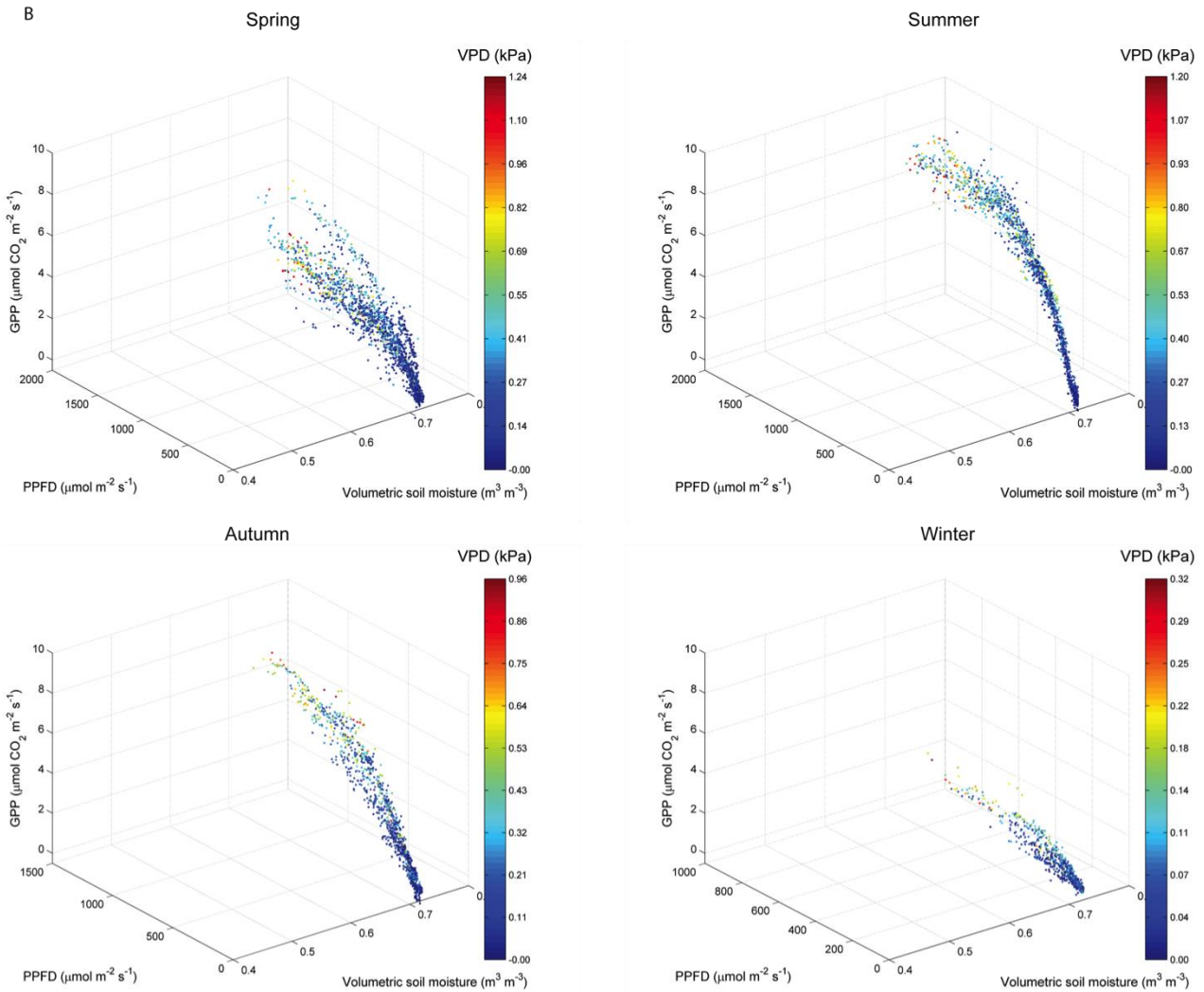

Figure 5.8 Three-dimensional scatter plots of the influence of VPD (kPa) on half-hourly EC-derived GPP at varying light levels and soil moisture content during each season at Lonielist (A) and Talaheel (B). Colour bars indicate vapour pressure deficit (kPa).

Low GPP fluxes were also observed at higher soil moisture content but as can be seen in Figure 5.8 this was caused by seasonality. This was particularly evident in winter where soil moisture content was high but GPP was low.

Using the results from the Spearman's rank correlation coefficient to inform independent variable inputs, a multiple regression analysis was undertaken at Lonielist and Talaheel. This analysis identified a very strong correlation between GPP and soil moisture, PPFD and VPD at both Lonielist ($R^2 = 0.91$, $P < 0.0001$) and Talaheel ($R^2 = 0.83$, $P < 0.0001$). This is consistent with the relationships observed in Figure 5.8. Similar to the Spearman's rank correlation coefficient analyses, temperature was not included in these analyses due to the potential effects of temperature in the data from the partitioning procedure. The partitioning of NEE into GPP is undertaken using temperature response curves therefore artefacts of this partitioning procedure could produce biased results. The effect of VPD and soil moisture content could not be assessed at Cross Lochs due to a broken soil moisture sensor.

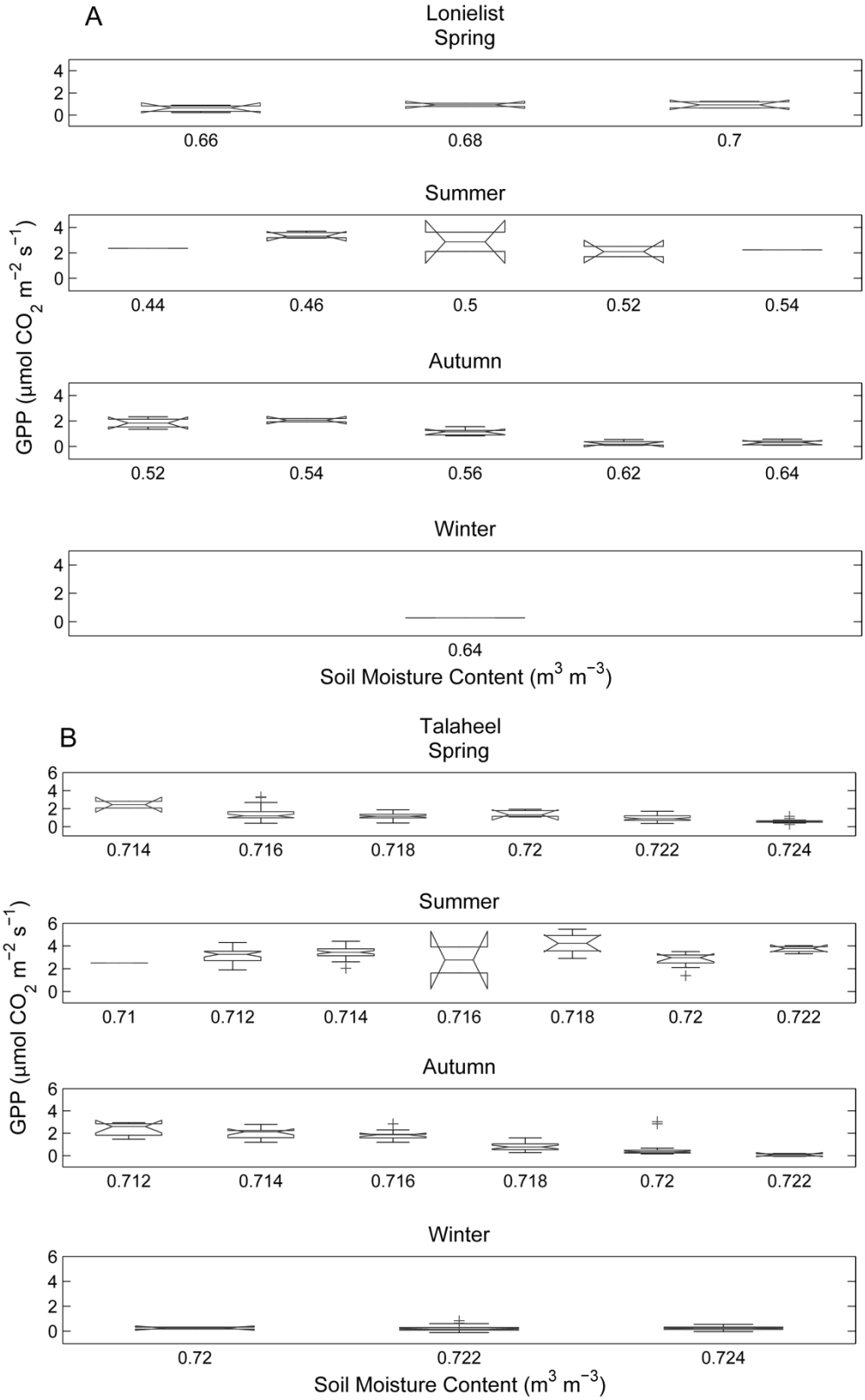

Figure 5.9 Relationship between soil moisture content and GPP at Lonielist (A) and Talaheel (B) during different seasons. Solid lines represent the median, with the boxes enclosing the 75th and 25th percentiles. The whiskers extend to the most extreme points not considered to be outliers, while outliers are plotted individually. Notches represent the 95% confidence intervals of the median.

5.5 Discussion

5.5.1 Effects of peatland restoration on GPP

In this study no significant difference was observed in GPP with time since restoration. However, annual C assimilation was greater in the undrained bog than the two restored sites even multiple decades after the onset of restoration. Similarly, Waddington and Price (2000) found that restoration increased GPP, as peatland vegetation began to colonise the site, but assimilation was still lower than that of undrained bogs in Quebec, Canada. Contrastingly, research using a dynamic chamber method in the Bois-des-Bel peatland in Quebec, Canada, observed higher C assimilation in restored peatlands than undrained sites (Strack and Zuback, 2013).

Annual GPP at the two restored sites was lower (Table 5.2) than the 6-year mean at Cross Lochs (Levy and Gray, 2015). Whilst environmental conditions play a role, it is thought that vegetation composition is a key driver in regulating C assimilation rates (Williams and Rastetter, 1999, Sims *et al.*, 2008, Poyatos *et al.*, 2014). Previous research has indicated *Sphagnum* mosses to be the greatest source of C assimilation in peatland environments (Weltzin *et al.*, 2000) with production positively correlated with *Sphagnum* moisture content (Grosvernier *et al.*, 1997). *Sphagnum* mosses have been found to have optimal water content for photosynthesis at 600-800% of dry weight, while photosynthesis declines rapidly when water content is reduced below optimal (Haraguchi and Yamada, 2011). Vegetation composition (Figure 5.0) showed Talaheel to have the largest *Sphagnum* and *Hypnum* moss coverage of the two restored sites, which would explain the greater CO_2 uptake from this site. However, the drier conditions at Lonielist are likely to result in lower GPP, with the dryness contributing to the lower coverage of *Sphagnum* and *Hypnum* mosses. Furthermore, areas of bare peat were also observed at Lonielist but not at Talaheel, which is also likely to account for some of the reduced assimilation at Lonielist. The significant correlation between GPP and NDVI (Spearman's $\rho = 0.1761$, $P = 0.001$), although weak, was indicative of a relationship between them. However, further research is required to better understand this relationship and understand how phenological changes and restoration affect this relationship.

Table 5.4 Literature searches of annual GPP flux rates from other peatland sites in the Northern Hemisphere. * Denotes this is a mean value from 12 sites in the Northern Hemisphere.

GPP (g C m^{-2} yr^{-1})	Reference
336	Peichl *et al.* (2014)
575	Levy and Gray (2015)
514*	Lund *et al.* (2010)
713	Syed *et al.* (2006)

Whilst greater C assimilation rates were observed in other Northern Hemisphere peatlands they are not dissimilar from those observed at Lonielist and Talaheel (Table 5.4). For instance, a synthesis of 12 northern peatlands (Lund *et al.*, 2010) found a mean annual GPP flux of 514 ± 206 g C m^{-2} yr^{-1}, which is lower than that observed at Talaheel (551 g C m^{-2} yr^{-1}) and slightly higher than that observed at Lonielist (501 g C m^{-2} yr^{-1}).

There is a dearth of information concerning C dynamics of restored northern peatlands, and particularly the GPP component of NEE. Studies that have investigated C dynamics of restored peatlands around the world have focussed on growing season fluxes (Strack and Zuback, 2013). Moreover, this lack of information is more acute on sites restored from forestry plantations. The intra-annual variability observed in this study suggests that peatlands restored from forestry maintain a very distinct seasonal pattern in GPP fluxes similar to that of other northern peatlands (Bubier *et al.*, 1998, Sottocornola and Kiely, 2010, Helfter *et al.*, 2014, Levy and Gray, 2015).

Seasonal GPP fluxes (Table 5.2) were in a similar range to those observed on other restored peatlands (Waddington *et al.*, 2010, Ballantyne *et al.*, 2014), with winter fluxes at Lonielist and Talaheel between 0 to 3.4 μmol CO_2 m^{-2} s^{-1}, whilst Cross Lochs fluxes (0 to 9.3 μmol CO_2 m^{-2} s^{-1}) were similar to undrained peatlands (Aurela *et al.*, 2009). Summer and autumn GPP fluxes from Lonielist and Talaheel were also in the range (0 to 11.82 μmol CO_2 m^{-2} s^{-1}) of other peatland restoration sites (Strack *et al.*, 2014).

5.5.2 Light response characteristics

Established relationships between PPFD and GPP (Gilmanov *et al.*, 2003) described by a rectangular hyperbola (Clement *et al.*, 2012), suggest that GPP increases with increasing light intensity. Light use efficiency (E_o) increased with time since restoration (Table 5.3) and was greatest at Cross Lochs, most likely due to the more typical bog-like vegetation composition and lack of structured microtopography. Seasonal differences were observed in E_o as would be

expected with reduced incoming solar radiation and phenological changes resulting in less photosynthesis in winter than in summer (Zhang *et al.*, 2006). However, a smaller range of E_o was found at Cross Lochs (0.029 to 0.043) indicating more efficient light use at Cross Lochs compared to Lonielist (0.011 to 0.035) and Talaheel (0.013 to 0.036). Light use efficiency was in a similar range (0.011 to 0.043 μmol m^{-2} s^{-1}) to other studies undertaken in restored peatlands (Waddington and Warner, 2001, Otieno *et al.*, 2009, Otieno *et al.*, 2012, Goodrich *et al.*, 2015). The restoration effect was observed in A_{max} with the highest values observed at Cross Lochs (5.762 to 12.498 μmol m^{-2} s^{-1}) and the lowest values observed at Lonielist (3.102 to 8.125 μmol m^{-2} s^{-1}) (Table 5.3); these were in a similar range of other peatlands (Komulainen *et al.*, 1999, Waddington and Warner, 2001, Goodrich *et al.*, 2015). However in spring, lower light use efficiency was observed at Talaheel compared to Lonielist. This is likely due to the influence of the earlier start to measurements at Talaheel, which was affected by snowfall in the spring of 2014. Snow cover limitations have been observed in other systems (Bosio *et al.*, 2014).

The light response curves obtained from Lonielist (Figure 5.2) and Talaheel (Figure 5.3) appeared to show at least two light response curves, particularly during summer and autumn, caused by differences in GPP during the different seasons (Medvigy *et al.*, 2013, Wang *et al.*, 2014). A potential explanation is the elevation angle of the sun changing each month, altering the amount of light penetrating the canopy and thus affecting GPP. Furthermore, the relationship between GPP and sun angle reaches an asymptote (Figure 5.5) where increasing sun angles do not increase GPP, and the highest GPP fluxes are not associated with the highest sun angles. The asymptote is not observed at Cross Lochs, which likely reflects the lack of data at high PPFD (~2000 μmol m^{-2} s^{-1}) and high sun elevation angles (>50°). The overestimation in the GPP model at high sun elevation angles and high PPFD, particularly at Lonielist, is indicative of a mechanism for suppression of GPP. It is also likely that the effects of VPD and soil moisture content (Section 5.6.3) had an influence upon some of these points and reduced GPP. However, it is postulated that the east-west aspect of microtopography (Chapter 6) and significant amounts of woody debris at Lonielist caused some degree of shading over smaller vegetation. Larger vegetation, reduced woody debris, and a south-north microtopographic aspect reduced the appearance of this effect at Talaheel. Further research is required to better understand this shading effect and its interactions with VPD and soil moisture.

PPFD is measured at a height of 3 m on the flux towers, however at ground level large woody debris and microtopography are likely to cast a shadow over the vegetation and thus there is a mismatch between the measurements and what is actually happening at the plant-soil interface and thus could lead to an apparent reduction in GPP. This therefore raises questions surrounding

the usefulness of above-canopy solar radiation measurements in peatlands restored from forestry plantations or on sites with significant canopy cover. Previous research has shown that plants grown in shaded conditions can be up to 25% less productive than plants in full light conditions (Chen *et al.*, 1994). Whilst no published research has observed this effect in restored peatlands, higher GPP fluxes in diffuse light due to the canopy structure and the area of photosynthetically active plant matter have been observed (Knohl and Baldocchi, 2008, Wohlfahrt *et al.*, 2008). This potentially explains the different response at Talaheel where longer restoration time has introduced a different canopy structure, reducing the impact of shading.

Light response relationships were difficult to assess at Cross Lochs (Figure 5.4) due to the poor frequency of data collection at this tower, which was attributed to two main factors. Firstly, significant periods of down time at the tower due to issues with the data logger and power. Secondly, due to the open-path analyser and its known poor performance during precipitation events (Chapter 3), data coverage was low resulting in noisy data as the analyser came in and out of signal.

5.5.3 Hydro-meteorological controls of GPP

The results from this research suggest a mechanism where GPP fluxes become suppressed at periods of high VPD (>1 kPa), low soil moisture content (<0.5 m^3 m^{-3} and high PPFD (>1000 μmol m^{-2} s^{-1}) (Figure 5.7). This relationship was particularly prevalent at Lonielist, where SMC was more variable than at Talaheel (Figure 5.9). Spearman's correlation suggested a strong positive relationship between VPD and GPP. However at high VPD (>1 kPa), a significantly strong negative correlation was observed between VPD and GPP at Lonielist (Spearman's ρ = -0.6447, $P < 0.0001$) whilst a significantly weak negative correlation was observed at Talaheel (Spearman's ρ = -0.3921, $P = 0.0362$). The switch from a strong positive correlation at low VPD (<1kPa), to a strong negative correlation between GPP and VPD at high VPD (>1 kPa), follows the results observed at Lonielist, where GPP was limited during periods of high VPD (>1 kPa) and low soil moisture content (<0.5 m^3 m^{-3}). The results of multiple regression analyses at Lonielist and Talaheel suggest an interactive effect of all three of these variables on GPP. When assessed together, over 90% of the variance in the data at Lonielist was explained by these three variables, whilst at Talaheel around 83% of the variance was explained by the three variables.

The data presented in Figure 5.9 highlights that soil moisture content alone is not able to explain differences in GPP. The seasonal differences in relationships between GPP and soil moisture content are suggestive of interactive relationship with other environmental variables. Therefore

soil moisture, in these restored ecosystems, cannot be used independently to explain the variation in GPP, but they must be considered along side other environmental variables and potential interactive effects between soil moisture content and other variables. As the correlation between GPP and soil moisture content varied seasonally, it is likely that temperature was a driving variable. As temperatures decreased through autumn and into winter, GPP reduced, but the soil moisture content increased due to the lower evaporation rates and higher precipitation inputs, therefore a negative correlation is observed between soil moisture and GPP. Whereas, through spring and into summer the temperatures were higher, GPP rates increased due to the increasing incident solar radiation. As seen in Figure 5.8, dry periods combined with high VPD (>1kPa), reduced GPP rates due to water stress, therefore higher soil moisture content during the summer was less likely to be a limiting factor and therefore increased GPP. Although this effect has not been seen before in peatlands, previous research has observed decreased GPP under wet conditions in grass species (Xu and Zhou, 2011). Therefore, vegetation composition could also have an impact, as these sites continue to recover and *Sphagnum* spp. continue to recolonise these ecosystems, this seasonal effect on GPP and soil moisture could potentially decrease and a more typical positive correlation be observed (Waddington and Price, 2000, Strack *et al.*, 2009).

Dang *et al.* (1991) suggested cooler temperatures at depth in the peat profile limited plant water uptake resulting in a significant portion of the water required by the plants being supplied from the shallower roots within the oxic peat profile (Lafleur *et al.*, 2005a). Low root-shoot hydraulic conductance of many peatland plants makes them susceptible to transpiration losses during periods of high VPD (Dang *et al.*, 1991, Lafleur *et al.*, 2005a, Touchette *et al.*, 2010). Moreover, due to the low hydraulic conductivity of peaty substrates, small decreases in water table depth can result in significant changes to the soil moisture content of the peat above the water table (Clymo, 2004, Lafleur *et al.*, 2005a). Research has found that the combination of shallow rooting depths and low hydraulic conductivity combined with high VPD (>1 kPa) and low soil moisture content results in plants closing their stomata in order to limit losses through transpiration (Bongi, 1990, Sperry, 2000). The closure of the stomata reduces photosynthesis and thus CO_2 uptake (Otieno *et al.*, 2012, Goodrich *et al.*, 2015).

The data observed at Lonielist and Talaheel agreed with this theory, where a lower GPP flux was observed during periods of low soil moisture content (<0.5 m^3 m^{-3}) and high VPD (>1 kPa) (Figure 5.8). The greater coverage of vascular and non-moss species at Lonielist (Figure 5.0) combined with a more variable water table is likely to account for the relationship between GPP and VPD. The greater coverage of *Sphagnum* and other moss species at Talaheel contributed to

the more stable water table and soil moisture content due to their moisture retention properties (Chirino *et al.*, 2006, Waddington *et al.*, 2011), resulting in a weaker relationship between GPP and VPD. Additionally, the greater coverage of non-stomatal vegetation such as *Sphagnum* reduced the loss of GPP during drier conditions (Otieno *et al.*, 2012, Goodrich *et al.*, 2015). Similar findings have been observed at other northern peatlands. Research by Otieno *et al.* (2012) at a mountain peatland in Germany found that GPP was reduced under high PPFD (>1000 μmol m^{-2} s^{-1}), low volumetric soil moisture content (<40%) and high VPD (>1 kPa). Here, the authors calculated that this reduction in GPP, due to stomatal closure, resulted in a net 20-30% loss of GPP in summer. Additionally, research undertaken at the Glencar bog in Ireland found that high values of air temperature, PPFD, VPD and low soil moisture content caused a desiccation of the moss layer, reducing the GPP contribution from moss species in the ecosystem (Sottocornola and Kiely, 2010). Although no desiccation of the moss layer was visually observed at any sites in the Flow Country during this research, future climate change in the Flow Country is expected to result in drier, warmer summers (Stocker *et al.*, 2013), potentially leading to a reduction in GPP if significant warm dry weather persists.

5.6 Conclusions

This chapter has presented the first year-round EC-measured GPP fluxes from a chronosequence of restored blanket bogs in the Northern Hemisphere. Although research has previously been undertaken on GPP fluxes in restored northern peatlands, many of these have focussed on growing season fluxes or have been measured using a chamber method due to the typically small extent of many peatland restoration sites.

There was no significant increase in GPP between the youngest site (Lonielist; restored 2003/04) and the oldest site (Talaheel; restored 1997/98). Distinct seasonal patterns were present in the data, with the maximum GPP flux observed in summer and the minimum in winter. Over annual timescales, although there were non-significant increases in assimilation rates, the restored sites were unable to assimilate as much C as the mean GPP flux over 6 years at the undrained bog at Cross Lochs.

Light use efficiency increased with time since restoration, although the efficiency at the restored sites never reached the same levels as that observed at the Cross Lochs control site. These differences are likely to have been caused by differences in the vegetation structure and composition, with typical bog species such as *Sphagnum* and *Hypnum* being concentrated in the wetter furrows, where they tended to be shaded by microtopography and large woody debris, which reduced GPP. This was particularly observed during periods of high measured PPFD and high solar elevation, where there is likely to be a discrepancy between the measured PPFD and the PPFD received at the plant-soil interface. As would be expected, incident PPFD was found to have the greatest correlation with GPP. However, soil moisture and VPD also had an impact on GPP by reducing the flux during periods of high VPD (>1 kPa), high PPFD (>1000 μmol m^{-2} s^{-1}) and low soil moisture content (<0.5 m^3 m^{-3}). During these periods, plants become water stressed forcing them to close their stomata thereby reducing photosynthesis. This was particularly evident at Lonielist where soil moisture content was less stable than at Talaheel.

~Chapter 6 ~

Microtopographic influences on CO_2 exchange in restored Flow Country peatlands

6.0 Abstract

Peatlands are dependent upon cool, wet conditions to accumulate peat and sequester carbon (C). Drainage or de-watering of peat can promote aerobic decomposition of the peat and a loss of C to watercourses and the atmosphere. Across the Northern Hemisphere, 15 million ha of peatlands have been drained for plantation forestry since the 1900s. Drainage requires ploughing of the peat, and the creation of distinct microtopographic features - furrows, ridges and a remnant of the original surface. Efforts are on-going in parts of the Northern Hemisphere to restore these forested peatlands to blanket bog. However, even though micro-scale gradients in redox and environmental conditions are known to be important C flux regulators in peatlands, little or no empirical data exists on the effects of artificial microtopography on C fluxes. C fluxes from the microtopographic features were studied using a dynamic chamber technique over a chronosequence of five sites over two separate years.

Significant differences were observed in respiration (R_{eco}) both among microforms and for the same microform at different sites across the chronosequence. At the newest restoration site (NR), ridge R_{eco} fluxes were significantly higher than those from the original surface and furrow. In contrast, at the oldest restoration site, similar R_{eco} fluxes were observed on ridges and original surfaces in both years; while R_{eco} fluxes from furrows were significantly lower. Statistical analyses of environmental variables found soil moisture and temperature had the greatest influence on R_{eco} across all microforms.

Gross primary productivity (GPP) measurements were only undertaken over one year at the oldest restoration site; however, no significant differences were observed in fluxes across microforms. Fluxes from the original surface were strongly influenced by a single photosynthetic hotspot, which was dominated by grasses and sedges, such as *Carex panicea* and *Molinia caerulea*, suggesting vegetation can play a key role in controlling GPP among microforms. Incoming solar radiation, soil moisture and temperature were observed to be key environmental variables. These results suggest that microforms present a significant source of CO_2 to the atmosphere and further restoration is required to restore net C sink functioning.

6.1 Introduction

Under undisturbed conditions, peatlands function as a net C sink with modest rates of organic matter decomposition (Holden, 2005). Perturbations such as peatland drainage can enhance aerobic decomposition, which may lead to peat erosion and enhanced gaseous and aqueous carbon (C) release (Holden *et al.*, 2004, Parry *et al.*, 2014). However, with many blanket peatlands now subject to environmental protection legislation, there has been a significant increase in the number of blanket peat restoration projects since the turn of the century (Parry *et al.*, 2014). Despite this, there remains a distinct lack of understanding of the impacts of restoration on C dynamics over multi-annual to decadal timescales, particularly in sites restored from forestry.

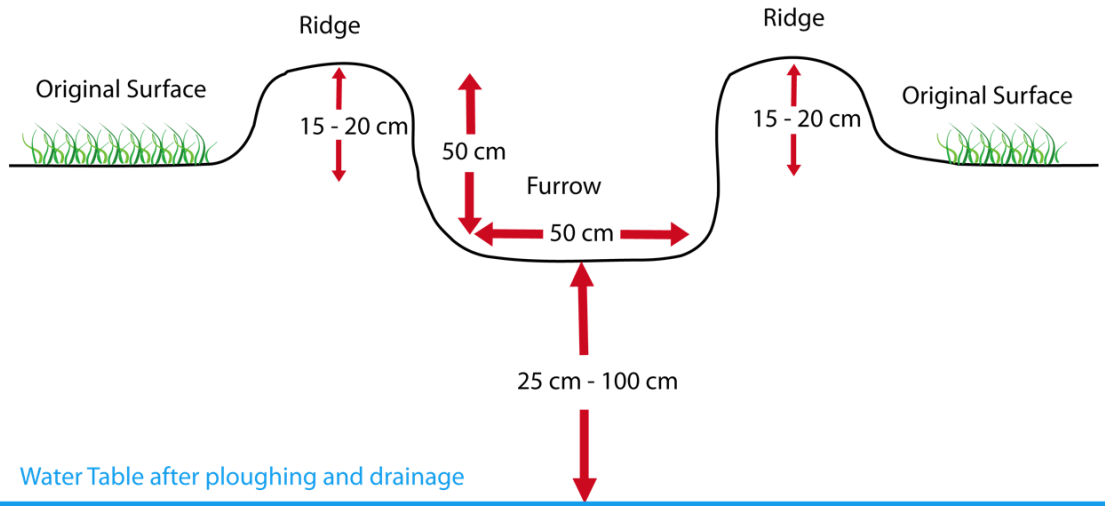

Figure 6.1 Schematic representation of the microtopographic features of a blanket bog ploughed and drained for forestry plantation. All measurements are given as approximations but are representative of those observed at the sites used in this study.

Peatland drainage lowers the water table, exposing a greater area of peat to aerobic conditions, which subsequently alter its physical, biogeochemical and hydrological functioning (Holden *et al.*, 2004, Parry *et al.*, 2014). In forested peatland ecosystems, re-profiling and ploughing of the peat creates three distinct microtopographic features; ridges, furrows and a remnant of the original surface (Figure 6.1 and Chapter 1). During restoration, drainage channels are blocked, typically using dams constructed from materials such as peat, heather bales or plastic sheeting in order to reduce water losses from the landscape and raise the water table height (Parry *et al.*, 2014). As the water table rises, it is likely to impact upon biogeochemical processes as anaerobic conditions begin to return to the peat system and decomposition slows, reducing the efflux of CO_2 (Waddington and Warner, 2001, Dixon *et al.*, 2014, Strack *et al.*, 2014). The restoration of afforested peatlands in the Flow Country does not include microtopographic re-profiling, as typically occurs in Canada and other Northern Hemisphere countries (Quinty and

Rochefort, 2003). In the Flow Country, felled trees are left to decompose in the furrows to act as a dam, due to cost of removing the trees from sites. It is thought that this will help the water table to naturally return to previous levels and provide organic matter for the formation of new peat.

In undrained peatlands, relationships between soil moisture, water table depth and soil respiration have been observed in hummock/hollow microtopographic structures (Kim and Verma, 1992, Nungesser, 2003, Luan and Wu, 2014). Consistently higher respiration rates have been observed from the drier hummock microsites than hollows, which tend to be wetter and closer to the water table (Kim and Verma, 1992). Environmental drivers, such as water table height and soil moisture content, tend to be relatively constant in undrained peatlands with variation tending to occur within the acrotelm (the area of peat containing living vegetation) due to the large pore structure and high saturated hydraulic conductivity of poorly decomposed organic matter (Kim and Verma, 1992, Evans *et al.*, 1999, Lapen *et al.*, 2000, Holden and Burt, 2003).

Little or no empirical data exists on the influence of man-made microtopographic (furrow/ridge) structures on C exchange and the key environmental drivers influencing C dynamics. Previous research has observed water tables in restored peatlands to be more variable than undrained sites due to changes in hydraulic conductivity, porosity, topography and organic matter inputs with water tables and soil moisture content observed to vary within the space of a few metres (Holden *et al.*, 2011, Parry *et al.*, 2014). This spatial variation in hydrological conditions, coupled with known interactions between hydrology and C dynamics, will likely influence the C exchange. It is therefore necessary to understand how C dynamics in man-made microtopographic features are affected by environmental conditions and how this changes with time since restoration. Improving our knowledge of the influence of man-made microtopographic features on C dynamics in restored peatlands can help with modelling of C cycling and predict the recovery trajectories of these restored ecosystems over multi-decadal timescales.

In order to understand how these structures respond to restoration and changing environmental conditions such as water table depth and soil moisture, ecosystem respiration (R_{eco}) fluxes were collected using a dynamic flux chamber technique across a chronosequence of sites in 2011/12 with data analysis conducted during 2012/13. Additionally, light response chamber measurements were undertaken at Talaheel during 2014/15 to understand the effects of microtopography on gross primary productivity (GPP), whilst also providing further data on

R_{eco} fluxes from a site at a more advanced stage of restoration. This chapter will answer the following questions:

1) How does R_{eco} from each microform change with time since restoration?

2) How do microforms affect GPP in restored blanket bogs?

3) What are the environmental factors controlling R_{eco} and GPP from microforms in restored blanket bogs?

6.2 Methods

Dynamic chamber measurements were undertaken across a chronosequence of restored sites (Table 6.2) on the Forsinard Flows National Nature Reserve (Figure 6.2) between July 2011 and July 2012. Further research was undertaken at Talaheel (Chapter 2), in response to the results from the previous data collection, between January 2014 and February 2015 to ascertain the effects of man-made microtopographic features on R_{eco} and GPP. Environmental variables, such as air temperature, soil temperature and soil moisture content, were also measured at each chamber to understand the key environmental drivers and how these change across different microforms.

6.2.1 Experimental Design

The experimental designs between the 2011/12 and 2014/15 studies were slightly different due to the different original aims of both studies. The experimental designs are discussed in Chapter 3, but are outlined briefly below.

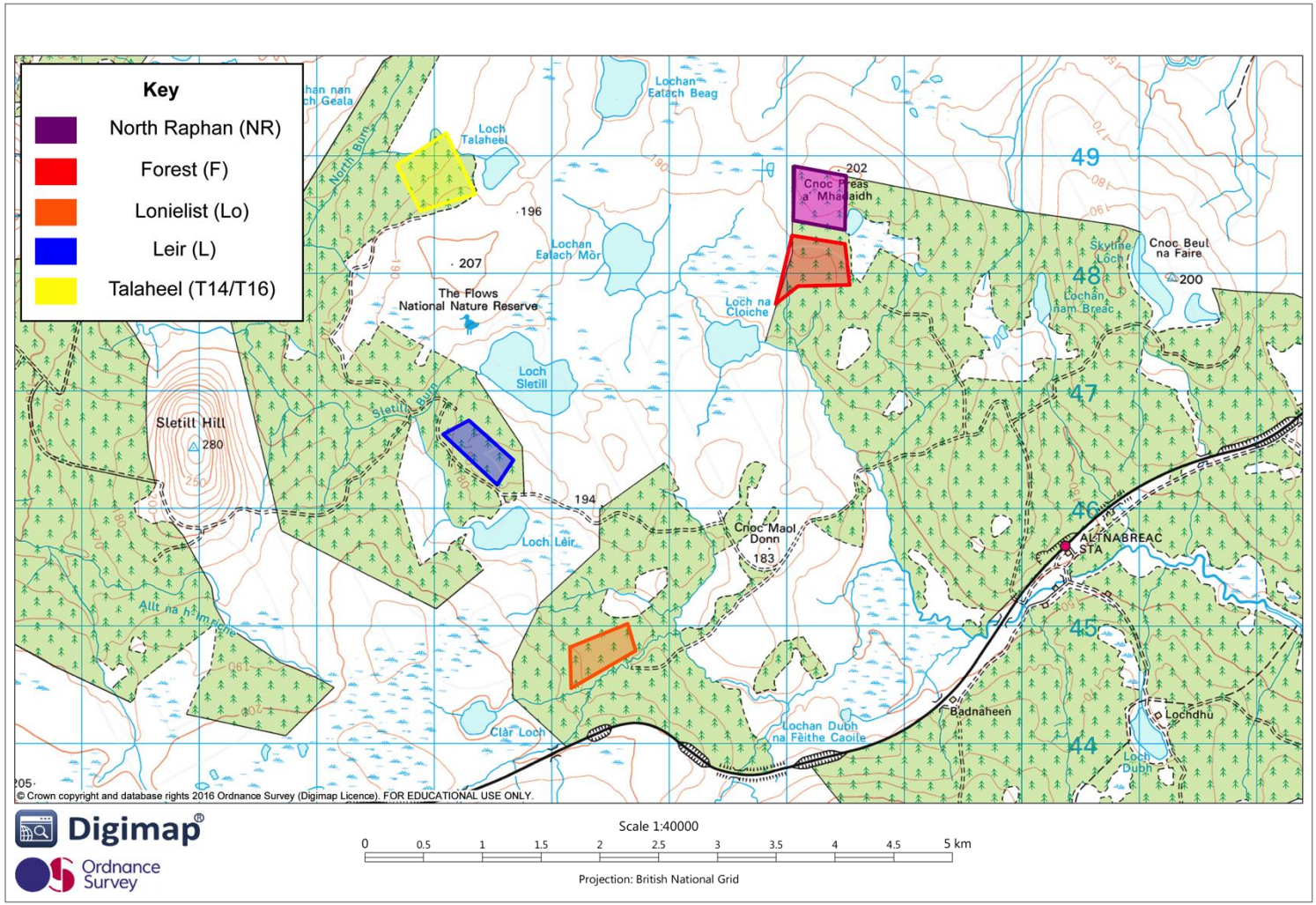

Figure 6.2. Map showing the site locations on Forsinard Flows National. Coloured polygons indicate locations of sites used in the chamber study (Image Source: Digimap, 2015).

6.2.1.1 - 2011/12

Two chambers were placed on each microform and replicated three times giving a total of 18 chambers per chronosequence age (Table 6.2). Four piezometers were also used at each site, two on the original surface and two in the furrow to provide water table measurements at the time of sampling. The chambers were measured during a single year from July 2011 to July 2012 (Table 6.1)

6.2.1.2 - 2014/15

One chamber was placed on each microform giving three chambers per site. This was replicated three times across Talaheel to provide spatial variability whilst retaining a focus on the microtopography. The chambers were measured over the course of a year from January 2014 to February 2015 as seen in Table 6.1 Sampling had to be reduced in autumn and winter, as the site was inaccessible due to adverse weather. Additionally, the ground nesting bird season limited access to some sites in the spring.

Table 6.1 Table of sample months for chamber measurements undertaken in 2011/12 and 2014/15

Year	January	February	March	April	May	June	July	August	September	October	November	December
2011												
2012												
2014												
2015												

Key	
	GC Measured Flux
	EGM-4 Measured Flux

6.2.2 Chamber and Analytical Methods

6.2.2.1 GC flux measurements during 2011/12

Chamber data collected in 2011/12 consisted of a two-component (base and lid) opaque dynamic flux chamber to quantify ecosystem respiration (R_{eco}) fluxes from microtopographic features across a chronosequence of restored sites. The flux chamber (height 40 cm) was fitted with a small fan and pressure port to ensure good mixing of the chamber headspace whilst allowing the internal chamber pressure to equilibrate with ambient air (Pumpanen *et al.*, 2004, Levy *et al.*, 2012). Each chamber was covered in reflective material to reflect incident solar radiation, reducing potential heating of the chamber. Gas fluxes were measured by enclosing an area of 0.031 m^2 for 18 minutes. Attached to each chamber was a 1.5 m sampling tube which was flushed three times before each headspace gas sample was taken. Four samples were collected at six-minute intervals using a gas tight syringe. These were then stored in pre-labelled, pre-evacuated 12 mL Exetainers® (Labco Ltd., Lampeter, UK). Collected gas samples were analysed with a Thermo TRACE GC ULTRA (Thermo Fisher Scientific Inc., Waltham, Massachusetts, USA) at the University of St Andrews. The instrument was equipped with a HayeSep-Q column to give chromatographic separation and the analyte concentration quantified using a flame ionisation detector (FID) with methaniser. The precision of the instrument was determined by calculating the coefficient of variation of the three different certified standards (CO_2: 372ppm, 998 ppm and 5006ppm - CK Gas, Ibstock, UK) analysed in each run, which were always below 5%.

6.2.2.2 IRGA C flux measurements during 2014/15

Transparent chambers were used in the 2014/15 study to account for photosynthesis and gain a fuller understanding of microtopographic effects on C dynamics. A two-component (base and lid) dynamic flux chamber, 30 cm in height, with a small fan was connected to an EGM-4 (PP-Systems, Amesbury, MA, USA) for instantaneous measurement of headspace CO_2 concentration changes over an area of 0.031 m^2. Headspace concentration was logged every four seconds over the enclosure time of two minutes. Each chamber was replicated twice, with the chamber then darkened using a shade cloth to ascertain the light response. Four shading levels were used; clear, approximately 25% shading, approximately 75% shading and dark.

A more detailed explanation of the methods for each of the chamber measurements is available in Chapter 3.

6.2.3 Environmental measurements

Measurements of key environmental variables, such as temperature and soil moisture, were undertaken at each chamber. Air and soil temperatures were measured using a type-k

thermocouple attached to a handheld meter (Omega Engineering Ltd., Manchester, UK). Four soil temperatures were taken immediately adjacent to the chamber base (< 5 cm from each chamber base; depth of 0–10cm). Chamber temperature was measured at the start and end of each measurement to ensure large temperature differences (> 3°C) were not experienced during sampling. In 2011/12, soil samples of known volume were taken immediately adjacent to each chamber (<5 cm from each chamber base in the top 10 cm of the peat) to assess the soil moisture content. These were returned to the lab, weighed and dried at 105°C for 24 hours before being weighed again to determine final dry weight (O'Kelly, 2007). Volumetric water content, bulk density and water-filled porosity were then calculated using established methods (Breuer *et al.*, 2000). In 2014/15, soil moisture content was determined using a soil moisture probe (ML2x Theta Probe, Delta-T Devices Ltd, Cambridge, UK). Four measurements were taken immediately adjacent to each flux chamber (< 5 cm from each chamber base in the top 10 cm of the peat). In 2014/15, measurements of Photosynthetically Active Radiation (PAR) were also undertaken at each chamber to ascertain the light response.

Table 6.2 Location and number of chambers at each site along with the method of analysis used. Furrow and ridge measurements are relative to the original surface.

Site (Name)	Restoration Year	Microtopographic aspect/orientation	Furrow depth/width (cm)	Ridge Height (cm)	Sample Year	Number of Chambers	Number of Replicates	Analysis Method
Forest (F)	NA	south	20/45	13	2011/12	6	3	GC
North Raphan (NR)	2012	south-east	20/45	13	2011/12	6	3	GC
Leir (L)	2008	south-west	27/48	15	2011/12	6	3	GC
Lonielist (LO)	2003/04	south-east	23/47	14	2011/12	6	3	GC
Talaheel (T14)	1997/98	south	26/50	14	2011/12	6	3	GC
Talaheel (T16)	1997/98	south	26/50	14	2014/15	3	3	EGM-4 IRGA

Table 6.3 Dominant live vegetation types at each site and microform, displaying the change from Lichens, liverworts and mosses to bryophytes and vascular bog species.

Site	**F**	**NR**	**L**	**LO**	**T14 & T16**
Name	**Forest Control**	**North Raphan**	**Leir**	**Lonielist**	**Talaheel**
Furrow	Mosses	Mosses	Other mosses	*Hypnum spp.*	*Sphagnum spp.*
	Hypnum spp.	*Hypnum spp.*	*Hypnum spp.*	*Eriophorum spp.*	*Eriophorum spp.*
	Liverworts	Liverworts	*Sphagnum spp*	*Sphagnum spp.*	*Hypnum spp.*
Ridge	Mosses	Mosses	*Calluna spp.*	*Calluna spp.*	*Eriophorum spp.*
	Lichen	Lichen	*Eriophorum spp.*	*Eriophorum spp.*	*Calluna spp*
	Liverworts	Liverworts	*Hypnum spp.*	Other mosses	*Hypnum spp.*
Original	Mossses	Mossses	Other mosses	*Eriophorum spp.*	*Hypnum spp.*
Surface	Lichen	Lichen	*Eriophorum spp.*	Other mosses	*Sphagnum spp.*
	Liverworts	Liverworts	*Hypnum spp.*	*Sphagnum spp.*	*Eriophorum spp.*

6.2.4 Vegetation monitoring

Vegetation communities were assessed using nine 1 m x 1 m quadrats at each of the sites, three on each microform with the coverage of living vegetation estimated. Table 6.3 presents the dominant vegetation types within each microform. Monitoring took place during 2011/12 for all sites and was repeated again in 2014/15 at T16 to see if further restoration and colonisation by higher plants had occurred.

6.2.5 Analyses

R_{eco} was estimated using dark measurements for both the 2011/12 and 2014/15 datasets. In 2014/15, when light measurements were collected, GPP was calculated by subtracting the net ecosystem exchange (NEE) from R_{eco} (Shaver *et al.*, 2007):

$$GPP = R_{eco} - NEE$$

(Eqn. 6.1)

The Lloyd and Taylor (1994) model (Chapter 4 - Eqn 4.2) was parameterised using R_{eco} data to assess the respiration fluxes at 10ºC. The response of GPP to light was assessed using a rectangular hyperbola model similar to that of Street *et al.* (2007),

$$GPP = \frac{P_{max} \cdot I}{k + I}$$

(Eqn. 6.2)

where, P_{max} is the light saturated photosynthetic rate (μmol CO_2 m^{-2} s^{-1}), I the incident photosynthetically active radiation (μmol PAR m^{-2} s^{-1}), and k the half-saturation constant of photosynthesis (μmol PAR m^{-2} s^{-1}).

The Q_{10} temperature coefficient was calculated as a measure of the rate of change in respiration as a result of a change in temperature of 10°C,

$$Q_{10} = \left(\frac{R_2}{R_1}\right)^{10/(T2-T1)}$$

(Eqn 6.3)

where R_2 and R_1 are the final and initial respiration rates respectively and T_2 and T_1 are the final and initial temperatures (°C), respectively.

Statistical analyses were performed using MATLAB Version 8.1.0.604 (R2013a) and Statistics Toolbox Version 8.2 (R2013a) (Mathworks Inc., Natick, MA, USA). Normality within the data were tested using a Kolmogorov-Smirnov test. As the data were not normally distributed, non-parametric methods were used. However, data were transformed where necessary to meet assumptions.

As all the data were skewed, Kruskal-Wallis with Fisher's LSD post-hoc tests were used to determine differences in CO_2 flux with time since restoration, and Wilcoxon rank sum tests were used to determine whether CO_2 efflux rates changed across different microforms.

Spearman's rank correlation coefficient tests were applied to assess the correlation between the environmental variables and R_{eco} and GPP fluxes, with the strength of the correlation determined as per Table 6.4. The results of the Spearman's rank correlation analyses were used to inform the independent variables for multiple regression analyses to assess the effect of key environmental drivers on R_{eco}. Independent variable data transformed using natural logarithms in order to meet normality assumptions. All values are presented as median ± interquartile range unless otherwise stated. Significance was accepted at $P < 0.05$. All flux data presented in this Chapter are presented in μmol CO_2 m^{-2} s^{-1} to aid comparison with the data presented in Chapters 4 and 5.

Table 6.4 Classification of the strength measure and Spearman's correlation coefficient used in this study.

Strength	Correlation Range
Very Weak	0 to 0.19
Weak	0.2 to 0.39
Moderate	0.4 to 0.59
Strong	0.6 to 0.79
Very Strong	0.8 to 1.0

6.3 Results

6.3.1 Microform effects on R_{eco}

When all the data were pooled, significant differences were observed in R_{eco} between microforms (Kruskal-Wallis with Fisher's LSD, $P < 0.0001$). When disaggregated by microform, the highest R_{eco} fluxes were observed on the ridges (Figure 6.3) at all sites, except in Talaheel in 2011/12 (T14) (Figure 6.3E) and 2014/15 (T16) (Figure 6.3F), where the original surface fluxes were higher (2.27 ± 2.58 μmol CO_2 m^{-2} s^{-1} and 2.38 ± 2.17 μmol CO_2 m^{-2} s^{-1}, respectively) although not significantly (Wilcoxon rank sum, $P = 0.7707$). Ridge R_{eco} fluxes were consistent across all sites with the only significant difference observed at Leir (L) (Kruskal-Wallis with Fisher's LSD, $P = 0.0308$).

The original surface followed a similar pattern to the ridge (Figure 6.3), although the fluxes were always lower (Kruskal-Wallis with Fisher's LSD, $P = 0.0021$), except in T16 and T14 as mentioned previously. Significant differences in fluxes from the original surface were only observed at North Raphan (NR) and L compared to the other sites (Kruskal-Wallis with Fisher's LSD, $P = 0.003$).

Furrow R_{eco} fluxes were consistently lower (Figure 6.3) than those observed from the ridge and original surface (Kruskal-Wallis with Fisher's LSD, $P < 0.0001$). In 2011/12, the difference in CO_2 fluxes between microforms was significantly different (Kruskal-Wallis, $P < 0.0001$), with post hoc tests showing furrow R_{eco} to be significantly lower than both the original surface and ridge. A similar significant relationship was also found in the 2014/15 data, with fluxes from furrows significantly lower (Kruskal-Wallis with Fisher's LSD, $P = 0.002$) than the original surface and ridge.

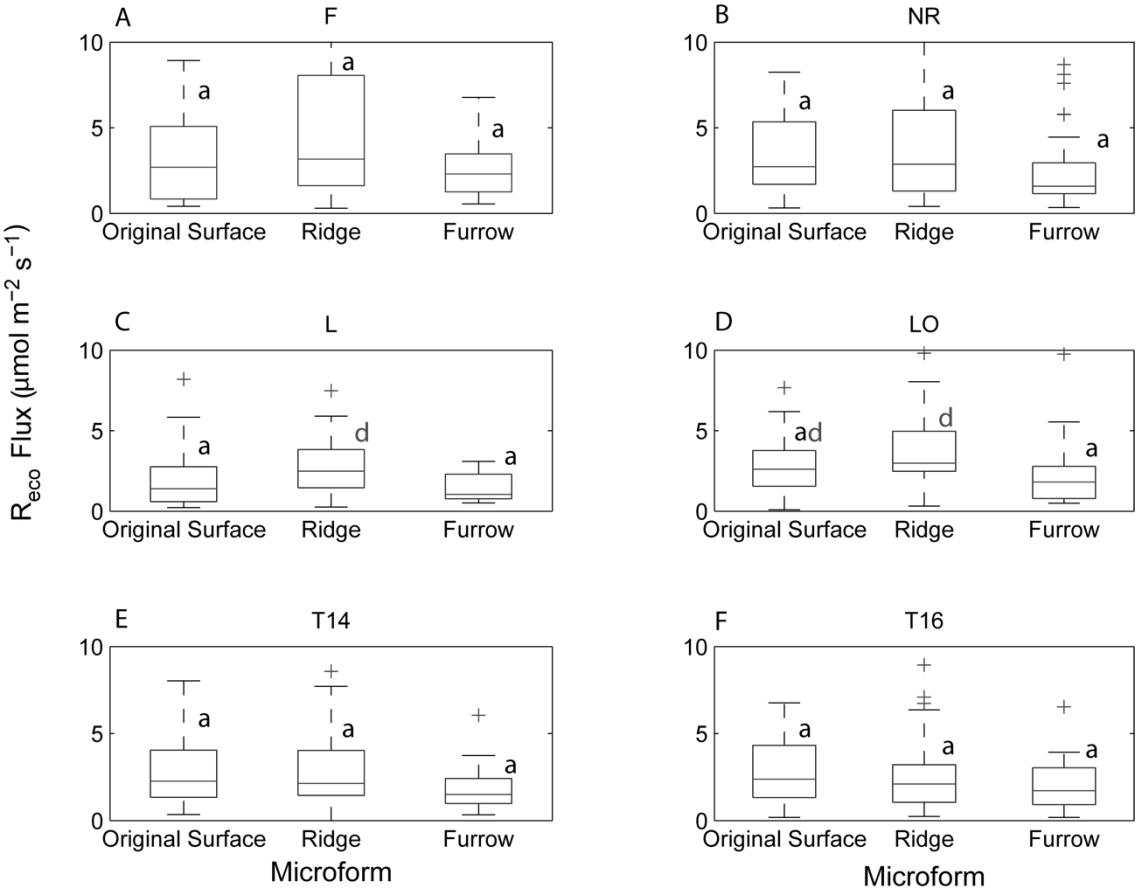

Figure 6.3 Boxplots of microform respiration fluxes across all sites (Table 6.2). Solid lines within boxes represent the median, with the boxes enclosing the 75th and 25th percentiles. The whiskers extend to the most extreme points not considered to be outliers, while outliers are plotted individually. Different letters indicate significant differences in intra-site microform R_{eco} fluxes.

Over the chronosequence (Figure 6.3), R_{eco} significantly decreased (Wilcoxon rank sum, P = 0.0208) with a median flux at NR of 2.55 ± 3.97 µmol CO_2 m^{-2} s^{-1} and a median flux at T16 of 2.14 ± 2.26 µmol CO_2 m^{-2} s^{-1}. There was also a significant decrease between the forested site (F) & T16 (Wilcoxon rank sum, P = 0.0307) showing that restoration is successful at reducing R_{eco} fluxes.

Inter-site ridge R_{eco} significantly decreased between F and T16 (Wilcoxon rank sum, P = 0.0189). However, no significant difference was observed in original surface R_{eco} fluxes between Lonielist (LO) and T14 (Wilcoxon rank sum P = 0.8102) and T16 (Wilcoxon rank sum, P = 0.9300). This is suggestive of ridges having a diminishing impact upon R_{eco} over time.

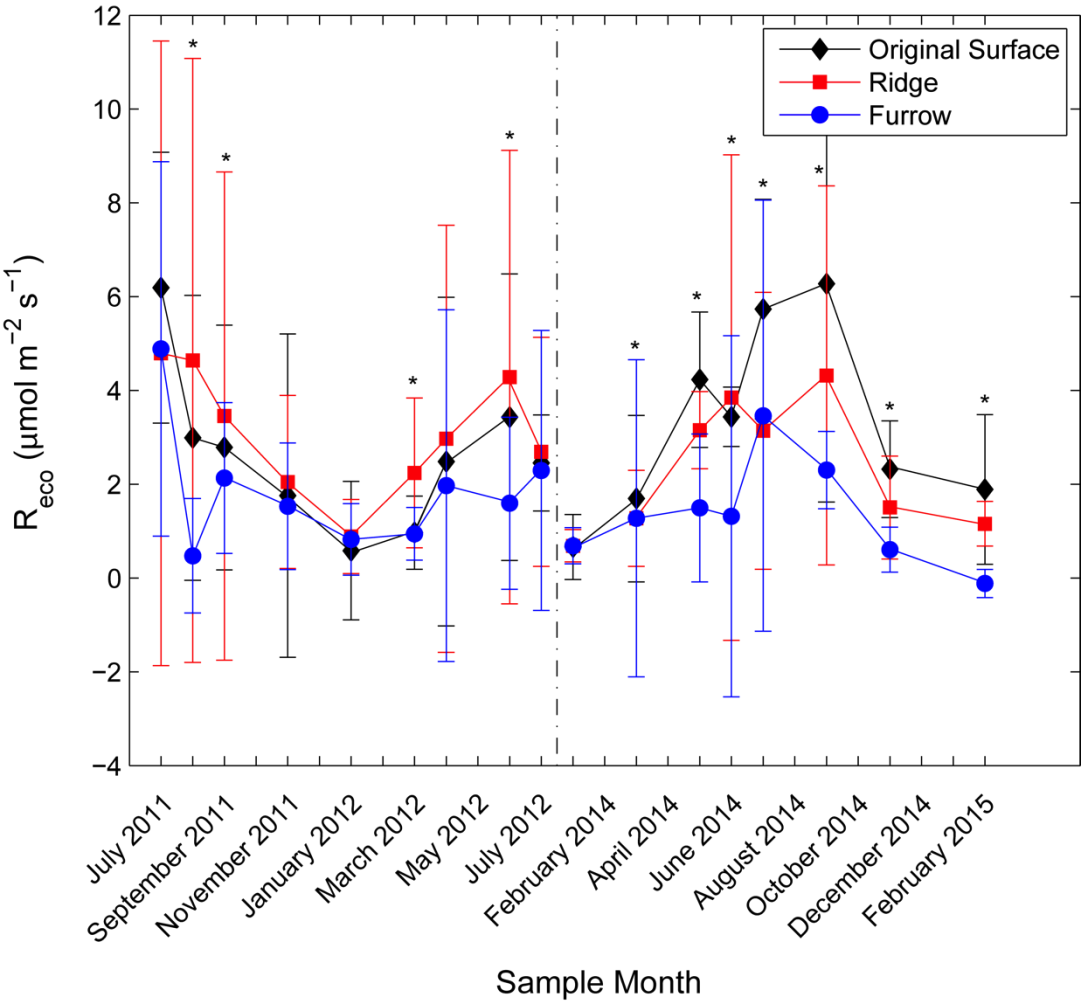

Figure 6.4 Pooled median ± interquartile range R_{eco} fluxes from each microform at each sample month. Dashed line represents break between the two sampling points. *Denotes significant differences in microform R_{eco} fluxes in that month.

The greatest difference in median microform fluxes over the chronosequence (F to T16) was observed on the ridges (Figure 6.3), where there was a difference of 1.07 µmol CO_2 m^{-2} s^{-1} compared to differences of 0.31 and 0.58 µmol CO_2 m^{-2} s^{-1} from the original surface and furrow respectively.

When all data were pooled, temporal variation in R_{eco} was evident (Figure 6.4) with significant differences observed between R_{eco} and sample month (Kruskal Wallis with Fisher's LSD, $P < 0.0001$). Significant differences (Kruskal Wallis, $P < 0.05$) were observed between microforms in every sample month during 2014/15 except January 2014 (Kruskal Wallis, $P = 0.1918$). In 2011/12, differences between microforms were only observed during August 2011 (Kruskal Wallis, $P = 0.049$), September 2011 (Kruskal Wallis, $P = 0.0064$), March 2012 (Kruskal Wallis, $P = 0.044$) and June 2012 (Kruskal Wallis, $P = 0.0024$). Greater differences are likely to be observed if 2011/12 data were disaggregated by site, rather than pooled.

6.3.2 Microform effects on GPP

When data were pooled no significant differences in GPP were observed among microforms (Figure 6.5 - Kruskal-Wallis, $P = 0.217$).

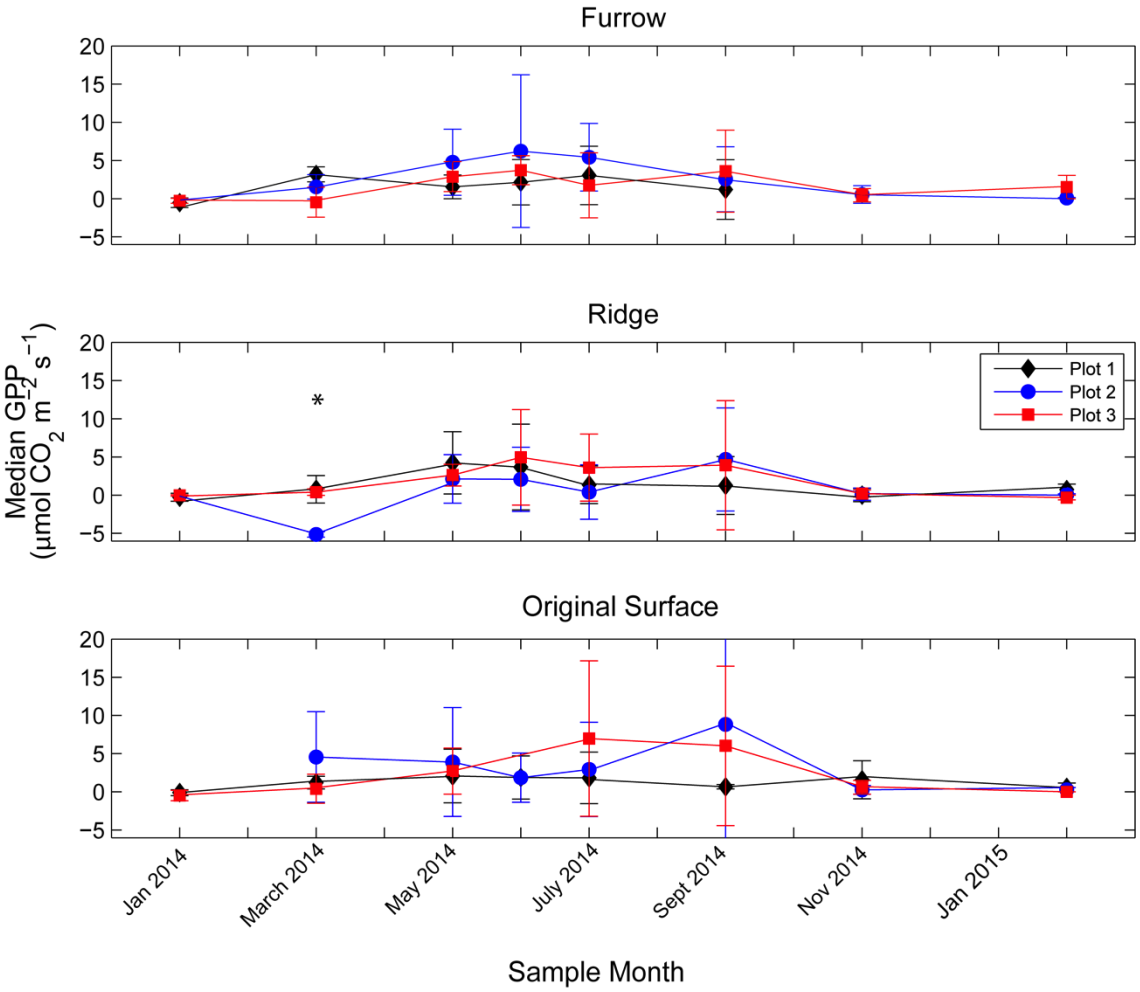

Figure 6.5 Chamber derived GPP fluxes from the microforms at each plot during the sampling period from January 2014 to February 2015. Data displayed are median ± interquartile range and stars indicate significant difference between microforms in that sampling month.

When disaggregated by sample month, the only significant difference observed was in March 2014 where ridges were significantly lower than both the original surfaces and furrows (Figure 6.5 - Kruskal-Wallis with Fisher's LSD, $P = 0.0259$). However, significant microform temporal variability (Figure 6.5) was observed in the original surfaces (Kruskal-Wallis with Fisher's LSD, $P < 0.0001$), ridges (Kruskal-Wallis with Fisher's LSD, $P < 0.0001$) and furrows (Kruskal-Wallis with Fisher's LSD, $P < 0.0001$), indicating a strong seasonal influence on GPP fluxes (Figure 6.5). The highest GPP fluxes were observed in the summer months of June (2.89 ± 4.39 µmol CO_2 m^{-2} s^{-1}) and July 2014 (2.90 ± 4.97 µmol CO_2 m^{-2} s^{-1}), whilst in January 2014

(0.32 ± 0.49 μmol CO_2 m^{-2} s^{-1}) and February 2015 (0.28 ± 0.75 μmol CO_2 m^{-2} s^{-1}) almost no photosynthesis was measured.

Median GPP fluxes were highest from furrow microforms (1.84 ± 4.33 μmol CO_2 m^{-2} s^{-1}), whilst lower median fluxes were observed on ridges (0.67 ± 3.78 μmol CO_2 m^{-2} s-1) and the original surface (0.80 ± 3.78 μmol CO_2 m^{-2} s^{-1}). However, modelled (Eqn 6.2) P_{max} values (Table 6.6) were greatest on the original surface (12.01 μmol CO_2 m^{-2} s^{-1}) and lower in the furrows (8.89 μmol CO_2 m^{-2} s^{-1}) and ridges (4.97 μmol CO_2 m^{-2} s^{-1}). It was postulated that GPP estimates from the original surface were strongly influenced by activity from a single photosynthetic "hotspot", which showed consistently high rates of photosynthesis over the duration of this study. This "hotspot" was retained in the analyses as its removal could potentially have led to an under-representation of GPP from this study site.

The "hotspot" flux was particularly obvious on the plot 3 original surface in July and September 2014 (Figure 6.5), giving rise to the larger median and interquartile ranges associated with fluxes in these months.

6.3.3 Environmental Controls on R_{eco}

When all data were pooled, R_{eco} showed weak positive correlations with soil (Spearman's ρ = 0.2561, P = <0.0001) and air temperature (Spearman's ρ = 0.2484, P = <0.0001). However, when disaggregated by sample year and microform, the strongest correlation was observed between R_{eco} and soil temperature on the ridges in both 2011/12 (Spearman's ρ = 0.3001, P < 0.0001) and 2014/15 (Spearman's ρ = 0.6526, P < 0.0001). The ridges were found to always have higher soil temperatures than the original surface and furrow (Table 6.6). Felling of trees had a significant impact upon soil temperatures with higher soil temperatures observed in the felled sites compared to the forested sites (Wilcoxon rank sum, P = 0.0036).

Q10 values (Table 6.5) also indicated similar trends with both air and soil temperature. The ridges showed the greatest response to increases in temperature both in the Q10 analyses and when using the Lloyd and Taylor (1994) model (Figure 6.7), particularly in the forest (2.8 μmol CO_2 m^{-2} s^{-1} at 10°C) and NR (2.9 μmol CO_2 m^{-2} s^{-1} at 10°C) However in 2014/15, Q10 values between the original surface and ridge were more similar (Table 6.5).

Table 6.5 Q10 values for chamber measurements undertaken in 2011/12 and 2014/15.

2011/12		
Microform	**Air Temperature**	**Soil Temperature**
Original Surface	2.3	2.5
Ridge	2.6	3.0
Furrow	2.1	2.3
2014/15		
Original Surface	2.5	2.8
Ridge	2.8	2.9
Furrow	2.4	2.6

Table 6.6 Median, Maximum and Minimum of selected environmental variables across all sites disaggregated by microform.

	Original Surface									Ridge								
	Air Temperature (°C)			Soil Temperature (°C)			Soil Moisture (%)			Air Temperature (°C)			Soil Temperature (°C)			Soil Moisture (%)		
	Median	Max	Min	Median	Max	Min	Median	Max	Min	Median	Max	Min	Median	Max	Min	Median	Max	Min
F	11.0	15.0	3.5	8.8	12.6	1.0	73.6	89.2	16.8	11.1	12.7	3.5	9.0	12.8	1.0	65.3	87.8	18.7
NR	11.3	18.7	1.2	9.1	12.9	1.0	71.0	85.7	18.7	11.3	18.7	1.2	9.3	13.2	1.0	61.0	80.8	18.3
L	11.4	16.7	3.3	7.3	12.9	1.0	73.9	85.3	50.4	11.4	16.7	3.3	7.7	12.9	1.0	66.3	80.9	33.7
LO	11.6	18.1	2.3	8.6	13.0	0.0	78.5	92.4	62.0	11.6	18.1	2.3	8.7	13.4	0.0	72.4	79.5	63.7
T14	11.5	14.7	8.9	10.5	12.1	4.9	72.7	87.9	44.1	11.6	14.7	8.9	10.6	12.4	4.9	66.8	78.2	22.5
T16	13.2	22.7	5.5	8.65	15.5	3.7	100	100	48.3	13.8	24.2	5.2	13.5	15.6	4.0	100	100	55.1

	Furrow								
	Air Temperature (°C)			Soil Temperature (°C)			Soil Moisture (%)		
	Median	Max	Min	Median	Max	Min	Median	Max	Min
F	11.0	13.0	3.5	8.4	12.6	1.0	78.0	101.	29.2
NR	11.3	18.7	1.2	8.9	12.9	1.0	69.0	85.3	7.1
L	11.4	16.7	3.3	7.1	12.9	1.0	74.4	92.0	60.3
LO	11.6	18.1	2.3	8.4	13.0	0.0	78.2	93.4	68.3
T14	11.6	14.7	8.9	10.3	12.1	4.9	73.3	83.6	53.1
T16	13.6	21.0	5.2	11.6	14.3	4.7	100	100	61.0

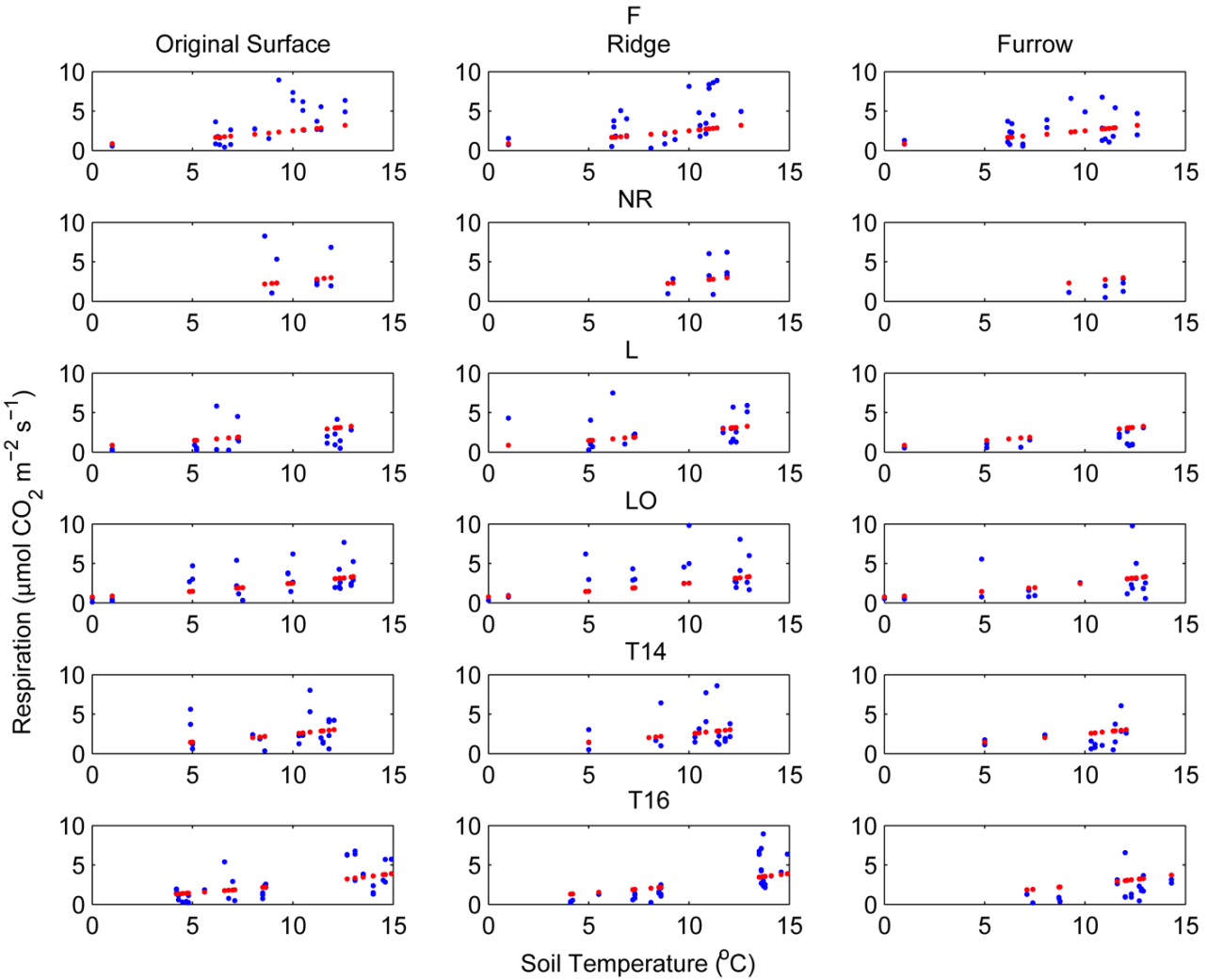

Figure 6.6 Relationship between soil temperature at 10cm and respiration fluxes. Red markers represent the respiration flux normalised to 10°c using the Lloyd and Taylor model (Lloyd and Taylor, 1994).

The furrows showed weak and very weak non-significant correlations between R_{eco} and soil temperatures in 2011/12 (Spearman's $\rho = 0.2628$, $P = 0.2124$) and 2014/15 (Spearman's $\rho = 0.1700$, $P = 0.3605$). Similar relationships were observed between air temperature and R_{eco} although the correlations were always slightly weaker. In both datasets the weakest correlations with air temperature were observed in the furrows (Spearman's $\rho = 0.2222$, $P = 0.009$ and Spearman's $\rho = 0.3344$, $P = 0.06$), which is expected due to the higher soil moisture content of these sites, furthermore the thermal conductivity is likely to cause a lag between air temperature and R_{eco}. The greatest correlations between air temperature and R_{eco} were observed in the ridges in both 2011/12 (Spearman's $\rho = 0.2620$, $P < 0.0001$) and 2014/15 (Spearman's $\rho = 0.6303$, $P < 0.0001$).

Pooled data showed R_{eco} to be non-significantly correlated with soil moisture content (Figure 6.7) (Spearman's $\rho = -0.1348$, $P = 0.052$). Data disaggregated by microforms in both the 2011/12 and 2014/15 datasets showed soil moisture content in the furrows (Spearman's $\rho = -0.0506$, $P = 0.5603$; Spearman's $\rho = -0.2041$, $P = 0.2707$ respectively) and the original surface (Spearman's $\rho = -0.1836$, $P = 0.0193$ and Spearman's $\rho = -0.1544$, $P = 0.3289$) to be negatively correlated with R_{eco}, although in all cases except 2011/12 original surfaces, soil moisture was not significantly correlated. In both 2011/12 (Spearman's $\rho = 0.0185$, $P = 0.8138$) and 2014/15 (Spearman's $\rho = 0.2050$, $P = 0.2043$) ridges were found to be non-significantly very weakly and weakly positively correlated with soil moisture. The lowest soil moisture content was observed in the ridges, whilst the furrows were always wetter with higher median soil moisture content (Table 6.6). Water table depth was found to have a very weak non-significant negative correlation with R_{eco} (Spearman's $\rho = -0.0487$, $P = 0.4126$), however, this is a very weak correlation and the high *P*-value indicates that this correlation may be due to chance.

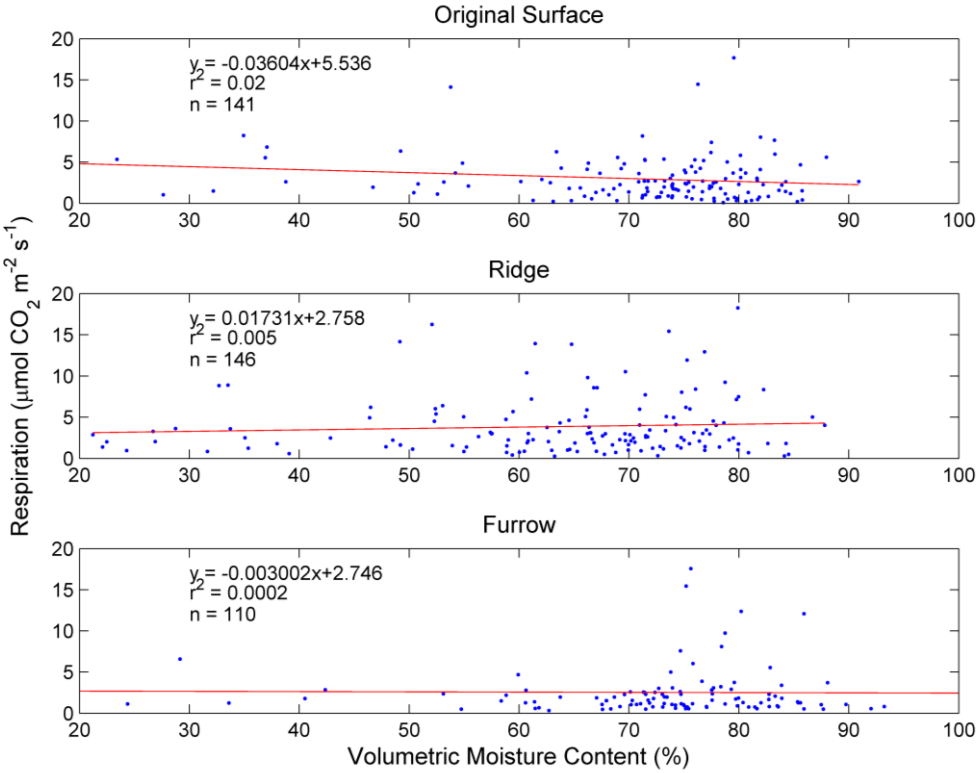

Figure 6.7 Respiration fluxes against volumetric moisture content at 10cm depth from each of the microforms. Lines are linear fits with the equation given within each of the plots.

Multiple linear regressions (MLR – Table 6.7) were run between R_{eco} and environmental variables identified in the Spearman's rank correlation analysis. However, soil moisture content was included despite showing no significant correlation as the respiration work undertaken in Chapter 4 showed soil moisture content to have a significant impact upon R_{eco}. In 2011/12, the strongest relationships were observed between soil temperature and soil moisture. On the original surface around 25% of the variation (Table 6.7) was explained by these two variables (R^2 = 0.2489, P < 0.0001), whilst on the ridge slightly less variation was explained (R^2 = 0.2003, P < 0.0001). The least variation was explained by these two variables in the furrow (R^2 = 0.1523, P = 0.0015). However the addition of other measured variables did not explain anymore of the variation. Similar to the Spearman's analysis, soil moisture content was negatively correlated with R_{eco} on the original surface (b = -5.3933) and furrow (b = -3.0766), whilst positive relationships were observed on the ridge (b = 4.3318). Positive relationships between soil temperature and R_{eco} were observed across the original surface (b = 1.0131), ridge (b = 7.7394) and furrow (b = 2.1812).

Similar to the 2011/12 dataset, the strongest relationships were observed between soil moisture content and soil temperature in the 2014/15 data, although the relationships were always stronger. On the original surface around 58% of the variation (R^2 = 0.5778) in R_{eco} was

explained by soil temperature (b = 15.09) and soil moisture (b = -4.19, P < 0.0001). Around 46% of the variance (R^2 = 0.4622) (Table 6.7) on the ridge was explained by soil moisture (b = 4.2417) and soil temperature (b = 9.6583). However in the furrows, only around 21% of the variation (R^2 = 0.2120) was explained by soil moisture (b = -4.2754) and soil temperature (b = 7.7086, P = 0.0001).

The results of the MLR and Spearman's rank correlation coefficient suggest that these two variables have the greatest influence on R_{eco} fluxes from restored ecosystems with microtopography playing an important role in the loss of CO_2 to the atmosphere. The weaker relationships observed in the 2011/12 dataset were likely caused by inter-site variation damping signals.

Table 6.7 Parameters from the multiple linear regression runs to show the influence of soil moisture and soil temperature on R_{eco} fluxes.

2011/12	**Original Surface**	**Ridge**	**Furrow**
R^2	0.2489	0.2003	0.1523
F	10.0256	10.5185	5.5716
P	<0.0001	<0.0001	0.0015
Error Variance	0.7309	0.6285	0.6158
	2014/15		
R^2	0.5778	0.4622	0.2120
F	52.9193	32.6546	8.1601
P	<0.0001	<0.0001	0.0001
Error Variance	1.4845	2.5455	1.2425

6.3.4 Environmental Controls on GPP

Pooled data indicated a strong positive significant correlation between GPP and PAR (Spearman's ρ = 0.7668, P < 0.0001). When disaggregated, GPP fluxes displayed moderate relationships with PAR across original surfaces (Spearman's ρ = 0.5433, P < 0.0001) and ridges (Spearman's ρ = 0.4947, P < 0.0001), and weak relationships in the furrows (Spearman's ρ = 0.2245, P < 0.0001). A rectangular hyperbola model applied to the data (Figure 6.8) found the greatest GPP on the original surface, with a maximum photosynthetic rate of 12.01 μmol CO_2 m^{-2} s^{-1} under full light conditions (Table 6.8) The lowest rate was observed on the ridges (P_{max} 4.97 μmol CO_2 m^{-2} s^{-1}). The quantum yield, describing the μmol of CO_2 fixed per μmol of photons absorbed, identified similar relationships.

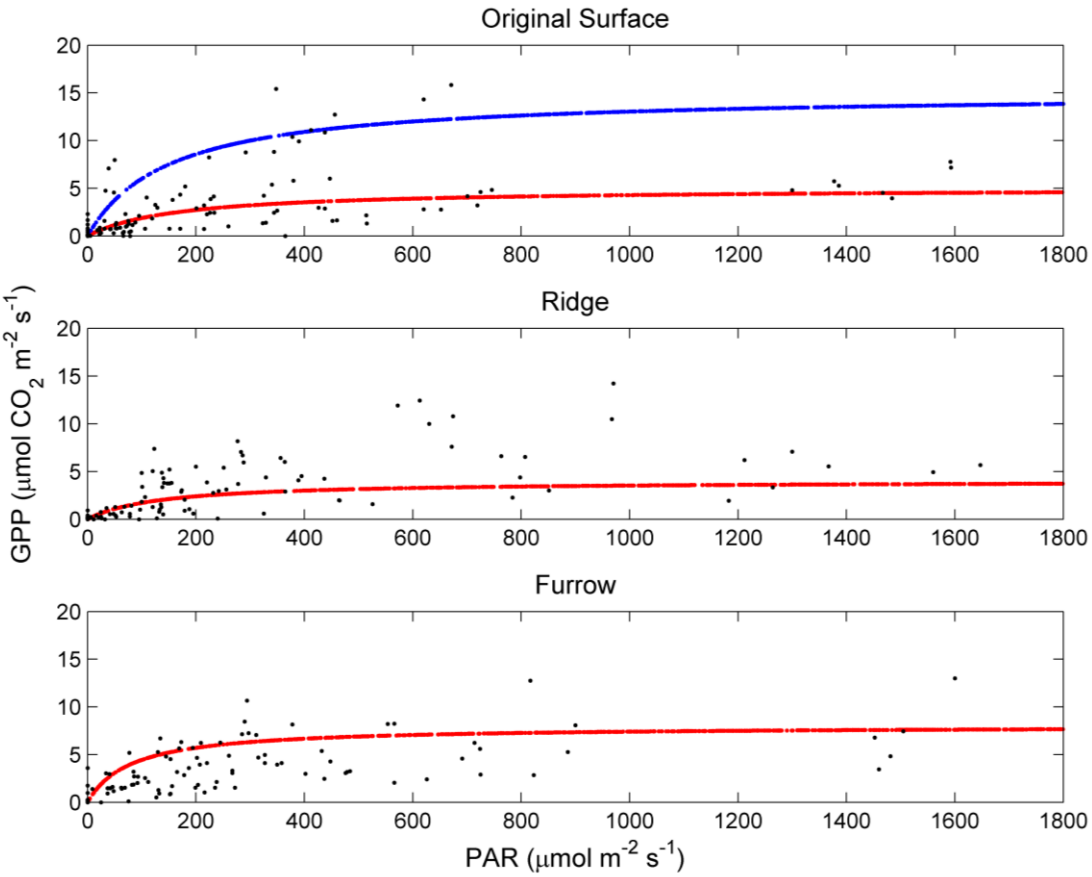

Figure 6.8 Photosynthesis irradiance curves of GPP and PAR from each of the microforms from Talaheel in the 2014/15 dataset. Black markers indicate the observed values; red markers indicate rectangular hyperbola modelled values. Blue markers indicate the second light response curve observed on the original surface due to hotspot activity.

In the original surface there appeared to be two light response curves (Figure 6.8 – high and low in Table 6.8), the greater of which (blue markers in Figure 6.8) reached a higher photosynthetic rate at lower PAR values. Further investigation of these data established that these values were associated with the photosynthetic "hotspot" activity mentioned in 6.3.2.

Amongst other environmental variables, GPP was positively correlated with soil and air temperature in the original surface and furrows (Spearman's $\rho = 0.4686$, $P < 0.0001$ & Spearman's $\rho = 0.3432$, $P < 0.0001$ respectively), whilst GPP fluxes were also negatively correlated with soil moisture on the original surface and furrows (Spearman's $\rho = -0.3109$, $P = 0.002$ & $\rho = -0.1774$, $P < 0.0001$). On ridges, GPP fluxes were positively correlated with soil temperature (Spearman's $\rho = 0.6005$, $P < 0.0001$), air temperature (Spearman's $\rho = 0.3178$, $P < 0.0001$) and soil moisture (Spearman's $\rho = 0.2818$, $P < 0.0001$).

Table 6.8 Light saturated photosynthetic rates and quantum yields (i.e. the slope of the line) from the PI curves displayed in Figure 6.9

Microform	P_{max} (μmol m^{-2} s^{-1}) (Confidence Intervals)	Quantum Yield (μmol m^{-2} s^{-1}) (Confidence Intervals)
Original Surface (high)	15.01 (14.39; 16.63)	0.138
Original Surface (low)	5.74 (5.22; 6.26)	0.128
Ridge	4.97 (3.41; 6.53)	0.127
Furrow	8.89 (7.97; 9.81)	0.135

6.3.5 Influence of Microtopography on NEE

Analysis of the net exchange in the 2014/15 dataset at T16 showed significantly greater NEE (i.e a greater sink/smaller source) than both the ridge and original surface (Kruskal-Wallis with Fisher's LSD, $P < 0.0001$).

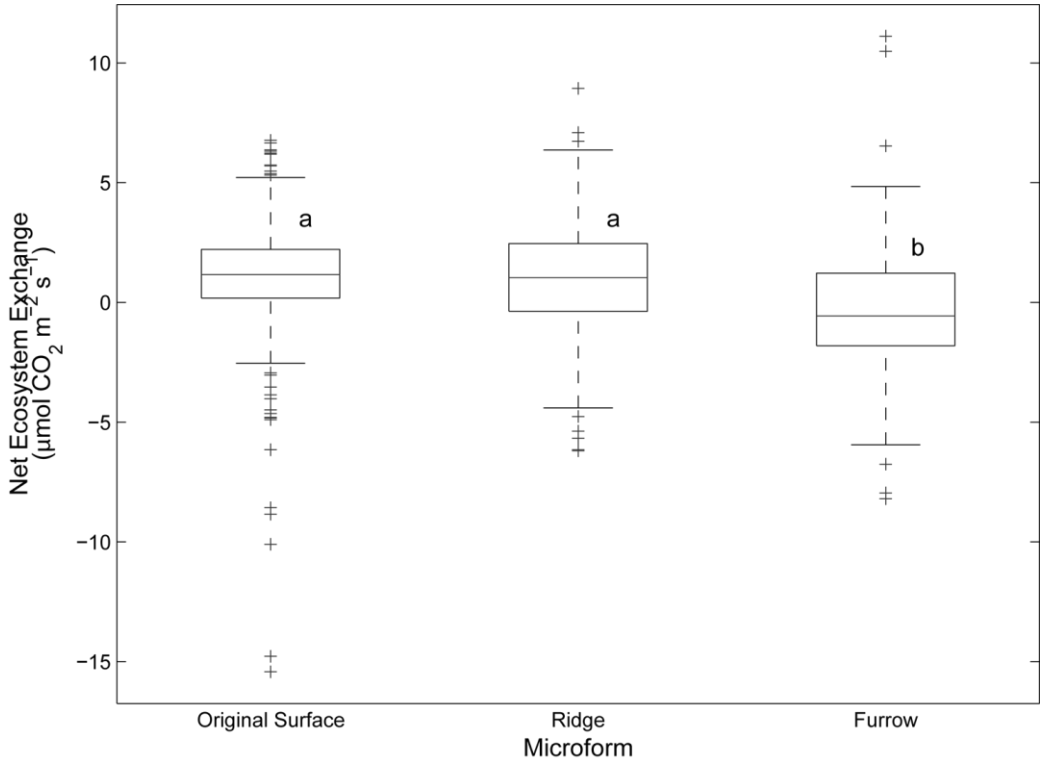

Figure 6.9 Net Ecosystem Exchange (NEE) across the three microforms at T16 in 2014/15. Solid lines within boxes represent the median, with the boxes enclosing the 75th and 25th percentiles. The whiskers extend to the most extreme points not considered to be outliers, while outliers are plotted individually.

The furrows were observed to be small net sinks for CO_2 (-0.56 ± 3.04 μmol CO_2 m^{-2} s^{-1}). However, the original surfaces and ridges were observed to be small net sources of CO_2 (1.16 ± 2.03 μmol CO_2 m^{-2} s^{-1} and 1.04 ± 2.83 μmol CO_2 m^{-2} s^{-1} respectively).

6.4 Discussion

6.4.1 Microtopographic effects on R_{eco} fluxes

Microforms had a significant influence on the exchange of CO_2 between the land surface and atmosphere. R_{eco} fluxes from ridges were found to be greater (Figures 6.3 and 6.4) than fluxes from original surfaces and furrows in younger restoration sites (Kruskal-Wallis, $P < 0.0001$). Analysis of environmental variables identified a weak negative correlation between soil moisture content and soil CO_2 fluxes (Spearman's $\rho = -0.1348$, $P = 0.0052$), although this varied between microforms (Figure 6.7), with a positive correlation observed on the ridges in both datasets (MLR $b = 4.3318$ and $b = 4.2417$). In peatland environments, hydrology and biogeochemical cycling are tightly coupled (Silvola *et al.*, 1996a, Waddington *et al.*, 2001) with soil respiration dependent upon changes in the surface temperature of the peat, as well as the moisture content at depth (Roulet *et al.*, 1993, Silvola *et al.*, 1996a, Updegraff *et al.*, 2001, Waddington *et al.*, 2001). In re-wetted peatlands, where previous drainage regimes resulted in aerobic conditions and greater decomposition of the peat (Parry *et al.*, 2014), substrates are likely to be depleted which could decrease respiration. Orchard and Cook (1983) observed that soils re-wetted to their original water content reduced the respiration rate by as much as 60% of the original respiration rate due to substrate depletion. However, in the case of these sites in the Flow Country, the incorporation of felled trees into the ecosystem is likely, at least in the first few years post felling, to result in increased R_{eco} due to the amount of organic material available to soil microbes for decomposition (Makiranta *et al.*, 2012).

Undrained peatlands are characterised by distinct natural microtopographic features called hummocks and hollows (Nungesser, 2003). Previous research has shown that higher R_{eco} fluxes tend to be associated with hummocks due to drier soil moisture conditions (Kim and Verma, 1992, Pelletier *et al.*, 2011). The research by Kim and Verma (1992) from a peatland in north central Minnesota, USA, found mean fluxes from hummocks and hollows of 9.8 ± 3.5 g C m^{-2} d^{-1} and 5.4 ± 2.9 g C m^{-2} d^{-1}, respectively, with the differences in soil moisture between the microsites being a reason for the variation in fluxes. However, although the microtopography observed on the restored sites is physically different to the hummocks and hollows observed in undrained peatlands, the observed relationships were very similar with raised areas (ridge, original surface) associated with higher R_{eco} fluxes similar to hummocks and furrows associated with lower R_{eco} fluxes as seen in hollows. The non-significance of soil moisture is likely due to the more stable water table at the older restoration sites and the low frequency of data collection, with rhizosphere soil moisture thought to change more rapidly than depth-integrated soil moisture, thereby exerting a greater control over R_{eco} (Zhang *et al.*, 2015). Therefore, low frequency chamber measurements may not show strong relationships with soil moisture content.

Soil temperature was positively correlated with R_{eco} across all microforms (Figure 6.6), although the greatest correlation was observed on the ridges (Spearman's $\rho = 0.3632$, $P < 0.0001$; MLR 2011/12 - $b = 1.0131$, $R^2 = 0.2003$; MLR 2014/15 - $b = 9.6583$, $R^2 = 0.4622$), which were also the driest microforms (Figure 6.7). Temperature is often cited as one of the most dominant environmental controls on temporal variations in peatland R_{eco} (Silvola *et al.*, 1996a, Freeman *et al.*, 2001, Lafleur *et al.*, 2005b, Dorrepaal *et al.*, 2009, Chojnicki *et al.*, 2010, Juszczak *et al.*, 2013). In dry peat environments, the thermal capacity decreases, leading to greater fluctuations in temperatures within the peat and greater respiration (Hobbie, 1996, Waddington *et al.*, 2002). The greatest R_{eco} was found on ridges, where the lowest median soil moisture content and highest soil temperatures were found. Similar results were found by Strack and Zuback (2013) at a restored peatland in Canada 10-years post restoration where the highest R_{eco} fluxes were observed in areas with a deep water table and warmer peat temperatures. The observed relationship between soil temperature and R_{eco} is likely to be an indicator of root respiration or root-derived microbial respiration being responsible for a large proportion of the R_{eco} flux with many plant roots occurring within the oxygenated zone above the water table (Bubier *et al.*, 1998). Previous research into respiration in bog ecosystems has found that between 30 – 70% of respiration is due to root-derived respiration processes (Silvola *et al.*, 1996b). Another indication of root respiration or root-derived microbial respiration is the seasonal pattern following that of the typical phenology of the vegetation (Silvola *et al.*, 1996b). This is seen by the high fluxes observed in summer and early autumn, when vegetation is likely to be at its most active.

Changes in vegetation composition between microforms is likely to, in part, explain some of the differences in R_{eco} between microforms and across the chronosequence. Respiration fluxes from the original surface and ridges were observed to increase, whilst furrow fluxes decreased at Lo compared to L while R_{eco} was observed to increase at Lo. This is believed to be due to intrinsic differences in the vegetation composition (Table 6.3) at Lo with a greater abundance of vascular plants in the original surface and ridge than at L, which was more dominated by mosses and the furrows, which were dominated by bryophytes. R_{eco} is known to vary with vegetation, with research highlighting that rates can significantly vary between different biome types (Raich and Schlesinger, 1992). Recent literature has suggested that vascular plant coverage can promote ancient C loss from peatlands, an effect not seen when only bryophytes are present (Walker *et al.*, 2016). Changes in vegetation across the chronosequence and microforms are therefore likely to have a significant impact upon R_{eco} with greater coverage of *Sphagnum* in the furrows of the older sites and greater coverage of vascular plants on the original surface and ridges. It is likely that the vegetation composition of the sites would have an impact upon R_{eco} as is seen in other

research (e.g. Raich and Schlesinger, 1992, Raich and Tufekcioglu, 2000, Ward *et al.*, 2013), especially as approximately 50% of the C taken up during photosynthesis is released back to the atmosphere through autotrophic respiration (Dawson and Smith, 2007, Smith *et al.*, 2010). As mentioned previously, root-derived respiration processes have the greatest impact upon respiration fluxes. This is therefore also going to be related to the vegetation, as different plants have different root structures and densities (Benasher *et al.*, 1994, Thomas *et al.*, 1996). Further research is required to understand the direct influence of vegetation on R_{eco} fluxes. This can be achieved through partitioning of autotrophic and heterotrophic respiration to better understand the dynamics of respiration and the relative proportions of autotrophic and heterotrophic respiration in R_{eco}.

6.4.2 Restoration age effects

Analysis of the chronosequence showed R_{eco} decreasing with increasing time since restoration (Figure 6.3). Furthermore, the effect of microtopography on R_{eco} also appeared to diminish with similar R_{eco} fluxes observed on the original surface and ridge microforms (Kruskal-Wallis, P = 0.1033) and significantly lower fluxes (Kruskal-Wallis, P = 0.0001) from furrows at T14 and T16. Younger restoration sites (L and LO) displayed significantly higher R_{eco} fluxes from ridges than the original surface and furrow (Kruskal-Wallis, P = 0.0308 and P = 0.0455 respectively). Land management practices have an effect on R_{eco} fluxes through the alteration of local microclimates, such as soil temperature, incident radiation and air temperature.(Chen *et al.*, 1999) The initial loss of canopy cover at NR is likely to have caused enhanced air and soil temperatures, as well as increasing incident radiation to ground vegetation (Bremer *et al.*, 1998). Besides the initial disturbance of machinery moving over the ground, the increase in soil temperatures through increased solar irradiance will potentially result in an increase in soil microbial activity and R_{eco} (Karhu *et al.*, 2014). In addition, the significantly increased (Wilcoxon rank sum, P = 0.0036) temperatures experienced in the felled sites compared to the standing forestry sites (Table 6.6) are likely to have resulted in increased decomposition of both the peat and root material (Hilasvuori *et al.*, 2013), thereby enhancing R_{eco}. Observed results indicate that R_{eco} from the original surfaces and furrows increased slightly after felling. As the trees tend to fall into the furrow once felled, providing a canopy cover, it is most likely that the increase in R_{eco} from this microform is due to the weight of the tree causing a compaction of the soil and forcing CO_2 trapped within soil pores to be forcibly released or released through diffusion as the trees slowly compact the peat (Ball *et al.*, 1999). Moreover, the decomposition of tree roots in the ridge is likely to account for higher R_{eco} rates from this microform, particularly in the younger restoration sites. The presence of significant volumes of needle litter

across all microforms will also lead to an enhancement of C fluxes as they begin to decompose and release C to the atmosphere.

Higher soil moisture conditions in the furrows of Lo compared with L are likely to have caused the lower R_{eco} flux. The negative correlation between soil moisture and R_{eco} (Spearman's ρ = -0.1348, P = 0.052) suggests that as soil moisture increases, R_{eco} decreases. Therefore as these sites become wetter due to rising water tables, R_{eco} is likely to decrease. This is demonstrated through the decreased R_{eco} in the furrows at T14 and T16. Although R_{eco} is closely linked to the hydrologic and biogeochemical dynamics of peatlands, this has been shown to be site specific (Juszczak *et al.*, 2013). The weak correlation between R_{eco} and water table depth is indicative of a link between the two, but further research is required. The water table is likely to show a greater correlation when analysed on a seasonal basis rather than a daily basis (Bubier *et al.*, 1998, Bubier *et al.*, 2003a, Lafleur *et al.*, 2005b). In this research a greater number of data points is likely to present a better understanding of water table dynamics over a season, especially in restored areas where the water table is likely to be less stable than in a blanket bog (Holden, 2005, Dixon *et al.*, 2014).

6.4.3 Gross Primary Productivity

GPP in the original surface at T16 was influenced by one plot, which in the summer and early autumn of 2014 displayed higher fluxes than the other plots (Figure 6.5). The only observed difference between this plot and other plots was a dominant cover of *Carex panicea*. Whilst *Carex panicea* was present in the other plot, this plot had a total cover of around 75% within it. Wolfenden and Diggle (1995) found that monoliths containing *Carex panicea* and other species, typical of base-rich communities show a positive response to net uptake (i.e. net uptake increased as CO_2 concentration increased) when exposed to elevated CO_2. Other research has also identified sedge-dominated sites to have higher net C accumulation rates than those with less sedge cover (Bubier *et al.*, 1998, Kwon *et al.*, 2006, Kivimaki *et al.*, 2008, He *et al.*, 2011). Other plots at T16 with high percentage cover of *Carex panicea* were found to have higher GPP flux rates than those with lower coverage of *Carex panicea*, particularly on the original surface. Higher GPP fluxes from the original surface in T16 are also likely to explain some of the higher R_{eco} fluxes observed from this microform. This is highlighted by the presence of two light response curves (Figure 6.8) on the original surface, the higher of which was associated with plots with higher *Carex panicea* coverage. Previous research has shown that approximately 50% of the C fixed during photosynthesis is cycled back to the atmosphere through autotrophic respiration (Dawson and Smith, 2007, Smith *et al.*, 2010). Therefore, higher CO_2 uptake will subsequently result in higher R_{eco} fluxes.

Lower GPP fluxes were observed on the ridges compared to the original surfaces and furrows (Figure 6.8). This is likely to be related to the vegetation composition with the furrows and original surfaces being associated with more productive vegetation families such as *Cyperaceae spp., Sphagnum spp.,* and *Eriophorum spp.* In contrast, ridges had greater coverage of non-*Sphagnum* mosses, *Ericaeae spp.* and lichens. However, this is in contradiction to work by Bubier *et al.* (1998), who found hollows to have a lower uptake rate than hummocks at all times of the year at a peatland in Manitoba, Canada. Maximum uptake rates from the hollow were in the range of 0.5 - 5 μmol m^{-2} s^{-1} while in the hummocks uptake rates ranged from around 0.5 - 9 μmol m^{-2} s^{-1}. Although fluxes in both this study and the study by Bubier *et al.* (1998) are in a similar range, the microtopography exerts a different forcing to that of a natural peatland hummock/hollow structure, most likely due to intrinsic differences in their chemical and physical structure.

6.4.4 Impacts of microtopography on restoration

These data highlight that man made microtopography results in significant R_{eco} fluxes with drier, warmer microforms were found to display higher R_{eco}. The furrows were consistently associated with lower R_{eco} due to the cooler, wetter conditions. Furthermore, Net exchange at T16 (Figure 6.9) showed the furrows to be significantly greater sinks for CO_2 (Kruskal-Wallis with Fisher's LSD, $P < 0.0001$) than the ridge and original surface, which were both, observed to be net sources. These data highlight that further restoration of these sites should include the removal of ridge microtopography and a flattening of the site. This should be undertaken by using the peat from the ridges to create a dam furrow, which will further raise and stabilise the water table. The data collected here suggest that this would significantly reduce R_{eco}, increase GPP and lead to greater NEE as bog vegetation, such as *Sphagnaceae* recolonize a greater area as the water table rises and makes the site more suitable for their growth. Waddington *et al.* (2010) found that within 3 years of restoration 50% of the land area had been vegetated, and of this 90% were moss and *Sphagnum* species. This was also coupled with an observed decrease in R_{eco} despite the fresh substrates from the recolonising vegetation. Similarly, Strack *et al.* (2016) observed lower R_{eco} and increased NEE due to wetter conditions at a restored peatland in Canada.

6.5 Conclusions

Little or no empirical data exists on the effects of peatland restoration on trace gas fluxes from previously afforested northern temperate peatlands (Billett *et al.*, 2010, Birkin *et al.*, 2011). This study represents, to the best of current knowledge, the first to have explored intra-annual variability on soil CO_2 exchange from a chronosequence of restored sites in the UK. Furthermore, this study has focussed upon the effect of microtopographic features upon the exchange of CO_2 and found these features to have a significant impact upon the exchange of CO_2.

Microforms have a significant effect on R_{eco} with the lowest fluxes observed from furrows and higher fluxes observed on ridges. Differences in R_{eco} fluxes were attributed to differences in soil moisture and soil temperature, with deeper water tables and higher temperatures observed on original surfaces and ridges where the highest R_{eco} fluxes were observed. The greater coverage of vascular plants on original surfaces is likely to increase the R_{eco} flux, and although this was not specifically investigated as part of this research, collected vegetation data suggest it may have an impact upon R_{eco} fluxes.

Whilst no significant differences were observed in GPP fluxes from different microforms, the highest GPP fluxes were observed from the original surface where there was a greater coverage of *Cyperaceae* species such as *Carex panicea,* which was responsible for an observed hotspot of CO_2 uptake. The primary controlling mechanism of GPP was light at photosynthetically active radiation. Other controlling mechanisms were soil temperature and soil moisture content similar to R_{eco}.

These data highlight the need for further restoration of these sites to remove the effects of microtopography on C dynamics by raising and stabilising the water table. These data suggest that further re-wetting of the site will reduce R_{eco}, whilst increasing GPP and NEE.

~Chapter 7~

Net Ecosystem Exchange of restored peatlands in the Flow Country of northern Scotland.

7.0 Abstract

Northern peatlands play a key role in mediating regional land - atmosphere exchange of greenhouse gases such as carbon dioxide (CO_2), with northern peatlands estimated to accumulate carbon (C) at a rate of 23 g C m^{-2} yr^{-1}. However, anthropogenic degradation of northern peatlands has led to their large-scale drainage, potentially resulting in large C losses from these normally C-accumulating ecosystems. In the UK, approximately 80% of peatlands are thought to be in a degraded state due to drainage for agriculture and forestry plantation. Significant efforts are now underway all over the Northern Hemisphere to restore degraded peatlands and return them to net C sinks in response to rapidly increasing atmospheric C concentrations and its links with climate change.

Net ecosystem exchange (NEE) is the difference between photosynthetic inputs and respiratory losses from an ecosystem and is the quantity directly measured by the eddy covariance technique. Little empirical data exists on annual NEE of important greenhouse gases such as CO_2 from restored peatlands. Using eddy covariance techniques over a chronosequence of two restored sites during one year, this study sought to examine time dependent change in NEE.

Results showed that peatland restoration is successful at returning these ecosystems to net C sinks over multi-decadal timescales, with the older restoration site (Talaheel; restored in 1997/98) being a net C sink of -71 g C m^{-2} yr^{-1}. However, a younger restoration site (Lonielist; restored in 2003/04) remained a source of C to the atmosphere with a flux of 80 g C m^{-2} yr^{-1}. NEE was largely controlled by changes in air temperature, incident solar radiation and soil moisture. Annual NEE fluxes from these sites were lower than a published 6-year mean value of -114 g C m^{-2} yr^{-1} from an undrained bog in the Flow Country. Talaheel fluxes were within the range of fluxes from other northern peatlands.

7.1 Introduction

Northern peatlands play a key role in modulating atmospheric carbon (C) budgets and biogenic trace gases which influences regional and global climate (Gorham, 1991, Frolking and Roulet, 2007). These ecosystems are estimated to contain approximately 500 ± 100 Pg of organic C (Gorham, 1991, Yu, 2012) equating to around a third of the total global terrestrial C pool (Post, 1982, Murrell *et al.*, 1998, Jobbagy and Jackson, 2000, Scharlemann *et al.*, 2014). Northern peatlands are estimated to accumulate C at a rate of approximately 23 g C m^{-2} yr^{-1} (Gorham, 1991, Roulet *et al.*, 2007, Nilsson *et al.*, 2008, Billett *et al.*, 2010), however, all over the world, anthropogenic activities have resulted in large-scale peatland drainage to increase the productivity of the land for crop or tree cultivation (Holden *et al.*, 2004, Hooijer *et al.*, 2010). Across the Northern Hemisphere approximately 15 million ha of peatlands have been drained for forestry (Holden *et al.*, 2004), whilst in the UK, over 500,000 ha of peatlands have been drained for non-native coniferous forestry plantations (Cannell, 1993). In Indonesia, peatlands cover around 13 Mha of Sumatra and Kalimantan, but research has shown that only 4% of the peatland area remains covered by pristine peat swamp forest, while 37% are covered by peat swamp forest in some state of degradation and at least 1.4 Mha of the peatlands are covered by industrial oil palm plantations (Miettinen and Liew, 2010).

Net ecosystem exchange (NEE) is defined as the difference between the photosynthetic inputs (gross primary productivity - GPP) and respiratory losses (ecosystem respiration - R_{eco}). In an unmanaged state, peatlands function as net sinks of C due to an imbalance between inputs from photosynthesis and the losses through respiration (Bellisario *et al.*, 1998, Bubier *et al.*, 1998, Flanagan and Syed, 2011, Armstrong *et al.*, 2015). Frolking *et al.* (1998) compiled data on NEE and photosynthetic photon flux density (PPFD) and found that peatlands are weak at capturing CO_2 in comparison to other ecosystems due to a lower gross uptake compared to forests and grasslands, but are associated with smaller respiration losses, making them greater C stores. High levels of precipitation, low evaporation rates due to cool temperatures, and small losses to leaching limit peatland C loss; while high water table levels result in anaerobic conditions within the peat, which slows overall rates of decomposition (Davidson and Janssens, 2006, Flanagan and Syed, 2011).

Hydrologic and climatic conditions such as the height of the water table, air and soil temperature, nutrient supply, and vegetation composition (Bellisario *et al.*, 1998, Holden *et al.*, 2004, Armstrong *et al.*, 2015) exert different pressures on R_{eco} (Chapter 4) and GPP (Chapter 5) and therefore influence NEE. For example, a lower water table increases oxygen diffusion into the peat profile, increasing heterotrophic respiration as microbes break down organic material

(Silvola *et al.*, 1996a, Juszczak *et al.*, 2013). As shown in Chapter 4, R_{eco} in these restored ecosystems is largely controlled by hydrologic and thermal conditions. Water table draw down, coupled with a lower thermal capacity of dry peat in drained peatlands, increases the temperature of peat, resulting in increased microbial activity and R_{eco} (Waddington *et al.*, 2002). However, restoration of the water table height is successful at reducing R_{eco} losses from these ecosystems.

Physical and chemical properties of peat influence the vegetation composition and microbial communities which indirectly affect C cycling within peatlands by modulating rates of peat decay and soil C losses (De Deyn *et al.*, 2008). In ombrotrophic bogs, where the nutrient supply is generally low as they only receive atmospheric inputs, GPP is typically limited by nitrogen (N) availability for vegetation (Strilesky and Humphreys, 2012). The photosynthetic capacity of a leaf is largely related to the availability of N to the leaf, which is roughly proportional to the chlorophyll content (Evans, 1989). However in fertilised bogs, research has shown that despite an increase in biomass and leaf area, GPP is reduced due to shading by bigger shrubs and increased litter accumulation (Bubier *et al.*, 2007). Furthermore, Bubier *et al.* (2007) found a loss of *Sphagnum* and *Polytrichum* mosses, due to the shading caused by bigger shrubs on fertilised bogs, which have a strong influence on C uptake and retention (Turetsky, 2003, Street *et al.*, 2013, Fritz *et al.*, 2014). In Chapter 5 it was shown that while incident solar radiation had the greatest influence on GPP, periods of high vapour pressure deficit (VPD; > 1 kPa), combined with periods of low soil moisture content (< 0.5 m^3 m^{-3}), limited GPP.

Eddy covariance measurements provide the best method for assessing intra-annual and inter-annual changes in land-atmosphere CO_2 exchange at the ecosystem scale (Roulet *et al.*, 2007, Aubinet *et al.*, 2012, Helfter *et al.*, 2014). Previous research on an undrained bog in the Flow Country of northern Scotland found the site to be a mean net sink of CO_2 over a 6-year period of -114 g C m^{-2} yr^{-1} (Levy and Gray, 2015). Parallel research from a peatland on the Manicouagan peninsula in Quebec, Canada, which contains ecosystems with similar characteristics to those in northern Scotland, found the site to be a net sink of -49 g C m^{-2} yr^{-1} (Pelletier *et al.*, 2015). Little or no empirical data exists on the *annual* net exchange from restored peatlands because previous research focussed only on growing season fluxes (Strack and Zuback, 2013). Furthermore, peatland restoration has mainly focussed on former peat cutting or horticultural sites, where the scale of restoration is unsuitable for the implementation of eddy covariance and chamber methods have instead been used (Waddington and Price, 2000). Waddington *et al.* (2010) found that a restored peatland in Quebec, Canada to be a net growing season CO_2 sink of around 20 ± 5 g C m^{-2}, two years after restoration. Furthermore, the authors combined the results with

previous work on dissolved organic carbon (DOC) export and suggested the peatland would return to an annual net C sink 6 to 10 years post restoration (Waddington *et al.*, 2010). In contrast, Samaritani *et al.* (2011) suggested that up to 50 years is required for net C accumulation to be regained after making measurements from a cutover peatland in the Swiss Jura Mountains 29 – 51 years after restoration. Strack and Zuback (2013) undertook year round measurements of NEE 10 years post restoration using closed dynamic chambers at the Bois-des-Bel peatland in Quebec, Canada, finding that both restored and natural peatlands were a source of C to the atmosphere. However, the authors noted that the restored NEE flux was significantly lower than from the unrestored site and attributed the net C source to the dry conditions during the sampling period (Strack and Zuback, 2013).

The aim of this research is to use eddy covariance to understand changes in annual NEE over a chronosequence of restored peatlands. Key questions include:

1) How does restoration affect NEE and its environmental drivers over a chronosequence of restored peatlands in Northern Scotland?

2) How do the NEE results obtained in this study compare to other Northern peatlands and how can this be used to inform restoration projects?

7.2 Site Descriptions

All work was undertaken on sites situated within the Forsinard Flows National Nature Reserve (58°23'59"N, 3°49'28"W) in Caithness and Sutherland, Northern Scotland. Talaheel (58°24'49"N, 3°47'52"W) was the oldest site on the reserve, encompassing an area of around 380 ha and was restored to blanket bog from Sitka spruce (*Picea sitchensis*) and lodgepole pine (*Pinus contorta*) plantation forestry in 1997/98. This site should provide an indication as to the timescales required for these sites to return to net C sinks. During the period of study, the site had a mean water table depth of 0.11 ± 0.05 m below the surface of the furrow, which was approximately 0.3 m below the original peat surface. Soil moisture content was relatively stable throughout the study period with a range of 0.71 to 0.73 m^3 m^{-3} (mean 0.72 m^3 m^{-3}). Mean air temperature over the study period was 7.0°C with a range of -8.1°C to 26.9°C. The peat at Talaheel had a mean C content of 50.1 ± 0.38% whilst N content was 1.42 ± 0.23%.

Lonielist (58°23'29"N, 3°45'59"W) was considered representative of a peatland at an intermediate stage of restoration with the site restored in 2003/04. The site had a mean water table depth of 0.10 ± 0.02 m below the furrow surface, which was approximately 0.3 m below the original peat surface. However, this site was not equipped with an automatic pressure transducer for measuring water table depth and was instead measured by hand at fortnightly to monthly intervals by volunteers. Soil moisture content was lower and more variable at Lonielist with a mean of 0.58 m^3 m^{-3} and a range of 0.43 to 0.69 m^3 m^{-3}. Mean air temperature at Lonielist was slightly higher at 7.5°C with a range of -8.1°C to 26.6°C. The peat at Lonielist had a mean C content of 49.7 ± 0.28% and a mean N content of 1.73 ± 0.20%.

Cross Lochs (58°22'13"N, 3°57'52"W) was an undrained blanket bog site within the Forsinard Flows National Nature Reserve. The site had not been subjected to any drainage management and the only human intervention on site had been deer management. The site had a mean water table of 0.06 ± 0.06 m below the surface of the peat. The mean air temperature at Cross Lochs was 8.2°C with a range of -1.9°C to 19.5°C. The peat had a mean C content of 49.6 ± 0.26% by weight and a mean N content of 1.76 ± 0.28% by weight.

Further information on each site is available in Chapter 2.

7.3 Methods

All of the NEE data presented in this chapter were collected using eddy covariance (EC) as described in Chapter 3. Eddy covariance measurements were undertaken on towers situated at the three sites, each equipped with a sonic anemometer and either an open-path or enclosed-path

CO_2 analyser at a measurement height of 3m. Additionally, each site was equipped with environmental sensors such as soil moisture, soil temperature and air temperature. EC measurements were recorded at a frequency of 10Hz and environmental measurements recorded once a minute.

7.3.1 Analysis

All EC data were processed as per the protocols described in Chapter 3. NEE data were gap filled using the marginal distribution sampling (MDS) method (Reichstein *et al.*, 2005) implemented through the R programme REddyProc (Reichstein and Moffat, 2014). This method is described in Chapter 3, but briefly the programme uses a moving window of ± 7 days to replace missing data with half-hour mean values for similar meteorological variables defined as solar radiation, air temperature and VPD with a deviation equal to 50 W m^{-2}, 2.5°C and 5.0 hPa, respectively. This window is increased to ± 14 days if similar meteorological conditions are not identified during the initial ± 7 day window.

All sites were subjected to the same statistical analyses, which were performed in MATLAB Version 8.1.0.604 (R2013a) with Statistics Toolbox Version 8.2 (R2013a) (Mathworks Inc., Natick, MA, USA). Normality within these data were tested using a Kolmogorov-Smirnov test. As none of the data were normally distributed, and thus did not meet the assumptions of analysis of variance (ANOVA), non-parametric statistical methods were used. For seasonal analyses, data were divided into standard meteorological seasons as per the analyses in previous chapters (Chapter 4 – Table 4.0). Furthermore, growing season fluxes were assessed using a protocol where the growing season was defined as the first day of a period of 5 consecutive days with a mean air temperature greater than 5°C. The end of the growing season was defined as the first day of a period of 5 consecutive days with a mean air temperature less than 5°C. All data are presented as median ± interquartile range unless otherwise stated.

Kruskal-Wallis was used in combination with Fisher's LSD post hoc analysis to assess the intra-annual variability in NEE. Wilcoxon rank sum analysis was used to assess differences between sites. Spearman's rank correlation coefficient was used to assess the correlation between environmental variables and NEE. The strength of the correlation was determined as per previous chapters (Chapter 5 – Table 5.1). The results of the Spearman's rank correlation analyses were used to inform multiple regression analyses. Due to the non-normality of the data, independent variables were transformed using natural logarithms to meet normality assumptions. For all statistical analyses significance was accepted at $P < 0.05$.

Throughout this chapter, the standard micrometeorological sign convention is used where negative NEE fluxes indicate movement from the atmosphere to the land surface (i.e. a sink) and positive NEE fluxes indicate movement from the land surface to the atmosphere (i.e. a source).

7.4 Results

7.4.1 Effects of Restoration on NEE

Significant differences were observed in NEE fluxes between the restored sites, with the younger site (Lonielist; restored in 2003/04) always being a larger source or smaller sink of CO_2 than the older site (Talaheel; restored in 1997/98 – Kruskal-Wallis, $P < 0.0001$). Daily mean NEE showed Lonielist (Chapter 2 - 2.3.1) to be a net source of CO_2 in early September 2014, while at Talaheel (Chapter 2 - 2.3.2) this did not occur until later in September 2014. Talaheel returned to a net sink in February 2015, whilst Lonielist did not return to a net sink until March 2015. In nearly all months, Talaheel was either a significantly greater daily mean sink or a smaller source of CO_2 than Lonielist (Kruskal-Wallis with Fisher's LSD, $P < 0.0001$), except in March 2015, where there was no significant difference (Wilcoxon rank sum, $P = 0.3476$). Moreover, in all months, Cross Lochs was a daily mean net sink for CO_2.

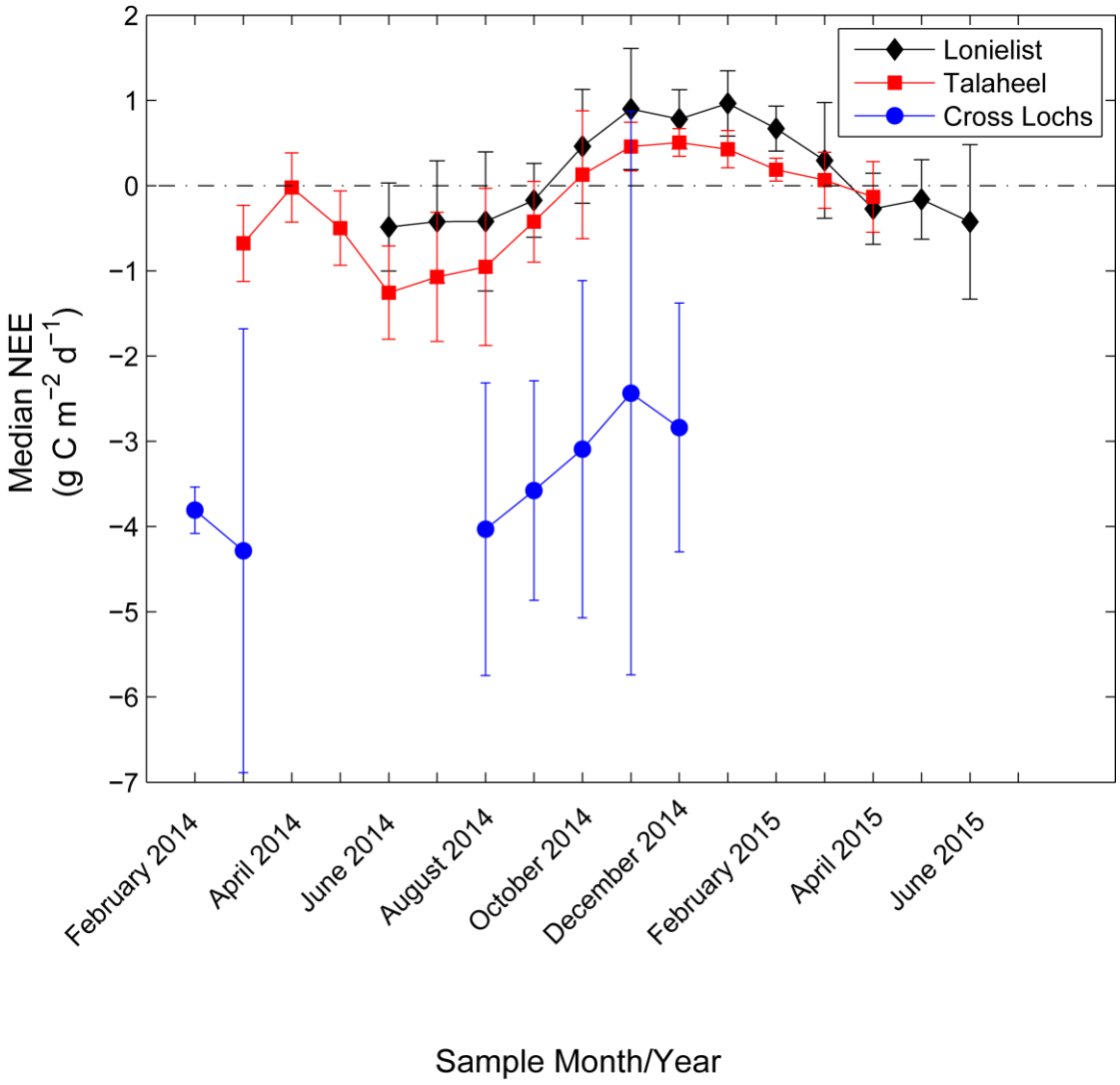

Figure 7.1 Daily mean NEE in each month from Lonielist (black), Talaheel (red) and Cross Lochs (blue). The shapes indicate the median and bars indicate the interquartile range.

The range of fluxes were greatest at Cross Lochs, where daily NEE fluxes were in the range of -9.61 to 0.87 g C m^{-2} d^{-1}, whilst at Talaheel NEE fluxes were in the range of -2.55 to 1.18 g C m^{-2} d^{-1}. At Lonielist, the range of fluxes was smaller -1.43 to 1.89 g C m^{-2} d^{-1}. The greatest median daily uptake at both Lonielist (-0.49 ± 0.52 g C m^{-2} d^{-1}) and Talaheel (-1.26 ± -0.55 g C m^{-2} d^{1}) was observed in June 2014 (Figure 7.1). The greatest median net loss of CO_2 at Lonielist occurred in November 2014 (0.90 ± 0.71 g C m^{-2} d^{-1}), whilst at Talaheel the greatest median net loss occurred in December 2014 (0.51 ± 0.16 g C m^{-2} d^{-1}). The monthly fluxes at Cross Lochs after July 2014 showed a similar trend to Lonielist and Talaheel with monthly net uptake reducing, although the site never became a monthly net source of CO_2 to the atmosphere (Figure 7.1).

The data display distinct seasonal trends (Figure 7.1) with the largest net sinks occurring in the summer months and small net sinks or net sources occurring in the winter months (Table 7.1). Seasonal median daily NEE fluxes were observed to be significantly different between all sites (Wilcoxon rank sum, $P < 0.0001$), with Lonielist always having higher NEE than both Talaheel and Cross Lochs (Wilcoxon rank sum, $P < 0.0001$). At Lonielist, net median daily CO_2 uptake was only observed in the summer, whilst all other months were found to be net sources to the atmosphere. During the thermal growing season, NEE at Lonielist was observed to be near neutral with a median flux of -0.02 ± 1.07 g C m^{-2} d^{-1}, but was a net source of CO_2 during the non-growing season (Table 7.1).

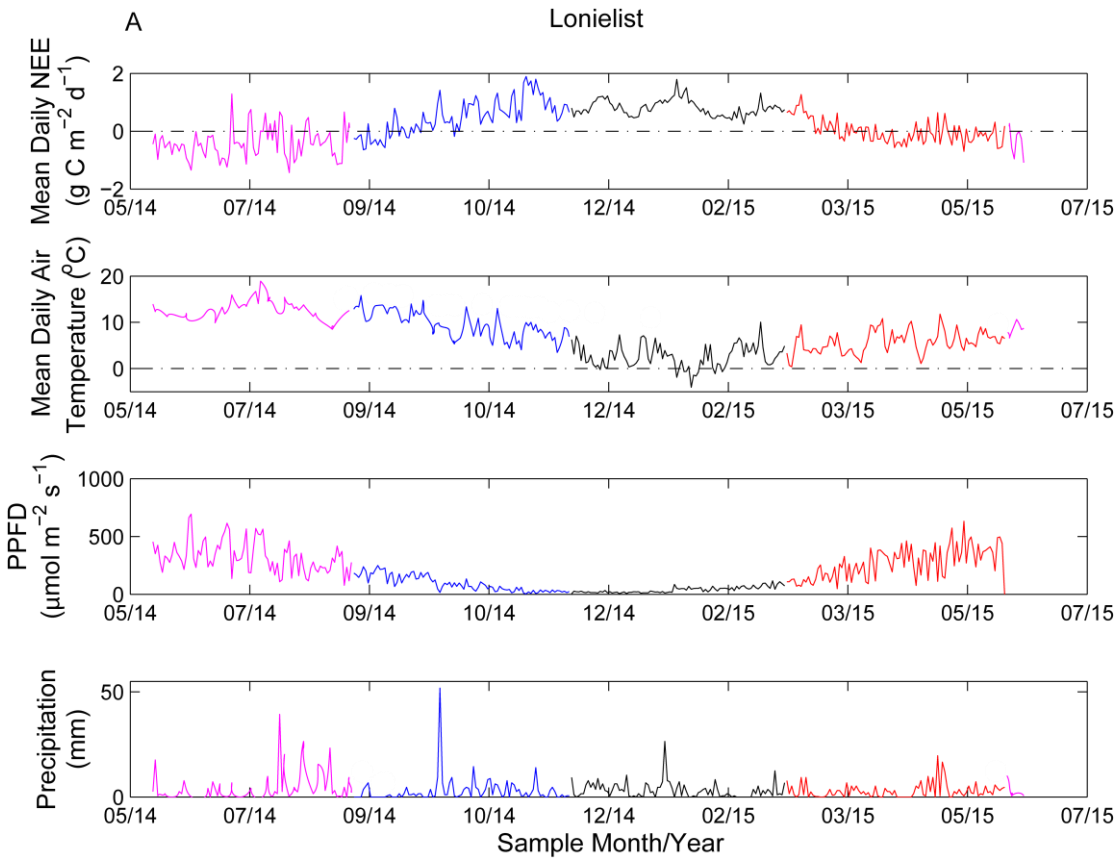

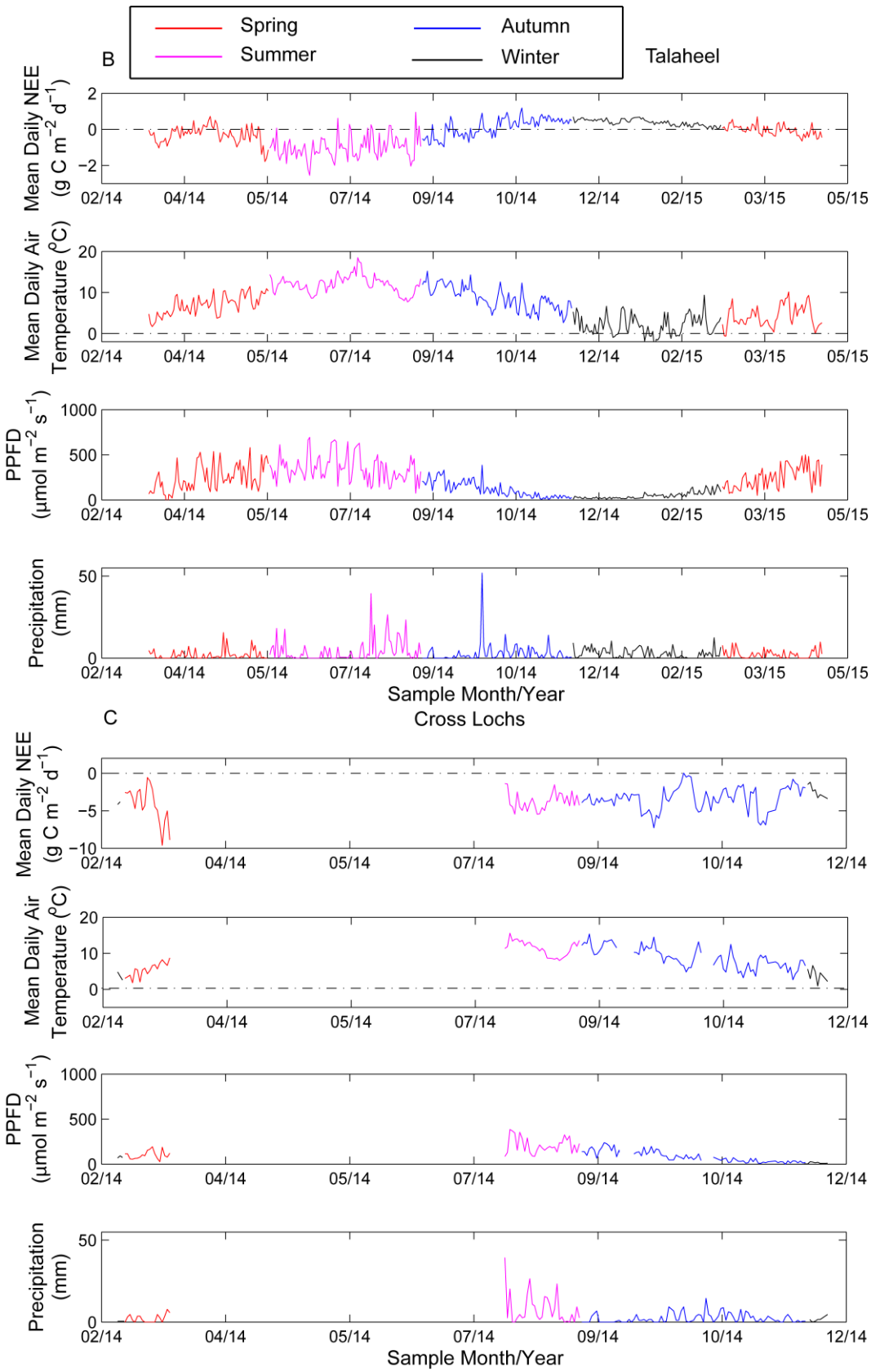

Figure 7.2 Trends in NEE from Lonielist (A), Talaheel (B), Cross Lochs (C) Meteorological data also provided for each site. Within each plot the daily seasonal signal is shown by use of colour. Note the differences in the x-axis between the plots.

Greater seasonal uptake was observed in spring and summer at Talaheel than at Lonielist (Table 7.1). Although Talaheel was near neutral in spring, similar to Lonielist, the net exchange was significantly different to Lonielist and provided a greater sink (Wilcoxon rank sum, P = 0.001). Greater uptake in summer and near-neutral conditions in spring and autumn resulted in a median daily growing season CO_2 sink at Talaheel (Table 7.1). The losses observed in the non-growing season at Talaheel were significantly lower than the growing season uptake (Wilcoxon rank sum, $P < 0.0001$). This was in contrast to Lonielist where non-growing season losses were significantly higher than the growing season (Wilcoxon rank sum, $P < 0.0001$). At Cross Lochs, mean net uptake was observed in both the growing (-3.47 ± 2.22 g C m^{-2} d^{-1}) and non-growing season (-3.33 ± 0.93 g C m^{-2} d^{-1}). However, net uptake was lower during the non-growing season.

Table 7.1 Seasonal median ± interquartile range daily NEE fluxes from Lonielist, Talaheel and Cross Lochs (g C m^{-2} d^{-1}). Small letters indicate significant differences ($P < 0.05$) within each site. Capital letters indicate significant differences ($P < 0.05$) between different sites. Common letters signify no significant difference.

	Lonielist	**Talaheel**	**Cross Lochs**
Spring (g C m^{-2} d^{-1})	-0.06 ± 0.55 aA	-0.16 ± 0.55 eB	-4.36 ± 3.23 iC
Summer (g C m^{-2} d^{-1})	-0.45 ± 0.68 bD	-1.08 ± 0.76 fE	-4.04 ± 1.72 jG
Autumn (g C m^{-2} d^{-1})	0.46 ± 0.89 cH	0.17 ± 0.84 gI	-3.34 ± 2.12 kJ
Winter (g C m^{-2} d^{-1})	0.76 ± 0.39 dK	0.38 ± 0.27 hL	-3.32 ± 1.51 iM
Growing Season (g C m^{-2} d^{-1})	-0.02 ± 1.07 nU	-0.35 ± 1.12 pV	-3.47 ± 2.22 rW
Non-Growing Season (g C m^{-2} d^{-1})	0.68 ± 0.43 oX	0.30 ± 0.34 qY	-3.33 ± 0.93 sZ

The loss of CO_2 to the atmosphere from the land surface in autumn and winter correlate to a reduction in mean daily PPFD (Figure 7.2A) at Lonielist (Spearman's $\rho = -0.7023$, $P < 0.0001$), Talaheel (Figure 7.2B - Spearman's $\rho = -0.7382$, $P < 0.0001$) and Cross Lochs (Figure 7.2C - Spearman's $\rho = -0.4511$, $P < 0.0001$), whilst a reduction in mean daily temperature (Figure 7.2) also resulted in a loss of CO_2 from the systems with a weak, but significant, correlation (Spearman's $\rho = -0.3702$, 0.3823 and 0.2621 respectively, $P < 0.0001$). During the spring and summer, increasing mean daily temperatures and PPFD increase CO_2 uptake from the atmosphere (Figures 7.2A, B and C), with NEE becoming more strongly negative (i.e. greater uptake). The lowest monthly precipitation was recorded in July 2014 with a total of 58 mm, whilst the preceding months of May and June 2014 were the second and third driest months with precipitation totals of 78 and 83 mm, respectively. The driest month of July 2014 correlated with a reduction in net uptake, suggesting a relationship between dry conditions and a reduction in uptake. Weak, but significant, correlations are observed between NEE and precipitation at Lonielist and Talaheel (Spearman's $\rho = 0.2689$, $P < 0.0001$ and $\rho = 0.2438$, $P =$

0.0076 respectively). Similar relationships are also observed in the soil moisture content (Spearman's $\rho = 0.2629$, $P < 0.0001$ and $\rho = 0.2728$, $P < 0.0001$ respectively).

Multiple regressions highlight that over daily timescales PPFD, soil temperature, soil moisture and VPD had the greatest significant influence on NEE at both Lonielist and Talaheel. At Lonielist, these four variables explained over 75% of the variation in NEE (MLR - $R^2 = 0.7576$, $P < 0.0001$), with PPFD observed to have the greatest influence on NEE (regression $R^2 = 0.7590$, $P < 0.0001$). At Talaheel, similar relationships were observed with the four environmental variables explaining over 70% of the variance in NEE (MLR - $R^2 = 0.7175$, $P < 0.0001$). Furthermore, PPFD was again observed to have the greatest influence individually on NEE (regression – $R^2 = 0.6333$, $P < 0.0001$). At Cross Lochs, no significant influence of environmental variables on NEE was observed (MLR – $R^2 = 0.1765$, $P = 0.0526$). However when assessed individually, PPFD was found to have the greatest influence (linear regression – $R^2 = 0.3099$, $P = 0.002$).

Over annual timescales, Talaheel was a net sink of CO_2 from the atmosphere (-71 g C m^{-2} yr^{-1}), whilst Lonielist was a net source of CO_2 to the atmosphere (80 g C m^{-2} yr^{-1}) (Table 7.2). In comparison to the 6-year annual mean from the Cross Lochs site (Levy and Gray, 2015), the sink strength at Talaheel (-71 g C m^{-2} yr^{-1}) was lower than that of Cross Lochs (-114 g C m^{-2} yr^{-1}).

Table 7.2 Annual NEE from Lonielist (restored in 2003/04), Talaheel (restored in 1997/98) and Cross Lochs. Figures from Cross Lochs are a 6-year mean between 2008-2013 (Levy and Gray, 2015)

	Lonielist	**Talaheel**	**Cross Lochs**
Annual NEE (g C m^{-2} yr^{-1})	80	-71	-114*

The constituent NEE fluxes of R_{eco} and GPP were previously presented in Chapters 4 and 5 respectively, but here it was clear that larger R_{eco} fluxes at Lonielist (Figure 7.3) compared to Talaheel (Figure 7.4) caused Lonielist to be a net source of CO_2 to the atmosphere. Whilst GPP showed very distinct seasonality, with small GPP fluxes in the winter (Figure 7.3), R_{eco} fluxes were always higher (Figure 7.3) although this is still lower than summer or autumn periods. Cumulative NEE highlighted that it is during this winter period when Lonielist (Figure 7.3) switched from a net sink to a net source, losing all of the C that had been taken up during the

summer period. The site began to lose CO_2 in September 2014 (around 100 days since start of experiment) and this was coupled with a distinct decrease in GPP (Figure 7.3).

Talaheel was a net C sink during the study period (Table 7.2). The greatest uptake was observed in the summer (Figure 7.4), driven by strong GPP uptake, whilst R_{eco} losses were lower. The site began to release CO_2 approximately two weeks after Lonielist, at the end of September 2014. This continued until the end of February 2015, when the site reached equilibrium where photosynthetic uptake was equal to respiratory losses (Figure 7.4). As can be seen in Figure 7.5, Cross Lochs was always a sink for CO_2 over the same time period. However, the large gaps in the data did not allow a full annual NEE to be calculated.

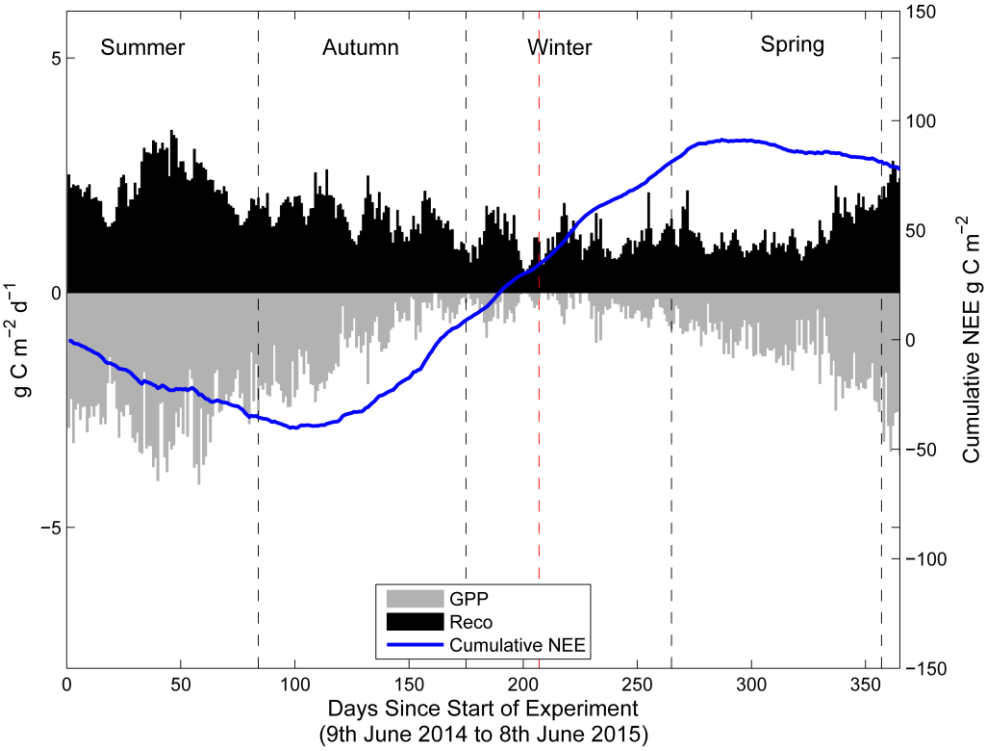

Figure 7.3 Daily GPP (grey) and R_{eco} (black) flux from Lonielist (restored in 2003/04) with cumulative NEE (blue) shown on the additional y-axis. Black dashed lines denote the seasons, whilst the red dashed line is 1st January 2015.

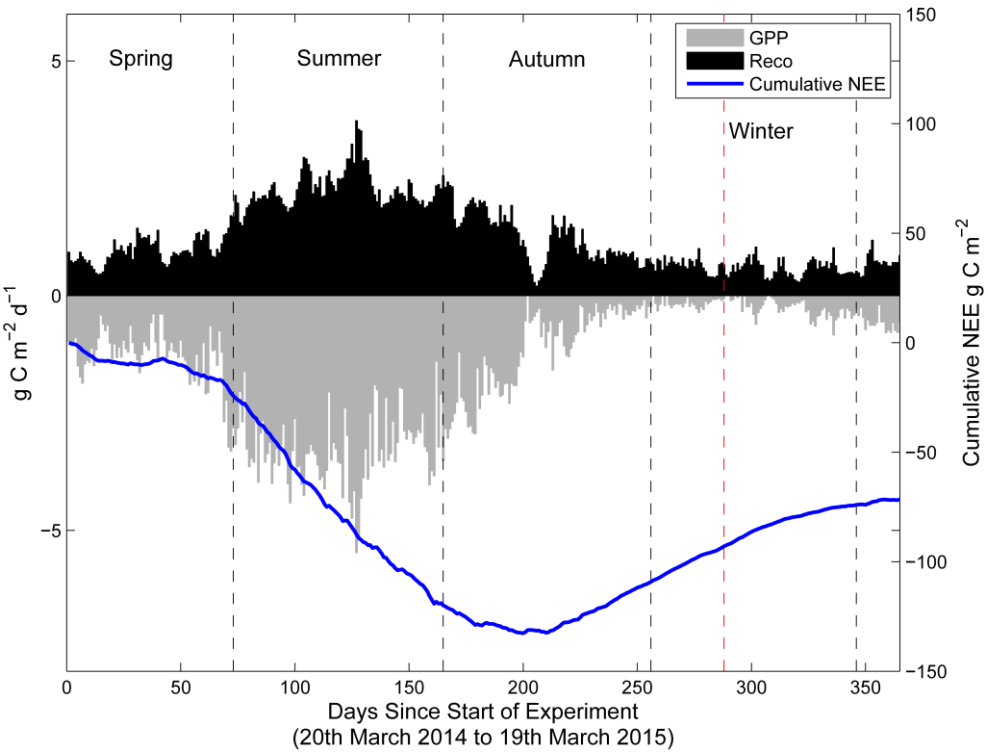

Figure 7.4 Daily GPP (grey) and R_{eco} (black) flux from Talaheel (restored in 1997/98) with cumulative NEE (blue) shown on the additional y-axis. Black dashed lines denote the seasons, whilst the red dashed line is 1st January 2015.

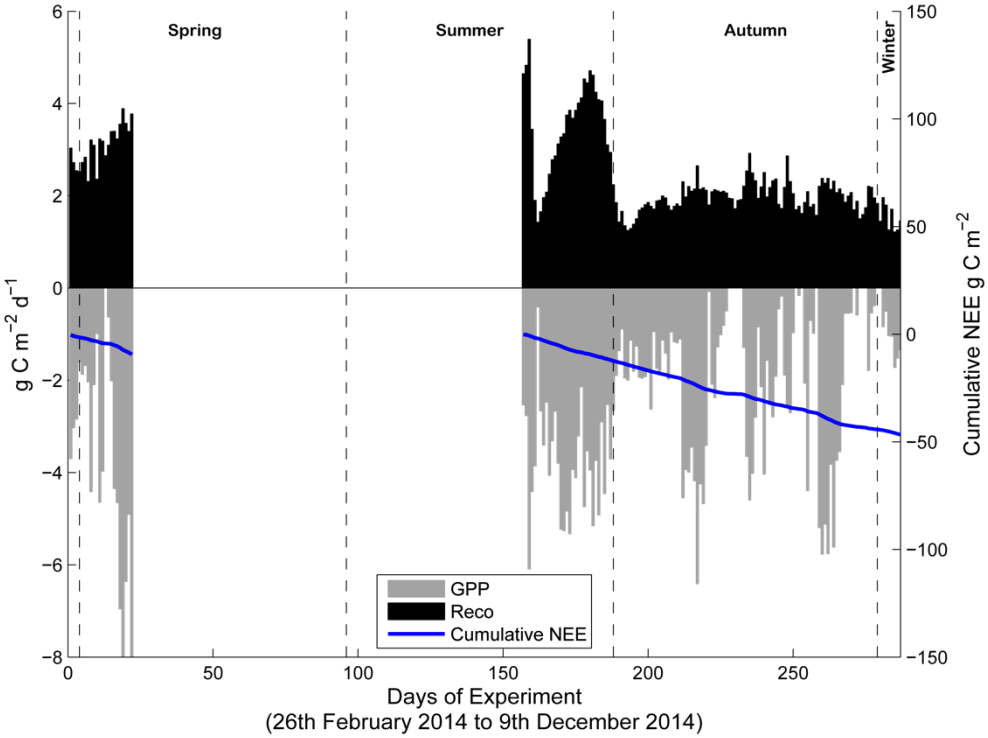

Figure 7.5 Daily GPP (grey), and R_{eco} (black) flux from Cross Lochs with the cumulative NEE (blue) shown on the additional y-axis. Black dashed lines denote the seasons.

Cumulative NEE showed similar patterns but highlighted the differences between Lonielist (Figure 7.3) and Talaheel (Figure 7.4). In spring, Talaheel was a strong net sink for CO_2 (-27.17 g C m^{-2}), whilst Lonielist was near neutral (0.11 g C m^{-2}). Lonielist was a net sink (-40.70 g C m^{-2}) in summer, whilst Talaheel was stronger (-95.76 g C m^{-2}). Both Lonielist and Talaheel were net sources in autumn (45.99 and 10.75 g C m^{-2} respectively) and winter (75.00 and 34.27 g C m^{-2} respectively), but Talaheel was always a weaker source.

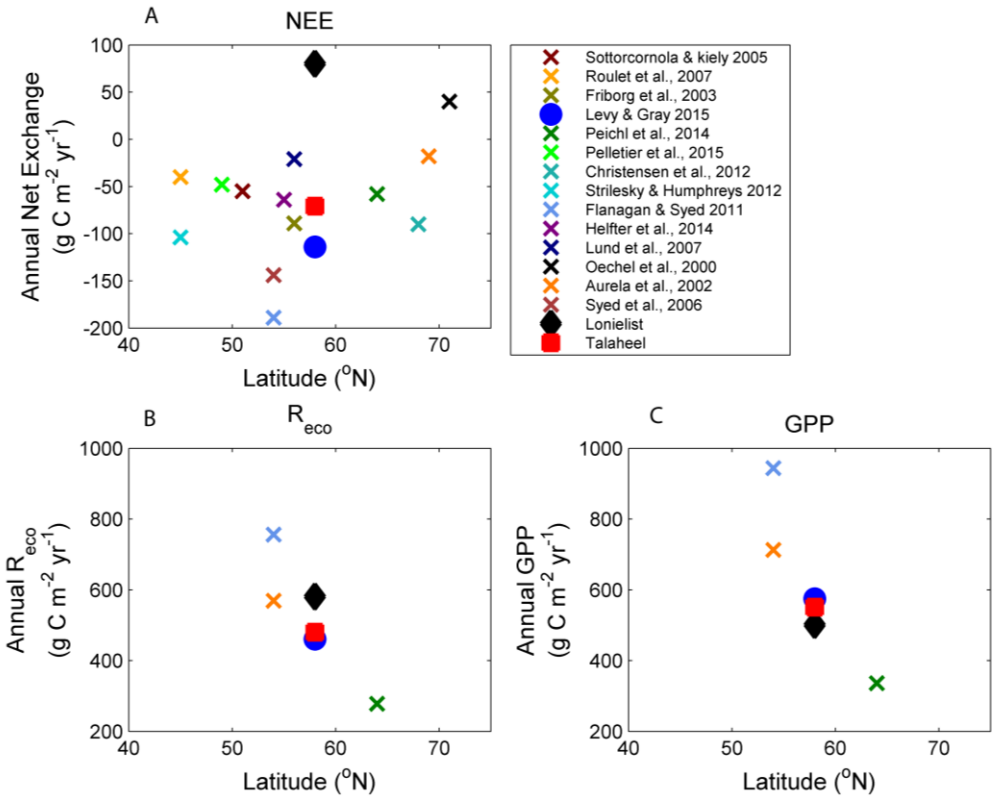

Figure 7.6 Annual NEE, R_{eco} and GPP at "natural" peatland sites in the Northern Hemisphere. *Strilesky and Humphreys figure based only on years with full annual measurements.

Comparison to other northern peatlands identified Talaheel NEE to be similar to "natural" peatlands at similar latitudes (Figure 7.6 A). Lonielist NEE was observed to be higher (i.e. a bigger source) than other "natural" peatlands, including those in the arctic. However, when GPP and R_{eco} were assessed against latitude, a near linear relationship was observed with both R_{eco} and GPP observed to decrease with latitude, which was not observed in latitudinal NEE. However no significant differences were observed between latitude and either R_{eco} (Kruskal-Wallis, $P = 0.2207$) or GPP (Kruskal-Wallis, $P = 0.1123$), although the lack of data, particularly at higher latitudes, is likely to influence these statistics.

7.5 Discussion

Current research into GHG exchange from restored peatlands suggests timescales of 6 – 50 years are required for restoration of the net C sink (Waddington *et al.*, 2010, Samaritani *et al.*, 2011). However, most of research has been undertaken on peat extraction sites rather than forested peatlands and focussed on growing season fluxes measured using static or dynamic chamber techniques. This makes it difficult to assess the timeline for the restoration of the net C sink due to the low frequency of measurements and the growing season bias in the data. Eddy covariance helps to reduce these issues by measuring continuously and integrating the flux over a large spatial area.

7.5.1 NEE and the controlling mechanisms

Annually, there was a significant difference between the two restored sites, with Lonielist being a net source of C to the atmosphere of 80 g C m^{-2} yr^{-1} and Talaheel being a net sink of -71 g C m^{-2} yr^{-1}. Unfortunately, due to equipment failures it wasn't possible to assess the net annual exchange for Cross Lochs over the same time period. However, previous work has shown this site to be a mean net sink of -114 g C m^{-2} yr^{-1} varying from -88 to -188 g C m^{-2} yr^{-1} on an annual basis (Levy and Gray, 2015). The annual loss of CO_2 from Lonielist was less than that of a restored former horticultural peat extraction site in the Boi-des-Bel peatland complex in Canada (148 g C m^{-2} yr^{-1}) which was restored in 1999/2000 (Strack and Zuback, 2013). However, this research was undertaken during a dry year, which is likely to have exacerbated emission to the atmosphere. This research in the Flow Country suggests that restoration and re-wetting of peatlands reduces the losses of CO_2 to the atmosphere (See Also: Nykanen *et al.*, 1995, Waddington and Price, 2000, Waddington *et al.*, 2002, Ojanen *et al.*, 2010), but that restoration of net sink ecosystem functioning takes longer than the 6 – 10 years previously proposed from research in Canada (Waddington *et al.*, 2010) and that timescales of 13-16 years are likely to be more realistic for higher latitude northern peatland ecosystems, although further research is required to better understand restoration timescales under different climatic conditions.

As previously mentioned (7.1), NEE is the difference between photosynthetic inputs and respiratory losses and therefore these are the main controlling factors on NEE. In Chapter 4, it was shown that there was a significant difference in R_{eco} (Kruskal-Wallis, $P < 0.0001$) between the younger restoration site (Lonielist; restored 2003/04 – 581 g C m^{-2} yr^{-1}) and the older restoration site (Talaheel; restored in 1997/98 – 480 g C m^{-2} yr^{-1}). In Chapter 5, it was shown that there was no significant difference of GPP (Kruskal-Wallis, $P = 0.2103$) between the younger restoration site (Lonielist; restored 2003/04 – 501 g C m^{-2} yr^{-1}) and the older restoration site (Talaheel; restored in 1997/98 – 551 g C m^{-2} yr^{-1}). Therefore, differences observed between

these two sites can be mainly attributed to R_{eco}. Differences in R_{eco} were partly attributed to the moisture content and temperature of the peat at Lonielist (Chapter 4 - multiple regression R^2 = 0.79, $P < 0.0001$) and Talaheel (multiple regression R^2 = 0.83, $P < 0.0001$). The thermal capacity of peat decreases with soil moisture content leading to greater diurnal temperature fluctuations (Waddington *et al.*, 2002). Higher soil temperatures in dry peat lead to greater soil microbial activity and increased respiration (Chapter 4 Figure 4.2). Significant differences (Kruskal-Wallis, $P < 0.0001$) were also observed in R_{eco} due to microtopography (Chapter 6) with R_{eco} fluxes from ridges and the original surfaces significantly higher than furrows. Similarly, no significant differences were observed in GPP fluxes between microforms (Kruskal-Wallis, $P = 0.217$).

Mean daily NEE showed distinct seasonality with the greatest uptake at Lonielist and Talaheel occurring in the summer, before reducing during autumn where Talaheel was near neutral. In winter, both sites were observed to be sources of CO_2 to the atmosphere, whilst in spring, both Lonielist and Talaheel were observed to be near neutral, although Talaheel was a slightly bigger sink than Lonielist. Similar relationships between seasonal changes and NEE fluxes were observed in the Mer Bleue peatland in Canada (Roulet *et al.*, 2007). Roulet *et al.* (2007) found NEE fluxes to be similar in magnitude to those observed at Lonielist and Talaheel with summer fluxes in the range 0 to -3 g C m^{-2} d^{-1}, whilst spring and autumn fluxes were in the range of 1 to -1 g C m^{-2} d^{-1}, and winter fluxes in the range of 0 to 0.5 g C m^{-2} d^{-1}. In my research elevated R_{eco} fluxes (Chapter 4) combined with lower GPP fluxes (Chapter 5) resulted in the lower NEE (i.e. greater source) in the winter. Winter GPP at Talaheel was around a tenth of the summer GPP, whilst winter R_{eco} was only around a third of the summer R_{eco} suggesting a substantial loss of CO_2 to the atmosphere.

At both Lonielist and Talaheel, the greatest mean daily net uptake was observed in June 2014 (-0.49 ± 0.52 g C m^2 d^{-1} and -1.26 ± 0.55 g C m^{-2} d^{-1} respectively), before slight reductions in July and August 2014. This has been attributed to lower increases in GPP than R_{eco} between June and July. The driest period at Talaheel and Lonielist during the study was July 2014, with total precipitation around 58 mm, whilst the preceding months of June and May 2014 were the second and third driest (approximately 78 mm and 83 mm respectively). Previous research by Lund *et al.* (2007) at a bog in southern Sweden also found that daily NEE uptake was greatest in June before decreasing slightly in July. The authors attributed this decrease to the desiccation of the *Sphagnum* mosses caused by a reduction in the water table height resulting in a reduction in photosynthetic capacity. Haraguchi and Yamada (2011) suggested that *Sphagnum* mosses have optimal water content for photosynthesis, 600 – 800% of their dry weight, above and below

which photosynthesis rapidly declines. As both Talaheel and Lonielist have at least 30% coverage of *Sphagnum* and *Hypnoid* mosses, it is likely that the reduction in net uptake in July 2014 was caused by the dry conditions of the site putting *Sphagnum* and *Hypnoid* mosses under water stress, limiting GPP and reducing net C uptake. Furthermore, relationships between GPP and VPD discussed in Chapter 5 are also likely to have had an impact in reducing the photosynthetic capacity of the sites, whilst the dry, warm conditions will have increased R_{eco}. Similar relationships between periods of high VPD and reduced photosynthetic capacity have been observed at undrained blanket bogs and other ecosystems (Cunningham, 2005, Otieno *et al.*, 2012, Goodrich *et al.*, 2015)

7.5.2 Latitudinal effects

It is expected that sites at lower latitudes would be greater sinks with a decreasing latitudinal NEE trend (Van Dijk and Dolman, 2004, Yuan *et al.*, 2009). Previous research has suggested that GPP drops off more rapidly towards the poles than R_{eco}, which leads to a general trend of decreasing NEE with increasing latitude (Van Dijk and Dolman, 2004, Yuan *et al.*, 2009). This explains the larger net source or smaller net sink status at higher latitudinal peatlands such as those in the arctic (Oechel *et al.*, 2000, Aurela *et al.*, 2002). However, whilst there was a general decreasing latitudinal NEE trend, there appeared to be more scatter, with a few studies indicating lower NEE fluxes at lower latitudes, in comparison to Cross Lochs and Talaheel.

When NEE was partitioned into the constituent parts of R_{eco} and GPP, there was a clear, but not significant, decreasing latitudinal trend. These results highlight the complexities involved in modelling NEE from ecosystems. The figure of -48.8 g C m^{-2} yr^{-1} (latitude 64ºN) presented by Pelletier *et al.* (2015) was only measured over one growing season using eddy covariance, with winter fluxes and the subsequent annual sum modelled using data from another peatland in the same area of Canada. Moreover, these data were not gap-filled due to the complexities of the landscape under measurement, which adds further uncertainty to the data. Furthermore, some of the Canadian measurements (Roulet *et al.*, 2007) reported significant snowfall during the study periods, resulting in a complete shutdown of GPP. The data presented in Figures 7.5B and 7.5C highlight the lack of literature with reported annual partitioned fluxes. Annual GPP and R_{eco} fluxes are crucial to fully understand C dynamics of peatland ecosystems and understand how future climatic change may affect C dynamics.

Annual NEE from Talaheel and Cross Lochs were similar to other studies at similar latitudes in the Northern Hemisphere. The closest site geographically to these sites in the Flow Country was Auchencorth Moss, near Edinburgh, where mean net exchange over 11 years was -64 g C m^{-2} yr^{-1}, with a range of -142 to -5.2 g C m^{-2} yr^{-1} (Helfter *et al.*, 2014). The site was drained over

100 years ago and was naturally re-vegetated by not clearing ditches, which allowed vegetation to infill the ditches, slowing water loss from the site. Research in a Siberian bog near Tomsk, Russia (56°N) found a net sink of -89 g C m^{-2} yr^{-1}, which is similar to that observed at Talaheel (Friborg *et al.*, 2003). Moreover, Figure 7.6 highlights the lack of annual exchange data from restored peatlands with only the data from Talaheel and Lonielist considered to be from a restored peatland.

7.5.3 Restoration implications

The restoration undertaken on these sites was completed in such a way as to encourage the re-growth of peat forming vegetation species such as *Sphagnum*, thus maximising GPP rather than reducing R_{eco}, as shown by the results presented in Chapters 4 and 5. The results of this research suggest that there needs to be a balance struck between maximising GPP and reducing R_{eco}.

Stakeholders, such as the Royal Society For The Protection Of Birds (RSPB) and others, undertaking forest-to-bog restoration should consider microtopographic re-profiling. This could be undertaken through flattening of ridges with ridge peat pushed into the furrows to create a peat dam behind which water can build up. The advantage of this is two fold: 1) it reduces microtopography, moisture and temperature gradients across microforms and thus R_{eco}; and, 2) it provides a wet surface for the establishment of *Sphagnum*, which helps to maximise GPP. Furthermore, similar to the restoration work undertaken in Canada and North America, *Sphagnum* re-colonisation could be achieved through the translocation of *Sphagnum* from surrounding areas of good quality blanket bog (Rochefort *et al.*, 2003). However, as no peat was extracted from these sites it is likely that *Sphagnum* will easily re-generate where conditions are appropriate.

The continued presence of woody debris on some of these restoration sites, even more than 10 years post restoration, results in a significant labile C pool which can increase R_{eco} losses to the atmosphere. Removal or reduction of this biomass through whole tree harvesting or mulching could accelerate the return of these ecosystems to net C sinks by reducing R_{eco} losses whilst increasing GPP, as vegetation shading is reduced (Chapter 5), resulting in a greater net C uptake.

7.5.4 Data Limitations

This chapter represents the first annual measurements of NEE using eddy covariance on peatlands restored from plantation forestry. Although the data have shown restoration to be successful at restoring the ecosystem C sink over multi-decadal timescales, the data are limited. Firstly, more data are required to better constrain inter-annual variation and provide more robust

error values around the annual sum. Inter-annual variation can be large, as seen at Cross Lochs, where although the 6-year mean NEE was -114 g C m^{-2} yr^{-1} the inter-annual variation gave a range of between -88 and -188 g C m^{-2} yr^{-1}.

Secondly, although these data cover temporal variations diurnally and over an annual cycle, it is limited in its scope to cover spatial variation, which for CO_2 can be large depending on hydrological and climatic conditions (Wright *et al.*, 2013, Armstrong *et al.*, 2015, Buczko *et al.*, 2015). Ideally, at least one more tower would be used on each site in order to better quantify spatial variations and instrumental uncertainty, allowing for better uncertainty estimates overall.

7.6 Conclusions

Little or no empirical data exists on the annual exchange of CO_2 from Northern peatland ecosystems undergoing restoration, particularly on sites restored from plantation forestry. Additionally, few peatland restoration sites have an areal extent large enough for the use of eddy covariance methods, meaning most studies examining NEE from restored peatlands are based upon chamber fluxes. Typically, these chamber measurements are undertaken in the growing season and thus do not capture the full annual NEE. This chapter represents the first annual measurements of NEE using eddy covariance on peatlands restored from plantation forestry. Overall, NEE increased (i.e. a greater sink) with time since restoration, with Talaheel a net sink of -71 g C m^{-2} yr^{-1}, whilst Lonielist was a source of 80 g C m^{-2} yr^{-1}. Both sites were lower than the 6-year mean NEE value from Cross Lochs of -114 g C m^{-2} yr^{-1} (Levy and Gray, 2015).

Differences in NEE from the two restored sites were largely controlled by significant differences in R_{eco} losses, thought to be due to the presence of microtopography and the significant quantities of woody debris still present at the younger restoration site (Lonielist; restored in 2003/04).

When compared to other Northern peatlands, the annual NEE flux from the older restoration site (Talaheel; restored 1997/98) was comparable to peatlands at similar latitudes (Figure 7.6). NEE from Lonielist was higher than values detailed in the literature from other Northern peatlands including those in the arctic. A distinct near-linear relationship was observed between GPP, R_{eco} and latitude (Figure 7.6), with higher values observed at lower latitudes and lower values at higher latitudes. However, this relationship was not observed in NEE values, highlighting the difficulties in modelling NEE due to the complex interactions of different ecosystem components and drivers, many of which are not yet fully understood.

~ Chapter 8 ~

Conclusions and Future Work

8.1 Conclusions

This chapter will summarise the key findings from the research into the effect of forest-to-bog restoration on net ecosystem exchange (NEE) of carbon dioxide (CO_2) from Flow Country peatlands and will begin by answering the questions set out in Chapter 1. Ideas for future research necessary to improve our understanding of C dynamics in peatlands restored from forestry will be discussed alongside recommendations of further restoration. Finally, this will be put into the context of the Scottish government's National Peatland Plan, which outlines the vision for peatlands to help Scotland meet its GHG emission targets and deliver improved biodiversity.

1. How do fluxes of R_{eco} and GPP change with time since restoration and what are the key environmental drivers?

1.1 R_{eco}

Significantly higher R_{eco} (Chapter 4) was observed at the younger restoration site (Lonielist; restored in 2003/04) compared to the older restoration site (Talaheel; restored 1997/98) at monthly, seasonal and annual timescales. Median seasonal R_{eco} fluxes were on average 23.4 % higher from Lonielist than Talaheel. The biggest difference was observed in winter where daily median R_{eco} fluxes were 42.0% higher at Lonielist (1.07 ± 0.43 µmol m^{-2} s^{-1}) than Talaheel (0.62 ± 0.24 µmol m^{-2} s^{-}). Seasonal R_{eco} fluxes from Lonielist were significantly higher than those observed at Talaheel and Cross Lochs (undrained), except in summer where no significant differences (Wilcoxon rank sum, P = 0.2474) were observed and there was a less than 1% difference in fluxes between the three sites (Lonielist - 2.19 µmol m^{-2} s^{-1}, Talaheel - 2.17 µmol m^{-2} s^{-1}, and Cross Lochs - 2.16 µmol m^{-2} s^{-1}). Additionally, Talaheel R_{eco} fluxes were significantly higher than Cross Lochs during winter (Wilcoxon rank sum, P = 0.0245). Annual R_{eco} fluxes were 21 % higher at Lonielist (581 g C m^{-2} yr^{-1}) than Talaheel (480 g C m^{-2} yr^{-1}) and 26 % higher than the 6-year mean of 461 g C m^{-2} yr^{-1} from Cross Lochs (Levy and Gray, 2015). Annual R_{eco} fluxes were only 4.1 % higher at Talaheel than Cross Lochs.

R_{eco} fluxes were primarily driven by temperature and soil moisture changes. The highest fluxes were observed during warm, dry periods, such as summer. The Q10 temperature co-efficient decreased with increasing time since restoration, suggesting that with a 10°C increase in temperature there was a smaller increase in R_{eco}. The R_{eco} flux was inversely related to soil moisture content at both Lonielist and Talaheel. Interactions between soil moisture and temperature were found to have the greatest influence on R_{eco} at both Lonielist and Talaheel.

1.2 GPP

Over annual timescales, no significant differences were observed in GPP between the youngest (Lonielist; restored in 2003/04) and oldest sites (Talaheel; restored in 1997/98). However, compared to the 6-year annual mean GPP flux from the undrained bog (Cross Lochs) (Levy and Gray, 2015), annual fluxes at Talaheel were 4.4% lower, whilst Lonielist fluxes were 14.8% lower, although these were not significantly different (Kruskal-Wallis, $P = 0.2103$). Seasonally, large differences were observed in summer between the different restored sites, for example mean daily productivity at Talaheel (3.34 ± 0.76 µmol CO_2 m^{-2} s^{-1}) was 23.7% higher than Lonielist (2.60 ± 0.84 µmol CO_2 m^{-2} s^{-1}).

Photosynthetic photon flux density (PPFD) was observed as the key driving environmental variable for GPP. However, limitations in GPP were observed at Lonielist under high solar angles, likely due to shading by woody debris and the aspect of the microtopography. Furthermore, interactions between soil moisture content and vapour pressure deficit (VPD) were observed to limit GPP. During periods of low soil moisture content (<0.5 m^3 m^{-3}), high VPD (>1 kPa), and high PPFD (>1000 µmol m^{-2} s^{-1}), GPP became limited as plants closed stomata to reduce water losses, resulting in a reduction in CO_2 uptake from the atmosphere. This effect was most clearly observed at Lonielist, although it was also observed at Talaheel; because soil moisture content was more stable at Talaheel, the magnitude of this effect was reduced. Unfortunately, due to a broken sensor at Cross Lochs it was not possible to assess the VPD-soil moisture effect in the undrained site to understand whether this was an effect of restoration or whether it is also seen in undrained sites.

2. What effect do microtopographic features created by the ploughing of the peat for plantation forestry have on NEE and what are the key environmental drivers?

Microtopography played a greater role in influencing R_{eco} than GPP, with significant differences observed between different microforms. R_{eco} from the ridges was significantly higher than that observed from the furrows. At the older site, Talaheel (T16 - restored in 1997/98), no significant difference was observed between the original surface and ridges, but furrow fluxes were significantly lower. These differences were attributed to differences in soil moisture content and soil temperature, with the ridges being drier and warmer than the furrows due to the thermal capacity of peat decreasing with soil moisture resulting in a greater temperature variation.

No significant differences were observed in GPP fluxes between microforms, although GPP fluxes were higher on the original surface due to greater coverage of grasses such as *Carex panicea* and *Molinia caerulea*. GPP was primarily controlled by PPFD; however similar to R_{eco}, soil moisture and temperature also influenced GPP fluxes across all microforms.

3. What impact does the restoration of blanket bogs from plantation forestry have on the Net ecosystem exchange of CO_2?

Restoration reduced losses of CO_2 with increasing time since the start of restoration, with restored systems shifting from a C source to a sink over multi-decadal timescales. However when compared to undrained blanket bogs, the sink strength at Talaheel (restored in 1997/98) was modest, and does not yet indicate a full recovery. Significant differences (Kruskal-Wallis, $P < 0.0001$) in seasonal NEE fluxes were observed between Lonielist and Talaheel; both sites were net C sinks during the summer, however daily NEE fluxes were 82% higher at Talaheel than Lonielist. In spring, both Lonielist and Talaheel were observed to be near neutral on a daily basis. During all other seasons, Lonielist and Talaheel were observed to be net sources with varying magnitudes of C emission. Over annual timescales, Lonielist was observed to be a source of CO_2 to the atmosphere (80 g C m^{-2} yr^{-1}), whilst Talaheel was a sink for CO_2 (-71 g C m^{-2} yr^{-1}). Analysis of other Northern peatlands indicated that the magnitude of the Talaheel C sink was similar to that of undrained "natural" peatlands in the Northern Hemisphere (-40 to -200 g C m^{-2} yr^{-1}), although lower than that of the 6-year mean NEE value from the nearest undrained bog at Cross Lochs (-114 g C m^{-2} yr^{-1}).

8.2 Limitations and Future Work

While this research has presented the first annual eddy covariance measurements from a peatland undergoing restoration from forestry to bog, further research is required to improve our knowledge of the C dynamics of these systems before, during and after restoration.

8.2.1 Replication

One of the weakest parts of the eddy covariance technique is the lack of replication, primarily due to the large cost associated with each tower. However, further research should be undertaken to replicate these results with a second tower on each site. Alternatively, as Forsinard Flows has many large areas of similar chronosequence age, replication could be undertaken on other sites of the same age. More sites would help to improve our knowledge of the uncertainties associated with the data by taking into account the spatial variation in CO_2 fluxes.

8.2.2 Inter-Annual Variability

To improve our knowledge of C dynamics in peatlands undergoing restoration and how these sites might be influenced by climatic change, further research is required to understand the drivers of inter-annual variability. Moreover, hydrological and vegetation changes can occur for many decades after the onset of restoration. It is therefore important that long-term measurements are undertaken to understand how changes in hydrology and vegetation composition affect C dynamics. Longer term monitoring will also allow uncertainties in annual budgets to be constrained and provide a better indication as to the source/sink status of these restored peatlands.

8.2.3 The Starting Point

In order to improve our knowledge of restoration, it is essential that the C dynamics of forested peatlands in the Flow Country be understood. It remains unclear as to whether forested peatlands actively accumulate C through productivity of the trees outweighing peat oxidation losses. Whilst previous research has taken place on forested peatlands in the UK (Hargreaves et al., 2003), this was based upon a few extrapolated seasonal measurements but did not take the poor growth and likely poor productivity of the trees in the Flow Country into account. Eddy covariance measurements of CO_2 above the forest canopy combined with chamber measurements on the forest floor should provide key information as to the C sink/source status of these systems and provide a missing piece of the Flow Country C budget. The C stock of the forests could also be assessed using allometric methods. Although this would be suitable to understand the amount C stored in the tree biomass, it would be very labour intensive and would not take the C flux from the trees or soil respiration into account.

8.2.4 Other GHG measurements

In an unmanaged state, peatlands are known to be sinks for CO_2 and sources of methane (CH_4). Methane is estimated to have a global warming potential around 25 times greater than that of CO_2 but a shorter residence time (Solomon *et al.*, 2007, Boucher *et al.*, 2009). However, this research has so far only considered net CO_2 exchange and therefore research is required to understand how increasing time since the start of restoration influences CH_4 fluxes. Changes in CH_4 fluxes over the course of the restoration/ecosystem recovery may affect the GHG balance and global warming potential of different-aged restoration sites. It is hypothesised that as CH_4 is produced under anaerobic conditions, fluxes are likely to become significant as the water table rises and stabilises nearer the peat surface, increasing the volume of peat under anaerobic conditions. Wetter conditions, combined with increased regional warming as a result of climate

change, could potentially have a positive feedback on the production of CH_4, further accelerating regional warming and altering C budgets for these sites.

N_2O has a global warming potential around 298 times that of CO_2 (Solomon *et al.*, 2007), however few studies consider N_2O dynamics in restored ecosystems. Human-affected peatlands have been found to be potential sources of N_2O due to human disturbance of the natural nitrogen (N) cycle (Teh *et al.*, 2011). N_2O production can be stimulated by increasing water content and the availability of substrates for denitrification. This could be significant, particularly in the first few years after deforestation on these sites, as the soil moisture content increases and there is a ready supply of substrate through decomposing tree material and new vegetation growth. Monitoring of felled sites in the future should include measurements of N_2O to improve our knowledge of N dynamics in these ecosystems.

8.2.5 Broader Analytical Basis

To better understand respiration dynamics it is important to improve our knowledge of the heterotrophic (Rh) and autotrophic (Ra) components of respiration at different restoration sites. Partitioning of respiration can be done either by the manual exclusion of roots from an area; so only heterotrophic respiration is measured or it can be measured using isotopic methods. The root exclusion method is very destructive, and it is difficult to completely remove all roots from one area. Additionally, the removal of roots alters the substrate supply to microbes by decreasing labile root inputs reducing respiration (Hopkins *et al.*, 2013). Colleagues at the University of Stirling using this method are currently undertaking work in the Flow Country, however, this work is centred on forested peatlands and does not take potential restoration effects on Rh and Ra into account.

Isotopic methods require the use of natural C tracers such as isotopically altered CO_2 to separate root respiration from microbial respiration (Hopkins *et al.*, 2013). Isotopic labelling experiments could be used such as pulse-chase experiments where a supply of isotopically altered CO_2 is traced to belowground tissues and the soil efflux (Brüggemann *et al.*, 2011). This method has the benefit of being less destructive, but can be costly.

The results obtained from vegetation surveys suggest similar types of vegetation are present in both Lonielist and Talaheel, but in different quantities. Changes to plant communities can change the proportion of recalcitrant and labile C through changes in litter quality and quantity. This can influence microbial decomposition of soil organic matter (SOM) as different microbial communities have differing abilities to breakdown plant derived C. Therefore, to better understand why changes in R_{eco} are occurring between sites and the main driving variables, it is

important to understand the microbial communities and any changes in these as restoration progresses. Furthermore, vegetation specific GPP could be measured using leaf cuvettes to better understand GPP from different vegetation types. These types of measurements can be achieved very quickly over a large area and repeated several times during the course of a day. The specific leaves used can also be later collected for measurements of leaf area, which can then be used to upscale to the plant level and ecosystem level if extensive vegetation surveys exist for the ecosystem.

Decomposition of woody debris is likely to have an impact upon $R_{eco,}$ with CO_2 produced during the decomposition process. Monitoring of CO_2 production directly from woody debris would provide vital information as to the influence of the woody debris on R_{eco}. This information, combined with tree volume and tree density data, should provide an indication as to the loss of C from the ecosystem as a direct result of tree felling, which can be used to better inform C budgets and the length of time required for C loss to be compensated for.

8.2.6 Different Restoration techniques

In the Flow Country, restoration had largely been centred on trees being felled and left to decompose on site as it was not economically viable to remove the trees due to their poor growth. However in the latest round of restoration, trials are being undertaken to clear fell sites, with the wood being sold for timber or biomass. Restoration enhancement trials are also being undertaken on older restoration sites across the Forsinard Flows Nature Reserve to crush remaining woody material into furrows, blocking the furrows using peat dams and removing the ridge microform, to leave the sites flatter and help to raise the water table. However, on these sites, whilst vegetation and hydrological monitoring are taking place, there are no plans for monitoring of C dynamics. Further research is needed to ascertain whether net ecosystem C functioning returns to these sites quicker with the enhanced restoration techniques. The monitoring could take the form of a chamber-based study to compare C dynamics between these sites, however this is unlikely to yield the long-term dataset required to fully understand changing C dynamics. Although not possible on all sites, many of the sites are large and flat enough for the implementation of multiple eddy covariance flux towers providing long-term, replicated, measurement of C dynamics.

Further research is currently on going in the Flow Country to assess the impact of restoration on the aqueous and gaseous evasion of C. Colleagues at the University of Stirling are measuring the gaseous emission of C using dynamic flux chambers at forested and restored sites, with a particular focus on new restoration techniques such as whole tree harvesting and mulching.

Fellow researchers at the University of Highlands and Islands are looking at the impacts of restoration on DOC concentrations in rivers and pore water.

8.3 Implication for Scottish Government Policy

A growing awareness of the global C cycle and the potential for ecosystems to sequester C from the atmosphere has put peatlands and peatland restoration in the research and policy limelight (Parry *et al.*, 2014, SNH, 2015). Whilst large scale planting and peat cutting has ended in Scotland, the decline of damaged peatlands continues due to peat oxidation, resulting in a net loss of C to the atmosphere. There is estimated to be approximately 600,000 ha of restorable peatland in Scotland, but so far only around 5,500 ha of this has undergone restoration (SNH, 2015). Publication of the National Peatland Plan by Scottish Natural Heritage (SNH) in August 2015 (SNH, 2015) set out the Scottish government's vision for peatlands to help Scotland meet its GHG emission targets and deliver improved biodiversity. The principle aim of the National Peatland Plan is to:

"Protect, manage and restore peatlands to maintain their natural functions, biodiversity and benefits."

A number of targets were set to achieve this aim; one of these is that by 2020 there is to be an improvement in the condition and protection of peatlands in Scotland and secondly by 2030 all Scottish peatlands will be in a healthy, resilient state. In terms of C functioning, this research has shown that sites restored 12 – 13 years ago are still large sources of C to the atmosphere of 80 g C m^{-2} yr^{-1}, while those restored 16 – 17 years previously, are modest sinks of -71 g C m^{-2} yr^{-1}. As approximately only 1% of the restorable peatlands in Scotland have so far undergone restoration (SNH, 2015), it is unlikely, given restoration timescales observed in this research, that all peatlands would be in a healthy, resilient state in terms of their C sequestration functioning by 2030. The restoration timescales seen in my research suggest that sites undergoing forest-to-bog restoration post 2016 are unlikely to meet the 2030 healthy and resilient target in terms of the C status. However, this research and research in other Northern peatlands (Waddington *et al.*, 2010, Strack and Zuback, 2013), has shown that restoration from forestry and other land uses is effective at reducing C losses to the atmosphere over multi-decadal timescales.

It is possible that new restoration techniques could accelerate the restoration of the C sink in these ecosystems. This research has shown that R_{eco} has the greatest influence on NEE in restored blanket bogs whilst microtopography was observed to have an influence on R_{eco} emissions, with drier microforms (ridges) associated with higher R_{eco}, whilst significantly lower

R_{eco} was observed in the wetter furrow microforms. Flattening of these microforms could result in a further raising and stabilisation of the water table, which this research suggests would reduce R_{eco}, and over timescales of a few years should encourage the re-colonisation of peat forming vegetation such as *Sphagnum*, which should increase GPP and net C uptake. Furthermore, improvements in technology have resulted in new restoration techniques such as whole tree harvesting or mulching. These techniques could also help to accelerate restoration by reducing the persistent loss of C to the atmosphere associated with biomass decomposition. This research also suggested there is potential for a reduction in GPP due to shading of vegetation by woody debris, therefore removing this could increase C uptake.

The National Peatland Plan is a movement in the right direction for the protection of peatland ecosystems. The inclusion of peatland emissions/sequestration in national C accounting highlights the benefits of peatlands for C sequestration and how restoration can help Scotland to continue to meet its climate change targets. However for this to be useful, robust C monitoring of peatland restoration projects is required to reduce uncertainties and limitations (Section 8.2) in the currently available data.

8.4 Recommendations

So far restoration of these sites has focussed on maximising GPP and has largely ignored R_{eco}. However, this research has shown that Reco primarily drives the net ecosystem exchange of restored peatland sites. Further restoration, as recommended below, should strike a balance between reducing R_{eco} and maximising GPP.

- Removal of microtopography from restored sites to flatten the sites. This will reduce R_{eco} and increase GPP resulting in greater uptake.

- Water table stabilisation. Flattening of sites should help to further raise and stabilise water tables, which will help to reduce R_{eco} and provide more ideal conditions for the colonisation of the ecosystem by *Sphagnum* spp.

- Removal of woody debris from sites. This will reduce the persistent high R_{eco} by reducing the labile C pool at restored sites.

- Current Scottish government policy requires all peatlands to be in a healthy state by 2030 – given restoration timescales observed in this research it is unlikely that peatlands, which are yet to undergo restoration, will meet this target.

- New restoration methods, such as mulching or harvesting with stump flipping combined with microtopography removal could help to reduce restoration times and improve the sink strength of the ecosystems.

- If, new restoration methods are implemented further research and monitoring of these sites will be required to understand the impact this will have upon restoration times and Scottish government policy.

8.4 Summary

Lonielist was observed to be a source of C to the atmosphere, whilst Talaheel was a C sink of similar magnitude to other undrained "natural" peatlands in the Northern Hemisphere. Differences in R_{eco} were observed to be the mechanism driving changes in NEE between the two restored sites during these respective stages of ecosystem recovery. At both Lonielist and Talaheel, soil moisture and temperature were observed to be key environmental variables for R_{eco}, whilst variables such as VPD, soil moisture and PPFD were observed to have an influence on GPP. This resulted in limitations in CO_2 uptake during periods of high VPD (>1 kPa), low soil moisture (<0.5 m^3m^{-3}) and high PPFD (>1000 µmol m^{-2} s^{-1}).

Over multi-decadal timescales, afforested peatland restoration is successful at reducing C losses and restoring the net C sink of the ecosystem. However, further restoration is required to raise and stabilise the water table, which should reduce R_{eco} losses and enhance the net C sink.

This thesis has broadened our understanding of peatland restoration in the Northern Hemisphere, especially in terms of the timescales required to return these sites to net C sinks. However, there remains an exciting body of research to improve our understanding and reduce uncertainties and limitations of C dynamics from forest-to-bog restoration.

References

2012. R. R Core Team.

AERTS, R. & CHAPIN, F. S. 2000. The mineral nutrition of wild plants revisited: A re-evaluation of processes and patterns. *Advances in Ecological Research, Vol 30,* 30**,** 1-67.

AINSWORTH, E. A. & LONG, S. P. 2005. What have we learned from 15 years of free-air CO2 enrichment (FACE)? A meta-analytic review of the responses of photosynthesis, canopy. *New Phytologist,* 165**,** 351-371.

ALM, J. S., L.; WALDEN, J.; NYKANEN, H.; MARTIKAINEN, P.J.; SILVOLA, J 1999. Carbon balance of boreal bog during a year with an exceptionally dry summer. *Ecology,* 80**,** 161 - 174.

ANDERSON, A. R., DAY, R. & PYATT, D. G. 2000. Physical and hydrological impacts of blanket bog afforestation at Bad a' Cheo, Caithness: the first 5 years. *Forestry,* 73**,** 467-478.

ANDERSON, D. E., VERMA, S. B., CLEMENT, R. J., BALDOCCHI, D. D. & MATT, D. R. 1986. Turbulence Spectra of Co2, Water-Vapor, Temperature and Velocity over a Deciduous Forest. *Agricultural and Forest Meteorology,* 38**,** 81-99.

ANDREWS, A. E., KOFLER, J. D., TRUDEAU, M. E., WILLIAMS, J. C., NEFF, D. H., MASARIE, K. A., CHAO, D. Y., KITZIS, D. R., NOVELLI, P. C., ZHAO, C. L., DLUGOKENCKY, E. J., LANG, P. M., CROTWELL, M. J., FISCHER, M. L., PARKER, M. J., LEE, J. T., BAUMANN, D. D., DESAI, A. R., STANIER, C. O., DE WEKKER, S. F. J., WOLFE, D. E., MUNGER, J. W. & TANS, P. P. 2014. CO2, CO, and CH4 measurements from tall towers in the NOAA Earth System Research Laboratory's Global Greenhouse Gas Reference Network: instrumentation, uncertainty analysis, and recommendations for future high-accuracy greenhouse gas monitoring efforts. *Atmospheric Measurement Techniques,* 7**,** 647-687.

ARMENTANO, T. V. & MENGES, E. S. 1986. Patterns of Change in the Carbon Balance of Organic Soil-Wetlands of the Temperate Zone. *Journal of Ecology,* 74**,** 755-774.

ARMSTRONG, A., HOLDEN, J., KAY, P., FOULGER, M., GLEDHILL, S., MCDONALD, A. T. & WALKER, A. 2009. Drain-blocking techniques on blanket peat: A framework for best practice. *J Environ Manage,* 90**,** 3512-9.

ARMSTRONG, A., WALDRON, S., OSTLE, N. J., RICHARDSON, H. & WHITAKER, J. 2015. Biotic and Abiotic Factors Interact to Regulate Northern Peatland Carbon Cycling. *Ecosystems,* 18**,** 1395-1409.

ARTZ, R. E. E., DONNELLY, D., ANDERSEN, R., MITCHELL, R., CHAPMAN, S. J., SMITH, J., SMITH, P., CUMMINS, R., BALANA, B. & CUTHBERT, A. 2014. Managing and restoring blanket bog to benefit biodiversity and carbon balance - a scoping study. *In:* HERITAGE, S. N. (ed.).

AUBINET, M., GRELLE, A., IBROM, A., RANNIK, U., MONCRIEFF, J., FOKEN, T., KOWALSKI, A. S., MARTIN, P. H., BERBIGIER, P., BERNHOFER, C., CLEMENT, R., ELBERS, J., GRANIER, A., GRUNWALD, T., MORGENSTERN, K., PILEGAARD, K., REBMANN, C., SNIJDERS, W., VALENTINI, R. & VESALA, T. 2000. Estimates of the annual net carbon and water exchange of forests: The EUROFLUX methodology. *Advances in Ecological Research, Vol 30,* 30**,** 113-175.

AUBINET, M., VESALA, T. & PAPALE, D. 2012. *Eddy Covariance: A practical Guide to Measurement and Data Analysis*, Springer Atmospheric Sciences.

AUBLE, D. L. & MEYERS, T. P. 1992. An Open Path, Fast Response Infrared-Absorption Gas Analyzer for H2o and Co2. *Boundary-Layer Meteorology,* 59**,** 243-256.

AURELA, M., LAURILA, T. & TUOVINEN, J. P. 2002. Annual CO2 balance of a subarctic fen in northern Europe: Importance of the wintertime efflux. *Journal of Geophysical Research-Atmospheres,* 107.

AURELA, M., LOHILA, A., TUOVINEN, J. P., HATAKKA, J., RIUTTA, T. & LAURILA, T. 2009. Carbon dioxide exchange on a northern boreal fen. *Boreal Environment Research,* 14**,** 699-710.

AUTON, C., MERRITT, J. & GOODENOUGH, K. 2011. *Moray and Caithness: A landscape Fashioned by Geology*, SNH Publishing.

AVERY, M. & LESLIE, R. 1990. *Birds and Forestry,* Poyser.

BADOREK, T., TUITTILA, E. S., OJANEN, P. & MINKKINEN, K. 2011. Forest floor photosynthesis and respiration in a drained peatland forest in southern Finland. *Plant Ecology & Diversity,* 4**,** 227-241.

BAIN, C. G., BONN, A., STONEMAN, R., CHAPMAN, S., COUPAR, A., EVANS, M. G., GEAREY, B., HOWAT, M., JOOSTEN, H., KEENLEYSIDE, C., LABADZ, J., LINDSAY, R., LITTLEWOOD, N., LUNT, P., C.J., M., MOXEY, A., ORR, H., REED, M., SMITH, P., SWALES, V., THOMPSON, D. B. A., THOMPSON, P. S., VAN DE NOORT, R., WILSON, J. D. & WORRALL, F. 2011. IUCN UK Commission of Inquiry on Peatlands. *In:* C.G., B. (ed.). Edinburgh: IUCN UK Peatland Programme.

BAINBRIDGE, I. P., MINNS, D. W., HOUSDEN, S. D. & LANCE, A. N. 1987. Forestry in the Flows of Caithness and Sutherland. Edinburgh.

BALDOCCHI, D., FALGE, E., GU, L. H., OLSON, R., HOLLINGER, D., RUNNING, S., ANTHONI, P., BERNHOFER, C., DAVIS, K., EVANS, R., FUENTES, J., GOLDSTEIN, A., KATUL, G., LAW, B., LEE, X. H., MALHI, Y., MEYERS, T., MUNGER, W., OECHEL, W., U, K. T. P., PILEGAARD, K., SCHMID, H. P., VALENTINI, R., VERMA, S., VESALA, T., WILSON, K. & WOFSY, S. 2001. FLUXNET: A new tool to study the temporal and spatial variability of ecosystem-scale carbon dioxide, water vapor, and energy flux densities. *Bulletin of the American Meteorological Society,* 82**,** 2415-2434.

BALDOCCHI, D. D. 2003. Assessing the eddy covariance technique for evaluating carbon dioxide exchange rates of ecosystems: past, present and future. *Global Change Biology,* 9**,** 1 - 14.

BALDOCCHI, D. D. H., B.B.; MEYERS, T.P. 1988. Measuring Biosphere-Atmosphere Exchanges of Biologically Related Gases with Micrometeorological Methods. *Ecology,* 69**,** 1331 - 1340.

BALDOCCHI, D. D. V. C. A. 1996. Energy and CO2 flux densities above and below a temperate broad-leaved forest and a boreal pine forest. *Tree Physiology,* 16**,** 5-16.

BALDOCK, D. 1984. *Wetland Drainage in Europe: The effects of Agricultural policy in Four EEC Countries*, International Institute for Environment and Development and the Institute for European Environmental Policy.

BALL, B. C., SCOTT, A. & PARKER, J. P. 1999. Field N(2)O, CO(2) and CH(4) fluxes in relation to tillage, compaction and soil quality in Scotland. *Soil & Tillage Research,* 53**,** 29-39.

BALLANTYNE, D. M., HRIBLJAN, J. A., PYPKER, T. G. & CHIMNER, R. A. 2014. Long-term water table manipulations alter peatland gaseous carbon fluxes in Northern Michigan. *Wetlands Ecology and Management,* 22**,** 35-47.

BARNETT, C., HOSSELL, J., PERRY, M. & PROCTER, C. 2006. A handbook of climate trends across Scotland. *SNIFFER project CC03, Scotland and Northern Ireland Forum for Environmental Research.*

BELLISARIO, L. M., MOORE, T. R. & BUBIER, J. L. 1998. Net ecosystem CO2 exchange in a boreal peatland, northern Manitoba. *Ecoscience,* 5**,** 534-541.

BELYEA, L. R. & BAIRD, A. J. 2006. Beyond "The limits to peat bog growth": Cross-scale feedback in peatland development. *Ecological Monographs,* 76**,** 299-322.

BELYEA, L. R. & CLYMO, R. S. 2001. Feedback control of the rate of peat formation. *Proceedings of the Royal Society B-Biological Sciences,* 268**,** 1315-1321.

BENASHER, J., CARDON, G. E., PETERS, D., ROLSTON, D. E., BIGGAR, J. W., PHENE, C. J. & EPHRATH, J. E. 1994. Determining Root Activity Distribution by Measuring Surface Carbon-Dioxide Fluxes. *Soil Science Society of America Journal,* 58**,** 926-930.

BILLETT, M. F., CHARMAN, D. J., CLARK, J. M., EVANS, C. D., EVANS, M. G., OSTLE, N. J., WORRALL, F., BURDEN, A., DINSMORE, K. J., JONES, T., MCNAMARA, N. P., PARRY, L., ROWSON, J. G. & ROSE, R. 2010. Carbon balance of UK peatlands: current state of knowledge and future research challenges. *Climate Research,* 45**,** 13-29.

BINGHAM, G. E., GILLESPIE, C. H. & MCQUAID, J. H. 1978. Development of a miniature, rapid response CO2 sensor. Lawrence Livermore National Laboratory Report UCRL-52440.

BIRKIN, L. J., BAILEY, S., BREWIS, F. E., BRUNEAU, P., CROSHER, I., DOBBIE, K., HILL, C., JOHNSON, S., SHEPERD, M. J. & SKATE, J. 2011. The requirements for improving greenhouse gases flux estimates for peatlands in the UK. *JNCC Report.*

BOND-LAMBERTY, B. & THOMSON, A. 2010. Temperature-associated increases in the global soil respiration record. *Nature,* 464**,** 579-U132.

BONGI, G. 1990. A Gas-Exchange Procedure to Evaluate Nonuniform Stomatal Closure Effects in Single Mesophyte Evergreen Leaves under High Vpd. *Current Research in Photosynthesis, Vols 1-4***,** D717-D720.

BORCHARD, N., SCHIRRMANN, M., VON HEBEL, C., SCHMIDT, M., BAATZ, R., FIRBANK, L., VEREECKEN, H. & HERBST, M. 2015. Spatio-temporal drivers of soil and ecosystem carbon fluxes at field scale in an upland grassland in Germany. *Agriculture Ecosystems & Environment,* 211**,** 84-93.

BOSIO, J., STIEGLER, C., JOHANSSON, M., MBUFONG, H. N. & CHRISTENSEN, T. R. 2014. Increased photosynthesis compensates for shorter growing season in subarctic tundra-8 years of snow accumulation manipulations. *Climatic Change,* 127**,** 321-334.

BOTCH, M. S., KOBAK, K. I., VINSON, T. S. & KOLCHUGINA, T. P. 1995. Carbon Pools and Accumulation in Peatlands of the Former Soviet-Union. *Global Biogeochemical Cycles,* 9**,** 37-46.

BOUCHER, O., FRIEDLINGSTEIN, P., COLLINS, B. & SHINE, K. P. 2009. The indirect global warming potential and global temperature change potential due to methane oxidation. *Environmental Research Letters,* 4**,** 1-5.

BRAGAZZA, L., BUTTLER, A., HABERMACHER, J., BRANCALEONI, L., GERDOL, R., FRITZE, H., HANAJIK, P., LAIHO, R. & JOHNSON, D. 2012. High nitrogen deposition alters the decomposition of bog plant litter and reduces carbon accumulation. *Global Change Biology,* 18**,** 1163-1172.

BREMER, D. J., HAM, J. M., OWENSBY, C. E. & KNAPP, A. K. 1998. Responses of soil respiration to clipping and grazing in a tallgrass prairie. *Journal of Environmental Quality,* 27**,** 1539-1548.

BREUER, L., PAPEN, H. & BUTTERBACH-BAHL, K. 2000. N2O emission from tropical forest soils of Australia. *Journal of Geophysical Research-Atmospheres,* 105**,** 26353-26367.

BRÜGGEMANN, N., GESSLER, A., KAYLER, Z., KEEL, S. G., BADECK, F., BARTHEL, M., BOECKX, P., BUCHMANN, N., BRUGNOLI, E., ESPERSCHÜTZ, J., GAVRICHKOVA, O., GHASHGHAIE, J., GOMEZ-CASANOVAS, N., KEITEL, C., KNOHL, A., KUPTZ, D., PALACIO, S., SALMON, Y., UCHIDA, Y. & BAHN, M. 2011. Carbon allocation and carbon isotope fluxes in the plant-soil-atmosphere continuum: a review. *Biogeosciences,* 8**,** 3457 - 3489.

BRUNEAU, P. M. C. & JOHNSON, S. M. 2014. Scotland's peatland - definitions & information resources.

BRUTSAERT, W. 1999. Aspects of bulk atmospheric boundary layer similarity under free-convective conditions. *Reviews of Geophysics,* 37**,** 439-451.

BUBIER, J., CRILL, P., MOSEDALE, A., FROLKING, S. & LINDER, E. 2003a. Peatland responses to varying interannual moisture conditions as measured by automatic CO2 chambers. *Global Biogeochemical Cycles,* 17.

BUBIER, J. L., BHATIA, G., MOORE, T. R., ROULET, N. T. & LAFLEUR, P. M. 2003b. Spatial and temporal variability in growing-season net ecosystem carbon dioxide exchange at a large peatland in Ontario, Canada. *Ecosystems,* 6**,** 353-367.

BUBIER, J. L., CRILL, P. M., MOORE, T. R., SAVAGE, K. & VARNER, R. K. 1998. Seasonal patterns and controls on net ecosystem CO2 exchange in a boreal peatland complex. *Global Biogeochemical Cycles,* 12**,** 703-714.

BUBIER, J. L., MOORE, T. R. & BLEDZKI, L. A. 2007. Effects of nutrient addition on vegetation and carbon cycling in an ombrotrophic bog. *Global Change Biology,* 13**,** 1168-1186.

BUCZKO, U., BACHMANN, S., GROPP, M., JURASINSKI, G. & GLATZEL, S. 2015. Spatial variability at different scales and sampling requirements for in situ soil CO2 efflux measurements on an arable soil. *Catena,* 131**,** 46-55.

BURBA, G. & ANDERSON, D. 2005. *Introduction to the Eddy Covariance method: general guidelines and conventional workflow,* Lincoln, Nebraska, USA, LI-COR inc.

BURBA, G. G., MCDERMITT, D. K., ANDERSON, D. J., FURTAW, M. D. & ECKLES, R. D. 2010. Novel design of an enclosed CO2/H2O gas analyser for eddy covariance flux measurements. *Tellus Series B-Chemical and Physical Meteorology,* 62**,** 743-748.

BURBA, G. G., MCDERMITT, D. K., GRELLE, A., ANDERSON, D. J. & XU, L. K. 2008. Addressing the influence of instrument surface heat exchange on the measurements of CO(2) flux from open-path gas analyzers. *Global Change Biology,* 14**,** 1854-1876.

BUSINGER, J. A. & ONCLEY, S. P. 1990. Flux Measurement with Conditional Sampling. *Journal of Atmospheric and Oceanic Technology,* 7**,** 349-352.

CAI, T. E. B., FLANAGAN, L. B. & SYED, K. H. 2010. Warmer and drier conditions stimulate respiration more than photosynthesis in a boreal peatland ecosystem: Analysis of automatic chambers and eddy covariance measurements. *Plant Cell and Environment,* 33**,** 394-407.

CANADELL, J. G., CIAIS, P., DHAKAL, S., DOLMAN, H., FRIEDLINGSTEIN, P., GURNEY, K. R., HELD, A., JACKSON, R. B., LE QUERE, C., MALONE, E. L., OJIMA, D. S., PATWARDHAN, A., PETERS, G. P. & RAUPACH, M. R. 2010. Interactions of the carbon cycle, human activity, and the climate system: a research portfolio. *Current Opinion in Environmental Sustainability,* 2**,** 301-311.

CANADELL, J. G., LE QUERE, C., RAUPACH, M. R., FIELD, C. B., BUITENHUIS, E. T., CIAIS, P., CONWAY, T. J., GILLETT, N. P., HOUGHTON, R. A. & MARLAND, G. 2007. Contributions to accelerating atmospheric CO2 growth from economic activity, carbon intensity, and efficiency of natural sinks. *Proc Natl Acad Sci U S A,* 104**,** 18866-70.

CANNELL, M. G. R. D., R.C.; PYATT D.G. 1993. Conifer plantations on drained peatlands in Britain: A net gain or loss of Carbon? *Forestry,* 66**,** 353 - 369.

CAO, L. & CALDEIRA, K. 2008. Atmospheric CO2 stabilization and ocean acidification. *Geophysical Research Letters,* 35.

CAO, M. K. & WOODWARD, F. I. 1998. Dynamic responses of terrestrial ecosystem carbon cycling to global climate change. *Nature,* 393**,** 249-252.

CHAPMAN, S. J., BELL, J., DONNELLY, D. & LILLY, A. 2009. Carbon stocks in Scottish peatlands. *Soil Use and Management,* 25**,** 105-112.

CHAPMAN, S. J. & THURLOW, M. 1998. Peat respiration at low temperatures. *Soil Biology & Biochemistry,* 30**,** 1013-1021.

CHARMAN, D. J. 1995. Patterned fen development in northern Scotland: Hypothesis testing and comparison with ombrotrophic blanket peats. *Journal of Quaternary Science,* 10**,** 327-342.

CHARMAN, D. J., BEILMAN, D. W., BLAAUW, M., BOOTH, R. K., BREWER, S., CHAMBERS, F. M., CHRISTEN, J. A., GALLEGO-SALA, A., HARRISON, S. P., HUGHES, P. D. M., JACKSON, S. T., KORHOLA, A., MAUQUOY, D., MITCHELL, F. J. G., PRENTICE, I. C., VAN DER LINDEN, M., DE VLEESCHOUWER, F., YU, Z. C., ALM, J., BAUER, I. E., CORISH, Y. M. C., GARNEAU, M., HOHL, V., HUANG, Y., KAROFELD, E., LE ROUX, G., LOISEL, J., MOSCHEN, R., NICHOLS, J. E., NIEMINEN, T. M., MACDONALD, G. M., PHADTARE, N. R., RAUSCH, N., SILLASOO, Ü., SWINDLES, G. T., TUITTILA, E. S., UKONMAANAHO, L., VÄLIRANTA, M., VAN BELLEN, S., VAN GEEL, B., VITT, D. H. & ZHAO, Y. 2013. Climate-related changes in peatland carbon accumulation during the last millennium. *Biogeosciences,* 10**,** 929-944.

CHEN, J. Q., SAUNDERS, S. C., CROW, T. R., NAIMAN, R. J., BROSOFSKE, K. D., MROZ, G. D., BROOKSHIRE, B. L. & FRANKLIN, J. F. 1999. Microclimate in forest ecosystem and landscape ecology - Variations in local climate can be used to monitor and compare the effects of different management regimes. *Bioscience,* 49**,** 288-297.

CHEN, S. G., SHAO, B. Y., IMPENS, I. & CEULEMANS, R. 1994. Effects of Plant Canopy Structure on Light Interception and Photosynthesis. *Journal of Quantitative Spectroscopy & Radiative Transfer,* 52**,** 115-123.

CHIRINO, C., CAMPEAU, S. & ROCHEFORT, L. 2006. Sphagnum establishment on bare peat: The importance of climatic variability and Sphagnum species richness. *Applied Vegetation Science,* 9**,** 285-294.

CHOJNICKI, B. H., MICHALAK, M., ACOSTA, M., JUSZCZAK, R., AUGUSTIN, J., DROSLER, M. & OLEJNIK, J. 2010. Measurements of Carbon Dioxide Fluxes by Chamber Method at the Rzecin Wetland Ecosystem, Poland. *Polish Journal of Environmental Studies,* 19**,** 283-291.

CHRISTIANSEN, J. R., KORHONEN, J. F. J., JUSZCZAK, R., GIEBELS, M. & PIHLATIE, M. 2011. Assessing the effects of chamber placement, manual sampling and headspace mixing on CH4 fluxes in a laboratory experiment. *Plant and Soil,* 343**,** 171-185.

CIAIS, P., SABINE, C., BALA, G., BOPP, L., BROVKIN, V., CANADELL, J. G., CHHABRA, A., DEFRIES, R., GALLOWAY, J., HEIMANN, M., JONES, C., LE QUERE, C., MYNENI, R. B., PIAO, S. & THORNTON, P. 2013. Carbon and Other Biogeochemical Cycles. *In:* STOCKER, T. F., QIN, D., PLATTNER, G.-K., TIGNOR, M., ALLEN, S. K., BOSCHUNG, J., NAUELS, A., XIA, Y., BEX, V. & MIDGLEY, P. M. (eds.) *Climate Change 2013: The Physical Science Basis. Contribution of Working Group I to the Fifth Assessment Report of the Intergovernmental Panel on Climate Change*. Cambridge University Press: Cambridge, United Kingdom and New York, NY, USA.

CLARK, J. M., LANE, S. N., CHAPMAN, P. J. & ADAMSON, J. K. 2008. Link between DOC in near surface peat and stream water in an upland catchment. *Science of the Total Environment,* 404**,** 308-315.

CLEMENT, R. 2004. *Mass and Energy Exchange of a Plantation Forest in Scotland using Micrometeorological Methods.* PhD PhD, University of Edinburgh.

CLEMENT, R. J., BURBA, G. G., GRELLE, A., ANDERSON, D. J. & MONCRIEFF, J. B. 2009. Improved trace gas flux estimation through IRGA sampling optimization. *Agricultural and Forest Meteorology,* 149**,** 623-638.

CLEMENT, R. J., JARVIS, P. G. & MONCRIEFF, J. B. 2012. Carbon dioxide exchange of a Sitka spruce plantation in Scotland over five years. *Agricultural and Forest Meteorology,* 153**,** 106-123.

CLYMO, R. S. 1984. The Limits to Peat Bog Growth. *Philosophical Transactions of the Royal Society of London Series B-Biological Sciences,* 303**,** 605-654.

CLYMO, R. S. 2004. Hydraulic conductivity of peat at Ellergower Moss, Scotland. *Hydrological Processes,* 18**,** 261-274.

CLYMO, R. S., PEARCE, D. M. E. & CONRAD, R. 1995. Methane and Carbon Dioxide Production in, Transport through, and Efflux from a Peatland [and Discussion]. *Philosophical Transactions of the Royal Society A: Mathematical, Physical and Engineering Sciences,* 351**,** 249-259.

COX, P. M., BETTS, R. A., JONES, C. D., SPALL, S. A. & TOTTERDELL, I. J. 2000. Acceleration of global warming due to carbon-cycle feedbacks in a coupled climate model. *Nature,* 408**,** 184-187.

CUBASCH, U., WUEBBLES, D., CHEN, D., FACCHINI, M. C., FRAME, D., MAHOWALD, N. & WINTHER, J.-G. 2013. Introduction. *In:* STOCKER, T. F., QIN, D., PLATTNER, G.-K., TIGNOR, M., ALLEN, S. K., BOSCHUNG, J., NAUELS, A., XIA, Y., BEX, V. & MIDGLEY, P. M. (eds.) *In: Climate Change 2013: The Physical Science Basis. Contributions of Working Group I to the Fifth Assessment Report of the Intergovermnental Panel on Climate Change*. Cambridge , United Kingdom and New York, NY, USA.

CUNNINGHAM, S. C. 2005. Photosynthetic responses to vapour pressure deficit in temperate and tropical evergreen rainforest trees of Australia. *Oecologia,* 142**,** 521-528.

DANG, Q. L., LIEFFERS, V. J., ROTHWELL, R. L. & MACDONALD, S. E. 1991. Diurnal-Variation and Interrelations of Ecophysiological Parameters in 3 Peatland Woody Species under Different Weather and Soil-Moisture Conditions. *Oecologia,* 88**,** 317-324.

DAVIDSON, E. A. & JANSSENS, I. A. 2006. Temperature sensitivity of soil carbon decomposition and feeedbacks to climate change. *Nature,* 440**,** 165 - 173.

DAWSON, J. J. C. & SMITH, P. 2007. Carbon losses from soil and its consequences for land-use management. *Science of the Total Environment,* 382**,** 165-190.

DE DEYN, G. B., CORNELISSEN, J. H. C. & BARDGETT, R. D. 2008. Plant functional traits and soil carbon sequestration in contrasting biomes. *Ecology Letters,* 11**,** 516-531.

DENMEAD, O. T. 2008. Approaches to measuring fluxes of methane and nitrous oxide between landscapes and the atmosphere. *Plant and Soil,* 309**,** 5-24.

DERWENT, R. G., SIMMONDS, P. G., MANNING, A. J. & SPAIN, T. G. 2007. Trends over a 20-year period from 1987 to 2007 in surface ozone at the atmospheric research station, Mace Head, Ireland. *Atmospheric Environment,* 41**,** 9091-9098.

DESJARDINS, R. L. 1974. Technique to Measure Co2 Exchange under Field Conditions. *International Journal of Biometeorology,* 18**,** 76-83.

DIAZ, S., LAVOREL, S., DE BELLO, F., QUETIER, F., GRIGULIS, K. & ROBSON, M. 2007. Incorporating plant functional diversity effects in ecosystem service assessments. *Proceedings of the National Academy of Sciences of the United States of America,* 104**,** 20684-20689.

DIXON, S. D., QASSIM, S. M., ROWSON, J. G., WORRALL, F., EVANS, M. G., BOOTHROYD, I. M. & BONN, A. 2014. Restoration effects on water table depths and CO2 fluxes from climatically marginal blanket bog. *Biogeochemistry,* 118**,** 159-176.

DON, A., SCHUMACHER, J. & FREIBAUER, A. 2011. Impact of tropical land-use change on soil organic carbon stocks - a meta-analysis. *Global Change Biology,* 17**,** 1658-1670.

DONEY, S. C., FABRY, V. J., FEELY, R. A. & KLEYPAS, J. A. 2009. Ocean Acidification: The Other CO2 Problem. *Annual Review of Marine Science,* 1**,** 169-192.

DORREPAAL, E., TOET, S., VAN LOGTESTIJN, R. S. P., SWART, E., VAN DE WEG, M. J., CALLAGHAN, T. V. & AERTS, R. 2009. Carbon respiration from subsurface peat accelerated by climate warming in the subarctic. *Nature,* 460**,** 616-619.

ERWIN, K. L. 2009. Wetlands and global climate change: the role of wetland restoration in a changing world. *Wetlands Ecology and Management,* 17**,** 71-84.

EVANS, J. R. 1989. Photosynthesis and Nitrogen Relationships in Leaves of C-3 Plants. *Oecologia,* 78**,** 9-19.

EVANS, M. G., BURT, T. P., HOLDEN, J. & ADAMSON, J. K. 1999. Runoff generation and water table fluctuations in blanket peat: evidence from UK data spanning the dry summer of 1995. *Journal of Hydrology,* 221**,** 141-160.

FALGE, E., BALDOCCHI, D., OLSON, R., ANTHONI, P., AUBINET, M., BERNHOFER, C., BURBA, G., CEULEMANS, R., CLEMENT, R., DOLMAN, H., GRANIER, A., GROSS, P., GRUNWALD, T., HOLLINGER, D., JENSEN, N. O., KATUL, G., KERONEN, P., KOWALSKI, A., LAI, C. T., LAW, B. E., MEYERS, T., MONCRIEFF, H., MOORS, E., MUNGER, J. W., PILEGAARD, K., RANNIK, U., REBMANN, C., SUYKER, A., TENHUNEN, J., TU, K., VERMA, S., VESALA, T., WILSON, K. & WOFSY, S. 2001. Gap filling strategies for defensible annual sums of net ecosystem exchange. *Agricultural and Forest Meteorology,* 107**,** 43-69.

FINNIGAN, J. J. 2004. A re-evaluation of long-term flux measurement techniques - Part II: Coordinate systems. *Boundary-Layer Meteorology,* 113**,** 1-41.

FINNIGAN, J. J., CLEMENT, R., MALHI, Y., LEUNING, R. & CLEUGH, H. A. 2003. A re-evaluation of long-term flux measurement techniques - Part I: Averaging and coordinate rotation. *Boundary-Layer Meteorology,* 107**,** 1-48.

FLANAGAN, L. B. & SYED, K. H. 2011. Stimulation of both photosynthesis and respiration in response to warmer and drier conditions in a boreal peatland ecosystem. *Global Change Biology,* 17**,** 2271-2287.

FOKEN, T. 2006. 50 years of the Monin-Obukhov similarity theory. *Boundary-Layer Meteorology,* 119**,** 431-447.

FOKEN, T. 2008. *Micrometeorology,* Berlin/Heidelberg, Springer.

FOKEN, T., AUBINET, M., FINNIGAN, J. J., LECLERC, M. Y., MAUDER, M. & U, K. T. P. 2011. Results of a Panel Discussion About the Energy Balance Closure Correction for Trace Gases. *Bulletin of the American Meteorological Society,* 92**,** Es13-Es18.

FOKEN, T., AUBINET, M. & LEUNING, R. 2012a. The Eddy Covariance Method. *In:* AUBINET, M., VESALA, T. & PAPALE, D. (eds.) *Eddy Covariance: A Practical guide to measurment and data analysis.* Dordrecht: Springer.

FOKEN, T., GÖCKEDE, M., MAUDER, M., MAHRT, L., AMIRO, B. D. & MUNGER, J. W. 2004. Post-field data quality control. *In:* LEE, X. E. A. (ed.) *Handbook of micrometeorology: a guide for surface flux measurement and analysis.* Dordrecht: Kluwer.

FOKEN, T., LEUNING, R., ONCLEY, S., MAUDER, M. & AUBINET, M. 2012b. Corrections and Data Quality Control. *In:* AUBINET, M., VESALA, T. & PAPALE, D. (eds.) *Eddy Covariance: A Practical Guide to Measurement and Data.* Dordrecht: Springer.

FOKEN, T. & ONCLEY, S. 1995. Workshop on Instrumental and Methodical Problems of Land-Surface Flux Measurements. *Bulletin of the American Meteorological Society,* 76**,** 1191-1193.

FOSTER, G. L. & ROHLING, E. J. 2013. Relationship between sea level and climate forcing by CO2 on geological timescales. *Proceedings of the National Academy of Sciences of the United States of America,* 110**,** 1209-1214.

FOWLER, D. H., K.J.; MACDONALD, J.A.; GARDINER, B. 1995. Methane and CO2 exchange over peatland and the effects of afforestation. *Forestry,* 68**,** 327 - 334.

FRATINI, G., MCDERMITT, D. K. & PAPALE, D. 2014. Eddy-covariance flux errors due to biases in gas concentration measurements: origins, quantification and correction. *Biogeosciences,* 11**,** 1037-1051.

FREEMAN, C., EVANS, C. D., MONTEITH, D. T., REYNOLDS, B. & FENNER, N. 2001. Export of organic carbon from peat soils. *Nature,* 412**,** 785-785.

FREEMAN, C., FENNER, N. & SHIRSAT, A. H. 2012. Peatland geoengineering: an alternative approach to terrestrial carbon sequestration. *Philosophical Transactions of the Royal Society a-Mathematical Physical and Engineering Sciences,* 370**,** 4404-4421.

FRIBORG, T., SOEGAARD, H., CHRISTENSEN, T. R., LLOYD, C. R. & PANIKOV, N. S. 2003. Siberian wetlands: Where a sink is a source. *Geophysical Research Letters,* 30.

FRIEDLINGSTEIN, P., BOPP, L., CIAIS, P., DUFRESNE, J.-L., FAIRHEAD, L., LETREUT, H., MONFRAY, P. & ORR, J. 2001. Positive feedback between future climate change and the carbon cycle. *Geophysical Research Letters,* 28**,** 1543 - 1546.

FRIEDLINGSTEIN, P. & SOLOMON, S. 2005. Contributions of past and present human generations to committed warming caused by carbon dioxide. *Proceedings of the National Academy of Sciences of the United States of America,* 102**,** 10832-10836.

FRITZ, C., LAMERS, L. P. M., RIAZ, M., VAN DEN BERG, L. J. L. & ELZENGA, T. J. T. M. 2014. Sphagnum Mosses - Masters of Efficient N-Uptake while Avoiding Intoxication. *Plos One,* 9.

FROLKING, S., ROULET, N. & FUGLESTVEDT, J. 2006. How northern peatlands influence the Earth's radiative budget: Sustained methane emission versus sustained carbon sequestration. *Journal of Geophysical Research-Biogeosciences,* 111.

FROLKING, S. & ROULET, N. T. 2007. Holocene radiative forcing impact of northern peatland carbon accumulation and methane emissions. *Global Change Biology,* 13**,** 1079-1088.

FROLKING, S. E., BUBIER, J. L., MOORE, T. R., BALL, T., BELLISARIO, L. M., BHARDWAJ, A., CARROLL, P., CRILL, P. M., LAFLEUR, P. M., MCCAUGHEY, J. H., ROULET, N. T., SUYKER, A. E., VERMA, S. B., WADDINGTON, J. M. & WHITING, G. J. 1998. Relationship between ecosystem productivity and photosynthetically active radiation for northern peatlands. *Global Biogeochemical Cycles,* 12**,** 115-126.

GALLAGHER, M. W., CHOULARTON, T. W., BOWER, K. N., STROMBERG, I. M., BESWICK, K. M., FOWLER, D. & HARGREAVES, K. J. 1994. Measurements of Methane Fluxes on the Landscape Scale from a Wetland Area in North Scotland. *Atmospheric Environment,* 28**,** 2421-2430.

GILBERT, J. 2007. RSPB Reserves 2007: A review of our work. RSPB.

GILMANOV, T. G., VERMA, S. B., SIMS, P. L., MEYERS, T. P., BRADFORD, J. A., BURBA, G. G. & SUYKER, A. E. 2003. Gross primary production and light response parameters of four Southern Plains ecosystems estimated using long-term CO2-flux tower measurements. *Global Biogeochemical Cycles,* 17**,** n/a-n/a.

GLENN, S., HEYES, A. & MOORE, T. 1993. Carbon-Dioxide and Methane Fluxes from Drained Peat Soils, Southern Quebec. *Global Biogeochemical Cycles,* 7**,** 247-257.

GOFFIN, S., AUBINET, M., MAIER, M., PLAIN, C., SCHACK-KIRCHNER, H. & LONGDOZ, B. 2014. Characterization of the soil CO2 production and its carbon isotope composition in forest soil layers using the flux-gradient approach. *Agricultural and Forest Meteorology,* 188**,** 45-57.

GOODRICH, J. P., CAMPBELL, D. I., CLEARWATER, M. J., RUTLEDGE, S. & SCHIPPER, L. A. 2015. High vapor pressure deficit constrains GPP and the light response of NEE at a Southern Hemisphere bog. *Agricultural and Forest Meteorology,* 203**,** 54-63.

GORHAM, E. 1991. Northern Peatlands: Role in the Carbon cycle and probable responses to climatic warming. *Ecological Applications,* 1**,** 182 - 195.

GOULDEN, M. L., MUNGER, J. W., FAN, S. M., DAUBE, B. C. & WOFSY, S. C. 1996. Measurements of carbon sequestration by long-term eddy covariance: Methods and a critical evaluation of accuracy. *Global Change Biology,* 2**,** 169-182.

GREEN, F. H. W. 1973. Aspects of Changing Environment - Some Factors Affecting Aquatic Environment in Recent Years. *Journal of Environmental Management,* 1**,** 377-+.

GREENUP, A. L., BRADFORD, M. A., MCNAMARA, N. P., INESON, P. & LEE, J. A. 2000. The role of Eriophorum vaginatum in CH4 flux from an ombrotrophic peatland. *Plant and Soil,* 227**,** 265-272.

GROSVERNIER, P., MATTHEY, Y. & BUTTLER, A. 1997. Growth potential of three Sphagnum species in relation to water table level and peat properties with implications for their restoration in cut-over bogs. *Journal of Applied Ecology,* 34**,** 471-483.

GUO, X., HUANG, M., PU, F., YOU, W. & KE, C. 2015. Effects of ocean acidification caused by rising CO2 on the early development of three mollusks. *Aquatic Biology,* 23**,** 147-157.

HALLDIN, S. & LINDROTH, A. 1992. Errors in Net Radiometry - Comparison and Evaluation of 6 Radiometer Designs. *Journal of Atmospheric and Oceanic Technology,* 9**,** 762-783.

HAMILTON, S. K., SIPPEL, S. J., CHANTON, J. P. & MELACK, J. M. 2014. Plant-mediated transport and isotopic composition of methane from shallow tropical wetlands. *Inland Waters,* 4**,** 369-376.

HANCOCK, M. H., GRANT, M. C. & WILSON, J. D. 2009. Associations between distance to forest and spatial and temporal variation in abundance of key peatland breeding bird species. *Bird Study,* 56**,** 53-64.

HARAGUCHI, A. & YAMADA, N. 2011. Temperature Dependency of Photosynthesis of Sphagnum spp. Distributed in the Warm-Temperate and the Cool-Temperate Mires of Japan. *American Journal of Plant Sciences,* 2**,** 716-725.

HARDING, R. J. & LLOYD, C. R. 2008. Evaporation and energy balance of a wet grassland at Tadham Moor on the Somerset Levels. *Hydrological Processes,* 22**,** 2346-2357.

HARGREAVES, K. J., MILNE, R. & CANNELL, M. G. R. 2003. Carbon balance of afforested peatland in Scotland. *Forestry,* 76**,** 299 - 317.

HASLWANTER, A., HAMMERLE, A. & WOHLFAHRT, G. 2009. Open-path vs. closed-path eddy covariance measurements of the net ecosystem carbon dioxide and water vapour exchange: A long-term perspective. *Agricultural and Forest Meteorology,* 149**,** 291-302.

HATALA, J. A., DETTO, M., SONNENTAG, O., DEVEREL, S. J., VERFAILLIE, J. & BALDOCCHI, D. D. 2012. Greenhouse gas (CO2, CH4, H2O) fluxes from drained and flooded agricultural peatlands in the Sacramento-San Joaquin Delta. *Agriculture Ecosystems & Environment,* 150**,** 1-18.

HE, Z. Y., BENTLEY, L. P. & HOLADAY, A. S. 2011. Greater Seasonal Carbon Gain across a Broad Temperature Range Contributes to the Invasive Potential of Phalaris Arundinacea (Poaceae; Reed Canary Grass) over the Native Sedge Carex Stricta (Cyperaceae). *American Journal of Botany,* 98**,** 20-30.

HEIMANN, M. & REICHSTEIN, M. 2008. Terrestrial ecosystem carbon dynamics and climate feedbacks. *Nature,* 451**,** 289-292.

HELFTER, C., CAMPBELL, C., DINSMORE, K. J., DREWER, J., COYLE, M., ANDERSON, M., SKIBA, U., NEMITZ, E., BILLETT, M. F. & SUTTON, M. A. 2014. Drivers of long-term variability in CO2 net ecosystem exchange in a temperate peatland. *Biogeosciences Discussions,* 11**,** 14981 - 15018.

HENDRIKS, D. M. D., DOLMAN, A. J., VAN DER MOLEN, M. K. & VAN HUISSTEDEN, J. 2008. A compact and stable eddy covariance set-up for methane measurements using off-axis integrated cavity output spectroscopy. *Atmospheric Chemistry and Physics,* 8**,** 431-443.

HENDRIKS, D. M. D., VAN HUISSTEDEN, J., DOLMAN, A. J. & VAN DER MOLEN, M. K. 2007. The full greenhouse gas balance of an abandoned peat meadow. *Biogeosciences,* 4**,** 411-424.

HERBST, M., FRIBORG, T., SCHELDE, K., JENSEN, R., RINGGAARD, R., VASQUEZ, V., THOMSEN, A. G. & SOEGAARD, H. 2013. Climate and site management as driving factors for the atmospheric greenhouse gas exchange of a restored wetland. *Biogeosciences,* 10**,** 39-52.

HIBBARD, K. A., LAW, B. E., REICHSTEIN, M. & SULZMAN, J. 2005. An analysis of soil respiration across northern hemisphere temperate ecosystems. *Biogeochemistry,* 73**,** 29-70.

HILASVUORI, E., AKUJARVI, A., FRITZE, H., KARHU, K., LAIHO, R., MAKIRANTA, P., OINONEN, M., PALONEN, V., VANHALA, P. & LISKI, J. 2013. Temperature sensitivity of decomposition in a peat profile. *Soil Biology & Biochemistry,* 67**,** 47-54.

HILL, T. C. W., M.; WOODWARD, F.I.; MONCREIFF J.B. 2011. Constraining ecosystem processes from tower fluxes and atmospheric profiles. *Ecological Applications,* 21**,** 1474 - 1489.

HOBBIE, S. E. 1996. Temperature and plant species control over litter decomposition in Alaskan tundra. *Ecological Monographs,* 66**,** 503-522.

HOJSTRUP, J. 1993. A Statistical-Data Screening-Procedure. *Measurement Science & Technology,* 4**,** 153-157.

HOLDEN, J. 2005. Peatland hydrology and carbon release: why small-scale process matters. *Philos Trans A Math Phys Eng Sci,* 363**,** 2891-2913.

HOLDEN, J. & BURT, T. P. 2003. Hydrological studies on blanket peat: the significance of the acrotelm-catotelm model. *Journal of Ecology,* 91**,** 86-102.

HOLDEN, J., CHAPMAN, P. J. & LABADZ, J. C. 2004. Artificial drainage of peatlands: hydrological and hydrochemical process and wetland restoration. *Progress in Physical Geography,* 28**,** 95-123.

HOLDEN, J., WALKER, J., EVANS, M. G., WORRALL, F. & BONN, A. 2008. A compendium of peat restoration and management projects. Defra report SP0556.

HOLDEN, J., WALLAGE, Z. E., LANE, S. N. & MCDONALD, A. T. 2011. Water table dynamics in undisturbed, drained and restored blanket peat. *Journal of Hydrology,* 402**,** 103-114.

HOLLAND, E. A., ROBERTSON, G. P., GREENBERG, J., GROFFMAN, P. M., BOONE, R. D. & GOSZ, J. R. 1999. Soil CO2, N2O and CH4 Exchange. *In:* ROBERTSON, G. P., COLEMAN, D. C., BLEDSOE, S. & SOLLINS, P. (eds.) *Standard Soil Methods for Long-Term Ecological Research.* USA: Oxford University Press.

HOLLINGER, D. Y. & RICHARDSON, A. D. 2005. Uncertainty in eddy covariance measurements and its application to physiological models. *Tree Physiology,* 25**,** 873-885.

HOOIJER, A., PAGE, S., CANADELL, J. G., SILVIUS, M., KWADIJK, J., WOSTEN, H. & JAUHIAINEN, J. 2010. Current and future CO2 emissions from drained peatlands in Southeast Asia. *Biogeosciences,* 7**,** 1505-1514.

HOPKINS, F., GONZALEZ-MELER, M. A., FLOWER, C. E., LYNCH, D. J., CZIMCZIK, C., TANG, J. & SUBKE, J. A. 2013. Ecosystem-level control on root-rhizosphere respiration. *New Phytol,* 199**,** 339 - 351.

HORST, T. W., SEMMER, S. R. & MACLEAN, G. 2015. Correction of a Non-orthogonal, Three-Component Sonic Anemometer for Flow Distortion by Transducer Shadowing. *Boundary-Layer Meteorology,* 155**,** 371-395.

HORST, T. W. & WEIL, J. C. 1992. Footprint Estimation for Scalar Flux Measurements in the Atmospheric Surface-Layer. *Boundary-Layer Meteorology,* 59**,** 279-296.

HOUBORG, R., ANDERSON, M. C., NORMAN, J. M., WILSON, T. & MEYERS, T. 2009. Intercomparison of a 'bottom-up' and 'top-down' modeling paradigm for estimating carbon and energy fluxes over a variety of vegetative regimes across the US. *Agricultural and Forest Meteorology,* 149**,** 1875-1895.

HOUSE, J. I., ORR, H. G., CLARK, J. M., GALLEGO-SALA, A. V., FREEMAN, C., PRENTICE, I. C. & SMITH, P. 2010. Climate change and the British Uplands: evidence for decision-making. *Climate Research,* 45**,** 3-12.

IBROM, A., DELLWIK, E., FLYVBJERG, H., JENSEN, N. O. & PILEGAARD, K. 2007a. Strong low-pass filtering effects on water vapour flux measurements with closed-path eddy correlation systems. *Agricultural and Forest Meteorology,* 147**,** 140-156.

IBROM, A., DELLWIK, E., LARSEN, S. E. & PILEGAARD, K. 2007b. On the use of the Webb-Pearman-Leuning theory for closed-path eddy correlation measurements. *Tellus Series B-Chemical and Physical Meteorology,* 59**,** 937-946.

ISE, T., DUNN, A. L., WOFSY, S. C. & MOORCROFT, P. R. 2008. High sensitivity of peat decomposition to climate change through water-table feedback. *Nature Geoscience,* 1**,** 763-766.

JARVIS, P. G., MASSHEDER, J. M., HALE, S. E., MONCRIEFF, J. B., RAYMENT, M. & SCOTT, S. L. 1997. Seasonal variation of carbon dioxide, water vapor, and energy exchanges of a boreal black spruce forest. *Journal of Geophysical Research-Atmospheres,* 102**,** 28953-28966.

JNCC 2011. Towards an assessment of the state of UK peatlands. *In:* HIGGINS, A., JONES, P., SHEPHERD, M., WEYL, R., BRUNEAU, P., COUPAR, A. & JOHNSON, S. (eds.) *JNCC report.* Joint Nature Conservation Committee.

JOBBAGY, E. G. & JACKSON, R. B. 2000. The vertical distribution of soil organic carbon and its relation to climate and vegetation. *Ecological Applications,* 10**,** 423-436.

JONES, E. P., ZWICK, H. & WARD, T. V. 1978. A fast response atmospheric CO2 sensor for eddy correlation flux measurement. *Atmospheric Environment,* 12**,** 845 - 851.

JOOSTEN, H. 2010. The Global Peatland CO2 Picture: Peatland status and drainage related emissions in all countries of the world.

JOOSTEN, H. & CLARKE, D. 2002. *Wise use of Mires and Peatlands - Background and Principles including a framework for decision-making,* Saarijärvi, Finland, International Mire Conservation Group and International Peat Society.

JUSZCZAK, R., HUMPHREYS, E., ACOSTA, M., MICHALAK-GALCZEWSKA, M., KAYZER, D. & OLEJNIK, J. 2013. Ecosystem respiration in a heterogeneous temperate peatland and its sensitivity to peat temperature and water table depth. *Plant and Soil,* 366**,** 505-520.

KAIMAL, J. C., CLIFFORD, S. F. & LATAITIS, R. J. 1989. Effect of Finite Sampling on Atmospheric Spectra. *Boundary-Layer Meteorology,* 47**,** 337-347.

KAIMAL, J. C. & FINNIGAN, J. J. 1994. *Atmospheric boundary layer flows: their structure and measurement,* Oxford, Oxford University Press.

KAIMAL, J. C., IZUMI, Y., WYNGAARD, J. C. & COTE, R. 1972. Spectral Characteristics of Surface-Layer Turbulence. *Quarterly Journal of the Royal Meteorological Society,* 98**,** 563-&.

KANE, R. P. & DEPAULA, E. R. 1996. Atmospheric CO2 changes at Mauna Loa, Hawaii. *Journal of Atmospheric and Terrestrial Physics,* 58**,** 1673-1681.

KARHU, K., AUFFRET, M. D., DUNGAIT, J. A. J., HOPKINS, D. W., PROSSER, J. I., SINGH, B. K., SUBKE, J. A., WOOKEY, P. A., AGREN, G. I., SEBASTIA, M. T., GOURIVEAU, F., BERGKVIST, G., MEIR, P., NOTTINGHAM, A. T., SALINAS, N. & HARTLEY, I. P. 2014. Temperature sensitivity of soil respiration rates enhanced by microbial community response. *Nature,* 513**,** 81-+.

KATUL, G. G., FINNIGAN, J. J., POGGI, D., LEUNING, R. & BELCHER, S. E. 2006. The influence of hilly terrain on canopy-atmosphere carbon dioxide exchange. *Boundary-Layer Meteorology,* 118**,** 189-216.

KETTRIDGE, N. & BAIRD, A. 2008. Modelling soil temperatures in northern peatlands. *European Journal of Soil Science,* 59**,** 327-338.

KIM, J. & VERMA, S. B. 1990. Carbon-Dioxide Exchange in a Temperate Grassland Ecosystem. *Boundary-Layer Meteorology,* 52**,** 135-149.

KIM, J. & VERMA, S. B. 1992. Soil Surface Co2 Flux in a Minnesota Peatland. *Biogeochemistry,* 18**,** 37-51.

KIM, J., VERMA, S. B., SHURPALI, N. J., HARAZONO, Y., MIYATA, A., YUN, J. I., TANNER, B. & KIM, J. W. 2000. Diurnal and seasonal variations in CH4 emission from various freshwater wetlands - Effects of growth stage, plant-mediated transport and water table elevations. *Non-Co2 Greenhouse Gases: Scientific Understanding, Control and Implementation***,** 131-136.

KIRSCHBAUM, M. U. F. 1995. The Temperature-Dependence of Soil Organic-Matter Decomposition, and the Effect of Global Warming on Soil Organic-C Storage. *Soil Biology & Biochemistry,* 27**,** 753-760.

KIVIMAKI, S. K., YLI-PETAYS, M. & TUITTILA, E. S. 2008. Carbon sink function of sedge and Sphagnum patches in a restored cut-away peatland: increased functional diversity leads to higher production. *Journal of Applied Ecology,* 45**,** 921-929.

KNOHL, A. & BALDOCCHI, D. D. 2008. Effects of diffuse radiation on canopy gas exchange processes in a forest ecosystem. *Journal of Geophysical Research-Biogeosciences,* 113.

KOBLICK, D. 2009. Vectorized Solar Azimuth and Elevation Estimation.

KOMULAINEN, V. M., NYKANEN, H., MARTIKAINEN, P. J. & LAINE, J. 1998. Short-term effect of restoration on vegetation change and methane emissions from peatlands drained for forestry in southern Finland. *Canadian Journal of Forest Research-Revue Canadienne De Recherche Forestiere,* 28**,** 402-411.

KOMULAINEN, V. M., TUITTILA, E. S., VASANDER, H. & LAINE, J. 1999. Restoration of drained peatlands in southern Finland: initial effects on vegetation change and CO2 balance. *Journal of Applied Ecology,* 36**,** 634-648.

KORMANN, R. & MEIXNER, F. X. 2001. An analytical footprint model for non-neutral stratification. *Boundary-Layer Meteorology,* 99**,** 207-224.

KOWALSKI, A. S., LOUSTAU, D., BERBIGIER, P., MANCA, G., TEDESCHI, V., BORGHETTI, M., VALENTINI, R., KOLARI, P., BERNINGER, F., RANNIK, U., HARI, P., RAYMENT, M., MENCUCCINI, M., MONCRIEFF, J. & GRACE, J. 2004. Paired comparisons of carbon exchange between undisturbed and regenerating stands in four managed forests in Europe. *Global Change Biology,* 10**,** 1707-1723.

KRISTENSEN, L. & JENSEN, N. O. 1979. Lateral Coherence in Isotropic Turbulence and in the Natural Wind. *Boundary-Layer Meteorology,* 17**,** 353-373.

KWON, H. J., OECHEL, W. C., ZULUETA, R. C. & HASTINGS, S. J. 2006. Effects of climate variability on carbon sequestration among adjacent wet sedge tundra and moist tussock tundra ecosystems. *Journal of Geophysical Research-Biogeosciences,* 111.

LAFLEUR, P. M., HEMBER, R. A., ADMIRAL, S. W. & ROULET, N. T. 2005a. Annual and seasonal variability in evapotranspiration and water table at a shrub-covered bog in southern Ontario, Canada. *Hydrological Processes,* 19**,** 3533-3550.

LAFLEUR, P. M., MOORE, T. R., ROULET, N. T. & FROLKING, S. 2005b. Ecosystem respiration in a cool temperate bog depends on peat temperature but not water table. *Ecosystems,* 8**,** 619-629.

LAGOMARSINO, A., DE ANGELIS, P., MOSCATELLI, M. C. & GREGO, S. 2009. The influence of temperature and labile C substrates on heterotrophic respiration in response to elevated CO2 and nitrogen fertilization. *Plant and Soil,* 317**,** 223-234.

LAIHO, R., VASANDER, H., PENTTILA, T. & LAINE, J. 2003. Dynamics of plant-mediated organic matter and nutrient cycling following water-level drawdown in boreal peatlands. *Global Biogeochemical Cycles,* 17.

LAL, R. 2004. Soil carbon sequestration to mitigate climate change. *Geoderma,* 123**,** 1-22.

LAPEN, D. R., PRICE, J. S. & GILBERT, R. 2000. Soil water storage dynamics in peatlands with shallow water tables. *Canadian Journal of Soil Science,* 80**,** 43-52.

LAPWORTH, A. & MCGREGOR, J. 2008. Seasonal variation of the prevailing wind direction in Britain. *Weather,* 63**,** 365-368.

LAUBACH, J. & MCNAUGHTON, K. G. 1998. A spectrum-independent procedure for correcting eddy fluxes measured with separated sensors. *Boundary-Layer Meteorology,* 89**,** 445-467.

LE QUÉRÉ, C. 2010. Trends in the land and ocean carbon uptake. *Current Opinion in Environmental Sustainability,* 2**,** 219-224.

LECLERC, M. Y. & THURTELL, G. W. 1990. Footprint Prediction of Scalar Fluxes Using a Markovian Analysis. *Boundary-Layer Meteorology,* 52**,** 247-258.

LEE, X., FINNIGAN, J. J. & PAW U, K. T. 2004. Coordinate systems and flux bias error. *Handbook of micrometeorology* Dordrecht, The Netherlands: Kluwer Academic.

LEE, X. H. 1998. On micrometeorological observations of surface-air exchange over tall vegetation. *Agricultural and Forest Meteorology,* 91**,** 39-49.

LEUNING, R. 2004. Measurements of trace gas fluxes in the atmosphere using eddy covariance: WPL corrections revisited. *In:* LEE, X., MASSMAN, W. J. & LAW, B. (eds.) *Handbook of Micrometeorology: A guide for surface flux measurement and analysis.* Dordrect, Netherlands: Kluwer Academic Publishers.

LEUNING, R., VAN GORSEL, E., MASSMAN, W. J. & ISAAC, P. R. 2012. Reflections on the surface energy imbalance problem. *Agricultural and Forest Meteorology,* 156**,** 65-74.

LEVY, P. E., BURDEN, A., COOPER, M. D. A., DINSMORE, K. J., DREWER, J., EVANS, C., FOWLER, D., GAIAWYN, J., GRAY, A., JONES, S. K., JONES, T., MCNAMARA, N. P., MILLS, R., OSTLE, N., SHEPPARD, L. J., SKIBA, U., SOWERBY, A., WARD, S. E. & ZIELINSKI, P. 2012. Methane emissions from soils: synthesis and analysis of a large UK data set. *Global Change Biology,* 18**,** 1657-1669.

LEVY, P. E. & GRAY, A. 2015. Greenhouse gas balance of a semi-natural peatbog in northern Scotland. *Environmental Research Letters,* 10.

LIMPENS, J., BERENDSE, F., BLODAU, C., CANADELL, J. G., FREEMAN, C., HOLDEN, J., ROULET, N., RYDIN, H. & SCHAEPMAN-STRUB, G. 2008. Peatlands and the carbon cycle: from local processes to global implications - a synthesis. *Biogeosciences,* 5**,** 1475-1491.

LINDSAY, R. A., CHARMAN, D. J., EVERINGHAM, F., O'REILLY, R. M., PALMER, M. A., ROWELL, T. A. & STROUD, D. A. 1988. The Flow Country - The peatlands of Caithness and Sutherland. *In:* RATCLIFFE, D. A. & OSWALD, P. H. (eds.).

LINTNER, B. R., BUERMANN, W., KOVEN, C. D. & FUNG, I. Y. 2006. Seasonal circulation and Mauna Loa CO2 variability. *Journal of Geophysical Research-Atmospheres,* 111.

LIVINGSTON, G. P. & HUTCHINSON, G. 1995. Enclosure-based measurement of trace gas exchange: applications and sources of error. *In:* MATSON, P., HARRISS, RC (ed.) *Biogenic Trace Gases: Measuring Emissions from Soil and Water.* Cambridge, MA, USA: Blackwell Science Ltd.

LLOYD, J. & TAYLOR, J. A. 1994. On the Temperature-Dependence of Soil Respiration. *Functional Ecology,* 8**,** 315-323.

LOHILA, A., AURELA, M., TUOVINEN, J. P. & LAURILA, T. 2004. Annual CO2 exchange of a peat field growing spring barley or perennial forage grass. *Journal of Geophysical Research-Atmospheres,* 109.

LOHILA, A., MINKKINEN, K., AURELA, M., TUOVINEN, J. P., PENTTILÄ, T., OJANEN, P. & LAURILA, T. 2011. Greenhouse gas flux measurements in a forestry-drained peatland indicate a large carbon sink. *Biogeosciences,* 8**,** 3203-3218.

LUAN, J. W. & WU, J. H. 2014. Gross photosynthesis explains the 'artificial bias' of methane fluxes by static chamber (opaque versus transparent) at the hummocks in a boreal peatland. *Environmental Research Letters,* 9.

LUGO, A. E. & BROWN, S. 1992. Tropical Forests as Sinks of Atmospheric Carbon. *Forest Ecology and Management,* 54**,** 239-255.

LUND, M., LAFLEUR, P. M., ROULET, N. T., LINDROTH, A., CHRISTENSEN, T. R., AURELA, M., CHOJNICKI, B. H., FLANAGAN, L. B., HUMPHREYS, E. R., LAURILA, T., OECHEL, W. C., OLEJNIK, J., RINNE, J., SCHUBERT, P. & NILSSON, M. B. 2010. Variability in exchange of CO2 across 12 northern peatland and tundra sites. *Global Change Biology,* 16**,** 2436-2448.

LUND, M., LINDROTH, A., CHRISTENSEN, T. R. & STROM, L. 2007. Annual CO2 balance of a temperate bog. *Tellus Series B-Chemical and Physical Meteorology,* 59**,** 804-811.

LUO, J., CHEN, Y. C., WU, Y. H., SHI, P. L., SHE, J. & ZHOU, P. 2012. Temporal-Spatial Variation and Controls of Soil Respiration in Different Primary Succession Stages on Glacier Forehead in Gongga Mountain, China. *Plos One,* 7.

MAHADEVAN, P., WOFSY, S. C., MATROSS, D. M., XIAO, X. M., DUNN, A. L., LIN, J. C., GERBIG, C., MUNGER, J. W., CHOW, V. Y. & GOTTLIEB, E. W. 2008. A

satellite-based biosphere parameterization for net ecosystem CO2 exchange: Vegetation Photosynthesis and Respiration Model (VPRM). *Global Biogeochemical Cycles,* 22.
MAHRT, L., LEE, X. H., BLACK, A., NEUMANN, H. & STAEBLER, R. M. 2000. Nocturnal mixing in a forest subcanopy. *Agricultural and Forest Meteorology,* 101**,** 67-78.
MAIER, M. & SCHACK-KIRCHNER, H. 2014. Using the gradient method to determine soil gas flux: A review. *Agricultural and Forest Meteorology,* 192**,** 78-95.
MAKIRANTA, P., LAIHO, R., PENTTILA, T. & MINKKINEN, K. 2012. The impact of logging residue on soil GHG fluxes in a drained peatland forest. *Soil Biology & Biochemistry,* 48**,** 1-9.
MALHI, Y., MCNAUGHTON, K. G. & VON RANDOW, C. 2004. Low Frequency atmospheric transport and surface flux measurements. *In:* LEE, X., MASSMAN, W. J. & LAW, B. (eds.) *Handbook of Micrometeorolgy: A guide for surface flux measurement and analysis.* Dordrecht: Kluwer Academic.
MALJANEN, M., SIGURDSSON, B. D., GUÐMUNDSSON, J., ÓSKARSSON, H., HUTTUNEN, J. T. & MARTIKAINEN, P. J. 2010. Greenhouse gas balances of managed peatlands in the Nordic countries – present knowledge and gaps. *Biogeosciences,* 7**,** 2711-2738.
MASSMAN, W. J. 1991. The Attenuation of Concentration Fluctuations in Turbulent-Flow through a Tube. *Journal of Geophysical Research-Atmospheres,* 96**,** 15269-15273.
MASSMAN, W. J. 2000. A simple method for estimating frequency response corrections for eddy covariance systems. *Agricultural and Forest Meteorology,* 104**,** 185-198.
MASSMAN, W. J. & CLEMENT, R. 2004. Uncertainty in Eddy Covariance Flux Estimates Resulting from Spectral Attenuation. *In:* LEE, X., MASSMAN, W. J. & LAW, B. (eds.) *Handbook of Micrometeorology.* Dordrecht: Kluwer Academic.
MASSMAN, W. J. & IBROM, A. 2008. Attenuation of concentration fluctuations of water vapor and other trace gases in turbulent tube flow. *Atmospheric Chemistry and Physics,* 8**,** 6245-6259.
MATHER, A. S. & MURRAY, N. C. 1988. The dynamics of rural land use change: The case of private sector afforestation in Scotland. *Land use Policy,* 5**,** 103 - 120.
MAUDER, M., FOKEN, T., CLEMENT, R., ELBERS, J. A., EUGSTER, W., GRUNWALD, T., HEUSINKVELD, B. & KOLLE, O. 2008. Quality control of CarboEurope flux data - Part 2: Inter-comparison of eddy-covariance software. *Biogeosciences,* 5**,** 451-462.
MCDERMITT, D., BURBA, G., XU, L., ANDERSON, T., KOMISSAROV, A., RIENSCHE, B., SCHEDLBAUER, J., STARR, G., ZONA, D., OECHEL, W., OBERBAUER, S. & HASTINGS, S. 2011. A new low-power, open-path instrument for measuring methane flux by eddy covariance. *Applied Physics B-Lasers and Optics,* 102**,** 391-405.
MCMILLAN, A. A. & POWELL, J. H. 1999. BGS rock classification scheme volume 4: Classification of artificial (man-made) ground and natural superficial deposits application to geological maps and datasets in the UK. NERC, British Geological Survey.
MCNEIL, P. & WADDINGTON, J. M. 2003. Moisture controls on Sphagnum growth and CO2 exchange on a cutover bog. *Journal of Applied Ecology,* 40**,** 354-367.
MEDVIGY, D., JEONG, S. J., CLARK, K. L., SKOWRONSKI, N. S. & SCHAFER, K. V. R. 2013. Effects of seasonal variation of photosynthetic capacity on the carbon fluxes of a temperate deciduous forest. *Journal of Geophysical Research-Biogeosciences,* 118**,** 1703-1714.
MEYERS, T. P., LUKE, W. T. & MEISINGER, J. J. 2006. Fluxes of ammonia and sulfate over maize using relaxed eddy accumulation. *Agricultural and Forest Meteorology,* 136**,** 203-213.
MIETTINEN, J. & LIEW, S. C. 2010. Status of Peatland Degradation and Development in Sumatra and Kalimantan. *Ambio,* 39**,** 394-401.
MILES, N. L., RICHARDSON, S. J., DAVIS, K. J., LAUVAUX, T., ANDREWS, A. E., WEST, T. O., BANDARU, V. & CROSSON, E. R. 2012. Large amplitude spatial and

temporal gradients in atmospheric boundary layer CO2 mole fractions detected with a tower-based network in the U.S. upper Midwest. *Journal of Geophysical Research-Biogeosciences,* 117.

MILLER, S. D., GOULDEN, M. L., MENTON, M. C., DA ROCHA, H. R., DE FREITAS, H. C., FIGUEIRA, A. M. E. S. & DE SOUSA, C. A. D. 2004. Biometric and micrometeorological measurements of tropical forest carbon balance. *Ecological Applications,* 14**,** S114-S126.

MINKKINEN, K. & LAINE, J. 1998. Long-term effect of forest drainage on the peat carbon stores of pine mires in Finland. *Canadian Journal of Forest Research-Revue Canadienne De Recherche Forestiere,* 28**,** 1267-1275.

MITCHELL, E. A. D., BUTTLER, A., GROSVERNIER, P., RYDIN, H., SIEGENTHALER, A. & GOBAT, J. M. 2002. Contrasted effects of increased N and CO2 supply on two keystone species in peatland restoration and implications for global change. *Journal of Ecology,* 90**,** 529-533.

MOFFAT, A. M., PAPALE, D., REICHSTEIN, M., HOLLINGER, D. Y., RICHARDSON, A. D., BARR, A. G., BECKSTEIN, C., BRASWELL, B. H., CHURKINA, G., DESAI, A. R., FALGE, E., GOVE, J. H., HEIMANN, M., HUI, D. F., JARVIS, A. J., KATTGE, J., NOORMETS, A. & STAUCH, V. J. 2007. Comprehensive comparison of gap-filling techniques for eddy covariance net carbon fluxes. *Agricultural and Forest Meteorology,* 147**,** 209-232.

MONCRIEFF, J., CLEMENT, R., FINNIGAN, J. & MEYERS, T. 2004. Averaging, detrending and filtering of eddy covariance time series. *In:* LEE, X., MASSMAN, W. J. & LAW, B. (eds.) *Handbook of micrometeorology: A guide for surface flux measurement and analysis.* Dordrecht: Kluwer Academic Publishers.

MONIN, A. S. & OBUKHOV, A. M. 1954. Osnovnye zakonomernosti turbulentnogo peremeshivanija v prizemnom sloe atmosfery (Basic Laws of Turbulent Mixing in the Atmosphere Near the Ground). *Trudy geofiz. inst.,* 24**,** 163-187.

MOORE, C. J. 1986. Frequency-Response Corrections for Eddy-Correlation Systems. *Boundary-Layer Meteorology,* 37**,** 17-35.

MORICE, C. P., KENNEDY, J. J., RAYNER, N. A. & JONES, P. D. 2012. Quantifying uncertainties in global and regional temperature change using an ensemble of observational estimates: The HadCRUT4 data set. *Journal of Geophysical Research-Atmospheres,* 117.

MULLER, J. B. A., PERCIVAL, C. J., GALLAGHER, M. W., FOWLER, D., COYLE, M. & NEMITZ, E. 2010. Sources of uncertainty in eddy covariance ozone flux measurements made by dry chemiluminescence fast response analysers. *Atmospheric Measurement Techniques,* 3**,** 163-176.

MURPHY, J. L. & MEASURES, C. I. 2014. Ocean Acidification: The Role of CO2. *Oceanography,* 27**,** 238-246.

MURRELL, J. C., MCDONALD, I. R. & BOURNE, D. G. 1998. Molecular methods for the study of methanotroph ecology. *Fems Microbiology Ecology,* 27**,** 103-114.

NEPSTAD, D. C., STICKLER, C. M., SOARES, B. & MERRY, F. 2008. Interactions among Amazon land use, forests and climate: prospects for a near-term forest tipping point. *Philosophical Transactions of the Royal Society B-Biological Sciences,* 363**,** 1737-1746.

NEWSON, M. D. 1992. Conservation management of peatlands and the drainage threat: hydrology, politics and the ecologist in the U.K. *Peatland ecosystems and man: an impact assessment symposium.* University of Dundee, Deparment of Biological Sciences in association with the international peat society.

NILSSON, M., SAGERFORS, J., BUFFAM, I., LAUDON, H., ERIKSSON, T., GRELLE, A., KLEMEDTSSON, L., WESLIEN, P. E. R. & LINDROTH, A. 2008. Contemporary carbon accumulation in a boreal oligotrophic minerogenic mire - a significant sink after accounting for all C-fluxes. *Global Change Biology,* 14**,** 2317-2332.

NOWAK, R. S., ELLSWORTH, D. S. & SMITH, S. D. 2004. Functional responses of plants to elevated atmospheric CO2 - do photosynthetic and productivity data from FACE experiments support early predictions? *New Phytologist,* 162**,** 253-280.

NUNGESSER, M. K. 2003. Modelling microtopography in boreal peatlands: hummocks and hollows. *Ecological Modelling,* 165**,** 175-207.

NYKANEN, H., ALM, J., LANG, K., SILVOLA, J. & MARTIKAINEN, P. J. 1995. Emissions of CH4, N2O and CO2 from a virgin fen and a fen drained for grassland in Finland. *Journal of Biogeography,* 22**,** 351-357.

NYKANEN, H., SILVOLA, J., ALM, J. & MARTIKAINEN, P. J. 1997. The Effect of Peatland Forestry on fluxes of carbon dioxide, methane and nitrous oxide. *In:* C.C. TRETTIN ET AL. (ed.) *Northern Forested Wetland: Ecology and Managment.* Boca Raton, FL: CRC/Lewis.

O'KELLY, B. C. 2007. Accurate determination of moisture content of organic soils using the oven drying method. *Drying Technology: An International Journal,* 22**,** 1767-1776.

OBERSTEINER, M., BOTTCHER, H. & YAMAGATA, Y. 2010. Terrestrial ecosystem management for climate change mitigation. *Current Opinion in Environmental Sustainability,* 2**,** 271-276.

OBUKHOV, A. M. 1946. Turbulentnost v temperaturnoj - neodnorodnoj atmosfere (Turbulence in an Atmosphere with a Non uniform Temperature). *Trudy inst. Theor. Geofiz.,* 1**,** 95-115.

OECHEL, W. C., VOURLITIS, G. L., HASTINGS, S. J., ZULUETA, R. C., HINZMAN, L. & KANE, D. 2000. Acclimation of ecosystem CO2 exchange in the Alaskan Arctic in response to decadal climate warming. *Nature,* 406**,** 978-981.

OFFICE, M. 2015. *Kinbrace climate* [Online]. Available: http://www.metoffice.gov.uk/public/weather/climate/gfm5qbgxz [Accessed 30/06/2015 2015].

OJANEN, P., MINKKINEN, K., ALM, J. & PENTTILA, T. 2010. Soil-atmosphere CO2, CH4 and N2O fluxes in boreal forestry-drained peatlands. *Forest Ecology and Management,* 260**,** 411-421.

ORCHARD, V. A. & COOK, F. J. 1983. Relationship between soil respiration and soil moisture. *Soil Biology & Biochemistry,* 15**,** 447 - 453.

OTIENO, D., LINDNER, S., MUHR, J. & BORKEN, W. 2012. Sensitivity of Peatland Herbaceous Vegetation to Vapor Pressure Deficit Influences Net Ecosystem CO2 Exchange. *Wetlands,* 32**,** 895-905.

OTIENO, D. O., WARTINGER, M., NISHIWAKI, A., HUSSAIN, M. Z., MUHR, J., BORKEN, W. & LISCHEID, G. 2009. Responses of CO2 Exchange and Primary Production of the Ecosystem Components to Environmental Changes in a Mountain Peatland. *Ecosystems,* 12**,** 590-603.

PAAVILAINEN, E. P., J. 1995. *Peatland Forestry,* Ecological Studies, Springer.

PAHLOW, M., PARLANGE, M. B. & PORTE-AGEL, F. 2001. On Monin-Obukhov similarity in the stable atmospheric boundary layer. *Boundary-Layer Meteorology,* 99**,** 225-248.

PANOFSKY, H. A. 1988. The Effect of Averaging Time on Velocity Variances. *Meteorology and Atmospheric Physics,* 38**,** 64-69.

PAPALE, D. 2012. Data Gap Filling. *In:* AUBINET, M., VESALA, T. & PAPALE, D. (eds.) *Eddy Covariance: A Practical Guide to Measurement and Data Analysis.* Dordrecht: Springer.

PAPALE, D., REICHSTEIN, M., AUBINET, M., CANFORA, E., BERNHOFER, C., KUTSCH, W., LONGDOZ, B., RAMBAL, S., VALENTINI, R., VESALA, T. & YAKIR, D. 2006. Towards a standardized processing of Net Ecosystem Exchange measured with eddy covariance technique: algorithms and uncertainty estimation. *Biogeosciences,* 3**,** 571-583.

PARRY, L. E., HOLDEN, J. & CHAPMAN, P. J. 2014. Restoration of blanket peatlands. *J Environ Manage,* 133**,** 193-205.

PATTEY, E., DESJARDINS, R. L. & ROCHETTE, P. 1993. Accuracy of the Relaxed Eddy-Accumulation Technique, Evaluated Using Co2 Flux Measurements. *Boundary-Layer Meteorology,* 66**,** 341-355.

PEDERSEN, A. R., PETERSEN, S. O. & SCHELDE, K. 2010. A comprehensive approach to soil-atmosphere trace-gas flux estimation with static chambers. *European Journal of Soil Science,* 61**,** 888-902.

PEICHL, M., OQUIST, M., LOFVENIUS, M. O., ILSTEDT, U., SAGERFORS, J., GRELLE, A., LINDROTH, A. & NILSSON, M. B. 2014. A 12-year record reveals pre-growing season temperature and water table level threshold effects on the net carbon dioxide exchange in a boreal fen. *Environmental Research Letters,* 9.

PELLETIER, L., GARNEAU, M. & MOORE, T. R. 2011. Variation in CO2 exchange over three summers at microform scale in a boreal bog, Eastmain region, Quebec, Canada. *Journal of Geophysical Research-Biogeosciences,* 116.

PELLETIER, L., STRACHAN, I. B., ROULET, N. T. & GARNEAU, M. 2015. Can boreal peatlands with pools be net sinks for CO2? *Environmental Research Letters,* 10.

PEYRON, O., GUIOT, J., CHEDDADI, R., TARASOV, P., REILLE, M., DE BEAULIEU, J. L., BOTTEMA, S. & ANDRIEU, V. 1998. Climatic reconstruction in Europe for 18,000 yr B.P. from pollen data. *Quaternary Research,* 49**,** 183-196.

PHILIP, J. R. 1963a. Damping of a Fluctuating Concentration by Continous Sampling through a Tube. *Australian Journal of Physics,* 16**,** 454-&.

PHILIP, J. R. 1963b. Theory of Dispersal during Laminar Flow in Tubes .1. *Australian Journal of Physics,* 16**,** 287-&.

PHILIP, J. R. 1963c. Theory of Dispersal during Laminar Flow in Tubes .2. *Australian Journal of Physics,* 16**,** 300-&.

POST, H., FRANSSEN, H. J. H., GRAF, A., SCHMIDT, M. & VEREECKEN, H. 2015. Uncertainty analysis of eddy covariance CO2 flux measurements for different EC tower distances using an extended two-tower approach. *Biogeosciences,* 12**,** 1205-1221.

POST, W. M. & KWON, K. C. 2000. Soil carbon sequestration and land-use change: processes and potential. *Global Change Biology,* 6**,** 317-327.

POST, W. M. E., W.R.; ZINKE P.J.; STANGENBERGER, A.G. 1982. Soil carbon pools and world life zones. *Nature,* 298**,** 156 - 159.

POYATOS, R., HEINEMEYER, A., INESON, P., EVANS, J. G., WARD, H. C., HUNTLEY, B. & BAXTER, R. 2014. Environmental and Vegetation Drivers of Seasonal CO2 Fluxes in a Sub-arctic Forest-Mire Ecotone. *Ecosystems,* 17**,** 377-393.

PRICE, J. S., HEATHWAITE, A. L. & BAIRD, A. J. 2003. Hydrological processes in abandoned and restored peatlands: An overview of management approaches. *Wetlands Ecology and Management,* 11**,** 65-83.

PRUDHOMME, C. & DAVIES, H. 2009. Assessing uncertainties in climate change impact analyses on the river flow regimes in the UK. Part 2: future climate. *Climatic Change,* 93**,** 197-222.

PUMPANEN, J., KOLARI, P., ILVESNIEMI, H., MINKKINEN, K., VESALA, T., NIINISTO, S., LOHILA, A., LARMOLA, T., MORERO, M., PIHLATIE, M., JANSSENS, I., YUSTE, J. C., GRUNZWEIG, J. M., RETH, S., SUBKE, J. A., SAVAGE, K., KUTSCH, W., OSTRENG, G., ZIEGLER, W., ANTHONI, P., LINDROTH, A. & HARI, P. 2004. Comparison of different chamber techniques for measuring soil CO2 efflux. *Agricultural and Forest Meteorology,* 123**,** 159-176.

QUINTY, F. & ROCHEFORT, L. 2003. Peatland Restoration Guide. Québec, Québec: Canadian Sphagnum Peat Moss Association and New Brunswick Department of Natural Resources and Energy.

RAICH, J. W. & POTTER, C. S. 1995. Global Patterns of Carbon-Dioxide Emissions from Soils. *Global Biogeochemical Cycles,* 9**,** 23-36.

RAICH, J. W. & SCHLESINGER, W. H. 1992. The Global Carbon-Dioxide Flux in Soil Respiration and Its Relationship to Vegetation and Climate. *Tellus Series B-Chemical and Physical Meteorology,* 44**,** 81-99.

RAICH, J. W. & TUFEKCIOGLU, A. 2000. Vegetation and soil respiration: Correlations and controls. *Biogeochemistry,* 48**,** 71-90.

RANNIK, U., ALTIMIR, N., RAITTILA, J., SUNI, T., GAMAN, A., HUSSEIN, T., HOLTTA, T., LASSILA, H., LATOKARTANO, M., LAURI, A., NATSHEH, A., PETAJA, T., SORJAMAA, R., YLA-MELLA, H., KERONEN, P., BERNINGER, F., VESALA, T., HARI, P. & KULMALA, M. 2002. Fluxes of carbon dioxide and water vapour over Scots pine forest and clearing. *Agricultural and Forest Meteorology,* 111**,** 187-202.

RANNIK, U., SOGACHEV, A. F., FOKEN, T., GÖCKEDE, M., KLJUN, N., LECLERC, M. Y. & VESALA, T. 2012. Footprint Analysis. *In:* AUBINET, M., VESALA, T. & PAPALE, D. (eds.) *Eddy Covariance: A Practical Guide to Measurement and Data Analysis.* Dordrecht: Springer.

RAUPACH, M. R., CANADELL, J. G. & LE QUERE, C. 2008. Anthropogenic and biophysical contributions to increasing atmospheric CO2 growth rate and airborne fraction. *Biogeosciences,* 5**,** 1601-1613.

REBA, M. L., LINK, T. E., MARKS, D. & POMEROY, J. 2009. An assessment of corrections for eddy covariance measured turbulent fluxes over snow in mountain environments. *Water Resources Research,* 45.

REBMANN, C., KOLLE, O., HEINESCH, B., QUECK, B., IBROM, A. & AUBINET, M. 2012. Data Acquistion and Flux Calculations. *In:* AUBINET, M., VESALA, T. & PAPALE, D. (eds.) *Eddy Covariance: A Practical Guide to Measurement and Data Analysis.* Dordrecht: Springer.

REDEKER, K. R., BAIRD, A. J. & TEH, Y. A. 2015. Quantifying wind and pressure effects on trace gas fluxes across the soil-atmosphere interface. *Biogeosciences,* 12**,** 7423-7434.

REICHSTEIN, M., FALGE, E., BALDOCCHI, D., PAPALE, D., AUBINET, M., BERBIGIER, P., BERNHOFER, C., BUCHMANN, N., GILMANOV, T., GRANIER, A., GRUNWALD, T., HAVRANKOVA, K., ILVESNIEMI, H., JANOUS, D., KNOHL, A., LAURILA, T., LOHILA, A., LOUSTAU, D., MATTEUCCI, G., MEYERS, T., MIGLIETTA, F., OURCIVAL, J.-M., PUMPANEN, J., RAMBAL, S., ROTENBERG, E., SANZ, M., TENHUNEN, J., SEUFERT, G., VACCARI, F., VESALA, T., YAKIR, D. & VALENTINI, R. 2005. On the separation of net ecosystem exchange into assimilation and ecosystem respiration: review and improved algorithm. *Global Change Biology,* 11**,** 1424-1439.

REICHSTEIN, M. & MOFFAT, A. M. 2014. REddyProc. *Data Processing and plotting utilities of (half-)hourly eddy covariance measurements.* R package version 0.6-0/r9 ed.

REN, X., SANDERS, J. E., RAJENDRAN, A., WEBER, R. J., GOLDSTEIN, A. H., PUSEDE, S. E., BROWNE, E. C., MIN, K. E. & COHEN, R. C. 2011. A relaxed eddy accumulation system for measuring vertical fluxes of nitrous acid. *Atmospheric Measurement Techniques,* 4**,** 2093-2103.

REVELLE, R. & SUESS, H. E. 1957. Carbon Dioxide Exchange between Atmosphere and Ocean and the Question of an Increase of Atmospheric Co2 during the Past Decades. *Tellus,* 9**,** 18-27.

REYNOLDS, O. 1895. On the dynamical theory of incompressible viscous fluids and determination of criterion. *Philosophical Transactions of the Royal Society of London,* A174**,** 935-982.

RICHARDSON, A. D., AUBINET, M., BARR, A. G., HOLLINGER, D., IBROM, A., LASSLOP, G. & REICHSTEIN, M. 2012. Uncertainty Quantification. *In:* AUBINET, M., VESALA, T. & PAPALE, D. (eds.) *Eddy Covariance: A Practical Guide to Measurement and Data Analsysis.* Dordrecht: Springer Atmospheric Sciences.

ROBINSON, M. & ARMSTRONG, A. C. 1988. The Extent of Agricultural Field Drainage in England and Wales, 1971-80. *Transactions of the Institute of British Geographers,* 13**,** 19-28.

ROCHEFORT, L., QUINTY, F., CAMPEAU, S., JOHNSON, K. & MALTERER, T. 2003. North American approach to the restoration of *Sphagnum* dominated peatlands. *Wetlands Ecology and Management,* 11**,** 3-20.

ROCHETTE, P. 2011. Towards a standard non-steady-state chamber methodology for measuring soil N2O emissions. *Animal Feed Science and Technology,* 166-67**,** 141-146.

ROULET, N. T., ASH, R., QUINTON, W. & MOORE, T. 1993. Methane Flux from Drained Northern Peatlands - Effect of a Persistent Water-Table Lowering on Flux. *Global Biogeochemical Cycles,* 7**,** 749-769.

ROULET, N. T., LAFLEUR, P. M., RICHARD, P. J. H., MOORE, T. R., HUMPHREYS, E. R. & BUBIER, J. 2007. Contemporary carbon balance and late Holocene carbon accumulation in a northern peatland. *Global Change Biology,* 13**,** 397-411.

RUNKLE, B. R. K., WILLE, C., GAZOVIC, M., WILMKING, M. & KUTZBACH, L. 2014. The surface energy balance and its drivers in a boreal peatland fen of northwestern Russia. *Journal of Hydrology,* 511**,** 359-373.

RUPPERT, J., MAUDER, M., THOMAS, C. & LUERS, J. 2006. Innovative gap-filling strategy for annual SUMS of CO2 net ecosystem exchange. *Agricultural and Forest Meteorology,* 138**,** 5-18.

RYDIN, H., GUNNARSON, U. & SUNDBERG, S. 2006. *The Role of Sphagnum in Peatland Development and Persistence*, Springer Berlin Heidelberg.

SAEKI, T., MAKSYUTOV, S., SASAKAWA, M., MACHIDA, T., ARSHINOV, M., TANS, P., CONWAY, T. J., SAITO, M., VALSALA, V., ODA, T., ANDRES, R. J. & BELIKOV, D. 2013. Carbon flux estimation for Siberia by inverse modeling constrained by aircraft and tower CO2 measurements. *Journal of Geophysical Research-Atmospheres,* 118**,** 1100-1122.

SAMARITANI, E., SIEGENTHALER, A., YLI-PETAYS, M., BUTTLER, A., CHRISTIN, P. A. & MITCHELL, E. A. D. 2011. Seasonal Net Ecosystem Carbon Exchange of a Regenerating Cutaway Bog: How Long Does it Take to Restore the C-Sequestration Function? *Restoration Ecology,* 19**,** 480-489.

SASAKAWA, M., MACHIDA, T., TSUDA, N., ARSHINOV, M., DAVYDOV, D., FOFONOV, A. & KRASNOV, O. 2013. Aircraft and tower measurements of CO2 concentration in the planetary boundary layer and the lower free troposphere over southern taiga in West Siberia: Long-term records from 2002 to 2011. *Journal of Geophysical Research-Atmospheres,* 118**,** 9489-9498.

SCHAEFER, K., LANTUIT, H., ROMANOVSKY, V. E., SCHUUR, E. A. G. & WITT, R. 2014. The impact of the permafrost carbon feedback on global climate. *Environmental Research Letters,* 9.

SCHARLEMANN, J. P. W., TANNER, E. V. J., HIEDERER, R. & KAPOS, V. 2014. Global soil carbon: understanding and managing the largest terrestrial carbon pool. *Carbon Management,* 5**,** 81-91.

SCHLESINGER, W. H. 1990. Evidence from Chronosequence Studies for a Low Carbon-Storage Potential of Soils. *Nature,* 348**,** 232-234.

SCHMID, H. P., GRIMMOND, C. S. B., CROPLEY, F., OFFERLE, B. & SU, H. B. 2000. Measurements of CO2 and energy fluxes over a mixed hardwood forest in the mid-western United States. *Agricultural and Forest Meteorology,* 103**,** 357-374.

SCHULZE, E. D., LLOYD, J., KELLIHER, F. M., WIRTH, C., REBMANN, C., LUHKER, B., MUND, M., KNOHL, A., MILYUKOVA, I. M., SCHULZE, W., ZIEGLER, W., VARLAGIN, A. B., SOGACHEV, A. F., VALENTINI, R., DORE, S., GRIGORIEV, S., KOLLE, O., PANFYOROV, M. I., TCHEBAKOVA, N. & VYGODSKAYA, N. N. 1999. Productivity of forests in the Eurosiberian boreal region and their potential to act as a carbon sink - a synthesis. *Global Change Biology,* 5**,** 703-722.

SCHUUR, E. A. G., MCGUIRE, A. D., SCHADEL, C., GROSSE, G., HARDEN, J. W., HAYES, D. J., HUGELIUS, G., KOVEN, C. D., KUHRY, P., LAWRENCE, D. M., NATALI, S. M., OLEFELDT, D., ROMANOVSKY, V. E., SCHAEFER, K., TURETSKY, M. R., TREAT, C. C. & VONK, J. E. 2015. Climate change and the permafrost carbon feedback. *Nature,* 520**,** 171-179.

SCOTLAND, N. R. F. 2013. *Scotland's Census Shaping our future* [Online]. National Records for Scotland. Available: http://www.scotlandscensus.gov.uk/ods-web/datavis.jsp?theme=Population_v4_September_2013 [Accessed 10/08/2015 2015].

SHAVER, G. R., STREET, L. E., RASTETTER, E. B., VAN WIJK, M. T. & WILLIAMS, M. 2007. Functional convergence in regulation of net CO2flux in heterogeneous tundra landscapes in Alaska and Sweden. *Journal of Ecology,* 95**,** 802-817.

SHEPPARD, P. A. 1947. The Aerodynamic Drag of the Earths Surface and the Value of Vonkarman Constant in the Lower Atmosphere. *Proceedings of the Royal Society of London Series a-Mathematical and Physical Sciences,* 188**,** 208-&.

SHOTYK, W. 1996. Natural and anthropogenic enrichments of As, Cu, Pb, Sb, and Zn in ombrotrophic versus minerotrophic peat bog profiles, Jura Mountains, Switzerland. *Water Air and Soil Pollution,* 90**,** 375-405.

SILVOLA, J., ALM, J., AHLHOLM, U., NYKANEN, H. & MARTIKAINEN, P. J. 1996a. CO2 fluxes from peat in boreal mires under varying temperature and moisture conditions. *Journal of Ecology,* 84**,** 219-228.

SILVOLA, J., ALM, J., AHLHOLM, U., NYKANEN, H. & MARTIKAINEN, P. J. 1996b. The contribution of plant roots to CO(2) fluxes from organic soils. *Biology and Fertility of Soils,* 23**,** 126 - 131.

SIMS, D. A., RAHMAN, A. F., CORDOVA, V. D., EL-MASRI, B. Z., BALDOCCHI, D. D., BOLSTAD, P. V., FLANAGAN, L. B., GOLDSTEIN, A. H., HOLLINGER, D. Y., MISSON, L., MONSON, R. K., OECHEL, W. C., SCHMID, H. P., WOFSY, S. C. & XU, L. 2008. A new model of gross primary productivity for North American ecosystems based solely on the enhanced vegetation index and land surface temperature from MODIS. *Remote Sensing of Environment,* 112**,** 1633-1646.

SMALLMAN, T. L., WILLIAMS, M. & MONCRIEFF, J. B. 2014. Can seasonal and interannual variation in landscape CO₂ fluxes be detected by atmospheric observations of CO₂ concentrations made at a tall tower? *Biogeosciences,* 11**,** 735-747.

SMITH, P., LANIGAN, G., KUTSCH, W. L., BUCHMANN, N., EUGSTER, W., AUBINET, M., CESCHIA, E., BEZIAT, P., YELURIPATI, J. B., OSBORNE, B., MOORS, E. J., BRUT, A., WATTENBACH, M., SAUNDERS, M. & JONES, M. 2010. Measurements necessary for assessing the net ecosystem carbon budget of croplands. *Agriculture Ecosystems & Environment,* 139**,** 302-315.

SNH 2005. The Peatlands of Caithness and Sutherland: Management Strategy 2005 - 2015. Scottish Natural Heritage.

SNH 2015. Scotland's National Peatland Plan: Working for our future. Edinburgh.

SOLOMON, S., PLATTNER, G. K., KNUTTI, R. & FRIEDLINGSTEIN, P. 2009. Irreversible climate change due to carbon dioxide emissions. *Proceedings of the National Academy of Sciences of the United States of America,* 106**,** 1704-1709.

SOLOMON, S., QIN, D., MANNING, M., CHEN, Z., MARQUIS, M., AVERYT, K. B., TIGNOR, M. & MILLER, H. L. 2007. Climate Change 2007: The Physical Science Basis: Contribution of working group I to the fourth assessment report of the intergovernmental panel on climate change. *In:* SOLOMON, S., QIN, D., MANNING, M., CHEN, Z., MARQUIS, M., AVERYT, K. B., TIGNOR, M. & MILLER, H. L. (eds.).

SOTTOCORNOLA, M. & KIELY, G. 2010. Hydro-meteorological controls on the CO2 exchange variation in an Irish blanket bog. *Agricultural and Forest Meteorology,* 150**,** 287-297.

SPERRY, J. S. 2000. Hydraulic constraints on plant gas exchange. *Agricultural and Forest Meteorology,* 104**,** 13-23.

STEFFENSEN, J. P., ANDERSEN, K. K., BIGLER, M., CLAUSEN, H. B., DAHL-JENSEN, D., FISCHER, H., GOTO-AZUMA, K., HANSSON, M., JOHNSEN, S. J., JOUZEL, J., MASSON-DELMOTTE, V., POPP, T., RASMUSSEN, S. O., ROTHLISBERGER, R., RUTH, U., STAUFFER, B., SIGGAARD-ANDERSEN, M. L., SVEINBJORNSDOTTIR, A. E., SVENSSON, A. & WHITE, J. W. C. 2008. High-resolution Greenland Ice Core data show abrupt climate change happens in few years. *Science,* 321**,** 680-684.

STELLA, P., KORTNER, M., AMMANN, C., FOKEN, T., MEIXNER, F. X. & TREBS, I. 2013. Measurements of nitrogen oxides and ozone fluxes by eddy covariance at a meadow: evidence for an internal leaf resistance to NO2. *Biogeosciences,* 10**,** 5997-6017.

STERN, N. 2007. *The Economics of Climate Change: The Stern Review,* Cambridge University Press.

STOCKER, T. F., QIN, D., PLATTNER, G.-K., TIGNOR, M., ALLEN, S. K., BOSCHUNG, J., NAUELS, A., XIA, Y., BEX, V. & MIDGLEY, P. M. 2013. *Climate Change 2013: The Physical Science Basis. Contribution of Working Group 1 to the Fifth Assessment Report of the Intergovernmental Panel on Climate Change,* Cambridge, United Kingdom and New York, NY, USA, Cambridge University Press.

STOWASSER, C., FARINAS, A. D., WARE, J., WISTISEN, D. W., RELLA, C., WAHL, E., CROSSON, E. & BLUNIER, T. 2014. A low-volume cavity ring-down spectrometer for sample-limited applications. *Applied Physics B-Lasers and Optics,* 116**,** 255-270.

STRACK, M., CAGAMPAN, J., HASSANPOUR FARD, G., KEITH, A. M., NUGENT, K., RANKIN, T., ROBINSON, C., STRACHAN, I. B., WADDINGTON, J. M. & XU, B. 2016. Controls on plot-scale growing season CO2 and CH4 fluxes in restored peatlands: Do they differ from unrestored and natural sites? *Mires and Peat,* 17**,** 1-18.

STRACK, M., KEITH, A. M. & XU, B. 2014. Growing season carbon dioxide and methane exchange at a restored peatland on the Western Boreal Plain. *Ecological Engineering,* 64**,** 231-239.

STRACK, M. & WADDINGTON, J. M. 2007. Response of peatland carbon dioxide and methane fluxes to a water table drawdown experiment. *Global Biogeochemical Cycles,* 21.

STRACK, M., WADDINGTON, J. M., LUCCHESE, M. C. & CAGAMPAN, J. P. 2009. Moisture controls on CO2 exchange in a Sphagnum-dominated peatland: results from an extreme drought field experiment. *Ecohydrology,* 2**,** 454-461.

STRACK, M. & ZUBACK, Y. C. A. 2013. Annual carbon balance of a peatland 10 yr following restoration. *Biogeosciences,* 10**,** 2885-2896.

STREET, L. E., SHAVER, G. R., WILLIAMS, M. & VAN WIJK, M. T. 2007. What is the relationship between changes in canopy leaf area and changes in photosynthetic CO2 flux in arctic ecosystems? *Journal of Ecology,* 95**,** 139-150.

STREET, L. E., SUBKE, J. A., SOMMERKORN, M., SLOAN, V., DUCROTOY, H., PHOENIX, G. K. & WILLIAMS, M. 2013. The role of mosses in carbon uptake and partitioning in arctic vegetation. *New Phytologist,* 199**,** 163-175.

STRILESKY, S. L. & HUMPHREYS, E. R. 2012. A comparison of the net ecosystem exchange of carbon dioxide and evapotranspiration for treed and open portions of a temperate peatland. *Agricultural and Forest Meteorology,* 153**,** 45-53.

STROUD, D. A., REED, T. M., PIENKOWSKI, M. W. & LINDSAY, R. A. 1987. Birds, Bogs and Forestry : the peatlands of Caithness and Sutherland. *Peterborough: Nature Conservancy council.*

STULL, R. B. 1988. *An Introduction to Boundary Layer Meteorology,* Dordrecht, Kluwer Academic.

SWINBANK, W. C. 1951. The Measurement of Vertical Transfer of Heat and Water Vapor by Eddies in the Lower Atmosphere. *Journal of Meteorology,* 8**,** 135-145.

SYED, K. H., FLANAGAN, L. B., CARLSON, P. J., GLENN, A. J. & VAN GAALEN, K. E. 2006. Environmental control of net ecosystem CO2 exchange in a treed, moderately rich fen in northern Alberta. *Agricultural and Forest Meteorology,* 140**,** 97-114.

TARNOCAI, C., CANADELL, J. G., SCHUUR, E. A. G., KUHRY, P., MAZHITOVA, G. & ZIMOV, S. 2009. Soil organic carbon pools in the northern circumpolar permafrost region. *Global Biogeochemical Cycles,* 23.

TAUB, D. 2010. Effects of Rising Atmospheric Concentrations of Carbon Dioxide on Plants. *Nature Education Knowledge,* 3.

TEH, Y. A., DIEM, T., JONES, S., HUARACA QUISPE, L. P., BAGGS, E., MORLEY, N., RICHARDS, M., SMITH, P. & MEIR, P. 2014. Methane and nitrous oxide fluxes across an elevation gradient in the tropical Peruvian Andes. *Biogeosciences,* 11**,** 2325-2339.

TEH, Y. A., SILVER, W. L., SONNENTAG, O., DETTO, M., KELLY, M. & BALDOCCHI, D. D. 2011. Large Greenhouse Gas Emissions from a Temperate Peatland Pasture. *Ecosystems,* 14**,** 311-325.

THOMAS, S. M., WHITEHEAD, D., ADAMS, J. A., REID, J. B., SHERLOCK, R. R. & LECKIE, A. C. 1996. Seasonal root distribution and soil surface carbon fluxes for one-year-old Pinus radiata trees growing at ambient and elevated carbon dioxide concentration. *Tree Physiology,* 16**,** 1015-1021.

TOUCHETTE, B. W., IANNACONE, L. R., TURNER, G. & FRANK, A. 2010. Ecophysiological responses of five emergent-wetland plants to diminished water supply: an experimental microcosm study. *Aquatic Ecology,* 44**,** 101-112.

TREWIN, N. H. 2003. *The Geology of Scotland,* Oxford, The Geological Society of London.

TUITTILA, E. S., KOMULAINEN, V. M., VASANDER, H. & LAINE, J. 1999. Restored cut-away peatland as a sink for atmospheric CO2. *Oecologia,* 120**,** 563-574.

TURETSKY, M. R. 2003. The role of bryophytes in carbon and nitrogen cycling. *Bryologist,* 106**,** 395-409.

TWINE, T. E., KUSTAS, W. P., NORMAN, J. M., COOK, D. R., HOUSER, P. R., MEYERS, T. P., PRUEGER, J. H., STARKS, P. J. & WESELY, M. L. 2000. Correcting eddy-covariance flux underestimates over a grassland. *Agricultural and Forest Meteorology,* 103**,** 279-300.

UEYAMA, M., HIRATA, R., MANO, M., HAMOTANI, K., HARAZONO, Y., HIRANO, T., MIYATA, A., TAKAGI, K. & TAKAHASHI, Y. 2012. Influences of various calculation options on heat, water and carbon fluxes determined by open- and closed-path eddy covariance methods. *Tellus Series B-Chemical and Physical Meteorology,* 64.

UPDEGRAFF, K., BRIDGHAM, S. D., PASTOR, J., WEISHAMPEL, P. & HARTH, C. 2001. Response of CO2 and CH4 emissions from peatlands to warming and water table manipulation. *Ecological Applications,* 11**,** 311-326.

VALENTINI, R., MATTEUCCI, G., DOLMAN, A. J., SCHULZE, E. D., REBMANN, C., MOORS, E. J., GRANIER, A., GROSS, P., JENSEN, N. O., PILEGAARD, K., LINDROTH, A., GRELLE, A., BERNHOFER, C., GRUNWALD, T., AUBINET, M., CEULEMANS, R., KOWALSKI, A. S., VESALA, T., RANNIK, U., BERBIGIER, P., LOUSTAU, D., GUOMUNDSSON, J., THORGEIRSSON, H., IBROM, A., MORGENSTERN, K., CLEMENT, R., MONCRIEFF, J., MONTAGNANI, L., MINERBI, S. & JARVIS, P. G. 2000. Respiration as the main determinant of carbon balance in European forests. *Nature,* 404**,** 861-865.

VAN DE WIEL, B. J. H., MOENE, A. F., JONKER, H. J. J. & CLERCX, H. J. H. 2011. The collapse of turbulence in the atmospheric boundary layer. *13th European Turbulence Conference (Etc13): Instability, Transition, Grid Turbulence and Jets,* 318.

VAN DIJK, A. I. J. M. & DOLMAN, A. J. 2004. Estimates of CO2 uptake and release among European forests based on eddy covariance data. *Global Change Biology,* 10**,** 1445-1459.

VAN GORSEL, E., LEUNING, R., CLEUGH, H. A., KEITH, H. & SUNI, T. 2007. Nocturnal carbon efflux: reconciliation of eddy covariance and chamber measurements using an alternative to the u(*)-threshold filtering technique. *Tellus Series B-Chemical and Physical Meteorology,* 59**,** 397-403.

VERMA, S. B., KIM, J. & CLEMENT, R. J. 1989. Carbon-Dioxide, Water-Vapor and Sensible Heat Fluxes over a Tallgrass Prairie. *Boundary-Layer Meteorology,* 46**,** 53-67.

VICKERS, D. & MAHRT, L. 1997. Quality control and flux sampling problems for tower and aircraft data. *Journal of Atmospheric and Oceanic Technology,* 14**,** 512-526.

WADDINGTON, J. M., GRIFFIS, T. J. & ROUSE, W. R. 1998. Northern Canadian wetlands: Net ecosystem CO2 exchange and climatic change. *Climatic Change,* 40**,** 267-275.

WADDINGTON, J. M., LUCCHESE, M. C. & DUVAL, T. P. 2011. Sphagnum moss moisture retention following the re-vegetation of degraded peatlands. *Ecohydrology,* 4**,** 359-366.

WADDINGTON, J. M. & PRICE, J. S. 2000. Effect of peatland drainage, harvesting, and restoration on atmospheric water and carbon exchange. *Physical Geography,* 21**,** 433-451.

WADDINGTON, J. M., ROTENBERG, P. A. & WARREN, F. J. 2001. Peat CO2 production in a natural and cutover peatland: Implications for restoration. *Biogeochemistry,* 54**,** 115-130.

WADDINGTON, J. M., STRACK, M. & GREENWOOD, M. J. 2010. Toward restoring the net carbon sink function of degraded peatlands: Short-term response in CO2 exchange to ecosystem-scale restoration. *Journal of Geophysical Research-Biogeosciences,* 115.

WADDINGTON, J. M. & WARNER, K. D. 2001. Atmospheric CO2 sequestration in restored mined peatlands. *Ecoscience,* 8**,** 359-368.

WADDINGTON, J. M., WARNER, K. D. & KENNEDY, G. W. 2002. Cutover peatlands: A persistent source of atmospheric CO2. *Global Biogeochemical Cycles,* 16**,** 1-7.

WALKER, T. N., GARNETT, M. H., WARD, S. E., OAKLEY, S., BARDGETT, R. D. & OSTLE, N. 2016. Vascular plants promote ancient peatland carbon loss with climate warming. *Global Change Biology,* 22**,** 1880 - 1889.

WANG, H., PRENTICE, I. C. & DAVIS, T. W. 2014. Biophysical constraints on gross primary production by the terrestrial biosphere. *Biogeosciences,* 11**,** 5987 - 6991.

WANG, K., LIU, C., ZHENG, X., PIHLATIE, M., LI, B., HAAPANALA, S., VESALA, T., LIU, H., WANG, Y., LIU, G. & HU, F. 2013. Comparison between eddy covariance and automatic chamber techniques for measuring net ecosystem exchange of carbon dioxide in cotton and wheat fields. *Biogeosciences,* 10**,** 6865-6877.

WANG, X. W., LI, X. Z., HU, Y. M., LV, J. J., SUN, J., LI, Z. M. & WU, Z. F. 2010. Effect of temperature and moisture on soil organic carbon mineralization of predominantly permafrost peatland in the Great Hing'an Mountains, Northeastern China. *Journal of Environmental Sciences,* 22**,** 1057-1066.

WARD, S. E., BARDGETT, R. D., MCNAMARA, N. P., ADAMSON, J. K. & OSTLE, N. 2007. Long-Term Consequences of Grazing and Burning on Northern Peatland Carbon Dynamics. *Ecosystems,* 10**,** 1069-1083.

WARD, S. E., BARDGETT, R. D., MCNAMARA, N. P. & OSTLE, N. J. 2009. Plant functional group identity influences short-term peatland ecosystem carbon flux: evidence from a plant removal experiment. *Functional Ecology,* 23**,** 454-462.

WARD, S. E., OSTLE, N. J., OAKLEY, S., QUIRK, H., HENRYS, P. A. & BARDGETT, R. D. 2013. Warming effects on greenhouse gas fluxes in peatlands are modulated by vegetation composition. *Ecol Lett,* 16**,** 1285-93.

WARREN, C. 2000. 'Birds, bogs and forestry' revisited: The significance of the flow country controversy. *Scottish Geographical Journal,* 116**,** 315 - 337.

WEBB, E. K., PEARMAN, G. I. & LEUNING, R. 1980. Correction of Flux Measurements for Density Effects Due to Heat and Water-Vapor Transfer. *Quarterly Journal of the Royal Meteorological Society,* 106**,** 85-100.

WELTZIN, J. F., PASTOR, J., HARTH, C., BRIDGHAM, S. D., UPDEGRAFF, K. & CHAPIN, C. T. 2000. Response of bog and fen plant communities to warming and water-table manipulations. *Ecology,* 81**,** 3464-3478.

WILCZAK, J. M., ONCLEY, S. P. & STAGE, S. A. 2001. Sonic anemometer tilt correction algorithms. *Boundary-Layer Meteorology,* 99**,** 127-150.

WILLIAMS, M. & RASTETTER, E. B. 1999. Vegetation characteristics and primary productivity along an arctic transect: implications for scaling-up. *Journal of Ecology,* 87**,** 885-898.

WILSON, J. D., ANDERSON, R., BAILEY, S., CHETCUTI, J., COWIE, N. R., HANCOCK, M. H., QUINE, C. P., RUSSELL, N., STEPHEN, L. & THOMPSON, D. B. A. 2014. Modelling edge effects of mature forest plantations on peatland waders informs landscape-scale conservation. *Journal of Applied Ecology,* 51**,** 204-213.

WILSON, K., GOLDSTEIN, A., FALGE, E., AUBINET, M., BALDOCCHI, D., BERBIGIER, P., BERNHOFER, C., CEULEMANS, R., DOLMAN, H., FIELD, C., GRELLE, A., IBROM, A., LAW, B. E., KOWALSKI, A., MEYERS, T., MONCRIEFF, J., MONSON, R., OECHEL, W., TENHUNEN, J., VALENTINI, R. & VERMA, S. 2002. Energy balance closure at FLUXNET sites. *Agricultural and Forest Meteorology,* 113**,** 223-243.

WILSON, R., ANCHUKAITIS, K., BRIFFA, K. R., BUNTGEN, U., COOK, E., D'ARRIGO, R., DAVI, N., ESPER, J., FRANK, D., GUNNARSON, B., HEGERL, G., HELAMA, S., KLESSE, S., KRUSIC, P. J., LINDERHOLM, H. W., MYGLAN, V., OSBORN, T. J., RYDVAL, M., SCHNEIDER, L., SCHURER, A., WILES, G., ZHANG, P. & ZORITA, E. 2016. Last millennium northern hemisphere summer temperatures from tree rings: Part I: The long term context. *Quaternary Science Reviews,* 134**,** 1-18.

WINDERLICH, J., GERBIG, C., KOLLE, O. & HEIMANN, M. 2014. Inferences from CO2 and CH4 concentration profiles at the Zotino Tall Tower Observatory (ZOTTO) on regional summertime ecosystem fluxes. *Biogeosciences,* 11**,** 2055-2068.

WOHLFAHRT, G., HAMMERLE, A., HASLWANTER, A., BAHN, M., TAPPEINER, U. & CERNUSCA, A. 2008. Disentangling leaf area and environmental effects on the response of the net ecosystem CO2 exchange to diffuse radiation. *Geophysical Research Letters,* 35.

WOHLFAHRT, G., HORTNAGL, L., HAMMERLE, A., GRAUS, M. & HANSEL, A. 2009. Measuring eddy covariance fluxes of ozone with a slow-response analyser. *Atmospheric Environment,* 43**,** 4570-4576.

WOLFENDEN, J. & DIGGLE, P. J. 1995. Canopy Gas-Exchange and Growth of Upland Pasture Swards in Elevated Co2. *New Phytologist,* 130**,** 369-380.

WORRALL, F., CHAPMAN, P. J., HOLDEN, J., EVANS, C., ARTZ, R. R. E., SMITH, P. & GRAYSON, R. 2010. Peatlands and Climate Change. *Report to the IUCN UK Peatland Programme.* Edinburgh.

WRIGHT, E. L., BLACK, C. R., TURNER, B. L. & SJOGERSTEN, S. 2013. Environmental controls of temporal and spatial variability in CO2 and CH4 fluxes in a neotropical peatland. *Global Change Biology,* 19**,** 3775-3789.

XU, Z. Z. & ZHOU, G. S. 2011. Responses of photosynthetic capacity to soil moisture gradient in perennial rhizome grass and perennial bunchgrass. *Bmc Plant Biology,* 11.

YAMAMOTO, Y., KITAHARA, N. & KANO, M. 2012. Long memory effect of past climate change in Vostok ice core records. *Thermochimica Acta,* 532**,** 41-44.

YU, Z. C. 2006. Holocene carbon accumulation of fen peatlands in boreal western Canada: A complex ecosystem response to climate variation and disturbance. *Ecosystems,* 9**,** 1278-1288.

YU, Z. C. 2012. Northern peatland carbon stocks and dynamics: a review. *Biogeosciences,* 9**,** 4071-4085.

YUAN, W. P., LUO, Y. Q., RICHARDSON, A. D., OREN, R., LUYSSAERT, S., JANSSENS, I. A., CEULEMANS, R., ZHOU, X. H., GRUNWALD, T., AUBINET, M., BERHOFER, C., BALDOCCHI, D. D., CHEN, J. Q., DUNN, A. L., DEFOREST, J. L., DRAGONI, D., GOLDSTEIN, A. H., MOORS, E., MUNGER, J. W., MONSON, R. K., SUYKER, A. E., STAR, G., SCOTT, R. L., TENHUNEN, J., VERMA, S. B., VESALA, T. & WOFSY, S. C. 2009. Latitudinal patterns of magnitude and interannual variability in net ecosystem exchange regulated by biological and environmental variables. *Global Change Biology,* 15**,** 2905-2920.

YVON-DUROCHER, G., CAFFREY, J. M., CESCATTI, A., DOSSENA, M., DEL GIORGIO, P., GASOL, J. M., MONTOYA, J. M., PUMPANEN, J., STAEHR, P. A., TRIMMER, M., WOODWARD, G. & ALLEN, A. P. 2012. Reconciling the temperature dependence of respiration across timescales and ecosystem types. *Nature,* 487**,** 472-476.

ZACHOS, J. C., DICKENS, G. R. & ZEEBE, R. E. 2008. An early Cenozoic perspective on greenhouse warming and carbon-cycle dynamics. *Nature,* 451**,** 279-283.

ZHANG, J. L., POORTER, L. & CAO, K. F. 2012. Productive leaf functional traits of Chinese savanna species. *Plant Ecology,* 213**,** 1449-1460.

ZHANG, L. M., YU, G. R., SUN, X. M., WEN, X. F., REN, C. Y., FU, Y. L., LI, Q. K., LI, Z. Q., LIU, Y. F., GUAN, D. X. & YAN, J. H. 2006. Seasonal variations of ecosystem apparent quantum yield (alpha) and maximum photosynthesis rate (P-max) of different forest ecosystems in China. *Agricultural and Forest Meteorology,* 137**,** 176-187.

ZHANG, Q., KATUL, G. G., OREN, R., DALY, E., MANZONI, S. & YANG, D. W. 2015. The hysteresis response of soil CO2 concentration and soil respiration to soil temperature. *Journal of Geophysical Research - Biogeosciences,* 120**,** 1605 - 1618.

ZHANG, S. F., WYNGAARD, J. C., BUSINGER, J. A. & ONCLEY, S. P. 1986. Response Characteristics of the UW Sonic Anemometer. *Journal of Atmospheric and Oceanic Technology,* 3**,** 315-323.

ZINNERT, J. C., SHIFLETT, S. A., VICK, J. K. & YOUNG, D. R. 2013. Plant functional traits of a shrub invader relative to sympatric native shrubs. *Ecosphere,* 4.

Appendix A

CO_2/H_2O Analyser Calibration Co-efficients

A1 – Talaheel LI-7500

This appendix provides details of the calibrations applied to the LICOR Biosciences LI-7500 open-path CO_2/H_2O gas analyser at Talaheel. Institutional constraints limited calibration of the analyser at a desired frequency over the course of the study. However, open-path analysers are known to be stable for long periods of time therefore longer periods between calibrations are acceptable. Due to the lack of a dew point generator only the CO_2 zero and span was calibrated. Both the zero and span were calibrated using certified standard gases. Dry, CO_2 free (certified to ±1%) research grade Nitrogen (N_2) was used (BOC Gases, Guildford, UK) for the zero gas, while the span was calibrated using CO_2 certified at 432ppm (BOC Gases, Guildford, UK). The H_2O channel was left at the factory pre-set value.

Table A1 Calibration coefficients for the LI-7500 open path CO_2/H_2O gas analyser at Talaheel

	CO_2 Channel		**H_2O Channel**	
Date	**Zero**	**Span**	**Zero**	**Span**
19/03/2014	0.87	0.98	0.76	0.94
16/04/2014	0.86	0.98	0.76	0.94
20/05/2014	0.84	0.99	0.76	0.94
16/09/2014	0.87	0.98	0.76	0.94
18/11/2014	0.85	1.01	0.76	0.94

19/01/2015	0.86	0.99	0.76	0.94
10/03/2015	0.89	1.01	0.76	0.94

The first field calibration of the sensor was carried out on the 19th March and caused only a small change in the calibration of the LI7500 of 0.2 ppm. After installation, strange values were noted in CO_2 readings, in conditions where you would not normally expect to see erroneous data. It was deduced that this may possibly be caused by condensation in the analyser head and that the internal chemicals were exhausted. The internal chemicals were replaced on the 15th April and after 24 hours the system checked and re-calibrated. Calibrations were then carried out approximately every 2-3 months (Table A1). Analyser windows were cleaned using isopropyl alcohol during every field visit and a water repellent (RainX, ITW Global, Houston, TX) applied to help aid water run off the analyser window, reducing the amount of downtime caused by precipitation.

A2 – Lonielist LI-7200

This appendix provides details of the corrections applied to the LICOR Biosciences LI-7200 enclosed-path CO_2/H_2O analyser at Lonielist. As this analyser was brand new at the time of setting up the factory calibration was accepted.

A3 – Cross Lochs EC150

This appendix provides details of the calibrations applied to the Campbell Scientific EC150 open-path CO_2/H_2O analyser at Cross Lochs. Similarly to Lonielist this was a new sensor that was put on the flux tower in February 2014. A zero-and-span procedure was carried out when the analyser was first installed in February 2014; however, due to institutional and equipment constraints it was not possible to carry out further calibrations of this analyser during the measurement period. The zero-and-span procedure was carried out using certified dry, CO_2 free (certified to ±1%) Nitrogen (BOC Gases, Guildford, UK). The span was calibrated using CO_2 certified at 400 ppm (BOC Gases, Guildford, UK). Similarly to Talaheel due to the lack of a dew point generator, the H_2O channel was left at the factory pre-set value.

	CO_2 Channel		**H_2O Channel**	
Date	**Zero**	**Span**	**Zero**	**Span**
20/02/2014	1.03	0.96	0.99	0.97

Analyser windows were cleaned at every field visit using isopropyl alcohol and a water repellent (RainX, ITW Global, Houston, TX) applied to help aid water run off the analyser window, reducing the amount of downtime caused by precipitation.

Appendix B

Flux Processing Protocol

This provides the processing list used in EdiRE (University of Edinburgh, Edinburgh, UK) to process raw data to fully processed fluxes. Although this process list is specifically for the Talaheel flux tower, the same processing protocols were employed at Cross Lochs and Lonielist.

Extract
Channel = 9
Label for Signal = Ux
Extract
Channel = 10
Label for Signal = Uy
Extract
Channel = 11
Label for Signal = Uz
Extract
Channel = 12
Label for Signal = Ts
Extract
Channel = 13
Label for Signal = Ds
Extract
Channel = 14
Label for Signal = VSolar
Extract
Channel = 15
Label for Signal = AirTC
Extract

Channel = 16
Label for Signal = e_hmp
Extract
Channel = 17
Label for Signal = CO2_LI7500
Extract
Channel = 18
Label for Signal = H2O_LI7500
Extract
Channel = 19
Label for Signal = Press_LI7500
Extract
Channel = 20
Label for Signal = irga_diag
Comments
Comment = Correct CSAT transducer wind shadowing. Based on 2015 and Horst 2006
1 chn statistics
Signal = Ux
Storage Label Mean = Ux_uncorr
Storage Label Std Dev = Ux_uncorr_std
1 chn statistics
Signal = Uy
Storage Label Mean = Uy_uncorr
Storage Label Std Dev = Uy_uncorr_std
1 chn statistics
Signal = Uz
Storage Label Mean = Uz_uncorr
Storage Label Std Dev = Uz_uncorr_std
Extract
Channel = 9
Label for Signal = Ua
Extract
Channel = 10
Label for Signal = Ub
Extract
Channel = 11
Label for Signal = Uc
Extract
Channel = 11
Label for Signal = theta
Extract
Channel = 11
Label for Signal = thetaB
Extract
Channel = 11
Label for Signal = thetaC
User defined fast
*Equation = -Ux*COS(3.14/3)+Uz*SIN(3.14/3)*
Number of signals = 3
Signal = Ua
Signal = Ux
Signal = Uz
User defined fast
*Equation = ((Ux+SQRT(3)*Uy)/2)*COS(3.14/3)+Uz*SIN(3.14/3)*
Number of signals = 4
Signal = Ub
Signal = Ux
Signal = Uy

Signal = Uz
User defined fast
*Equation = ((Ux-SQRT(3)*Uy)/2)*COS(3.14/3)+Uz*SIN(3.14/3)*
Number of signals = 4
Signal = Uc
Signal = Ux
Signal = Uy
Signal = Uz
User defined fast
Equation = ACOS(Ua/(SQRT(Ux^2+Uy^2+Uz^2)))
Number of signals = 5
Signal = theta
Signal = Ua
Signal = Ux
Signal = Uy
Signal = Uz
User defined fast
Equation = ACOS(Ub/(SQRT(Ux^2+Uy^2+Uz^2)))
Number of signals = 5
Signal = thetaB
Signal = Ub
Signal = Ux
Signal = Uy
Signal = Uz

User defined fast
Equation = ACOS(Uc/(SQRT(Ux^2+Uy^2+Uz^2)))
Number of signals = 5
Signal = thetaC
Signal = Uc
Signal = Ux
Signal = Uy
Signal = Uz
User defined fast
*Equation = Ua/(0.84+0.16*sin(thetaA))*
Number of signals = 2
Signal = Ua
Signal = theta
User defined fast
*Equation = Ub/(0.84+0.16*sin(thetaB))*
Number of signals = 2
Signal = Ub
Signal = thetaB
User defined fast
*Equation = Uc/(0.84+0.16*sin(thetaC))*
Number of signals = 2
Signal = Uc
Signal = thetaC
User defined fast
*Equation = (-2*Ua +Ub+Uc)/(3*cos(3.14/3))*
Number of signals = 4
Signal = Ux
Signal = Ua
Signal = Ub
Signal = Uc
User defined fast
*Equation = (Ub-Uc)/(sqrt(3)*cos(3.14/3))*

Number of signals = 4
Signal = Uy
Signal = Ua
Signal = Ub
Signal = Uc
User defined fast
*Equation = (Ua +Ub+Uc)/(3*sin(3.14/3))*
Number of signals = 4
Signal = Uz
Signal = Ua
Signal = Ub
Signal = Uc
1 chn statistics
Signal = Ux
Storage Label Mean = Ux_corr
1 chn statistics
Signal = Uy
Storage Label Mean = Uy_corr
1 chn statistics
Signal = Uz
Storage Label Mean = Uz_corr
Storage Label Std Dev = Uz_std_corr
Plot Value
Left Axis Value = Ux_corr
Right Axis Value = Ux_uncorr
Match Left/Right Axes = x
Plot Value
Left Axis Value = Uy_corr
Right Axis Value = Uy_uncorr
Match Left/Right Axes = x
Plot Value
Left Axis Value = Uz_corr
Right Axis Value = Uz_uncorr
Match Left/Right Axes = x
Plot Value
Left Axis Value = Uz_std_corr
Right Axis Value = Uz_std_uncorr
Match Left/Right Axes = x
Comments
Comment = Calculate RH from hmp
Comment = Coefficients for the sixth order approximating saturation vapor pressure ploynomial (Lowe, Paul R., 1977.: An approximating ploynomial for computation of saturation vapor pressure, J. Appl. Metoer., 16, 100-103).
Extract
Channel = 16
Label for Signal = RH_hmp
Extract
Channel = 15
Label for Signal = T_hmp
1 chn statistics
Signal = RH_hmp
Storage Label Mean = mean_RH_hmp
Gas conversion time series
Signal = CO2_LI7500
Convert from = Molar density mmol/m3
Convert to = Concentration umol/mol
1st Offset = 0
1st Gain = 1

1st Curvature = 0
Signal T, C = AirTC
Signal P, kPa = Press_LI7500
Value P, kPa =
Signal H2O = H2O_LI750
Units H2O = Molar density mmol/m3
Molecular Weight = 44
2nd Offset = 0
2nd Gain = 1
2nd Curvature =
1 chn statistics
Signal = CO2_LI7500
Storage Label Mean = mean_CO2LI7500
Plot Value
Left Axis Value = mean_CO2LI7500
Set Values
Number of Variables = 7
Storage Label = A_0
Assignment value = 6.107800
Storage Label = A_1
Assignment value = 0.4436519
Storage Label = A_2
Assignment value = 0.01428946
Storage Label = A_3
Assignment value = 0.0002650648
Storage Label = A_4
Assignment value = 0.000003031240
Storage Label = A_5
Assignment value = 0.00000002034081
Storage Label = A_6
Assignment value = 0.00000000006136821
User defined fast
From Time =
To Time =
*Equation=100*e_hmp/(0.1*(A_0+T_hmp*(A_1+T_hmp*(A_2+T_hmp*(A_3+T_hmp*(A_4+T_hmp*(A_5+T_hmp*A_6)))))))*
Number of signals = 3
Signal = RH_hmp
Signal = e_hmp
Signal = T_hmp
Variable = A_0
Variable = A_1
Variable = A_2
Variable = A_3
Variable = A_4
Variable = A_5
Variable = A_6
1 chn statistics
Signal = RH_hmp
Storage Label Mean = mean_RH_hmp
Plot Value
Left Axis Value = mean_RH_hm
Comments
Comment = Clean Data
Despike
Standard Deviations = 5
Spike width = 4
Spike % consistency = 30

Replace spikes = x
Outlier Standard Deviations = 9
Despike – Vickers
Signal = Ts
Window size, minutes = 5
Window step, points = 10
Initial standard deviation = 3.5
Standard deviation increment, % = 0.2
Max spike width = 3
Max number of passes = 10
Comments
Comment = Calculate the wind direction before rotations
Comment = Wind speed is calculated as part of the coordinate rotation
Comment = Save Ux, Uy, and Uz Components before rotation
Wind direction
Signal (u) = Ux
Signal (v) = Uy
Orientation = 244
Wind Direction Components = U+N_V+W
Wind Direction Output = N_0_deg-E_90_deg
Storage Label Wind Direction = Wind_Dir
Storage Label Wind Dir Std Dev = Wind_Dir_Std
1 chn statistics
Signal = Ux
Storage Label Mean = mean_Ux

1 chn statistics
Signal = Uy
Storage Label Mean = mean_Uy
1 chn statistics
Signal = Uz
Storage Label Mean = mean_Uz
Comments
Comment = Calculate sensor separation lags for lag removal
User defined
Storage Label = LI7500_sslag
*Equation = (0.15*cos((Wind_Dir - 260)*3.14/180))/max(SQRT(Ux_corr*Ux_corr +Uy_corr*Uy_corr),0.05)*
Variable = Wind_Dir
Variable = Ux_corr
Variable = Uy_corr
Plot Value
Left Axis Value = LI7500_sslag
Comments
Comment = Lag removal
Cross Correlate
Signal = Uz
Signal which lags = H2O_LI7500
Correlation type = Covariance
Storage Label Peak Time = H2O_LI7500_lag
Plot cross correlation
From Time =
To Time =
User defined
Storage Label = LI7500_H2Olag
Equation =-0.05+LI7500_sslag
Variable = mean_RH_hmp
Variable = LI7500_sslag

Remove Lag|
Signal = H2O
Min Lag (sec) = 0.0
Lag (sec) = LI7500_H2Olag
Max Lag (sec) = 5
Below Min default (sec) = 0
Above Max default (sec) = 0
Cross Correlate
Signal = Uz
Signal which lags = CO2_LI7500
Correlation type = Covariance
Storage Label Peak Time = CO2_LI7500_lag
Plot cross correlation
From Time =
To Time =
User defined
Storage Label = LI7500_CO2lag
Equation = -0.05+LI7500_sslag
Variable = mean_RH_hmp
Variable = LI7500_sslag
Remove Lag
Signal = CO2_LI7500
Min Lag (sec) = 0
Lag (sec) = LI7500_CO2lag
Max Lag (sec) = 5
Below Min default (sec) = 0
Above Max default (sec) = 0
Cross Correlate
Signal = Uz
Signal which lags = CO2del_umm_m
Correlation type = Covariance
Storage Label Peak Time = CO2_lag
Plot cross correlation
From Time =
To Time =
Comments
Comment = Coordinate Rotation
Rotation coefficients
Signal (u) = Ux
Signal (v) = Uy
Signal (w) = Uz
Storage Label Alpha = alpha
Storage Label Beta = beta
Storage Label Gamma = gamma
Rotation
Signal (u) = Ux
Signal (v) = Uy
Signal (w) = Uz
Alpha = alpha
Beta = beta
Gamma = gamma
Do 1st Rot = x
Do 2nd Rot = x
Cross Correlate
Signal = Uz
Signal which lags = CO2_LI7500
Correlation type = Covariance
Storage Label Peak Time = CO2LI7500_Lag_Postrotation

Cross Correlate
Signal = Uz
Signal which lags = H2O_LI7500
Correlation type = Covariance
Storage Label Peak Time = H2OLI7500_Lagpostrotation
Comments
Comment = means
1 chn statistics
Signal = AirTC
Storage Label Mean = mean_AirTC
1 chn statistics
Signal = CO2_LI7500
Storage Label Mean = mean_CO2LI7500
1 chn statistics
Signal = H20_LI7500
Storage Label Mean = mean_H_LI7500
1 chn statistics
Signal = Press_LI7500
Storage Label Mean = mean_Press_LI7500
Storage Label Maximum = max_Press_LI7500
Storage Label Minimum = min_Press_LI7500
1 chn statistics
Signal = Ts
Storage Label Mean = mean_Ts

Spectra
Signal = Ts
Window = Hamming
Output Spectra = x
Sort Output = x
Detrend data = Low
Cospectra
Signal 1 = Uz
Signal 2 = Ts
Window = Hamming
Output Cospectra = x
Sort Output = x
Detrend data, Signal 1 = Low
Detrend data, Signal 2 = Low
Plot spectral
Left Axis Spectra = Spectra
Right Axis Spectra = Cospectra
Left Axis Logarithmic = x
Right Axis Logarithmic = x
Spectra
Signal = CO2_LI7500
Window = Hamming
Output Spectra = x
Sort Output = x
Detrend data = Low
Cospectra
Signal 1 = Uz
Signal 2 = CO2_LI7500
Window = Hamming
Output Cospectra = x
Sort Output = x
Detrend data, Signal 1 = Low

Detrend data, Signal 2 = Low
Plot spectral
Left Axis Spectra = Spectra
Right Axis Spectra = Cospectra
Left Axis Logarithmic = x
Right Axis Logarithmic = x
Spectra
Signal = H2O_LI7500
Window = Hamming
Output Spectra = x
Sort Output = x
Detrend data = Low
Cospectra
Signal 1 = Uz
Signal 2 = H2O_LI7500
Window = Hamming
Output Cospectra = x
Sort Output = x
Detrend data, Signal 1 = Low
Detrend data, Signal 2 = Low
Plot spectral
Left Axis Spectra = Spectra
Right Axis Spectra = Cospectra
Left Axis Logarithmic = x
Right Axis Logarithmic = x

Plot Value
Left Axis Value = minC
Right Axis Value = maxC
Match Left/Right Axes = x
Plot Value
Left Axis Value = minH
Right Axis Value = maxH
Match Left/Right Axes = x
Comments
Comment = Perform High frequency filtering
Raw Subset
Subset start time(s) = 0
Subset length(s) = 1800
Signal for condition = Ds
Condition operators = Between
Condition (lower limit) = -0.5
Condition upper limit = 1.5
Storage Label % removed = pct_remove_sonic
Number of signals = 12
Signal Subset = Ux
Signal Subset = Uy
Signal Subset = Uz
Signal Subset = Ts
Signal Subset = Ds
Signal Subset = Vsolar
Signal Subset = AirTc
Signal Subset = e hmp
Signal Subset = H2O_LI7500
Signal Subset = CO2_LI7500
Signal Subset = Press_LI7500
Signal Subset = irga_diag

Raw Subset
Subset start time(s) = 0
Subset length(s) = 1800
Signal for condition = irga_diag
Condition operators = Between
Condition (lower limit) = -0.5
Condition upper limit = 1.5
Storage Label % removed = pct_remove_irga
Number of signals = 4
Signal Subset = H2O_LI7500
Signal Subset = CO2_LI7500
Signal Subset = Press_LI7500
Signal Subset = irga_diag
Plot Value
Left Axis Value = pct_remove_sonic
Right Axis Value = pct_remove_OPirga
Match Left/Right Axes = x
Comments
Comment = Skip remaining calculations is less than 50% of data remains.
Skip Next
Skip conditional variable = pct_remove_sonic
Skip condition operators = >
Skip condition (lower limit) = 50
Skip next items = -1
Default is skip =

Skip Next
From Time =
To Time =
Skip conditional variable = pct_remove_irga
Skip condition operators = >
Skip condition (lower limit) = 50
Skip next items = -1
Default is skip =
Cross Correlate
Signal = Uz
Signal which lags = CO2_LI7500
Correlation type = Covariance
Storage Label Peak Time = CO2LI7500_Lag_Postrotation
Cross Correlate
Signal = Uz
Signal which lags = H2O_LI7500
Correlation type = Covariance
Storage Label Peak Time = H2OLI7500_Lagpostrotation
Comments
Comment = Calculate useful and necessary means
1 chn statistics
Signal = Ts
Storage Label Mean = mean_Ts
Virtual Temperature Raw
Signal T(C) = Ts
Signal H2O = H2O_LI7500
Pressure, kPa = mean_Press_LI7500
Water vapour units = Molar density, mmol/m3
Temperature conversion = Calculate true from virtual-sonic
1 chn statistics
Signal = Ts

Storage Label Mean = mean_Ts
1 chn statistics
Signal = Ux
Storage Label Mean = mean_wind_spd
Storage Label Std Dev = std_wind_spd
1 chn statistics
Signal = Ds
Storage Label Mean = mean_diag_sonic
Plot Value
Left Axis Value = mean_diag_sonic
Comments
Comment = Calculate fluxes
Gas conversion
Storage Label = e
Measured variable = mean_H_LI7500
Convert from = Molar density mmol/m3
Convert to = Partial Pressure kPa
Temperature (C) = mean_Ts
Pressure (kPa) = mean_Press_LI7500
Water vapour = mean_H_LI7500
Water vapour units = Molar density mmol/m3
Molecular weight (g/mole) = 18
Sensible heat flux coefficient
Storage Label = rhocp
Vapour pressure (KPa) = e
Temperature (C) = mean_Ts
Pressure (KPa) = mean_Press_LI7500
Latent heat of evaporation
Storage Label = lambda
Temperature (C) = mean_AirTC
Pressure (KPa) = mean_Press_LI7500
Friction Velocity
Signal (u) = Ux
Signal (v) = Uy
Signal (w) = Uz
Storage Label U (uw vw) = friction_velocity*
Gas conversion time series
Signal = H2O_LI7500
Convert from = Molar density mmol/m3
Convert to = Absolute density g/m3
1st Offset = 0
1st Gain = 1
1st Curvature = 0
Signal T, C = Ts
Signal P, kPa = Press_LI7500
Signal H2O = H2O_LI7500
Units H2O = Molar density mmol/m3
Molecular Weight = 18
2nd Offset = 0
2nd Gain = 1
2nd Curvature = 0
Gas conversion time series
Signal = CO2_LI7500
Convert from = Concentration umol/mol
Convert to = Molar density umol/m3
1st Offset = 0
1st Gain = 1
1st Curvature = 0

Signal T, C = Ts
Signal P, kPa = Press_LI7500
Value H2O = e
Units H2O = Partial pressure kPa
Molecular Weight = 44
2nd Offset = 0
2nd Gain = 1
2nd Curvature = 0
2 chn statistics
Signal = Uz
Signal = Ts
Storage Label Flux = H
Flux coefficient = rhocp
2 chn statistics
Signal = Uz
Signal = CO2_LI7500
Storage Label Flux = OPFc
Flux coefficient = 1
2 chn statistics
Signal = Uz
Signal = H2O_LI7500
Storage Label Flux = OPLE
Flux coefficient = lambda

Plot Value
Left Axis Value = H
Right Axis Value = OPLE
Plot Value
Left Axis Value = OPFc
Right Axis Value = friction_velocity
Set Values
Number of Variables = 6
Storage Label = Height
Assignment value = 3.37
Storage Label = Sonic_Path
Assignment value = 0.1
Storage Label = Zero_Plane
Assignment value = 0.2
Storage Label = Sample_Freq
Assignment value = 10
Storage Label = irga_path
Assignment value = 0.152
Storage Label = OPsonic_irga_sep
Assignment value = 0.15
Set Value
Storage Label = OPirga_Path
Assignment value = 0.125
Stability - Monin Obhukov
Storage Label = MO_Stability
Measurement height (m) = Height
Zero plane displacement (m) = Zero_Plane
Virtual Temperature (C) = mean_Ts
H flux (W/m2) = H
H flux coef, RhoCp = rhocp
Scaling velocity (m/s) = friction_velocity

Plot Value
Left Axis Value = MO_stability
User defined
Storage Label = P_HorstMassman_fx
*Equation = IIF(MO_stability<=0,0.11368,0.12712+0.25387*MIN(MO_stability,3))*
Variable = MO_stability
User defined
Storage Label = P_HorstMassman_N
*Equation = IIF(MO_stability<=0,6.8763,2.8395-0.15979*MIN(MO_stability,3))*
Variable = MO_stability
User defined
Storage Label = P_HorstMassman_mu
*Equation = IIF(MO_stability<=0,0.18462,0.25414+0.019015*MIN(MO_stability,3))*
Variable = MO_stability
Load co-spectra
Load spectra of type = Model Horst/Massman
Spectral model = WX
Monin-Ohbukov stability = MO_stability
Wind speed (m/s) = mean_wind_spd
Measurement ht (m) = Height
Zero plane (m) = Zero_plane
Boundary layer ht (m) = 1000
Spectral peak frequency = P_HorstMassman_fx
Spectral broadness parameter = P_HorstMassman_mu
Spectral gain parameter = P_HorstMassman_N

Plot spectral
Left Axis Spectra = Loaded
Frequency response
Storage Label = Freq_resp_H
Correction type = WX
Measurement height (m) = Height
Zero plane displacement (m) = Zero_Plane
Boundary layer height (m) = 1000
Stability Z/L = MO_Stability
Wind speed (m/s) = mean_wind_spd
Sensor 1 Flow velocity (m/s) = mean_wind_spd
Sensor 1 Sampling frequency (Hz) = Sample_Freq
Sensor 1 Path length (m) = Sonic_Path
Sensor 1 Time constant (s) = 0.01
Sensor 1 Tube attenuation coef =
Sensor 2 Flow velocity (m/s) = mean_wind_spd
Sensor 2 Sampling frequency (Hz) = Sample_Freq
Sensor 2 Path length (m) = Sonic_Path
Sensor 2 Time constant (s) = 0.01
Sensor 2 Tube attenuation coef =
Path separation (m) = 0
Get spectral data type = Loaded
Get response function from = model
Frequency response
Storage Label = Freq_resp_tau
Correction type = UW
Measurement height (m) = Height
Zero plane displacement (m) = Zero_Plane
Boundary layer height (m) = 1000
Stability Z/L = MO_Stability
Wind speed (m/s) = mean_wind_spd
Sensor 1 Flow velocity (m/s) = mean_wind_spd

Sensor 1 Sampling frequency (Hz) = Sample_Freq
Sensor 1 Path length (m) = Sonic_Path
Sensor 1 Time constant (s) = 0.01
Sensor 1 Tube attenuation coef =
Sensor 2 Flow velocity (m/s) = mean_wind_spd
Sensor 2 Sampling frequency (Hz) = Sample_Freq
Sensor 2 Path length (m) = Sonic_Path
Sensor 2 Time constant (s) = 0.01
Sensor 2 Tube attenuation coef =
Path separation (m) = 0
Get spectral data type = Loaded
Get response function from = model
Frequency response
Storage Label = Freq_resp_OPFc
Correction type = WX
Measurement height (m) = Height
Zero plane displacement (m) = Zero_Plane
Boundary layer height (m) = 1000
Stability Z/L = MO_Stability
Wind speed (m/s) = mean_wind_spd
Sensor 1 Flow velocity (m/s) = mean_wind_spd
Sensor 1 Sampling frequency (Hz) = Sample_Freq
Sensor 1 Path length (m) = Sonic_Path
Sensor 1 Time constant (s) = 0.01
Sensor 2 Flow velocity (m/s) = mean_wind_spd
Sensor 2 Sampling frequency (Hz) = Sample_Freq
Sensor 2 Path length (m) = OPirga_Path
Sensor 2 Time constant (s) = 0.02
Path separation (m) = OPsonic_irga_sep
Get spectral data type = Loaded
Get response function from = model
Frequency response
Storage Label = Freq_resp_OPLE
Correction type = WX
Measurement height (m) = Height
Zero plane displacement (m) = Zero_Plane
Boundary layer height (m) = 1000
Stability Z/L = MO_Stability
Wind speed (m/s) = mean_wind_spd
Sensor 1 Flow velocity (m/s) = mean_wind_spd
Sensor 1 Sampling frequency (Hz) = Sample_Freq
Sensor 1 Path length (m) = Sonic_Path
Sensor 1 Time constant (s) = 0.01
Sensor 2 Flow velocity (m/s) = mean_wind_spd
Sensor 2 Sampling frequency (Hz) = Sample_Freq
Sensor 2 Path length (m) = OPirga_Path
Sensor 2 Time constant (s) = 0.02
Path separation (m) = OPsonic_irga_sep
Get spectral data type = Loaded
Get response function from = model
Plot Value
Left Axis Value = Freq_resp_OPLE
Plot Value
Left Axis Value = Freq_resp_OPFc
Plot Value
Left Axis Value = Freq_resp_H
Plot Value
Left Axis Value = Freq_resp_tau

Mathematical operation
Storage Label = Hc
Measured variable A = H
*Operation = **
Measured variable B = Freq_resp_H
Mathematical operation
Storage Label = OPFcc
Measured variable A = OPFc
*Operation = **
Measured variable B = Freq_resp_OPFc
Mathematical operation
Storage Label = OPLEc
Measured variable A = OPLE
*Operation = **
Measured variable B = Freq_resp_OPLE
Plot Value
Left Axis Value = mean_CO2
Match Left/Right Axes = x
Plot Value
Left Axis Value = H
Right Axis Value = Hc
Match Left/Right Axes = x
Plot Value
Left Axis Value = mean_CO2LI7500
Match Left/Right Axes = x
Plot Value
Left Axis Value = min_H_LI7500
Right Axis Value = max_H_LI7500
Match Left/Right Axes = x
Plot Value
Left Axis Value = min_Press_LI7500
Right Axis Value = max_Press_LI7500
Match Left/Right Axes = x
Plot Value
Left Axis Value = mean_irga_diag
Match Left/Right Axes = x
Plot Value
Left Axis Value = OPFc
Right Axis Value = OPFcc
Match Left/Right Axes = x
Plot Value
Left Axis Value = OPLEc
Right Axis Value = OPLE
Match Left/Right Axes = x
Webb correction
Storage Label = WebbCO2
Scalar value type = Concentration (umol/mol)
Scalar value = mean_CO2LI7500
Water vapour value type = Concentration (mmol/mol)
Water vapour value = mean_H_LI7500
Temperature (C) = mean_Ts
Pressure (KPa) = mean_Press_LI7500
H flux (W/m2) = H
LE flux (W/m2) = OPLEc
H flux coef, RhoCp = rhocp
LE flux coef, L = lambda
Scalar molecular wt. = 44
Scalar flux type = Fx (umol/m2/s)

Webb correction
Storage Label = WebbH2O
Scalar value type = Partial Pressure (kPa)
Scalar value = e
Water vapour value type = Partial Pressure (kPa)
Water vapour value = e
Temperature (C) = mean_Ts
Pressure (KPa) = mean_Press_LI7500
H flux (W/m2) = H
LE flux (W/m2) = OPLE
H flux coef, RhoCp = rhocp
LE flux coef, L = lambda
Scalar molecular wt. = 18
Scalar flux type = LE (W/m2)|
Mathematical operation
Storage Label = OPFccc
Measured variable A = OPFcc
Operation = +
Measured variable B = WebbCO2
Mathematical operation
Storage Label = OPLEcc
Measured variable A = OPLEc
Operation = +
Measured variable B = WebbH2O

Plot Value
Left Axis Value = WebbCO2
Right Axis Value = OPFcc
Match Left/Right Axes = x
Plot Value
Left Axis Value = OPFcc
Right Axis Value = OPFccc
Match Left/Right Axes = x
Plot Value
Left Axis Value = OPLEcc
Right Axis Value = OPLEc
Match Left/Right Axes = x
Comments
Comment = Flux footprint calculation
Integral Turbulence
Signal = Ts
Signal(w) = Uz
Storage Label QC value = QC_wT_Turbulence
Type of signal = X
Friction velocity (U) = friction_velocity*
Monin Ohbukov stability = MO_Stability
Latitude, deg = 58
1 chn statistics
Signal = Uy
Storage Label Std Dev = std_V
Plot Value
Left Axis Value = std_V
Plot Value
Left Axis Value = mean_wind_spd
Plot Value
Left Axis Value = QC_wT_Turbulence
Footprint
Storage Label = TalaheelFP

Fetch (m) = 1000
Measurement height (m) = Height
Wind speed (m/s) = mean_wind_spd
Friction velocity (m/s) = friction_velocity
Std dev of V velocity (m/s) = std_V
Stability Z/L = MO_Stability
Wind direction (deg) = Wind_Dir
Wind speed limit = 0.05
Friction velocity limit = 0.001
Stability limit (+/-) = 5
Fetch calculation step, m = 5
Footprint average
Storage Label = TalaheelFPOP
Unique footprint tag = FPtag
Conditional variable = 1.0
Condition operators = >
Condition (lower limit) = 0
Output File = C:\Users\Grahame\Documents\PhD\FLOW COUNTRY DATA\Talaheel\Processed Data\New Data (2015)\Footprint Day\a Talaheel All.csv
Footprint average
Storage Label = Avg_FP
Unique footprint tag = tag_AVP
Conditional variable =
Condition operators =
Condition (lower limit) =
Condition upper limit =
Output File = C:\Users\Grahame\Documents\PhD\FLOW COUNTRY DATA\Talaheel\Processed Data\New Data (2015)\Footprint Day\Avg_footprint.csv

Appendix C

Eddy Covariance Terms

C1 Reynolds Decomposition

Reynolds decomposition (Figure 1) is used to describe the decomposition of the time-series of each variable into a mean $\bar{\zeta}$ and fluctuating part ζ', which can be written as (Aubinet *et al.*, 2012):

$$\zeta = \bar{\zeta} + \zeta' \qquad \textbf{(C1.1)}$$

where:

$$\bar{\zeta} = \frac{1}{T}\int_{t}^{t+T} \zeta(t)dt \qquad \textbf{(C1.2)}$$

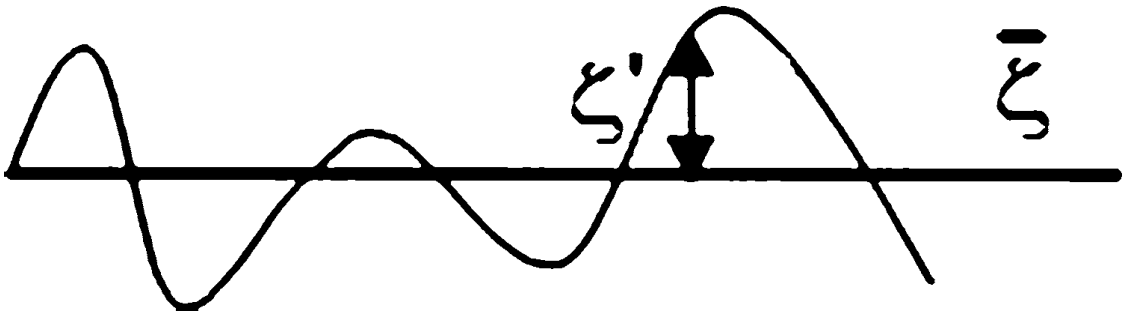

Figure 1 Schematic interpretation of the Reynolds decomposition of the value ζ (Foken, 2008)

In order to apply the Reynolds decomposition a number of averaging rules need to be applied these are called Reynolds postulates, where *a* is a constant (Aubinet *et al.*, 2012):

i. $\overline{\zeta'} = 0$

ii. $\overline{\zeta\xi} = \bar{\zeta}\bar{\xi} + \overline{\zeta'\xi'}$

iii. $\overline{\bar{\zeta}\xi} = \bar{\zeta}\,\bar{\xi}$

iv. $\overline{a\zeta} = a\bar{\zeta}$

v. $\overline{\zeta + \xi} = \bar{\zeta} + \bar{\xi}$

(C1.3)

In the strictest sense, these relationships are only valid when averaging by an ensemble averaging scheme, such that the averaging is carried out over many realisations under identical conditions (Kaimal and Finnigan, 1994, Aubinet *et al.*, 2012). However, in atmospheric measurements this is not possible, so averages are often computed on the basis of time series of statistical quantities by assuming that time averages are equivalent to ensemble averages, this is ergodic hypothesis (Kaimal and Finnigan, 1994). Fluctuations have to be statistically stationary during the averaging time in order for this assumption to be fulfilled.

C2 Monin-Obukhov Similarity Theory

The Monin-Obukhov similarity theory describes non-dimensionalised mean flows and temperatures in the surface layer under non-neutral conditions as a function of the dimensionless height parameter (*z*) (Monin and Obukhov, 1954, Foken, 2006). The Obukhov length, (*L)* is used to describe the effect of buoyancy on turbulent flows above the roughness sub layer (Obukhov, 1946). As *L* was defined in the Monin-Obukhov similarity theory, the Obukhov length is often referred to as the Monin-Obukhov length. In order to describe Obukhov length, Obukhov (1946), used gravity acceleration (*g*), surface temperature(T_0), friction velocity (u_*), kinematic heat flux (*q*), specific heat (C_p) and air density (ρ) to build this equation:

$$L = -\frac{v_*^3}{k\left(\frac{g}{T_0}\right)\left(\frac{q}{c_p\rho}\right)}$$

(C1.4)

Where k is the Von Kármán constant. This constant, 0.4, describes the logarithmic velocity profile of a turbulent flow near the boundary and can be determined by taking measurements of the surface drag and the velocity profile (Sheppard, 1947). Vertical fluxes are assumed to be constant with height in the surface layer. Atmospheric turbulence properties or statistics, such as gradient or covariance, when properly scaled, are universal functions of the stability parameter ζ *(=z/L)* (Brutsaert, 1999, Pahlow *et al.*, 2001).

C3 Terms of the Eddy Covariance Equation

In order to visualise the EC theory, under ideal conditions, we can think of an imaginary box enclosing the surface of interest (Figure C2). Within this box we can measure the flow through the sides and estimate the amount of the scalar, c[3], leaving the surface over a known period of time, thus we can measure the flux of *c* from the surface to the atmosphere.

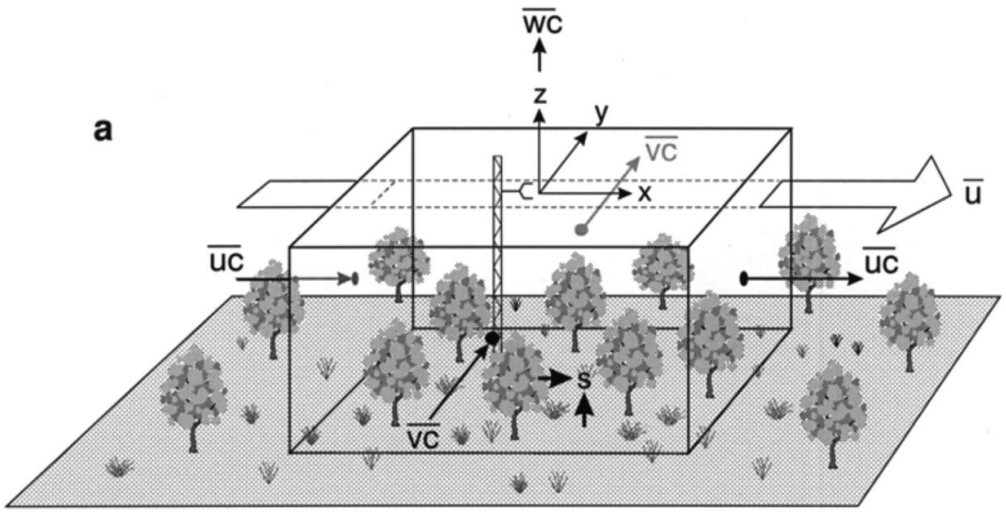

Figure C2 Diagrammatic representation of the imaginary box over an ecosystem to demonstrate the EC theory (Finnigan *et al.*, 2003).

[3] *c* is used to describe any atmospheric constituent that can be used as a resource by an ecosystem or is necessary to measure in order to understand ecosystem functioning. In this research, the constituents of interest are water vapour, CO_2 and energy in the form of latent heat and sensible heat.

However, in order for the box to behave like a "free" atmosphere it also has to include diffusive transport and flow (*u*, *v*, *w*), into and out of the box, in three ordinal directions (x, y, z), which are the primary directions in which we are interested. To understand the exchange processes occurring, changes in the storage of *c* over the measurement period within the box must also be known. These changes occur due to a divergence in the respective flows into and out of the box (Finnigan *et al.*, 2003). It is the change in *c* across the box in three ordinal directions that we are most interested in.

Assuming the scalar *c* does not experience a change of state the condition of the box can be expressed as (Baldocchi, 1988, Stull, 1988, Clement, 2004):

$$\frac{\partial c}{\partial t} + u\frac{\partial c}{\partial x} + v\frac{\partial c}{\partial y} + w\frac{\partial c}{\partial z} = Dc\frac{\partial^2 c}{\partial x^2} + Dc\frac{\partial^2 c}{\partial y^2} + Dc\frac{\partial^2 c}{\partial z^2} + F$$

(C1.5)

The first term in equation C1.5 is a storage term, while the next three represent the transport of the scalar *C* in the three orthogonal wind directions, *x*, *y* and *z*. The three terms on the right hand side of the equals sign represent the molecular diffusion exchange of the scalar *c*, while the surface flux is represented by the *F* term. In order to calculate this, we must make a number of assumptions about the system and aerodynamic field of flow such as the field of flow in the horizontal plane is homogenous and thus horizontal divergences of advective and eddy fluxes disappear. Another assumption is that the time averaged eddy flux measured at a single point is representative of the whole area.

C3.1 Storage

The first term in equation C1.5, $\frac{\partial c}{\partial t}$, describes how the magnitude of the scalar *c* varies as a function of time within the volume of the imaginary box. The vertical transport term diverges in the scenario of horizontal homogeneity.

Biomass and soil temperature changes are included in the sensible heat storage term because these terms represent fluxes occurring at the surface of the source and therefore are needed to account for the components of the surface when attempting the close the energy budget. However, problems arise if the additional sensible heat storage terms are added to sensible heat fluxes for analysis other than energy balance closure. Storage equations can be applied to fluxes/budgets of CO_2 and H_2O as the content of CO_2 and H_2O within the soil and biomass can

change over the measurement period. However, these changes are usually too small to be accurately measured unless over longer time periods.

In the context of the imaginary box, the storage term can be described by (Clement, 2004):

$$S_c = \sum_i K_{ci} \frac{\Delta c_i}{\Delta t} \Delta z_i$$

(C1.6)

Where S_c is the storage term related to the flux measurement period, Δt. The change in *c* over the measurement period, Δc_i, represents the difference in the ensemble average of *c* as measured at the beginning and end of the measurement period. If a finite number of sensors were placed along a vertical transect within the box, and each vertical measurement taken (*i*) taken at the beginning and end of the measurement period this is assumed to representative of the ensemble averages. Each ensemble average is then assumed to be representative for the layer of thickness, Δz. The variable *Kc* is used to convert the units of *c* into appropriate units so as to express the change in storage as a flux. The total change in storage is calculated for each layer and summed to give the total change in storage across the entire imaginary volume.

The storage term change depending on the ecosystem. For example, for CO_2 in an ecosystem with short vegetation the storage term is quite small, while an ecosystem with much taller vegetation, such as a forest, will have a bigger storage term. The storage term tends to be greatest around sunrise and sunset, when you reach a transition between respiration and photosynthesis and a transition between the stable nocturnal boundary layer and daytime convective turbulence respectively. Over a 24-hour period, it is expected that the storage term sums out to zero.

C3.2 Diffusion

In the imaginary box (Figure C2) the diffusion terms (**C1.7**), describe the transport of *C* across the walls by diffusion:

$$Dc \frac{\partial^2 c}{\partial x^2} + Dc \frac{\partial^2 c}{\partial y^2} + Dc \frac{\partial^2 c}{\partial z^2}$$

(C1.7)

In reality these terms are generally considered to be insignificant (Finnigan *et al.*, 2003). This is due to the magnitude of both the kinematic viscosity and the spatial rate of change of *C*, which would be zero if the flat, homogeneous surface assumptions were correct. However, very close

to the surface, such as in the interfacial zone, this may not be the case and could be the primary transport mechanism. However, at this point, the effect of the diffusion can be incorporated into the source strength specification (Finnigan *et al.*, 2003)

C3.3 Transport

The next three terms represent the movement of the scalar *c* in the three orthogonal wind directions, *x, y* and z:

$$u\frac{\partial c}{\partial x} + v\frac{\partial c}{\partial y} + w\frac{\partial c}{\partial z}$$

(C1.8)

Equation C1.5 can be reduced under assumptions of incompressibility and horizontal homogeneity to (Stull, 1988):

$$\frac{\partial wc}{\partial z}$$

(C1.9)

If the Reynolds decomposition (equation C1.1) is applied to equation C1.5 it can be split down into its mean and fluctuating components (Aubinet *et al.*, 2012):

$$\frac{\partial \overline{wc}}{\partial z} + \frac{\partial \overline{w'c'}}{\partial z}$$

(C1.10)

Transport terms can be obtained in terms of the product of the mean and fluctuating components of the vertical velocity and *C* by integration with respect to the vertical component and the equation becomes:

$$\overline{wc} + \overline{w'c'}$$

(C1.11)

Now that storage and transport terms have been shown to reduce under assumptions, such as homogeneity and incompressibility and the Reynolds decomposition theory the equation for the determination of net ecosystem exchange of the scalar *c* can be expressed as:

$$F = \overline{w'c'} + S_c$$

(C1.12)

This equation states that the flux is equal to the sum of the mean air density and mean covariance between instantaneous deviations in the vertical wind speed and mixing ratio.

C4 Errors and Corrections

C4.1 Frequency Response

It is necessary to correct EC fluxes for frequency attenuation because of limitations in sensor response times, path length averaging, signal processing and flux averaging periods. All EC sensors display some degree of high frequency attenuation, which is caused by the relatively slow response of the scalar sensors; instruments are often characterised by time constants of around 0.1s or greater (Massman, 2000). The spatial separation of instruments and volume averaging effects caused by the sensor design can also cause high frequency attenuation. It is possible to see some degree of attenuation in the low frequencies caused by the flux being estimated by blocking averaging over a set length of time such as 30 minutes (Panofsky, 1988, Kaimal *et al.*, 1989, Massman, 2000). With any EC system some degree of flux loss is inevitable, correcting the fluxes can be done with a variety of different methods. One such method is to correct flux measurements *in situ* (Laubach and McNaughton, 1998). This method has the advantage of being free of co-spectral shape, despite assuming co-spectral similarity between heat and water vapour fluxes. However, it requires more than one measurement of the virtual temperature flux. Other correction methods use spectral transfer functions (Moore, 1986), which give reasonable estimates of the correction factors. However, this method requires *a priori* assumptions to be made about the co-spectral shape, which can cause the correction factor to be incorrect if the assumed shape differs significantly from the true co-spectrum (Massman, 2000). At present, the use of spectral transfer functions is still the most commonly accepted method of correcting fluxes for frequency attenuation (Aubinet *et al.*, 2000).

The method of Moore (1986) sometimes referred to as the integrated method, uses a co-spectral shape for an assumed unattenuated flux and transfer function, dependent on the frequency, to describe the proportion of the true flux that is lost at different frequencies. Model transforms are applied to the data by:

$$C'(n) = C(n) \cdot T_i(n) \Big|_{i}^{\#\, transforms}$$

(C1.13)

where T_i is the modelled data. The model and reference transforms can be calculated as follows with T_R being the reference transform

$$C'(n) = \left| C(n) \cdot T_i(n) \cdot T_R(n) \right|^{\#\, transforms}_{i}$$

(C1.14)

The model and calculated transform can be combined to give:

$$C'(n) = \left| C(n) \cdot T_i(n) \cdot T_c(n) \right|^{\#\, transforms}_{i}$$

(C1.15)

Equations C1.14 and C1.15 are then combined to give:

$$C'(n) = C(n) \cdot T_R(n) \cdot T_C(n)$$

(C1.16)

Equation C1.16 gives the equation for which the reference and calculated transforms can be applied. These transforms are then integrated to give the covariance (*cov*) and the deviation from the mean of the covariance (*cov'*):

$$Cov = \sum_{i=0}^{j-1} \left(\frac{c(i) + (c(i+1)}{2} \right) \cdot [\ln(n(i+1)) - \ln(n(i))]$$

$$Cov' = \sum_{i=0}^{j-1} \left(\frac{c'(i) + (c'(i+1)}{2} \right) \cdot [\ln(n(i+1)) - \ln(n(i))]$$

(C1.17)

The final part of the frequency correction in EdiRe calculates the correction factor which can be applied to measured fluxes to account for factors such sensor response times, tube attenuation, path length averaging by using the two calculated parts from equation C1.17:

$$Correction = \frac{Cov}{Cov'}$$

(C1.18)

C4.2 Sensor Separation

A separation between scalar sensors and the sonic anemometer is unavoidable (Moore, 1986, Twine *et al.*, 2000). Due to the bulky nature of most sensors, having these too close to the sonic anemometer can cause flow distortion effects, which can result in large errors in the covariance (Laubach and McNaughton, 1998).

If we consider a time series of vertical wind velocity, represented by *w(t)* and a time series of a scalar represented by *a(t)* then the vertical turbulent flux of *a* over an averaging period is given by the covariance $\overline{w'a'}$. The spectra of this covariance can be decomposed as:

$$\overline{w'a'} = \int_0^\infty C^{wa}(f)df,$$

(C1.19)

Where $C^{wa}(f)$ represents the true cospectra of *w* and *a* and *f* the frequency. However, the decomposition shown in equation C1.19 represents an ideal measurement where, *w* and *a* are obtained at the same point in space and time and in reality this does not happen. If the two sensors are separated by a distance, s, then the co-spectra is subjected to a degree of high frequency loss, with the covariance spectra now being represented as:

$$\overline{w'a'_s} = \int_0^\infty C_s^{wa}(f)df.$$

(C1.20)

Moore (1986) proposed that this separation could be represented by co-spectral transfer function, T_s (n), defind as the ratio, $S_{\alpha'\beta}(n)/S_{\alpha\beta}(n)$, of the co-spectra for the quantities α' and β and quantities α and β, where α and α' represent the two sensors and β the separation. The angle between the separation path and the wind vector will have a bearing upon the co-spectrum of α and α'. If the path is parallel to the wind then the two sensors should measure the same turbulent fluctuations based on Taylor's frozen field hypothesis[4], but there will be a phase shift between the two sets of measurements. If the separation is perpendicular to the wind, then the fluctuations will be different but there will not be a phase shift (Moore, 1986).

C4.3 Tube Attenuation

[4] This is an assumption that advection contributed by turbulent circulations is small and therefore the advection of a field of turbulence past a fixed point can be taken to be entirely due to the mean flow

The tube attenuation co-efficient is a correction, applied to any analyser that employs an intake tube. It is necessary to apply this correction because analysers, that use intake tubes, can see a smoothing of the observed fluxes as some of the atmospheric constituents of interest, becoming attenuated in the tube due to flow within the tube (Philip, 1963a, Massman, 1991). In 1963 a model was developed for the attenuation of an atmospheric constituent in a tube with laminar flow (Philip, 1963b, Philip, 1963c). However, until 1991 no equivalent turbulent flow model existed (Massman, 1991), despite it being of vital importance to the accuracy of the EC approach that attenuation within the tube is accounted for.

Massman (1991) proposed a transfer function for calculating the tube attenuation co-efficient during turbulent flow:

$$T(w) = \exp(-(w^2 \ \Lambda La)/u^2)$$

(C1.21)

Where, $\Lambda(= vRe\,|Im(\lambda)|2\Omega \mathrm{D}_{\max})$ is termed the attenuation coefficient, *La* is the tube length and *u* the mean flow velocity. D_{max} is the turbulent diffusivity, which can vary laterally; *Re* is the Reynolds number and *v* the kinematic viscosity of air.

It has been demonstrated that relative humidity (RH) can have a large effect on fluxes of H_2O and to a less extent CO_2 (Clement, 2004, Ibrom *et al.*, 2007a, Massman and Ibrom, 2008) due to tube attenuation. Ibrom et al, 2007 found that the correction for this in a beech forest in Denmark amounted on average to 42% of the measured flux for H_2O and 4% for CO_2.

C5 Flux Processing Terms

C5.1 De-spiking

Firstly the data are despiked, this is a quality control measure employed to remove noise, constant values, spikes and dropouts. These issues can be caused by instrumental problems, electronic noise and water contamination on the sonic transducers. Noise and spikes are similar in nature but present different challenges when attempting to detect and remove from the data. Noise is difficult to determine, as it cannot be differentiated from the signal in magnitude or time. However, the amplitude, and the abruptness with which they occur allow spikes to be detected more easily. A procedure to define thresholds of spike detection by a point-to-point autocorrelation was suggested by (Hojstrup, 1993), which was proceeded by test criteria for QC of turbulent time series independent of the statistical distribution (Vickers and Mahrt, 1997). The first step in data de-spiking is to identify physical limits for the measured data, such that seasonal cycles can be incorporated so as not to truncate the measurement signal and remove

data due to shifts in meteorological conditions. The next step is to check the data relative to the standard deviation of the averaging interval. A method proposed by Schmid *et al.* (2000) suggests that spikes be identified as a value χ_i, which deviates more than the product of a discrimination factor, D, and the standard deviation σ_j from the mean value $\overline{\chi_j}$ (Aubinet *et al.*, 2012)

$$\left|\chi_i - \bar{\chi}_j\right| \geq D \cdot \sigma_j \rightarrow spike$$

(C1.22)

C5.2 Co-ordinate Rotations

Coordinate rotations are carried out as each term in the mass balance (C1.5) is a scalar and thus independent of coordinate frame. Due to the measurements being taken from a single point, the coordinate frame must be chosen so that the sole divergence measured approximates the total divergence (Finnigan *et al.*, 2003). This is so that the vertical axis of the sonic is aligned to the normal of the surface. A homogeneous boundary layer is assumed where the mean moments of the wind and scalar field in the surface-normal, cross streamline direction is much larger than streamwise gradients. Not only does this work in one-dimensional, horizontally homogeneous mean wind fields but also it is also valid in two- or three-dimensional wind flows where the measurement is carried out away from changes in the topography. Under these conditions, the orientation of the coordinate system is obtained when the instrument is oriented in the plane spanned by the mean wind vector and the normal of the surface. Errors in this are known as tilt errors, and an error of <2° can result in an error of around 5% in scalar fluxes. However, during stable conditions, momentum flux errors can be as high as 100% of the flux (Lee *et al.*, 2004).

The rotation is typically applied through one of two methods; Double rotation and planar fit, both of which are typically applied over 30 minute averages. The first rotation aligns $\bar{u}$ into the mean direction, which forces $\bar{v}$ to 0, resulting in the yaw angle α. The second rotation is performed to cancel out the, $\overline{w}$, which results in the pitch angle β. This rotation is a powerful way to level the anemometer to the surface in homogeneous flow. However there is a potential for over-rotation if there is an offset in the measurement of the *w* component it may be interpreted as a tilt. The planar-fit method was proposed by Wilczak *et al.* (2001) after research by Lee (1998) found that a non-zero mean vertical velocity may exist over tall vegetation or complex terrain over a time period of 30 minutes and should be taken into account. The method is based on an assumption that the vertical wind component is only equal to zero over long averaging periods such as weeks, representing different flow dynamics over the site under

investigation. The coordinate rotation must be carried out before any other processing occurs; in this research the double rotation method was chosen.

C5.3 Lag Determination

The time lag determination is required as the two time series (wind and scalar) are slightly offset from one another; however instantaneous measurements of both components are needed. These differences are caused by differences in electronic signals, spatial separation between sensors and tube travel time. Delays caused by signals can be due to conversion or computation by individual sensor software; these delays are generally small and constant. This means that these delays can be known and dealt with directly. Sensor separation causes the two components to be measured at two different points in time and space. The use of tubes in closed path systems produces a larger lag time, as time is needed for the air to travel down the tube to the analyser. A mass flow controller can be used in these systems to keep the time delay on this constant, allowing for an easier calculation of the lag time. The lag is determined for each averaging interval by performing a cross correlation between the scalar and vertical wind component. The selected time lag is the time delay that produces the highest correlation between the scalar and vertical velocity. Lag times for H_2O can be affected by relative humidity and thus should be taken into account for further lag time determinations.

C5.4 Uncorrected Flux Determination

Uncorrected fluxes of CO_2, and LE can now be calculated through the covariance of the vertically rotated wind speed and the mixing ratio of the scalar. Sensible heat flux can be calculated from the fluctuations of the vertical wind and sonic temperature. Coefficients must be calculated for LE and H must be calculated. For H the coefficient is used to convert the units of the of the covariance of vertical velocity and temperature, for example °c m^{-1} s^{-1}, into energy flux units of W m^{-2}. The LE coefficient has a similar function but is used to covert units of the covariance of the vertical velocity and absolute humidity (g m^{-1} s^{-1}) to energy flux units of W m^{-2}. In order to calculate the uncorrected fluxes the components must be in appropriate units. This step is dependent upon the system being used and what units are being outputted from the sensor. As most scalar analysers measure a concentration such as μmol/mol (ppm), this needs to be converted to appropriate molar density units such as μmol/m^3. Once units have been converted the uncorrected fluxes can be calculated by calculating the covariance of vertical wind speed with the scalar.

C5.4 Correcting Fluxes

The correction of frequency dependent flux losses requires knowledge of the proportion of flux attenuation across all measured frequencies, the true flux spectral behaviour or the attenuated

flux at a certain frequencies. However, attenuation can reduce the flux at high frequencies to magnitudes so low that true fluxes cannot be recovered accurately. Therefore frequency response corrections presume knowledge of the true flux spectral behaviour (Clement, 2004).

The frequency response of a system can be seen in the co-spectra for that sensor. Co-spectral models are a set of equations for different atmospheric conditions (stable, unstable and neutral) and use measured and calculated parameters such as stability (z/L), non-dimensionalised frequency (f=n(z-d)/U), measurement height (z), zero plane displacement (d) and mean wind speed (U) to obtain the co-spectral energy at each frequency (nC(n)).

C5.5 WPL correction

Density fluctuations of a scalar *c* occur due water vapour density and temperature fluctuations, which are not associated with the net transport of *c,* this can be particularly large for trace gases such as CO_2 (Webb *et al.*, 1980, Leuning, 2004). During warm and wet conditions, high frequency measurements could create an appearance of CO_2 uptake when there is no actual CO_2 flux, due to the expansion of the air. A correction for this was proposed by Webb *et al.* (1980) and is now referred to as the WPL correction:

$$\overline{F_c}(hm) = \overline{w'pc'} + \mu \left(\frac{\overline{pc}}{\overline{pd}}\right) \overline{w'pv'} + (1 + \mu\sigma)\left(\frac{\overline{pc}}{\overline{\theta}}\right) \overline{w'\theta'}$$

(C1.23)

Where, $\mu = m_d/m_v$ is the ratio of molar masses of dry air and water vapour and $\sigma = \overline{p_v/p_d}$ the ratio of the densities of water vapour dry air. A key governing constraint used by Webb *et al.* (1980) iss that during steady, horizontally homogeneous conditions there is no horizontal advection, meaning there is no net flux of dry air at the measurement height, *hm.* The sensitivity of the WPL correction is dependent upon the ratio between the concentration of the scalar and the flux, with large WPL corrections expected for small fluxes with high background concentrations (Ibrom *et al.*, 2007b). Typically this is applied to both open- and closed-path analysers, however, it is not required if the analyte is brought to a constant pressure and temperature prior to analysis.

C5.6 Final Corrected Flux

Now that the obtained raw data has been processed and corrected the final flux can simply be calculated, by multiplying the uncorrected flux by the frequency response correction. However, this does not take into account the WPL correction and thus this must also be added on. This is usually a simple step within eddy covariance data processing software.